INFORMATION TO USERS

This manuscript has been reproduced from the microfilm master. UMI films the text directly from the original or copy submitted. Thus, some thesis and dissertation copies are in typewriter face, while others may be from any type of computer printer.

The quality of this reproduction is dependent upon the quality of the copy submitted. Broken or indistinct print, colored or poor quality illustrations and photographs, print bleedthrough, substandard margins, and improper alignment can adversely affect reproduction.

In the unlikely event that the author did not send UMI a complete manuscript and there are missing pages, these will be noted. Also, if unauthorized copyright material had to be removed, a note will indicate the deletion.

Oversize materials (e.g., maps, drawings, charts) are reproduced by sectioning the original, beginning at the upper left-hand corner and continuing from left to right in equal sections with small overlaps. Each original is also photographed in one exposure and is included in reduced form at the back of the book.

Photographs included in the original manuscript have been reproduced xerographically in this copy. Higher quality 6" x 9" black and white photographic prints are available for any photographs or illustrations appearing in this copy for an additional charge. Contact UMI directly to order.

UMI

A Bell & Howell Information Company
300 North Zeeb Road, Ann Arbor, MI 48106-1346 USA
313/761-4700 800/521-0600

Development of Raney-Ni Gas Diffusion Electrodes for Fuel-cells

BY

SLEEM-UR-RAHMAN

A Dissertation Presented to the

FACULTY OF THE COLLEGE OF GRADUATE STUDIES

KING FAHD UNIVERSITY OF PETROLEUM & MINERALS

DHAHRAN, SAUDI ARABIA

In Partial Fulfillment of the
Requirements for the Degree of

DOCTOR OF PHILOSOPHY
In
CHEMICAL ENGINEERING

August, 1995

UMI Number: 9543508

UMI Microform 9543508
Copyright 1995, by UMI Company. All rights reserved.

This microform edition is protected against unauthorized
copying under Title 17, United States Code.

UMI

300 North Zeeb Road
Ann Arbor, MI 48103

KING FAHD UNIVERSITY OF PETROLEUM AND MINERALS
DHAHRAN 31261, SAUDI ARABIA

COLLEGE OF GRADUATE STUDIES

This dissertation, written by **SLEEM-UR-RAHMAN** under the direction of his Dissertation Advisor, and approved by his Dissertation committee, has been presented to and accepted by the Dean of the College of Graduate Studies, in partial fulfillment of the requirements for the degree of **DOCTOR OF PHILOSOPHY IN CHEMICAL ENGINEERING.**

Dissertation Committee

Dr. Muhammad A. Al-Saleh (Chairman)

Dr. Selahttin Gultekin (Co-chairman)

Dr. Abdullah S. Al-Zakri (Member)

Dr. Hussein K. Abdel-Aal (Member)

Dr. Abdul Muttaleb Y. Jaber (Member)

Department Chairman

Dean, College of Graduate Studies

Date : Aug 20, 1995

Dedicated to my mother and father.
May Allah forgive them
and bestow His mercy on them.

ACKNOWLEDGMENT

All praises to Almighty Allah Who taught man what he knew not. Thanks to Him for bestowing me with the courage and patience to carry out this work.

My sincere appreciation and thanks is for my dissertation advisor Dr. Muhammad A. Al-Saleh for is constant help, guidance and encouragement through out the course of my studies.

I wish to thank Dr. S. Gultekin, my dissertation co-advisor, for his invaluable suggestions, comments and cooperation. I am also thankful to Prof. A. S. Al-Zakri, Vice Rector for Graduate Studies and Research, Prof. H. K. Abdel Aal and Dr. A. M. Y. Jaber (Chemistry Department) for serving as dissertation committee members and for their helpful advice and criticism.

Acknowledgment is due to King Fahd University of Petroleum & Minerals for various facilities I used for this work. The financial support by the King Abdulaziz City for Science and Technology through the Hysolar Project is gratefully acknowledged. The help from the KFUPM Research Institute (CAL/MCL and Division 1) is highly appreciated.

I am thankful to Dr. D. Al-Harbi, Chairman, Chemical Engineering Department, for his cooperation and help during this work. Also, I want to thank all chemical engineering faculty for their help.

I wish to thank Prof. Schnurnberger and Mr. Guelzow of DLR, Germany; Dr. Loughlin, Dr. Mirza and Dr. Fatehi for their suggestions at various stages of the work.

I would like to thank Dr. W. Z. Khan for his cooperation. Also, special thanks to our technicians Mr. J. Chapman, Mr. Mehdi Al-Saffar, Mr. Ibrahim Al-Salem, Mr. Syed Kamal, Mr. Bashir Ahmed, Mr. Romeo, Mr. Mariano and Mr. Ahmedullah.

I would like to thank all of my friends and fellow graduate students for their help at various stages, especially Asjad Khan, Shakeel Ahmed, Nadhir Al-Baghli, Mohd. Sami, Azhar Saeed, Zafar Haider of KFUPM; Dr. Asif Hussain and Dr. Mukhtar Khan of IIT, Bombay; and Dr. Rajesh Tyagi of NRC, Canada.

Last, but not the least, I wish to thanks my wife, Farhat for her help, support and patience.

SLEEM-UR-RAHMAN
Dhahran
August, 1995.

TABLE OF CONTENTS

Page

List of Tables x

List of Figures xii

ABSTRACT-Arabic xviii

ABSTRACT-English xix

Chapter1 : Introduction 1

1.1. Definition of Fuel Cells 1

1.2. Advantages and Disadvantages 3

1.3. Classification of Fuel Cells 4

1.4. Applications of Fuel Cells 4

1.5. H2/O2 Alkaline Fuel Cells 8

1.6 Electrode kinetics and Modes of Polarization 11

1.7. Methods and techniques for Fuel-cell studies 11

1.8. Objectives of This Study 14

1.8.1. Experimental Objectives 14

1.8.2. Theoretical Objectives 16

References 17

Chapter 2 : Literature Review **18**

2.1. Introduction 18

2.2. Electrocatalysts 18

2.2.1. Requirements of the Fuel-cell Electrocatalysts 18

2.2.2. Hydrogen Oxidation Electrocatalysts 19

A. Noble Metal Electrocatalysts 19

B. Nickel Electrocatalysts 21

C. Miscellaneous Electrocatalysts 21

2.2.3. Mechanism of Oxygen Reduction 22
2.2.4. Electrocatalysts for Oxygen Reduction 23
A. Carbon Materials 23
B. Pt and Pt-Alloys 24
C. Silver 26
D. Transition Metal Complexes 26
E. Bulk Doped Organometals 27
F. Perovskites and other Oxides. 27
2.3. Fuel Cell Electrodes 28
2.3.1. Historical Background 28
2.3.2. Single Layer Homoporous Electrode 29
2.3.3. Variants of DSK Electrodes 30
A. DSK electrodes from platinum metals 30
B. Triple Layered Electrodes 30
C. Non pyrophoric Electrodes 30
2.3.4. MSK-Electrode (55) 31
2.3.5. Electrodes on Plastic Supports 32
2.3.6 Controlled Wetting Electrodes 32
A. The General Electric Electrode 32
B. The Union Carbide Electrode 35
2.3.7. Dual Layer and Dual Porosity Electrodes 35
2.3.8. The Single-Layered Hydrophobic Electrodes 40
2.3.9. Spongy Raney Ni Electrode 40
2.4. Electrode Preparation Techniques and Electrocatalysts 41
2.4.1. Introduction 41
2.4.2. Techniques of Electrode Preparation 42

A. The DSK Electrodes 42
B. PTFE Bonded Raney Ni Electrodes 43
C. PTFE Bonded Carbon Electrode 45
2.5. Mathematical Models for Gas Diffusion Electrodes 51
2.5.1. Introduction 51
A. Homogeneous Model 53
B. Quasi-homogeneous Model 53
C. Statistical Models 53
2.5.2. Simple Pore Model 54
2.5.3. Thin Film and Meniscus Model 57
A. The Thin Film Model 57
B. The Meniscus Model 61
2.5.4. Hydrophobic Electrode Models 64
2.5.5. Hydrophilic Electrode Models 65
2.5.6. Cylindrical Gas Pore Model 66
2.5.7. Models Based on Macrokinetics and Electrode Effectiveness 67
2.5.8. Flooded Agglomerate Models 67
References 73
Chapter 3 : Electrode Preparation by Filtration Method 81
3.1. Introduction 81
3.2. Dry Method 81
3.3. The Filtration Method 82
3.4. Advantages of the Filtration Method 83
3.5. Passivation of the Raney-Ni Catalyst 83
3.5.1. Conventional Method 84
3.5.2. Passivation by H2O2 Treatment 86
References 89

Chapter 4 : Experimental Procedure and the Set-Up 90
4.1. Preparation of the Gas Diffusion Electrodes 90
4.1.1. Introduction 90
4.1.2. Materials Used 90
A. Raney Ni- Al alloy 90
B. Nickel Mesh 93
C. The PTFE Powder 93
D. Potassium Hydroxide 93
E. Surfactants 93
4.1.3. Prepration of the catalyst 95
A. Leaching of Raney-Ni-Al Alloy 95
B. Washing of the catalyst 95
C. Passivation of Raney- Ni catalyst 99
4.1.4. Reactive Mixing 101
4.1.5. Preparation of Slurry 101
4.1.6. Formation of the Filter-cake 101
4.1.7. Cold Rolling 103
4.1.8. Removal of the Surfactant 106
4.2. Testing of the Electrode Performance 106
4.2.1. Introduction 106
4.2.2. The Half-cell Set-up 106
4.2.3. Procedure of Activation and Measurement of Polarization 109
A. Potentiostat and Related Circuit 109
B. IR-drop Compensation 111
C. Activation of Passivated Raney-Ni Electrode. 112
D. Polarization of Activated Electrodes. 114

References 115

Chapter 5: Parametric Study of Electrode Preparation by Filtration Method 116

5.1. Introduction 116

5.2. Experimental Design 116

5.2.1. Parameters Affecting the Performance 117

5.2.2. The Partial Factorial Design 120

5.2.3. Result and Discussion 123

A. Analysis of Data at 100 mA/cm2 123

B. Analysis of Data at 150 mA / cm2 130

5.3. Effects of Parameters on Electrode Performance 139

5.3.1. Effect of PTFE Content 139

5.3.2. Effect of Milling Time 142

5.3.3. Effect of Cooling while Reactive Mixing 142

References 145

Chapter 6 : Characterization of the Materials and the Electrode 146

6.1. Introduction 146

6.2. BET Surface Area 147

6.3. Mercury Intrusion Porosimetery 148

6.4. Scanning Electron Microscopy (SEM) 153

6.5. X-ray Diffraction 160

6.6. Density of the Powder by Helium Displacement 160

6.7. Particle Size Distribution 162

Reference 164

Chapter 7 : Mathematical Model for the Performance of the Fuel Cell Electrode 165

7.1 The Flooded Spherical Agglomerate Model 165

7.2 The Modified Flooded Spherical Agglomerate Model 170

7.2.1. The Grain 174

7.2.2. The film 175

7.2.3. The Macropores 176

7.2.4. Ionic Overpotential 177

7.3. Solution of Model Equations 179

7.4. Result and Discussion 182

7.4.1. Estimation of the Model Parameters 184

A. Conductivity of the Electrolyte: 184

B. Estimation of Henry's Constant 186

C. Diffusion Coefficients in Macropores: 186

D. Diffusivities in KOH Solution 187

E. Other Parameters and Constants 188

7.4.2. Effects of Various Parameters on the Polarization Behavior 188

7.5.3 Polarization Curves at Different Temperatures 194

References 201

Chapter 8 : Results and Discussions **203**

8.1. Introduction 203

8.2. Passivation of the Raney-Ni Catalyst 204

8.3. Reactive Mixing 208

8.4 Performance Testing and Reproducibility 211

8.5. Effect of Various Parameters on the Performance of the Electrodes 215
A. PTFE Content 218
B. Milling Time 220
C. Cooling while Milling 223
D. Clearance between the Rolls 224
E. Removal of the Surfactant 227
8.6. Comparison of the Electrode Performance 227
8.7. Long Term Performance Test 237
Reference 242
Chapter 9 : Conclusions and Recommendations 243
9.1. Conclusions 243
A. Electrode Preparation 243
B. Mathematical Model 245
C. Passivation of Raney-Ni 246
9.2. Recommendations 246
Nomenclature 250
APPENDICES 252
Appendix-A : Computer Programs for Running the Experiments 253
Appendix-B : Electrode Polarization Data for Experimental Design 267
Appendix-C : Electrode Polarization Data for the Effect of PTFE Content 284
Appendix-D : Electrode Polarization Data for the Effect of Milling Time 290
Appendix-E : Electrode Polarization Data at Different Temperatures 297
Appendix-F : Computer Program for Solving Model Equation in Chapter 7 304
Appendix-G : Sample Run of Electrode Preparation 315

LIST OF TABLES

Page

Table 1.1 : Classification of Fuel Cells on the Basis of Electrolyte 5

Table 1.2 : Classification of Fuel cell..... 6

Table 1.3 : Potential Fuel Cell applications..... 7

Table 1.4 : Threshold Capital Values for different Fuel cell Applications 9

Table 2.1. : Pt and Pt alloys used for oxygen reduction..... 25

Table 2.2 : Properties of a Typical Shell Electrode 33

Table 2.3 : Properties of a Typical General Electric Electrode 36

Table 2.4 : Properties of a Typical Union Carbide Electrode 38

Table 2.5 : Properties of a Typical Bacon Dual Layer Electrode 39

Table 4.1 : Properties of Raney-Ni Alloy..... 92

Table 4.2 : Parameters of Leaching..... 96

Table 4.3 : Comparison of Positive Feedback and Current Interruption..... 113

Table 5.1 : Higher and Lower Levels of Parameter Values..... 121

Table 5.2 : Construction of 2^{5-1} Factorial Design..... 122

Table 5.3 : Plan of the Experiments 124

Table 5.4 : Overpotentials at 100 mA/cm^2 and 150 mA/cm^2 125

Table 5.5 : Estimated Effects at 100 mA/cm^2 126

Table 5.6 : ANOVA at 100 mA/cm^2..... 127

Table 5.7 : Estimated Effects at 150 mA/cm^2 133

Table 5.8 : ANOVA at 150 mA/cm^2 134

Table 5.9 : Base Vales of Parameters Affecting the Electrode Performance 140

Table 6.1 : The BET Surface Area of Various Samples 149

Table 7.1 : Estimated and Fitted Parameters for the modified Model at Different Temperatures 185

Table 8.1 : Reproducibility of the Half-cell Set-up 217

Table 8.2 : Estimated and Fitted Parameters for the modified Model at Different Temperatures (Filtration Method) 235

Table 8.3 : Other Parameters for the Model (Electrode Prepared by Filtration Method) 236

Table 8.4 : Comparison of the Performance of Various Electrodes 240

LIST OF FIGURES

Page

Fig. 1.1 : Schematic of Alkaline Fuel Cell in Operation 2

Fig. 1.2 : A Typical Hydrogen-Oxygen Fuel-cell Polarization curve 12

Fig. 1.3 :Schematic Diagram of the Half Cell Assembly 13

Fig. 2.1 : Photomicrograph of a General Electric Electrode 34

Fig. 2.2 : Cross-section of a Union Carbide Electrode 37

Fig. 2.3 : Schematic Diagram for Electrode Preparation by Dry-Method 46

Fig. 2.4 : The Flow-sheet for Electrode Preparation by Rolling Method 47

Fig. 2.5 : Process Flow-sheet for Electrode Manufacturing by Pressing Method 49

Fig. 2.6 : Process Flow-Sheet for the Preparation of Thin Carbon Electrodes (Spraying) 50

Fig. 2.7 : Schematic Diagram of the Simple Pore Model 55

Fig. 2.8 : The Thin Film Model 59

Fig. 2.9 : The Thin Film Model (Kenjo et al.) 62

Fig. 2.10 : The Meniscus Model 63

Fig. 2.11 : Flooded Agglomerate Model (Giner et al.) 69

Fig. 2.12 : Flooded Agglomerate Model (Iczkwoski et al.) 70

Fig. 2.13 : Schematic Diagram of the Model of a Complete Fuel-cell 72

Fig. 3.1 : Apparatus for Passivation by Conventional Method 85

Fig. 3.2 : Apparatus for Passivation by H_2O_2 Treatment 88

Fig. 4.1 : Flow-diagram of Electrode Preparation by Filtration Method 91

Fig. 4.2 : SEM Micrograph of PTFE Particles..... 94

Fig. 4.3 : Apparatus for Leaching of Raney-Ni Alloy..... 97

Fig. 4.4 : Apparatus for Washing the Leached Raney-Ni 98

Fig. 4.5 : Apparatus for Passivation of Raney-Ni 100

Fig. 4.6 : High Speed Mill for Reactive Mixing 102

Fig. 4.7 : Apparatus for Electrode Formation by filtration Method..... 104

Fig. 4.8 : The Rolling machine..... 105

Fig. 4.9 : General View of the Performance Testing Set-up 107

Fig. 4.10 : Schematic Diagram of the Half-cell Assembly..... 108

Fig. 4.11 : Schematic Diagram of the Set-up for Performance Testing 110

Fig. 5.1: Relative Effectiveness of the Designs. 118

Fig. 5.2 : Plot of Main Effects for 100 mA/cm^2. 128

Fig. 5.3 : Standardized Pareto Chart for 100 mA/cm^2. 129

Fig. 5.4 : Standard Probability Plot 100 mA/cm^2. 131

Fig. 5.5 : Plot of the Residuals w.r.t. run number 100 mA/cm^2. 132

Fig. 5.6 : Standardized Pareto Chart for 150 mA/cm^2. 135

Fig. 5.7 : Plot of Main Effects for 150 mA/cm^2. 136

Fig. 5.8 : Standard Probability Plot 150 mA/cm^2 137

Fig. 5.9 : Plot of the Residuals w.r.t. run number 150 mA/cm^2. 138

Fig. 5.10 : Effect of PTFE Content on the Electrode Performance 141

Fig. 5.11 : Effect of Milling Time on the Electrode Performance 143

Fig. 5.12 : Effect of Cooling During Reactive Mixing on the Electrode Performance 144

Fig. 6.1 : BET Isotherm for the Passivated Raney-Ni 150

Fig. 6.2 : BET Isotherm for the Milled Raney-Ni 151

Fig. 6.3 : BET Isotherm for the Electrode 152

Fig. 6.4 : Cumulative Void Volume Distribution for the Passivated Raney-Ni 154

Fig. 6.5 : Cumulative Void Volume Distribution for the Milled Raney-Ni 155

Fig. 6.6 : Cumulative Void Volume Distribution for the Electrode 156

Fig. 6.7 : Micrograph of the Cross-section of the Electrode 157

Fig. 6.8 : Micrograph of the of Catalyst Side of the Electrode 158

Fig. 6.9 : Micrograph of the of Mesh-side of the Electrode 159

Fig. 6.10 : Micrograph of the Mesh-side of the Electrode Produced by Dry Method 161

Fig. 6.11 : Histogram for the Particle Size Distribution of the Milled Raney-Ni 163

Fig. 7.1 : Micrograph of the Ni/PTFE electrode from mesh side (Magnification =400x) 166

Fig. 7.2 : Schematic diagram of spherical grain model 168

Fig. 7.3 : Polarization curves obtained from the spherical grain model and experimental data 171

Fig. 7.4 : . Schematic diagram of the fuel cell electrode and Raney Ni-PTFE grain 173

Fig. 7.5 : Flow chart for the FORTRAN program to solve model equations 183

Fig. 7.6 : Effect of film thickness on Polarization of electrode using parameters at 348 K 190

Fig. 7.7 : Effect of exchange current density on polarization of electrode using parameters at 348 K 191

Fig. 7.8 : Effect of grain radius on polarization of electrode using parameters at 348 K 192

Fig. 7.9 : Effect of diffusivity of H_2 in the electrolyte on polarization of electrode using parameters at 348 K 193

Fig. 7.10 : Effect of diffusivity of H_2 in the macropores on polarization of electrode using parameters at 348 K 195

Fig. 7.11 : Reactant pressure profiles in the electrode at different macropore diffusivities at ηo = 44 mV and other parameters at 348 K 196

Fig. 7.12 : Comparison of the experimental data with old and modified model (T= 308 and 318 K) 197

Fig. 7.13 : Comparison of the experimental data with old and modified model (T=328 and 348 K) 198

Fig. 7.14 : Exchange current density vs. 1/T (Arrhenious Plot) 199

Fig. 8.1 : XRD Pattern of the Raney-Ni Sample Passivated by Conventional Method 205

Fig. 8.2.a : SEM Micrograph of the Conventionally Passivated Raney-Ni (500X magnification) 206

Fig. 8.2.b : SEM Micrograph of the Conventionally Passivated Raney-Ni (5000X magnification) 207

Fig. 8.3 : XRD Pattern for the Raney-Ni Sample Passivated by H_2O_2 Treatment 209

Fig. 8.4 : SEM Micrograph for the Raney-Ni Sample Passivated by H_2O_2 Treatment. 210

Fig. 8.5.a : SEM Micrographs of Milled Raney-Ni (Magnification 500x) 212

Fig. 8.5.b : SEM Micrographs of Milled Raney-Ni (Magnification 5000x) 213

Fig. 8.6 : A typical Activation Plot..... 214

Fig. 8.7 : A Typical Plot for Test of Activation..... 216

Fig. 8.8 : Effect of the PTFE Content on the Performance of the Electrode..... 219

Fig. 8.9 : Effect of the PTFE Content on the Performance of the Electrode made by Wet Method 221

Fig. 8.10 : Effect of the Milling Time on the Performance of the Electrode 222

Fig. 8.11 : Effect of the Cooling while Milling on the Performance of the Electrode 225

Fig. 8.12 : Effect of the Clearance between the Calender Rolls on the Performance of the Electrode..... 226

Fig. 8.13 : Effect of the Surfactant Removal on the Performance of the Electrode 228

Fig. 8.14 : Polarization of Electrode at 25°C..... 229

Fig. 8.15 : Polarization of Electrode at 35°C..... 230

Fig. 8.16 : Polarization of Electrode at 45°C..... 231

Fig. 8.17 : Polarization of Electrode at 55°C..... 232

Fig. 8.18 : Polarization of Electrode at 65°C..... 233

Fig. 8.19 : Polarization of Electrode at 75°C..... 234

Fig. 8.20 : Arrhenious Plot of Exchange Current Density for Electrode Made by Filtration Method..... 238

Fig. 8.21 : Comparison of the Polarization with Electrode Prepared by Mund et al. 239

Fig. 8.22 : Long Term Performance of the Filtration Method Electrode 241

Fig. 9.1 : Continuous Production of the Fuel-cell Electrodes 248

Fig. 9.2 : Proposed Machine for Electrode Production 249

ملخص الأطروحـــه

الأســـم : د . سليم الرحمن

العنـــوان : تطوير أقطاب النيكل الغازيه لخلايا الوقود

التخصص : الهندسه الكيميائيه

التاريـــخ : أغسطس ١٩٩٥م

تم في هذه الدراسه أقتراح طريقه جديده لتحضير الأقطاب الغازيه لخلايا الوقود والتي تتغلب على بعض الصعوبات التي كانت موجوده في الطريقه التقليديه المسماه بالطريقه الجافه والمقترحه بواسطة الأستاذ ونسل . يتم في الطريقه المقترحه طحن العامل المساعد مع ماده بوليميريه في طاحونه ذات سرعه عاليه وحاده مشابه للتي تستعمل في الطريقه الجافه . ومن ثم يتم خلط المسحوق المنتج مع ماده سطحيه لعمل طين سائل للقيام بترشيحه على أوراق ترشيح لتكوين طبقه مساميه ذات سماكه متجانسه . ثم تدلفن هذه الطبقه في جهاز دلفنه مع شبكه معدنيه . وأخيراً يسخن المنتج في ماده الأسيتون لأزالة ما بقي من المواد السطحيه لأنتاج الأقطاب الغازيه بالشكل النهائي .

لأختبار ودراسة الطريقه الجديده المقترحه تم أختيار النيكل الأسفنجي كعامل مساعد ومادة البوليتترا فلورأيثيلين (PTFE) كماده ماسكه . يستخدم هذا القطب أنود في خلايا الوقود القاعديه . لقد تم تقويم أداء الأقطاب المنتجه بالطريقه المقترحه بأستقطابها جلفنوستا تيكلي حيث وجد أن فرط الجهد في درجات حراره (٢٥ ، ٤٥ ، ٥٥ ، ٦٥ ، ٧٥ درجه مئويه) أقل من تلك المقاسه لأقطاب مماثله تم أستحضارها بالعمليه الجافه . توجد هنالك خمسه عوامل مؤثره في تحضير الأقطاب وهي محتوي PTFE ، وقت السحق ، عملية التبريد أثناء السحق ، مسافة الفسح في عجلات ماكنه الدلفنه ، وإزالة الماده السطحيه من القطب . تم أستخدام الطريقه الرياضيه المسماه العوامل الجزئيه لتحديد أهمية العوامل السابقة الذكر على أداء الأقطاب المنتجه . حيث وجد أن محتوى PTFE ووقت السحق والتأثير المتبادل بينهما هما أهم العناصر المؤثره في تحضير الأقطاب . حيث وجد أيضاً من التجارب المعمليه أن ٨ ٪ من PTFE و٦٠ ثانيه لوقت السحق في وجود التبريد هما الأفضل في أنتاج الأقطاب الغازيه . لقد تم في هذه الدراسه أيضاً تعديل وتطوير النموذج الرياضي للحبيبات الدائريه ومطابقته للنتائج المستحصله للأقطاب الغازيه المستعمله في خلايا الوقود القاعديه . يفترض هذا النموذج الرياضي أن القطب مكون من حبيبات دائريه من المعادن الأسفنجيه و PTFE مملوء بالأكترولييت بينما الغاز يملاء الفجوات الكبيره . بالأضافه إلى تحليل الأنتشار ، والتفاعل داخل الحبيبات في نموذج الحبيبات الدائريه ، أضاف النموذج المطور مقاومه غازيه في الفجوات الكبيره وفرض وجود طبقه من الكترولييت محيطه بالحبيبه . لقد تمت مقارنه النموذج الأصلي والمطور للنتائج المخبريه المستحصله في عملية الأستقطاب لاكسده الهيد روجين بأستعمال أقطاب النيكل على PTFE . لقد وجد أن توقعات النموذج المعدل كانت أقرب للنتائج المخبريه .

كما تم أستعمال النموذج الرياضي المطور لأيجاد كثافة التيار التبادلي ومعامل إنتقال الشحنه وطاقه التنشيط لافضل قطب غازي تم تحضيره بأستخدام طريقة الترشيح . حيث كانت القيم المستحصله على التوالي في درجه حراره ٢٥ درجه مئويه هي ٢٤× ١٠ ميللي أمبير / سم٢ ، ٦٢ر٠ ، ٩ر٧٣ كيلو جول / مول .

درجـــة الدكتوراه

جامعة الملك فهد للبترول والمعادن

الظهران ٣١٢٦١

المملكـه العربيـة السعوديـــه

DISSERTATION ABSTRACT

NAME : SLEEM-UR-RAHMAN
TITLE : Development of Raney-Ni Gas Diffusion Electrodes for Fuel-cells
MAJOR : CHEMICAL ENGINEERING
DATE : AUGUST, 1995

A novel method of preparing the gas diffusion electrodes for fuel-cells is proposed which overcomes the problems of conventional 'Dry Method'. In this method, the catalyst is milled with a polymer binder and a slurry of the milled catalyst is made using a surfactant. This slurry is filtered on a filter paper to give a uniform filter cake. This is rolled with a metallic mesh which works as charge collector. The remaining traces of the surfactant are washed off with boiling solvent to get the final electrode.

To demonstrate, test and study the effectiveness of the method, Raney-Ni catalyst and Polytetrafluoroethylene (PTFE) binder were used to make electrodes. These electrodes were used as anode in an alkaline fuel-cell. The performance tests of galvanostatic polarization at 25, 45, 55, 65 and 75°C showed that the new electrodes performed better.

Five parameters which may affect the performance, namely; PTFE content, milling time, cooling while milling, clearance between the calendars and the removal of the surfactant were considered in the experimental design. The PTFE content, milling time, their interaction and cooling were found significant using a partial factorial design (2^{5-1}). The performance of these electrodes were best at 8% PTFE and milling for 60 seconds while cooling was ON.

The spherical grain model for the performance was modified with the assumptions that the electrode is made of spherical agglomerates of Raney metal and PTFE, flooded with electrolyte, while the gas is occupying the macropores. In addition to the analysis of the diffusion and reaction inside the grains in the spherical grain model, this model includes the resistance of gas diffusion into the macropores and a thin electrolyte film surrounding the grain. The original and modified models were compared with the experimental polarization data of hydrogen oxidation on a Ni/PTFE electrode in KOH. The newly developed model predicts the experimental data very well in all regions. This model was used to obtain exchange current density (i_0), charge transfer coefficient(α) and activation energy (E) for the best electrode prepared by the filtration method. The values of these parameters at 25°C were 24.0×10^{-5} mA/cm^2, 0.62 and 73.9 KJ/mol respectively.

DOCTOR OF PHILOSOPHY DEGREE
KING FAHD UNIVERSITY OF PETROLEUM & MINERALS
Dhahran-31261, Kingdom of Saudi Arabia.

1

Introduction

1.1. Definition of Fuel Cells

A fuel cell is a device that directly converts the chemical energy of reactants (a fuel and an oxidant) into low voltage d.c. electricity. Unlike primary and secondary batteries, this electrochemical conversion does not consume materials that form an integral part of its structure. It rather uses the fuel and oxidant stored outside the cell. Thus a fuel cell is an energy converter only. Since ideally no part of it should undergo any irreversible chemical change, it can continue to operate as long as it is fed with suitable fuel and oxidant and reaction products are removed.

A fuel cell comprises of two electrodes immersed in an electrolyte. Fuel is supplied to the fuel electrode (anode) and oxidant is fed to the oxidant electrode (cathode) as shown in Fig. 1.1 for H_2-O_2 fuel-cell. The electrodes are kept at a distance from each other to provide useful work because this separation prevents direct reaction of the fuel and oxidant which in turn may cause a kind of short circuit with no electricity generation. Simultaneous and separate occurrence of the oxidation of fuel at anode and reduction of oxidant at cathode causes a potential difference that promotes electron flow in the external circuit.

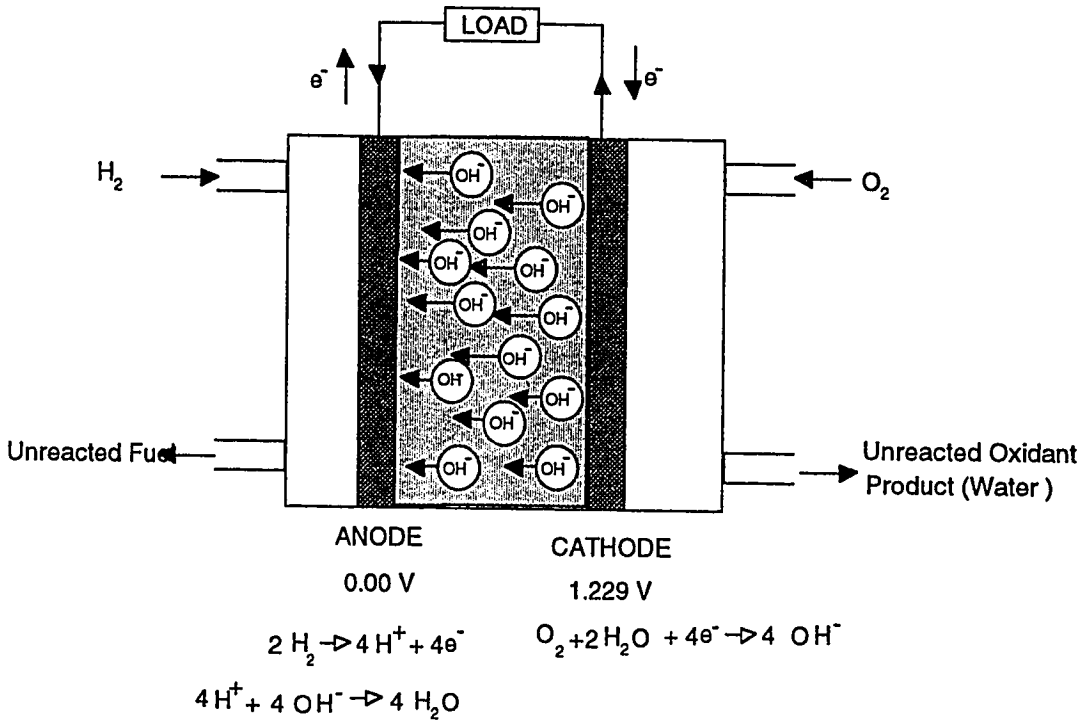

Fig. 1.1 : Schematic of Alkaline Fuel Cell in Operation

Principally any spontaneous chemical reaction could be suitable for a fuel cell but most of the attention has been focused on combustion reactions. Among these, Hydrogen/Oxygen fuel cells are the most popular ones.

1.2. Advantages and Disadvantages

The most prominent advantage of the fuel-cell is that the chemical energy is directly converted into electrical energy avoiding the limitation of Carnot Cycle. This results into higher efficiencies (1). Other main intrinsic advantages are absence of moving parts, low noise levels, high reliability, high power and energy densities with respect to volume, low operating temperatures and low pollution levels (2,3).

Fuel cell power plants have potential benefits of peak shaving, load following and intermediate and base load power generation in electric utility and for industrial applications. Fuel cell plant efficiencies are independent of the rated power above 100kW.

Fuel-cells can be made in variety of sizes, and they are modular. This permits the local power plants at several locations in the grid system to reduce the transmission losses. This advantage is particularly important in congested urban centers where the needed transmission and distribution facilities are expensive to install (4,5).

The fuel-cell power plants have capabilities of waste heat utilization such as space heating, hot water and absorption cooling. The combined effeciency for electricity and heat production can be as high as 90%. Therefore these plants are good for

large industries which need co-generation of electricity and high grade heat.Although fuel cells offer very attractive advantages as cited above there are some disadvantages associated with them which include high initial cost of the system, large weight and volume of gaseous fuel storage, liquefaction expenses of hydrogen gas, cleaning requirements of the fuel and oxidant gases, carbon dioxide degradation of the electrolyte, specific power limitation, and deactivation of precious metal catalyst by sulfur compound and by carbon monoxide.

1.3. Classification of Fuel Cells

The classification of the fuel cells can be done based on electrolyte, electrode, electrocatalyst, temperature and end use (6). Out of these, classification on the basis of electrolyte is the most relevant. This is shown in Table 1.1 (3). Another way of classification on the basis of usage and material of construction is given in Table 1.2.

1.4. Applications of Fuel Cells

The fuel cell was practically used first time in Gemini spacecraft of 1960s. This followed by a chain of spacecrafts with fuel cells including Apollo and Space Shuttle. Their excellent energy output per weight and the fact that the water is the only by-product make them important for space applications. Applications that can best absorb the relatively high capital cost or in which benefits of using the fuel cells compensate the high initial cost will be most likely, the most practical in future. Table 1.3 lists their potential applications together with their relative importance (7).

Table 1.1 : Classification of Fuel Cells on the Basis of Electrolyte (5)

	Alkaline Fuel Cell (AFC)	Phosphoric Acid Fuel-Cell (PAFC)	Solid Oxide Fuel Cell (SFC)	Solid Polymer Electrolyte Fuel Cell	Molten Carbonate Fuel Cell
Electrolyte	NaOH or KOH	o-Phosphoric Acid	Ion-conducting oxides(ZrOwithYO)	Ion-Conducting Membrane	KLiC (Molten)
Fuel	Pure H_2	H_2 and CO	H_2 and CO	Pure H_2	H_2 and CO
Operating Temperature	<100 °C	<200 °C	800-1000 °C	<100 °C	~800 °C
Electrode Material	Metal or Carbon	Carbon	Ceramics	Carbon	Metal-based
Configuration	Mono/bipolar	Bipolar	Mono/bipolar	Mono/bipolar	Bipolar

Table 1.2 : Classification of Fuel cell (5)

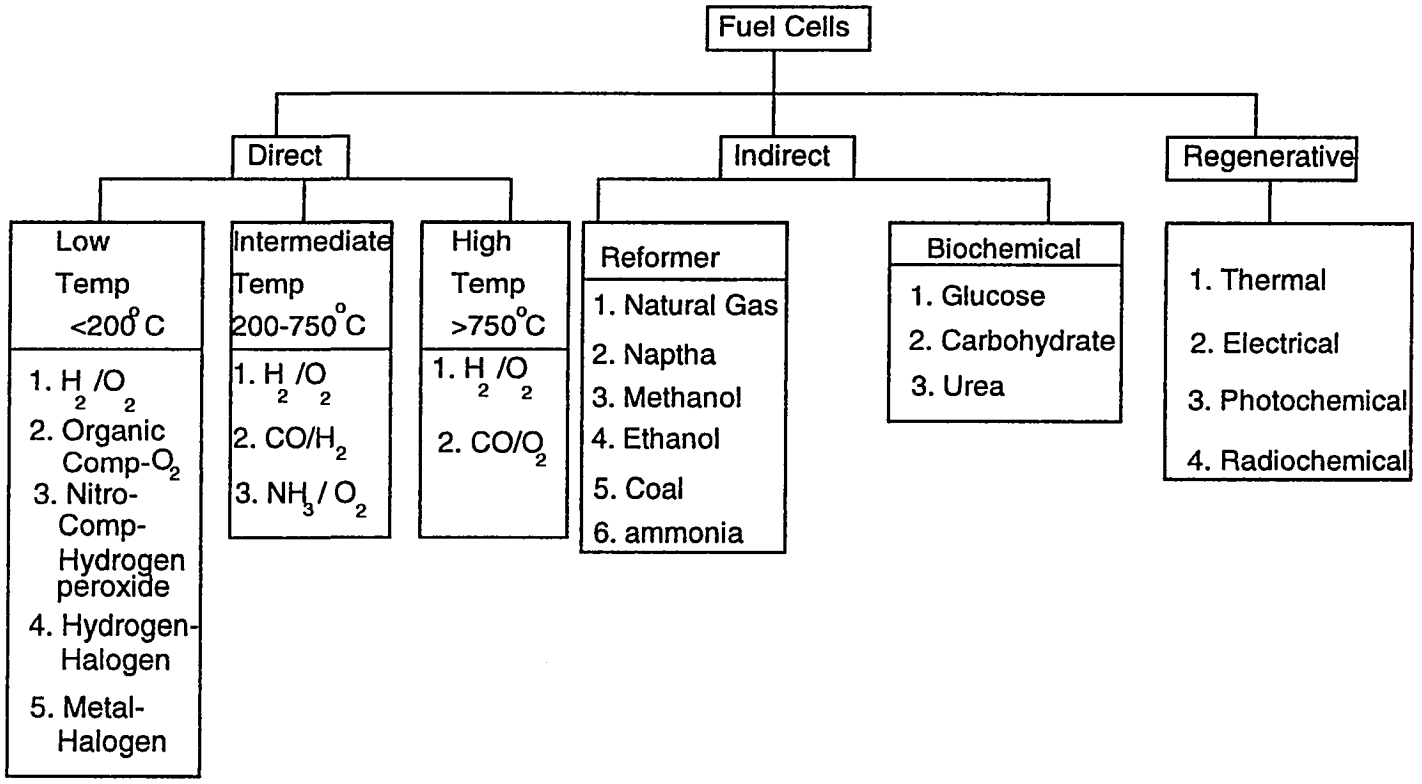

Table 1.3 : Potential Fuel Cell applications (5)

Application		Efficiency		Emission/Noise		Cost
		Weight/Volume	Fuel Cost	Environmental	Detectibality	
Remote	Space	2	3	3	3	3
	Submarine	1-2	2	3	2	2-3
Portable	Military	1-2	3	3	2	2-3
	Recreational	3	2	3	3	1
Utility	Small(<1 MW)	3	2	2	3	1-2
	Large	3	2	2	3	2
Other	Emergency	3	3	2	3	1
	Transportation	1	2	2	3	1

Where : 1= Very Important, difficult to achieve targets.
2= Very important, targets achievable.
3= Relatively unimportant (compared with other requirements)

Remote power applications include submarine, navigation aids, automatic weather stations, remote beacons, pipeline cathodic protection and communication etc. As portable power generation they compete with diesel engines. Their reliability, system weight, fuel efficiency and nondetectability give them upper hand in military usage.

Utility is another important area where fuel cells are being used. These applications can be classified into the following three categories :

a: On-site power plant requiring 40-400kW

b: Electric Power Plants (5-50 MW)

c: Electric Power Plants (100-500 MW)

Transportation is among the attractive applications of fuel cells. But commercially successful fuel cell based transportation systems demand inexpensive fuel cells. Table 1.4 shows threshold capital cost for different applications. This suggests the easy commercial uses will involve electric utility, on site and cogeneration units (7).

1.5. H_2/O_2 Alkaline Fuel Cells

Among the low temperature H_2/O_2 fuel cells alkaline fuel cells with KOH and acidic fuel cells with phosphoric acid are the most important. Alkaline fuel cells have several advantages over the acidic ones. Among these are better cathode performance, lower cost of material of construction and lesser corrosion. One of their major problems is formation of carbonates with carbon dioxide impurity in the fuel or oxidant (8). Although there are not much cost data available, alkaline

Table 1.4 : Threshold Capital Values for different Fuel cell Applications (5)

Applications	Threshold Cost (1984 $ per kW installed)
Space	>10,000
Military	4,000
Utility Small (<1MW)	2,000*
Utility Large	1,500*
Emergency Power	1,000
Transportation	100

* Includes industrial cogeneration.

fuel cells are considered more beneficial for low temperature applications (9). In this study attention is focused on alkaline H_2/O_2 cell with KOH as electrolyte.

A typical H_2/O_2 fuel cell operation and conventions are shown in Fig. 1.1. At the anode, hydrogen is oxidized to form water and simultaneously at the cathode, oxygen is reduced to form hydroxyl ions. Electrons are released in the process and they flow in the external circuit. The charge transfer takes place through the electrolyte by hydroxyl ions. The electrode reactions and the overall reaction of this process are as follows :

Anodic Reaction $H_2(g) + 2OH^-(aq) \longleftrightarrow 2H_2O + 2e$

Cathodic Reaction $\frac{1}{2}O_2(g) + H_2O(l) + 2e^- \longleftrightarrow 2OH^-(aq)$

Overall Reaction $H_2(g) + O_{2(g)} \longrightarrow H_2O$

$\Delta G° = -56.7$ kcal

$\Delta H° = -68.3$ kcal

$E° = 1.229$ V

If non-porous planer electrode is used in a fuel-cell using gaseous reactants, the current densities produced are of the order of micro to milliamperes per square centimeter. These values are too small to be used in a practical fuel-cell system. This neccecciates the use of porous electrodes. A good electrode structure must be able to bring gas and electrolyte together so that the reaction can be easy and rapid and must be able to keep them apart to prevent undesirable mass-transfer such as

bubbling, floating or weeping. This is another reason why enlarged surface area and porous structure are required for gas diffusion electrodes.

1.6 Electrode kinetics and Modes of Polarization

The passage of electric current through a fuel-cell changes the potential of the elctrode. This phenomenon is known as polarization. The difference between the potential at a particular current density and the open circuit potential is the overpotential of an electrode. In a fuel-cell the working potential is lesser than the rest potential. A typical polarization curve is shown in Fig. 1.2 for hydrogen-oxygen fuel-cell. This concept is elucidated in this figure. It is evident that the overpotential is a measure of total losses occuring in the different processes in the fuel-cell. Therefore a polarization curve is an index of the performance of the electrodes and the cells. Smaller overpotential at a given current density indicate more effecient electrode. The overall overptential of a cell is a result of a number of processes occuring in the fuel-cell. There can be losses in different locations.

1.7. Methods and techniques for Fuel-cell studies

A complete fuel-cell is used for initial screening for life testing by studying the performance of fuel and oxidant electrodes over extended periods of time. On the other hand, using a half-cell, the reaction on each electrodes can be studied separately. In this case it is necessary to supply current from an external source. The overall reaction taking place in this half cell is not the same as that occuring in the complete cell. A schamatic diagram for the operation of a half cell is shown in Fig. 1.3. The cell is provided with a reference electrode and a counter electrode besides a working electrode assembly which comprises the electrode to be studied. The half cell is placed in a thermostated bath. It is also possible to measure IR-free

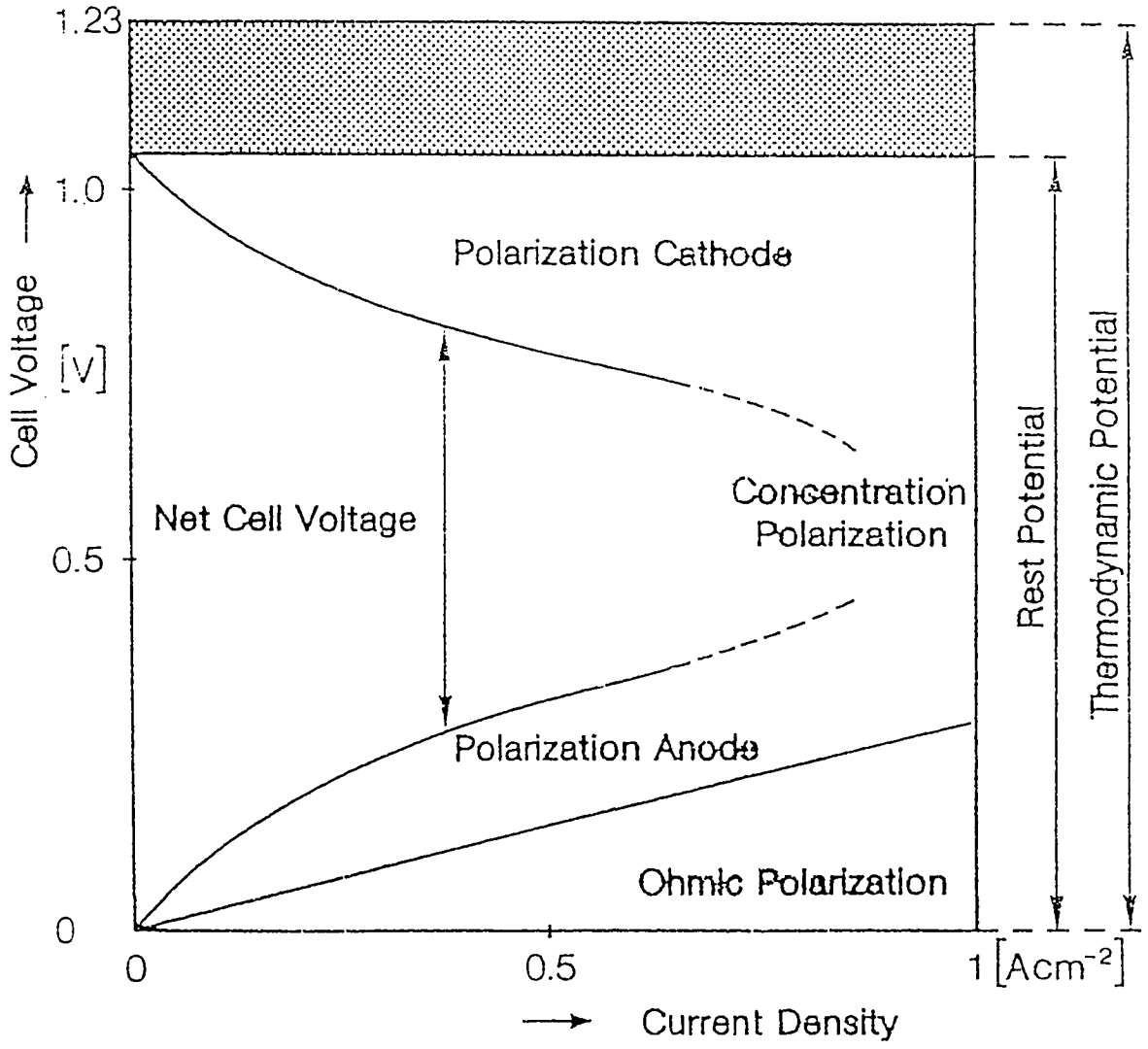

Fig. 1.2 : A Typical Hydrogen-Oxygen Fuel-cell Polarization curve

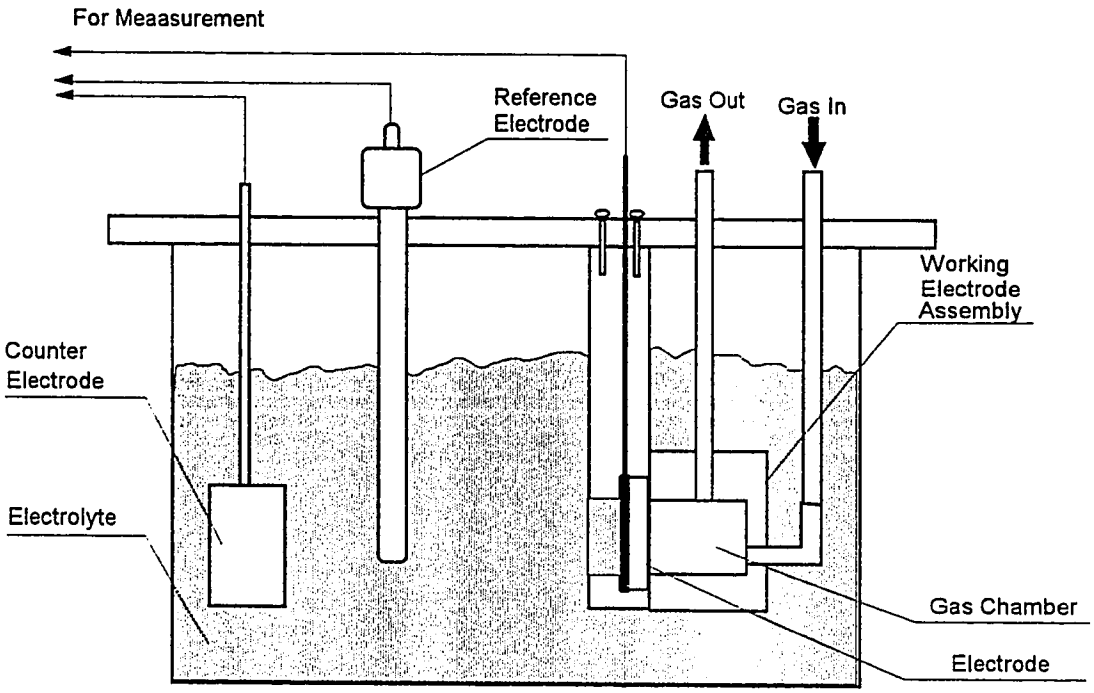

Fig. 1.3 :Schematic Diagram of the Half Cell Assembly

potential of the electrode using current interruption or positive feedback techniques. In this work , the experiments are carried out using a half cell and the IR-drop was estimated using current interruption technique.

1.8. Objectives of This Study

The objectives of this study can be divided into two parts; experimental and theoretical. The first part which is experimental comprises of the preparation of gas diffusion electrodes for fuel-cells, their characterization and performance testing. Study of the effect of different parameters on the performance is also included. The second part consists of development of a mathematical model for the performance of the gas diffusion electrodes. These objectives are discussed in greater details in the forthcoming sections.

1.8.1. Experimental Objectives

The PTFE bonded Raney-Ni electrodes are produced by recently developed dry method proposed by A. Winsel (10). This method involves reactive mixing of PTFE with catalyst. The resulting fluffy powder has to be rolled into a horizontal pair of calenders. This requires not only the precision in composition and mixing parameters but the preparation depends on the way powder flows in the funnel supplying catalyst to the calender rolls. It is difficult to control the flow rate of the powder. Even the slightest variation in the flow rate of powder will result into uneven electrode. This eventually results into poor performance. One objective of this work is to develop a method which obviates these shortcomings of the dry method. A method called "Filtration Method" is proposed in this work. It is described in detail in Chapter 3.

There are number of parameters which may affect the performance of the electrodes made by the newly developed method. There are a variety of statistical methods for designing the experiments which help in deciding the significantly important parameters. A partial factorial design is to be used for this purpose.

The parameters found significant by the use of partial factorial design are to be varied to study the effect of these parameters on the polarization and to optimize the electrode performance.

The polarization curves of the optimum electrode is to be obtained at different temperature in the range of 25-75 °C. The electrode is to be tested for long period of time.

The optimum electrode is to be characterized using various techniques. This is done to obtain parameters for the mathematical model and to establish the structure-function relationship. The techniques to be used are :

BET surface area.
Mercury Intrusion Porosimetery
Scanning Electron Microscope
X-ray Diffraction
EDS

The Raney-Ni, after leaching, has to be passivated to remove the pyrophoricity of the catalyst. It is conventionally done by drying the catalyst in the vacuum and reacting the dried mass with small doses of oxygen. This method required precise detection and control of oxygen and temperature. Any accidental overdose of

oxygen may result into catalyst sintering. To avoid this situation a more reliable method is to be developed.

1.8.2. Theoretical Objectives

A mathematical model was developed by Celiker et al. (11) based on the hypothesis of spherical grains of Raney Ni-PTFE catalyst. This model failed to predict polarization behavior at higher overpotential and to show the limiting current. This was due to the omission of mass transfer resistances. This model is modified by incorporating the macropore resistance. In addition, it is proposed that there exist a thin film of electrolyte on the surface of each spherical grain. The reactant gas which is present in the macropores has to diffuse into this film before reaching the catalyst. The resistance offered in this diffusion process is also taken care of. The results of this model is compared with that of the previous model and experimental data. The model is discussed in Chapter 7.

References

1. Lindstorm, O., *Chemtech*, August, 490 (1988).

2. Kordesch, K., *Hydrogen Energy Progress VI*, 1201 (1984).

3. Tilak, B.V., R.S. Yeo and S. Srinivasan, *Comprehensive Treatise of Electrochemistry, Plenum Press*, **3**, 39 (1981).

4. Printice, G., *Chemtech*, Aug., 490 (1988).

5. Srinivasan, S., Journal of the Electrochemical Society, 136, No. 2, 41c-48c (1977).

6. Sandstede, G., *From Electrocatalysis to Fuel Cells* , Battelte Research Center and the University of Washington Press (1972).

7. Fickell, A.P., *Encyclopedia of Physical Sciences*, 5,626 (1987).

8. Thallar, L.H., R.E.Martin and J.K. Stedman, *2nd Annual IECEC Conference*, Philadelphia (1987).

9.Kordesch, K., *International Journal of Hydrogen Energy*, 8,9,709 (1983).

10. Winsel, A., O. Fuhrer, K. Ruthling and C. Fischer, *Ber. Bunsenges. Phys. Chem.*, 94,926 (1990).

11. Celiker, H., M.A.Al-Saleh, S.Gultekin and A.S.Al-Zakri, *Journal of the Electrochemical Society*, **138**, 6, 1991.

2

Literature Review

2.1. Introduction

In this chapter available fuel-cell literature has been reviewed. The attention is focused on the electrocatalysts, electrodes, electrode preparation techniques and the mathematical models for their performance.

2.2. Electrocatalysts

2.2.1. Requirements of the Fuel-cell Electrocatalysts

A fuel-cell electrocatalyst should posses electronic conductivity, should be stable in the fuel-cell environment, and should display suitable adsorption characteristics for reactants and/or reaction intermediates. A primary requirement of any electrocatalyst is the stability in the operating environment. For this reason, corrosion testing always comprises the first step in the screening process for a candidate electrocatalyst. Corrosion testing usually begins with simple immersion of material in the electrolyte at fuel-cell operating temperature in the presence of the reactant. It is followed by potentiostatic testing in the absence of reactants. Finally long term tests are performed under actual fuel-cell operating conditions. An electrocatalyst must be significantly active. The evaluation of the electrochemical activity is usually done by evaluating the polarization curve for the reaction in the

electrolyte of interest on the desired electrocatalyst of well defined composition and surface area. The exchange current density is estimated by extrapolation back to the reversible potential.

To function correctly, an electrocatalytic particle in the porous electrode must be located at a site of electron exchange between the reactants and the products, and must serve as a conduction path way for electrons to current collectors. If the electrocatalyst is a poor conductor or a semi-conductor, it must be supported or dispersed within a conducting material.

2.2.2. Hydrogen Oxidation Electrocatalysts

The reaction kinetics, mechanism, and modes of electrocatalysis for the hydrogen oxidation reaction are known in considerable details (1,2). The hydrogen oxidation is rapid compared with that for oxygen reduction because it involves only breaking of one single bond, along with two electron transfer steps per molecule. In contrast, oxygen reduction requires the breaking of a double bond and four combined electron-atom transfer steps. In oxygen reduction there is evidence that reaction intermediates are irreversibly adsorbed because of the affinity of the substrate catalytic species to form a very stable covalent product. In contrast, the hydrogen intermediates are much more reversibly adsorbed, making the desorption step much easier.

A. Noble Metal Electrocatalysts

Among the metals that are able to withstand the corrosive conditions in the electrolytes at the appropriate hydrogen potentials, platinum is generally considered to be the most effective electrocatalysts for hydrogen oxidation. Other stable noble metals are platinum group metals (gold, silver and

mercury), all of which are thermodynamically stable to practical hydrogen electrode potentials. (3). The relative activities for hydrogen reaction in acid electrolyte on clean catalyst surfaces descend in the order:

Platinum, Rhodium> Palladium > Ruthenium >> Gold, WCx (4)

On platinum the gross exchange current density is about 140 mA/cm^2 at 160°C in phosphoric acid and the limiting current is 10 A/cm^2. This shows remarkable polarization of just 5mV per 100 mA / cm^2 in practical fuel cells (5). Due to these reasons the platinum is the prime choice as anode catalyst. Although not entirely unique in its properties as electrocatalyst, platinum does have a combination of properties that promotes electrocatalytic properties. Its vacant d-orbitals are such that the metal-reactant bond is neither too strong in which case the reaction products would be unable to desorb, nor too weak which would saturate the surface with intermediates preventing further adsorption of reactants. Under anode reaction conditions platinum does not form oxide layer which would reduce rates for hydrogen activation by blocking sites (6) as they do for oxygen reduction. Platinum has both a good affinity for adsorption of hydrogen atoms, as well as high surface diffusion coefficients (7). In the light of these facts, it can be concluded that although the individual electrocatalytic modalities of platinum are not unique, but they are fortuitously combined in a single material. This has spurred the research for the search of equivalent electrocatalyst. Other noble materials have occasionally been alloyed with platinum for hydrogen reduction. But in general, these metals are not used alone for this purpose.

B. Nickel Electrocatalysts

Although the pure nickel is about three orders of a magnitude less active than platinum for hydrogen electrode processes, it is preferred due to its low cost. The activity can approach to that of noble metals by the use of highest surface area Raney Nickel. Nickel is thermodynamically stable as bulk metal to +110mV/SHE at pH 14 and 25°C, where as at pH 0 its domain of stability is -550 mV / SHE (3). This permits its use only in alkaline media. In alkaline media, a reduced nickel oxide layer, probably consisting of $Ni(OH)_2$ forms on the metal surface. This layer is capable of adsorbing hydrogen.(8).This is the reason why the surface-oxidized nickel is found more active electrocatalytically than the bare nickel. This may be due to an increase in the roughness of the surface on the reduction of oxidized surface.

Sintered nickel alone has been used as an electrocatalyst in alkaline Bacon cell(9) and in molten carbonate fuel-cells. The activity or stability of nickel catalyst is reported to be improved by doping with noble metals (Pt or Pd), cadmium or lead(10), copper or vanadium, addition of transition metal salts of titanium, maganese, zirconium, vanadium, chromium, tungsten, cobalt and copper to porous nickel hydrogen anodes. The improvement in activity can also be obtained by alloying iron, titanium or molybdenum(7).

C. Miscellaneous Electrocatalysts

Following substances have also been reported to work as electrocatalyst in hydrogen reduction :

Nickel Boride (11,12,13,14)

Mixed Metals

$LnM_{4.5\text{-}5.5}$ [where ln= La or Sm, M=Ni,Co]

$M_xMn_{3-x}O4$ [where M=Cu,Ni or Ag, x=1-5]

Cu_2Ni_{1-z}, Mn_2O_4 [$z \leq 0.7$]

XY_2O_4 [X=Fe, Zn, Mn, Co, Mg, Cd, Cu and Y=Fe, Cr, Mn, Ni or Co]

Tungsten Catalysts

Sodium Tungsten Bronzes (15)

Tungsten Oxide (16)

Tungsten Carbide (17,18)

2.2.3. Mechanism of Oxygen Reduction

Oxygen reduction is considered to proceed by the following two pathways:

a: Direct four-electron pathways

Alkaline solutions:

$$O_2 + 2H_2O + 4e^- \rightarrow 4OH^-$$

Acid solutions:

$$O_2 + 4H^+ + 4e^- \rightarrow 2H_2O$$

B: Peroxide Pathways

Alkaline solutions:

$$O_2 + H_2O + 2e^- \rightarrow HO_2^- + OH^-$$

followed by either of these

$$HO_2^- + H_2O + 2e^- \rightarrow 3OH^-$$

$$2HO_2^- \rightarrow 2OH^- + O_2$$

Acidic solutions:

$$O_2 + 2H^+ + 2e^- \rightarrow H_2O_2$$

followed by either of these

$$H_2O_2 + 2H^+ + 2e^- \rightarrow 2H_2O$$

$$2H_2O_2 \rightarrow 2H_2O + O_2$$

The extent to which each of these pathways is involved at a particular electrode surface is usually established with the rotating ring-disc electrode technique. While reducing through the two electron pathway, peroxyl ions may reach high concentration near the electrode. This limits the electrode current density due to the larger polarization because of the ion layer. Therefore two electron pathway is not desired in the fuel cell electrode reactions. According to the mechanism the electrode materials (electrocatalysts) can be divided into two categories (19).

Category I : Reduction predominantly through peroxide pathway

a. Graphite and most of the carbons

b. Metals : Gold, Mercury and most of the oxide covered metals.

c. Oxides: Most of the transition metal oxides

d. Transition metal macrocycles

Category II : Reduction through 4 Electron pathway

a. Platinum, Platinum alloys, platinum family metals

b. Other metals : Silver, palladium

c. Oxides : some Perovskites, pyrochlores

d. Some transition metal macrocycles.

2.2.4. Electrocatalysts for Oxygen Reduction

A. Carbon Materials

The carbon materials have been used by many researchers lately for the manufacturing of the oxygen reducing cathodes (20), although their use in the oxygen or air cells with zinc as negative electrode was established already in the primary battery industry (21). Various research groups are involved in the

improvement of the carbon electrodes. Variety of manufacturing techniques and electrocatalysts have thus come forth. Although carbon does not have transition metal character, it fulfills the first four requirements for a good electrocatalyst. Reduction proceeds principally through the peroxide pathway. However peroxide activity can be depressed by loading some other catalysts on carbon. Exact mechanism in the presence of carbon is not yet clearly understood. It involves the interaction of oxygen with the functional group at the surface of carbon. Lamp black, heat treated acetylene black and furnace black are few examples of carbon materials that have been used (19). In a recent study coconut shell charcoal has been tried (22). It is reported to show better performance than any other carbon. Electrodes made with this material gave 500-2000 A/m^2 current densities for 200 hours. When loaded with Pt current densities were 2000-5200 A/m^2 for 1200 hours. Performance was even better when Pt bimetals were used. Pretreatment with steam and NH_3 enhanced the performance further. After the discovery of the use of Organometals for oxygen reduction, Organometals were also used as loading material (22,23,24,25,26).

B. Pt and Pt-Alloys

Due to their high electrocatalytic activity, high stability and electronic conductivity Pt and Pt alloys are indubitably the best commercial materials for oxygen cathodes. Reduction on their surfaces proceeds through desirable four-electron pathway. A number of Pt alloys have been used. These are chronologically mentioned in Table 2.1.

Table 2.1. : Pt and Pt alloys used for oxygen reduction

Alloy	Year	Author	Remarks
Pt	1975	Kunz,R. & Gruver,G.(27)	United Technology
Pt-Ti Pt-V Pt-Mn	1977	Jalan, V.M. Landsman, D.A. (28)	United Technology
Pt-V Pt-Mo	1980	Jalan, V.M.(29)	United Technology
Pt-Cr	1982	Landsman, D.A. Luczak, F.S.(30)	United Technology
Pt-Cr-Co	1984	Luczak, F.J. Landsman, D.A(31).	Alloy is in ternary phase United Technology
Pt-Ti	1986	Beard, B. Ross, P. (32)	Impregnation of TiO_2 on Pt-C
Pt-Cr	1986	Paffett, M. Bens, J. Gottesfielg, C. (33)	United Technology
Pt-Co	1990	Bruce, C. Ross, P. (34)	Pt-Co in ordered phase

C. Silver

Reduction on silver goes through the 4 electron pathway. It can only be used in alkaline media. Silver is also being used as Raney silver with carbon. It has very good activity but it suffers from poor stability and shorter lives (35). Following materials have been doped with silver resulting into better performance:gold, zinc, mercury and nickel.

D. Transition Metal Complexes

In the effort of finding out cheaper substitutes of Pt and other costly metals, macrocyclic chelates have been extensively studied. Several Phthalocynines and Porphrines of transition metals were reported to be active. These compounds are in liquid form and are used in homogeneous catalytic reduction reactions. When used in electrode manufacturing they are mostly heterogenized over the surface of a suitable high surface area material e.g. active carbon.

Vasudevan et al (24) have tried cobalt Phthalocynines with following groups

- Imido
- Carboxyl
- Co[bis(3,4) phthalimido carbonyl] phthalacynine
- Co [bis(3,4) dicarboxy benzonyl]phthlocynine
- NN'diphenyl Co [bis(3,4) dicarboxyl benzonyl] phthalocynine diimides

Shukla (26) reported that the activities of the phthalacynines(Pc) and Porphrines (PP) are as follows

$$Fe\ Pc > Co\ Pc \sim Co\ T\ PP > Ni\ Pc >> Mn\ Pc \sim C$$

Kirchenmann et al (36) studied porphrines of Fe and Co with several substituted groups. They reported following order of the activities:

a: Fe PP

$CN > -H > -NH_2 > -OCH_3 > -NO_2 > -N(CH_3)_2 > -COOH$

b: Co PP

$-CN > -COOH > -N(CH_3)_2 > -H > -NO_2 > -OCH_3 > -NH_2$

Kivisaari et al (37) found CoTMPP (Cobalt tetramethyl porphirine) to be an excellent electrocatalyst.

E. Bulk Doped Organometals

Macrocycles of transition metals are usually doped over the surface of a high surface area conducting material e.g. carbon. The disadvantage in this practice is that only a few monolayers are responsible for catalytic activity. It was proposed that if transition metal and the coordinated ligands are dispersed throughout the bulk of the conducting material, the performance will be better. This can be achieved by two methods. First method involves the introduction of metal and nitrogen into cationic exchange resin. This can either be done by exchanging a transition metal and NH_4OH or by chelation compounds. In the second method, gas phase precursors are mixed in a reactor and pyrolyzed to form the catalyst. For example : $C_2H_2 + NH_3 + Fe$ containing organometals are mixed and pyrolyzed(38).

F. Perovskites and other Oxides.

Perovskites are metal oxides with general formula ABO_3. They are active electrocatalyst. But their activity drops very fast (39). Shimuzu (40) studied

various Co and Mn pervoskites. For various values of x, $La_{1-x}Ca_xMO_3$ with M=Co or Mn are reported to be active. Anderson et al. studied lead pyrochlores. They claimed that this material was better than Pt-Au catalyst used in NASA fuel cells (41).

2.3. Fuel Cell Electrodes

2.3.1. Historical Background

The concept of fuel cell was discovered by W.R.Grove in 1839 (42). Besides this remarkable invention he observed that the electrochemical reaction takes place at the junction of three phases, namely; the electrode, the electrolyte and the reactant gas. In his own words *"As the chemical or catalytic action .....could only be supposed to take place with ordinary platina foil, at the line or water mark where the liquid, gas and platina met, the chief difficulty was to obtain anything like a notable surface of action."* (43). The difficulty in achieving this notable surface of action is the major challenge in the manufacturing of fuel cell electrodes.

Grove's work was advanced by L. Mond and C. Langer in 1889 (44) with the use of porous matrix filled with electrode. The electrodes were made of platinum black and platinum powder. These electrodes were fixed on both sides of the porous diaphragm of non conducting material which was saturated with the electrolyte. This was able to provide about 3.6 mA/cm^2 at 0.73 volt. F Haber and coworkers in 1905 (45) used fuel cell with solid electrolyte (fused glass). The platinum and gold electrodes were fixed on both sides of this fused glass electrolyte. This experiment showed that reversible potential can be achieved with very low currents. Baur, Treadwell and

Trumpler (46) used porous magnesia to hold the electrolyte. The term 'Gas Diffusion electrode' was given by Alferd Scimid(47) who systematically and successfully investigated them. Although these electrodes were not fuel cell electrodes, the concept of diffusing gas was important. He developed cylindrical porous graphite electrodes with a porous layer of electrodeposited platinum at the outer surface, hydrogen entering through a concentric cylindrical boring that terminated at the proper distance above the bottom of the electrode. The pores of the platinum layer were smaller than that of the graphite, thus providing dual layer and dual porosity electrode. Here graphite layer worked as gas diffusion layer. One another way of achieving surface of action was proposed by Tobler(48). The electrode is a mass of granulated graphite in which the grains are in intimate contact with a central current collector, are bathed in electrolyte, and are retained by a cylindrical cotton stocking. The gas enters through the fritted glass in the bottom.

2.3.2. Single Layer Homoporous Electrode

The applicability of Raney Nickel for hydrogen electrode was established long back in 1938 by Traus and Aubry(49). They discovered that the hydrogen potential is established reversibly at Raney Ni in alkaline solutions. A mechanically strong electrode can not, however, be made from the Raney Ni powder by pressing, sintering and finally dissolving out the aluminum with warm alkali. The single layer Justi electrodes (50) were first to solve this problem. This electrode was known as DSK (Doppeleskelett Katalysator) electrode. This means that the electrode has a skeleton which provides strength and electrical conductivity and a second skeleton is an electrocatalyst. In these electrodes carbonyl nickel served as first skeleton while Raney Ni worked as electrocatalyst.

2.3.3. Variants of DSK Electrodes

A. DSK electrodes from platinum metals

Raney alloy of platinum, palladium, rhodium (Pt-Al, Pd-Al, Rh-Al) is prepared and ground to grain size of 25-40 μ. This powder is blended with noble metal powder to give supporting skeleton. Sodium chloride is added to form macropores. This blend is pressed at 10 ton/cm^2 into discs of 12 mm diameter. Unlike Justi electrodes this electrode is not sintered. These electrodes were able to produce 300 mA/cm^2 in KOH (51).

B. Triple Layered Electrodes

Burshtein et al. (49) developed a triple layered electrode in which active layer of skeleton nickel is sandwiched between two inactive layers of carbonyl nickel (coarse-pored supporting layer and fine pored surface layer). The active layer was made of Raney-Ni-Ti alloy by pulverizing and dissolving aluminum. Addition of titanium stabilizes the skeleton structure and makes the active layer non pyrophoric.

C. Non pyrophoric Electrodes

(i) Electrodes by Dousek, Jansta and Riha (52)

This group proposed a method of preparing non pyrophoric nickel catalyst. In this method the adsorbed hydrogen is removed before the catalyst is dried. This is carried out under mild conditions either by neutralization of alkali with tartaric acid followed by desorption of hydrogen in distilled water at 90°C, or by reaction of hydrogen with oxygen. The non pyrophoric nickel powder obtained in this way is used to make double layered electrodes. At 90°C these electrodes extended 500mA/m^2 at an overvoltage of 50mV.

(ii) Electrodes by Jung and vanDohren (53)

The aluminum from the catalyst alloy is removed with plenty of KOH solution. The washing with distilled water is done till neutrality is achieved. The adsorbed hydrogen is removed by oxidizing quantitatively with KIO_3, $KBrO_3$ or $KClO_3$. The catalyst is washed completely. These electrodes have three layers which are : a fine-pored layer of Mond nickel powder, a working layer of a mixture of pre-activated Raney-nickel and Mond-nickel powder with sodium carbonate as filler and a gas diffusing layer of Mond-nickel with potassium chloride filler. In order to make electrode, these layers are hot pressed at 450°C and 0.5 ton/cm^2. It is observed that the activity of the electrode is enhanced by addition of 0.1 to 0.5 % of promoter metal e.g. platinum and copper.

(iii) Electrodes by Brown and Bovery (54)

This is another variant of Justi single layer electrode. The nickel and aluminum are mixed, pressed hot or cold and sintered just like any other Justi variant. The major difference is the method of achieving non-pyrophoric character. It is done by impregnation. Impregnation is not discussed very well in the literature.

2.3.4. MSK-Electrode (55)

The catalytic activity of the skeleton nickel electrode depends strongly on its dispersed surface structure rather than on its method of preparation. Mono skeleton nickel (MSK) electrodes are prepared with only one kind of nickel skeleton (powder). This is done by mixing powdered nickel and aluminum, pressing and sintering and finally dissolving out aluminum with alkali.

2.3.5. Electrodes on Plastic Supports

The major problem of hydrodynamic unstability of Justi electrode was answered by Shell electrodes (56) which used porous plastic materials as supports. The porous plastic materials like porvic were used. Porvic is a commercial polyvinyl chloride sheet having uniform pores. In order to make electrodes, a thin electrically conducting film of gold or silver is evaporated into the pores of plastic sheet. Thus obtained metallic layer is thickened by electrodiposition. In this way 0.1 -2 μ thick film of gold or silver is anchored in the pores of the plastic material. The electrocatalyst is placed over this film by spraying or electrodiposition. The properties of a typical sheet electrode is shown in Table 2.2.

2.3.6 Controlled Wetting Electrodes

A. The General Electric Electrode

Controlled wetting is one of the best solution to the hydrodynamic unstability of the electrodes. In the General Electric electrodes (57), it is done by using a hydrophobic material on the gas side of the electrode. A cross-sectional micrograph is shown in Fig. 2.1. A thin layer of porous Teflon on the gas side provides hydrophobicity. The procedure of making these electrodes is as follows : A slurry of electrocatalyst with an aqueous suspension of duPont PTFE T-30 is sprayed on an aluminum foil. This is dried to form a thin film. A hydrophobic film to be used on the gas side is made by spraying T-30 on another aluminum foil. The supporting screen is placed in contact with the two layers to form a sandwich that is hot pressed (350°C) at 2000-4000psi for 2-5 minutes. The aluminum foil is dissolved away with alkali and the resultant electrode is washed repetitively with distilled water. These electrodes are versatile. They accommodate various electrocatalysts and are

Table 2.2 : Properties of a Typical Shell Electrode (56)

	Overall thickness (cm)	0.077
Metal Layer	Material	Ag or Au + Pd or Pt
	Thickness(μ)	3-4
	Porosity	50
	Pore diameter (μ)	3-4
	Number of pores/cm^2	~ $1.3X10^6$
Plastic Layer	Material	Porvic M
	Thickness(cm)	o.o76
	Porosity	85
	Pore diameter (μ)	3-4
	Number of pores/cm^2	~ $2.2X10^6$

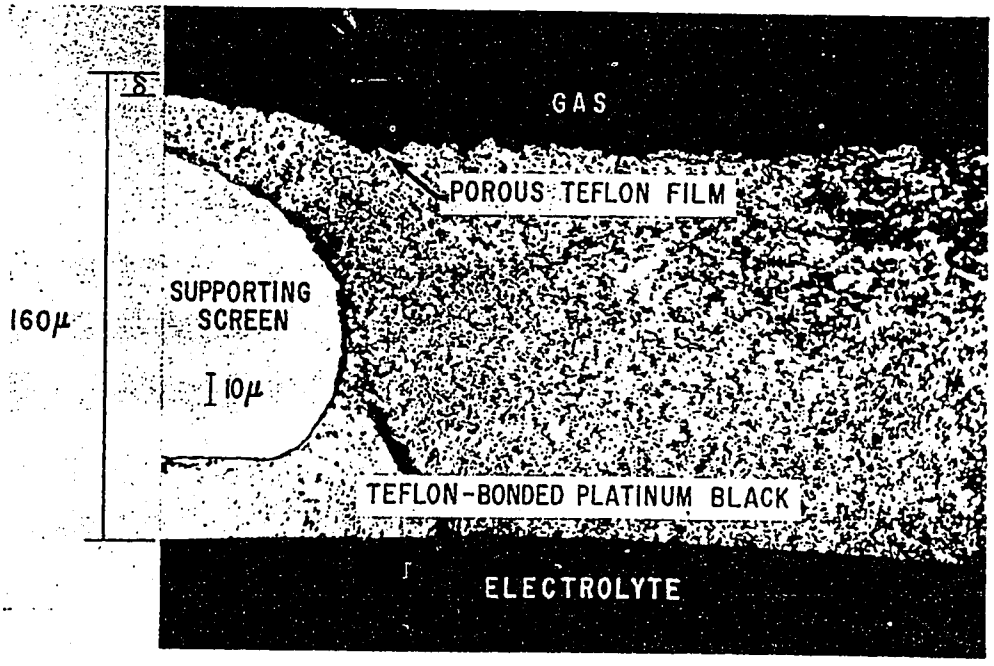

Fig. 2.1 : Photomicrograph of a General Electric Electrode (57)

suitable for operation in acid or alkaline solutions. Properties of a typical General Electric electrode is shown in Table 2.3.

B. The Union Carbide Electrode

These are thin carbon electrodes. Although the carbon electrodes have been manufactured for long time, the major contribution was in 1964 by Kordecsh et al.(58). A typical cross section is shown in Fig. 2.2. This electrode has three layers. The active layer which will be in contact with the electrolyte, is made of active carbon. This carbon is activated by addition of electrocatalyst. In this layer a hydrophobic material (polyethylene) is also added. The quantity of polyethylene is 20 %. This amount is reduced to 4-10 % in other layers. The bottom layer is the porous nickel sheet. The properties of a typical electrode is given in Table 2.4.

2.3.7. Dual Layer and Dual Porosity Electrodes

Dual layer and dual porosity electrodes due to Bacon (59) is one of the milestone in the history of the fuel cell electrodes. The hydrodynamic stability and objectionable mass transfer were taken care of by using two layers of different mean pore size. The fine pores filled with electrolyte act as a seal for the gas. The coarser layer of the electrode is prepared from carbonyl nickel powder (2-3 μ) with 20 % of ammonium carbonate as spacer. This mixture is lightly pressed and sintered for 30 minutes. The fine layer on one side of this layer is made by applying a suspension of Grade A carbonyl nickel (4-5 μ). The electrode is sintered again at 800°C. The properties of a typical Bacon electrode is shown in Table 2.5 (54).

Table 2.3 : Properties of a Typical General Electric Electrode (57)

	Overall thickness	0.012-0.030
PTFE Film	Thickness (cm)	0.1-10
	Particle diameter (μ)	0.2-0.5
	Porosity (%)	40-60
	Pore diameter (μ)	0.01-1.0
	Number of pores/cm^2	2X10^8
Electrocatalyst Layer	Thickness (cm)	0.01-0.03
	Diameter of Pt particles (μ)	0.01
	Diametyer of PTFE particles (μ)	0.2-0.5
	Porosity (%)	40-60
	Pore diameter (μ)	0.1-1.0
	Number of pores/cm^2	2X10^8
Support Screen	Material	Pt, Ag, Ni etc.
	Wire diameter (cm)	0.007-0.020
	Mesh (wires/inch)	40-80

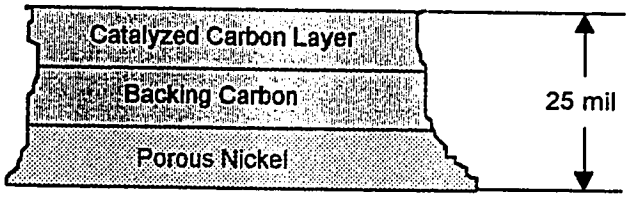

Fig. 2.2 : Cross-section of a Union Carbide Electrode (58)

Table 2.4 : Properties of a Typical Union Carbide Electrode (58)

	Overall thickness (cm)	0.025-0.125
Porous metal backing	Thickness (μ)	Nickel
	Porosity (%)	0.015-0.075
	Mean pore diameter (μ)	68-80
	Number of pores/cm^2	$0.5\text{-}4X10^5$
	Wet proof agent	PTFE
Bonded carbon multiple layer	Thickness (cm)	0.010-0.050
	Particle diameter (μ)	5-20
	Wetproof agent	Polyethylene
	Porosity (%)	40-60
	Pore diamete (μ)r	4-15
	Number of pores/cm^2	$5X10^4 - 1X10^5$
	Amount of catalyst (mg/cm^2)	1-3

Table 2.5 : Properties of a Typical Bacon Dual Layer Electrode (59)

	Overall thickness (cm)	0.15-0.40
Large-pore layer	Material	Grade B carbonyl Ni
	Particle diameter (μ)	2-3
	Thickness (cm)	0.12-0.37
	Porosity (%)	70
	Pore diameter (μ)	32
	Number of pore/cm^2	8.7X10^4
Small-pore layer	Material	Grade A carbonyl Ni
	Particle diameter (μ)	4-5
	Thickness (cm)	0.03
	Porosity (%)	57
	Pore diameter (μ)	16
	Number of pore/cm^2	2.8X10^5

2.3.8. The Single-Layered Hydrophobic Electrodes

The single layered hydrophobic electrodes are relatively new. There are variety of methods for making these electrodes. The electrodes made by Winsel(60), Kordesch(61), Motoo(62) et al. may be categorized in this category. These electrodes are made essentially of a catalyst and a polymer binder (usually PTFE). The catalyst particles are microporous. When a binder is used to form the electrode some channels are formed among the catalyst particles. These channel have polymer binder adhered to them. This makes these channels hydrophobic. In this way, the electrode has two porosity's like a heterogeneous catalyst pellet namely; microporosity in the particles themselves and the macroporosity in the channels among the catalyst particles. The catalyst is chosen in away that it is hydrophilic (Raney- Ni, Raney-Ag, Pt dispersed on the active carbon). Therefore when it comes in contact with the electrolyte, electrolyte floods the micropores of the particles. The macropores being hydrophobic doe not allow electrolyte to stay there. The macropores are therefore available for the reactant gas diffusion. The gas diffuses into these macropores and then into the electrolyte in the micropores. As a result all three phases required for the reaction are brought together. The various manufacturing methods are discussed elsewhere in this dissertation.

2.3.9. Spongy Raney Ni Electrode

Tomido and co-workers(63) proposed a new method of making hydrogen electrodes. This utilizes spongy Raney nickel. In this method molten aluminum is sprayed on both sides of a spongy plate of nickel as substrate with an acetylene-oxygen flame gun. Then, the spongy nickel electrodes are activated by alloying at a given temperature from 550 to 750°C. Subsequently leaching with alkaline solution is done to remove aluminum. This type of

electrodes have shown good thermal and electrical conductivity and also mechanical strength by itself. Their polarization resistances are very low. The characteristics of the electrodes improve with increase in the temperature of heat treatment of alloying. The performance of the electrodes prepared by this method are reported to be better than that of Mund(64) and Kenjo (65) electrodes.

2.4. Electrode Preparation Techniques and Electrocatalysts

2.4.1. Introduction

The performance of a fuel-cell electrode can be optimized in two ways; by improving the physical structure and by using a more active electrocatalyst. A good structure of electrode must provide ample of surface area, provides maximum contact of catalyst, reactant gas and electrolyte, facilitate gas transport and provide good electronic conductance. In this fashion the structure should be able to minimize losses. A variety of electrode preparation techniques have been proposed which have improved the structure. The Electrocatalysts are used to improve activity and thus the rate of reaction. Rate of reaction is the current density in the context of fuel-cells, as the product is electron instead of molecules. A multitude of electrocatalyst have been used for hydrogen oxidation and oxygen reduction. In this chapter a general literature review on the preparation methods and the electrocatalysts is being presented.

2.4.2. Techniques of Electrode Preparation

A. The DSK Electrodes

The DSK electrodes are prepared as follows : Raney nickel is obtained by 50% nickel and 50 % aluminum at 1350 °C under protective layer of calcium chloride. This brittle alloy when cooled is ground to give a fine powder (3-5 μ). This powder is blended with twice its weight of carbonyl nickel (5 μ). The blended powder is spreaded over a circular die over which a thin layer of carbonyl nickel is evenly spreaded. Then the die is pressed at 3800 Kg/cm^2 until 2-4 mm thick disc is formed. Thus obtained discs are sintered at 7000°C and leached with 6N KOH at 40 °C. This electrode is highly pyrophoric and must be kept out of contact with oxygen.

Since their invention, the DSK electrodes have been improved continually. The maximum current that can be drawn from these electrodes had increased from 35 to 750 $mAcm^{-2}$ at 80°C from 1953 to 1957 (66). The pyrophoric character of these electrodes is eliminated by controlled oxidation with ambient air. The adsorbed hydrogen on the surface of the catalyst is oxidized under gradual addition of air. In the subsequent step of oxygen addition, parts of nickel surface is oxidized to NiO and $Ni(OH)_2$ (in the presence of water). The kinetics of the nickel oxidation depends significantly on the water film present on the nickel surface. It works as oxygen diffusion barrier. A situation critical to the oxidation may occur if, at too abundant oxygen access , the catalyst powder is locally heated up evaporating the retarding water film at this spot. Consequently the oxidation is accelerated and the catalyst gets heated up still more. In this way the nickel powder will burn completely and become useless. Therefore a slow 'cold combustion' of the nickel surface with no evaporation of water film is needed (67,68,69).

The performance of the depyrophorised Raney-Ni electrode is reported to be enhanced with the addition of 2% Ti in the Raney-alloy (69,70,71). The annealing of the depyrophorised electrode in hydrogen atmosphere increased the long term performance of the electrodes (71). A number of electrocatalysts (mostly oxides of transition metals) were tested by Tarabic et al (72). These catalysts were mixed with 25% carbonyl nickel, 50% nickel carbonate, 25 % oxalic acid to make DSK electrodes. It is found that the electrode performance decreases in the following order of the electrocatalysts: ammonium wolframate > cobalt acetate > copper basic carbonate > ammonium vanadate.

B. PTFE Bonded Raney Ni Electrodes

In most of the Raney nickel electrodes that have thus far been studied, electrolyte penetration into the electrode pores is prevented from the gas pressure applied on the pores from the other side of the electrode. To attain a balance between the gas pressure and the capillary force, a very good uniformity in the pore size distribution and a careful gas pressure control are required. Contrary to this, the electrodes with hydrophobic agents do not impose such requirements. The water proofing agents used with Raney nickel catalyst in fuel cell electrodes suffer from electrolyte drowning (73). PTFE (Polytetrafluoroethylene) is the one hydrophobicity agent which is reported repetitively in the literature. The reason is its stability against heat and various types of the electrolytes. The PTFE particles are apt to cross-link with one other when they are milled with catalyst powder. The fraction of the cross-linked PTFE particles on the milling seems to increase with mixing time and temperature. The hydrophobicity of the electrode and the catalytic surface area covered with PTFE, which influence the polarization, depends not only

upon the content of PTFE added but also upon its cross linkage. Thus, the polarization characteristics vary with milling conditions. This is the main reason for their poor reproducibility. There are two methods of preparing PTFE bonded fuel cell electrodes, namely dry and wet methods depending upon the form of PTFE used (74).

(i) Wet Method

In the wet method aqueous PTFE emulsions are used. The procedure used by Jenseit (74) is as follows : The depyrophorised Raney Ni powder is first mixed with promoters e.g. Cu_2O. This mixture is added to the PTFE suspensions. Isopropanol is added to stabilize the rubber like resultant mixture. During this mixing the suspension of PTFE breaks and water is removed. This paste is heated in order to evaporate some water and isopropanol resulting into a plastisizable mass. Cold rolling of this mass is done to obtain a felt of 0.2 to 0.5 mm thickness. Finally this felt is rolled with a nickel net which also works as current collector. The cold rolling results into more cross linkage of catalyst particles with PTFE strands.

Kenjo(65) reports the use of D-1 PTFE suspension containing 60% of PTFE. The mixture with the catalyst is milled for one hour at 20±2°C. The paste is calender rolled into 0.1 to 0.2 mm thick sheet. The surfactants are removed by boiling the sheet in acetone. Thus obtained sheet is used as catalyst layer. Gas side layers are prepared by using nickel black powder blended with PTFE dispersion. These two layers are rolled with a mesh of stainless steel to get the final electrodes. In a later communication Kenjo(75) showed that the use of dopants like chromium and titanium improves and stabilizes the polarization characteristics of Raney nickel electrodes.

(ii) Dry Method

Use of dry PTFE powder in making fuel cell electrodes is relatively new. Sauer (76) patented the method of making air electrodes using activated carbon and PTFE powder. He used a fast rotating sharp blade cutter head to achieve fragmentation. It is believed that at least some part of the PTFE is evaporated and precipitated on the carbon particles. This milled mixture is subsequently rolled into a foil and then with a metal gauze to obtain finished electrodes. Dry PTFE powder with Raney nickel catalyst was used by A. Winsel (60) to prepare fuel cell hydrogen electrodes. In this method 5-8 wt% of PTFE is added to the catalyst. The blend is milled into a high speed machine with sharp blades. It formed a network of PTFE threads and lumps with catalyst grains in between. According to Schnurnberger (77) high speed blade milling of the catalyst particles with PTFE leads to PTFE coating on the catalyst grains. The next step is the rolling of this fluffy PTFE-catalyst mixture into a calendar to form a tape. This tape is further rolled onto a wire mesh of nickel. Fig. 2.3 shows the manufacturing schematic of this procedure. The method is continuous and mass production of the electrodes is possible. The electrodes made in this way are continuous, flexible and homogeneous (78).

C. PTFE Bonded Carbon Electrode

(i) Rolling Technique

It involves rolling or calendering a mixture of carbon, PTFE powder and suspension agents e.g. light fraction of petroleum or toluene (61). The sugar is generally used as filler or spacer. Schautz (79) has studied and tried to optimized the rolling procedure. A flow diagram for the production is shown in Fig. 2.4. For making the active layer the catalyst, PTFE powder, carbon

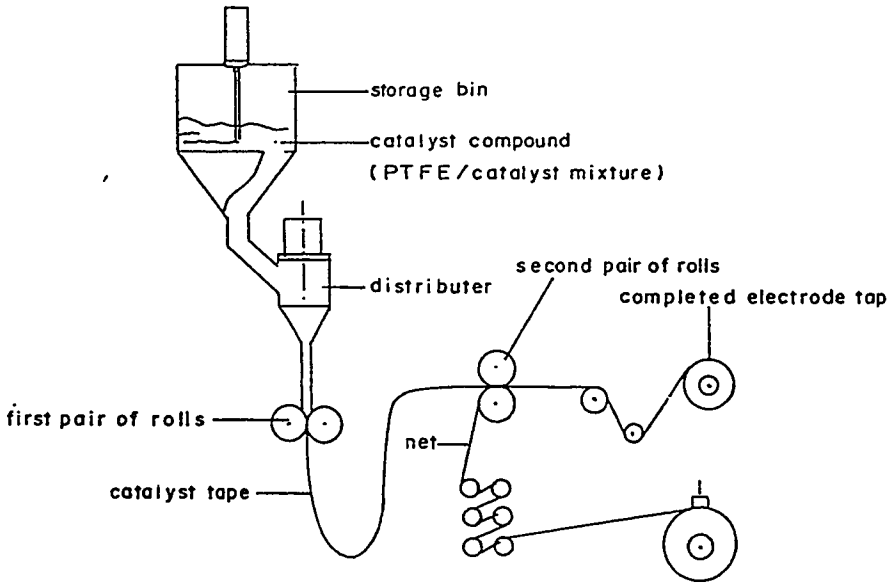

Fig. 2.3 : Schematic Diagram for Electrode Preparation by Dry-Method (60)

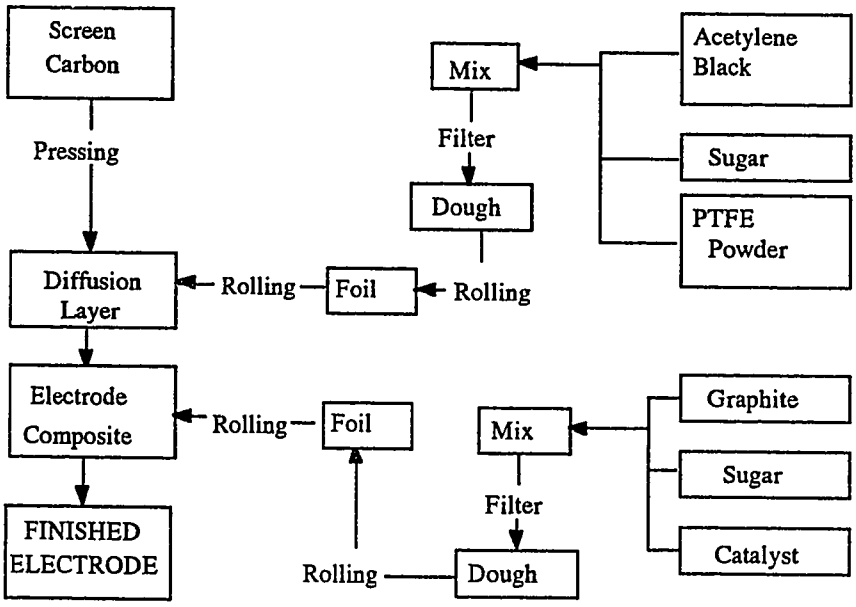

Fig. 2.4 : The Flow-sheet for Electrode Preparation by Rolling Method (79)

and sugar are mixed and rolled separately. Carbon powder, sugar and PTFE are mixed and rolled independently to get the gas diffusion layer. These two layers are rolled together with nickel screen followed by washing and sintering to obtain the finished electrode.

(ii) Pressing Technique

A mixture of carbon powder, PTFE powder and filler is pressed to get the electrodes. The active layer that contains catalyst is pressed separately. Diffusion layer, which originally has ammonium carbonate as filler, is pressed alone. The filler is removed before these two layers are pressed together with a conducting screen. Subsequently sintering and reduction take place to get the finished electrode. Fig. 2.5 shows a typical flow diagram for the production by this technique (80).

(iii) Spraying Techniques

In this method a very diluted aqueous suspension of PTFE with carbon (with or without catalyst) is sprayed over the porous nickel sheet. Instead of PTFE suspension, polyethylene powder dissolved in solvent like xylene or tetrachloro ethylene may also be used. The ratio between carbon and PTFE is determined by weight and dilution of the viscous mixture is adjusted to the spraying gun. The steps used in spraying technique are shown in Fig. 2.6 (81,82).

(iv) Approach of Motoo et al

This group proposed a technique on the basis of theoretical analysis of the catalyzed (Pt) electrodes (62). They hypothesized that the reactant gas dissolves on 'the gas dissolving sites' at gas-liquid interface. From these

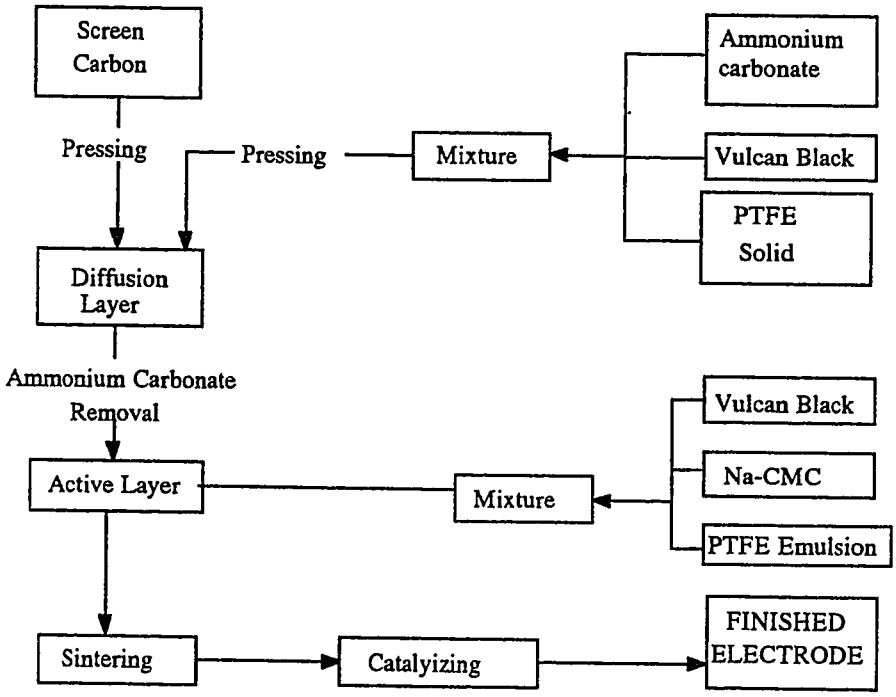

Fig. 2.5 : Process Flow-sheet for Electrode Manufacturing by Pressing Method (74)

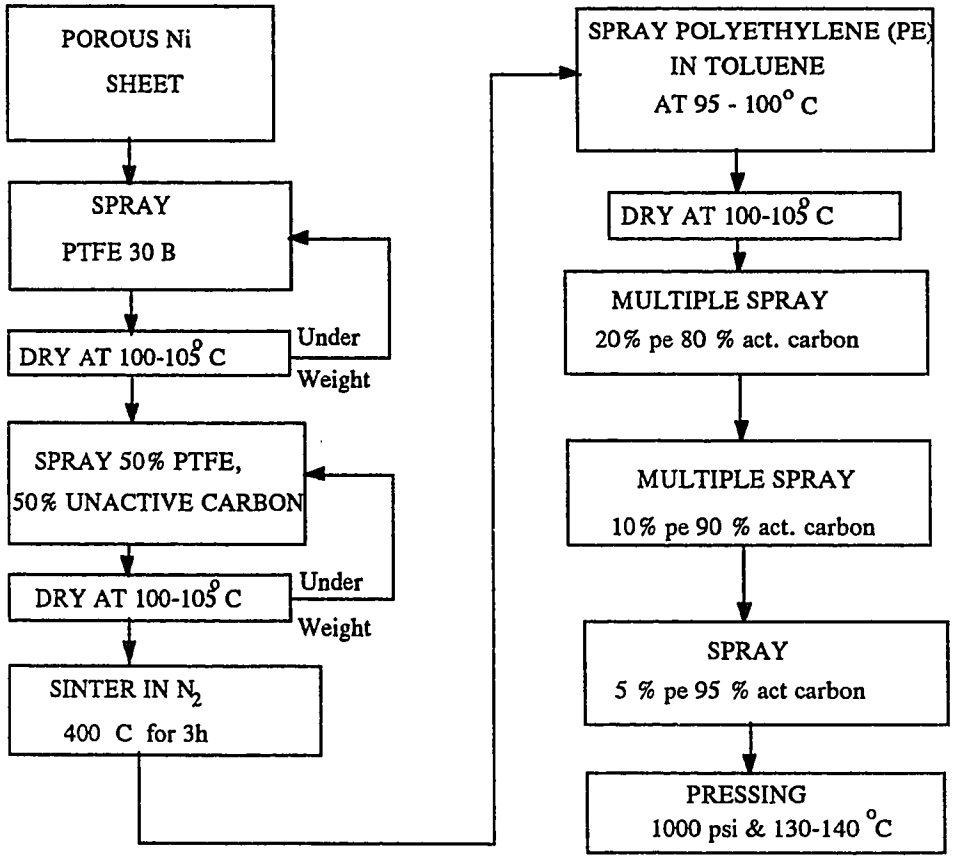

Fig. 2.6 : Process Flow-Sheet for the pReparation of Thin Carbon Electrodes (Spraying) (74)

dissolving sites the reactant transfers to the catalyst sites by diffusion. For better performance of the electrodes, it is necessary that the diffusion path between these two kind of sites should be minimum. To achieve this, the gas should be supplied to all of the gas dissolving sites. This could be done by introducing gas supplying networks through the layer. The channels of this network should have gas dissolving sites at their outer walls. The greater the number of the gas dissolving sites to which enough reactant has supplied, the shorter the diffusion distance. The number of the catalyst sites to which the reactant should be supplied from one gas dissolving site is inversely proportional to the number of gas dissolving sites. Therefore the number of the gas dissolving sites must be as high as possible in order to obtain the desirable low overpotential and high current density. This requires that most of the catalyst clusters should exist in the electrolyte networks and enough reactant gas should be supplied to whole clusters via the shortest pathway. Following method is proposed to fulfill these requirements (83). To ensure the wettability, catalyst bearing carbon was heated at 600°C in air and then boiled with concentrated HNO_3. Fine networks for electrolyte and channels for gas supply are ensured by milling the catalyzed carbon and PTFE dispersion in an ultrasonic colloidal mill. The resultant mass is hot pressed (360°C, 5 Kg/cm^2) and sintered to get the final electrode (84,85).

2.5. Mathematical Models for Gas Diffusion Electrodes

2.5.1. Introduction

In the recent years, it has become common to find models in which the elements of the hypothesis are expressed in mathematical form. Modeling is not only used to predict the theoretical behavior but it is also used for

optimization, analyzing experimental data, correlating and scaling experimental data, comparising between different alternatives. There have been numerous attempts of mathematical modeling the behavior of gas diffusion electrodes for fuel-cells. The performance of these electrodes depends on the distribution of the liquid and gaseous reagents, rate of transport processes, and the local kinetics of the electrochemical reactions.

A detailed knowledge of structural features of the structure, materials and prevalent conditions is needed to describe the performance of the electrode theoretically (86). The theoretical analysis of the porous electrodes in particular is complicated for several reasons. Firstly, being hetrogeneously porous, the structural details are lacking. Secondly, the potential and the mass transfer distribution is non-linear and multidimensional. Thirdly, defining active zone mathematically is difficult as the reaction takes place at the juncture of the three phases, namely; gaseous reactant, liquid electrolyte and solid electrocatalyst.

With this complication it becomes necessary to simplify the situation by making certain assumptions. A variety of simplifications or idealization have been used in different models. The differences in these models are also due to diversified design of porous gas diffusion electrodes(87).

The major objectives of these models are to calculate total current, to determine the distribution of the processes into the depth of the electrode and to establish the principal factors influencing the above characteristics. The total current collected from the electrode is the resultant effects of a number of processes e.g. local kinetics, diffusion, convection, charge transfer, and

electronic conduction. It is impossible to segregate these process in a process electrode.

The models proposed for the description of these electrodes can be classified in the following three categories:

a. Homogeneous model

b. Quasi-homogeneous model

c. Descrete or statistical model

A. Homogeneous Model

In these models, the interconnected multiphase system is treated as a single homogeneous phase by replacing the distributed homogeneous sources/sinks by appropriate homogeneous or volume entities. This avoids precise definition regarding the structural details of porous matrix and also the geometry of the zone of electrochemical activity.

B. Quasi-homogeneous Model

In this case, the current density-overpotential relationships are deduced by modeling the three-phase boundary regions and relating these results to the pore structures elucidated through homogenization and a knowledge of the boundary distributions.

C. Statistical Models

Instead of ignoring the structure of the porous matrix, one may idealize it by adopting simple concept such as single-pore or lattice models. In the single pore approach, one may assume that the porous structure are made up of non-

interacting pores characterized by two parameters; radius of the solid capillary and distance parameter representing the packing of these solids. Taking into account the pore geometry, one may solve the boundary value problem and develop ensemble-averaged parameters. The interconnected pore medium can also be described by all lattice modeling where each lattice influences the flux adjacent to it.

In the literature following models are frequently cited:

1. Simple Pore Model
2. Thin Film and Meniscus Model
3. Hydrophobic Electrode Model
4. Hydrophilic Electrode Model
5. Cylindrical Gas Pore Model
6. Model based on Macrokinitics and Electrode Effectiveness
7. Flooded Agglomerate Model

2.5.2. Simple Pore Model

This model was developed by Austin et al. (88) who proposed that reactant gas diffuses into the pores, dissolves in the electrolyte and further diffuses in solution to reach the catalytic sites where the three-phase boundary of solid-liquid gas comes into contact. Srinivasan et al. (89) have also studied this models extensively to describe the behavior of partially wettable electrocatalysts. A schematic diagram of the simple pore model proposed by Srinivasan et al. (90) is shown in Fig. 2.7. When all forms of polarization are

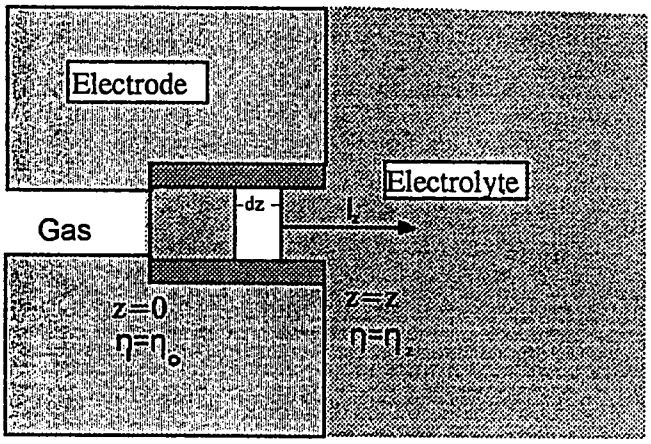

Fig. 2.7 : Schematic Diagram of the Simple Pore Model (90)

present, the differential equation describing the potential variation in the pore is given as:

$$\frac{d^2\eta}{dz^2} = \frac{2i_0}{\rho r_2}\left\{\frac{C}{C_o}\exp\left(\frac{\beta\eta F}{RT}\right) - \exp\left(\frac{-(1-\beta)\eta F}{RT}\right)\right\} \qquad [2.1]$$

Where η is the overpotential, C and C_o the surface and bulk concentration of the reactant respectively, z the distance coordinate, r_2 the pore radius, β the symmetry factor, F the Faraday constant, T the temperature, R the gas constant, and ρ is the specific conductance of the electrolyte. Solution of Eqn [2.1.] with the boundary conditions:

$$\eta = \eta_o \qquad \text{at} \qquad z = 0 \qquad [2.2]$$

$$i = \rho\pi r_2^2 \frac{d\eta}{dz} \qquad \text{at} \qquad z=0 \qquad [2.3]$$

results in the following relationship for the current distribution and total current per pore (i_t) :

$$\frac{i_z}{i_t} = \left[\left(\frac{dc}{d\alpha}\right)_{\alpha=\alpha_1} - \left(\frac{dc}{d\alpha}\right)\exp(mx/2)\right] \Big/ \left(\frac{dc}{d\alpha}\right)_{\alpha=\alpha_1} \qquad [2.4]$$

Where,

$$\frac{dc}{d\alpha} = 1 - \exp(-y_0)\frac{K_1(\alpha_2)I_1(\alpha) - I_1(\alpha_2)K_1(\alpha)}{K_0(\alpha_1)I_1(\alpha_2) - I_0(\alpha_1)K_1(\alpha_2)} \qquad [2.5]$$

where i_z is the total current generated from $z=0$ to $z=z$ and i_l is the total current generated from $z = 0$ to $z = l$, α_l and m are dimensionless groups in terms of physical and electrochemical parameters, x is the dimensionless axial coordinate, y_0 is the dimensionless overpotential at $z = 0$, and l is the length of the pore.

$$i_l = -2\pi r_2^2 \rho \frac{RT}{lF} \{ab\exp(y_0)\}^{1/2} \left(\frac{dc}{d\alpha}\right)_{\alpha=\alpha_l} \qquad [2.6]$$

Eqns. [2.4] and [2.6] take simple forms under some limiting conditions such as activation-concentration control and activation-ohmic control.

2.5.3. Thin Film and Meniscus Model

Experiments with partially submerged electrodes show that the electrode reaction takes place mainly in a region where the electrolyte forms a thin meniscus and a film at a the electrode-gas interface. This facilitates molecular diffusion of the gaseous reactant through the film in the electrode. For various geometries of meniscus and film, mathematical analysis have been carried out by several authors (88, 90-95).

A. The Thin Film Model

The thin film model was introduced by Will(96) who developed a mathematical treatment including only diffusion and ohmic polarization effect. Will(97) also experimentally confirmed the validity of this model for the ionization of hydrogen on partially immersed Pt electrode in H_2SO_4 solutions. Other investigators (90,95,98,99) generalized the thin film model by considering activation polarization in addition to concentration and ohmic

polarization. Lindstorm(100) postulated that there was a thin electrolyte film on the walls of the gas filled pores of gas diffusion electrodes. Transport limitations in the gas phase are also considered by Lindstorm(101) in which the thin film model is applied to the Bacon type electrodes. Bennion and Tobias(102) studied the axial diffusion of electrolyte ions in O_2 electrode according to thin model.

A schematic diagram of the thin film model is given in Fig 2.8. The rate of the electrode reaction in an element *dz* is given by :

$$dI_z = 2\pi r_2 dz i_0 \left[\frac{C}{C_0} \exp\left(\eta F / 2RT \right) - \exp\left(-\eta F / 2RT \right) \right] \qquad [2.7]$$

Potential drop in element *dz* would be written as :

$$d\eta = I_z \frac{dz}{K\pi\left(r_2^2 - r_1^2\right)} \qquad [2.8]$$

and the potential distribution is expressed as :

$$-\frac{d^2\eta}{dz^2} = \frac{\left\{4r_2 i_0 / K(r_2^2 - r_1^2)\right\}\sinh(\eta F / 2RT)}{1 + (r_2 i_0 / DnFC^o)\ln\left(r_2/r_1\right)\exp(\eta F / 2RT)} \qquad [2.9]$$

Current generated from $z = 0$ to $z = z$ is given by :

$$I_z = 2K\pi(r_2^2 - r_1^2)\frac{RT}{lF}\left(\frac{dy}{dx}\right)_{x=x} \qquad [2.10]$$

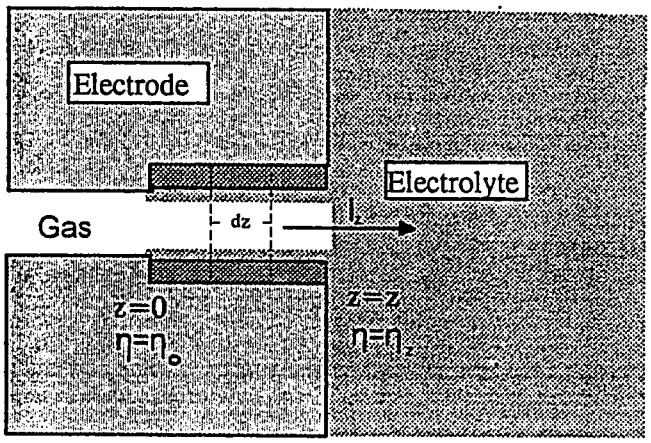

Fig. 2.8 : The Thin Film Model (96)

and the total current generated from $z=0$ to $z= 1.0$ is given as :

$$I_t = 2K\pi(r_2^2 - r_1^2)\frac{RT}{lF}\left(\frac{dy}{dx}\right)_{x=l} \qquad [2.11]$$

where x and y are the dimensionless distance and overpotential respectively.

It is not possible to solve Eqn. [2.9] analytically in a general case. For this reason, a numerical solution is necessary to study the influence of various parameters such as i_0, K, D, C°, r_2,r_1, η_0.

Mund (103) developed a thin film model by considering that the whole catalytic surface of the pores is covered by thin electrolyte films. These films are thin enough to permit the gas molecule to diffuse at substantial rate. The gas molecules are dissolved into the films, and the electrode reaction takes place at the electrolyte catalyst interface. The whole catalytic surface participates in the electrode reaction. This contrasts with the three phase boundary mechanism. On the basis of this model, Mund (103,104) has expressed the polarization resistance, w, as a function of the catalyst loading, d, in the form :

$$w = \sqrt{\rho k}\left(\coth\frac{\sqrt{\rho d^2}}{k}\right) \qquad [2.13]$$

where ρ is the electrode resistivity in the catalyst layers, and k, the polarization resistance of the catalyst.

Kenjo and Nakajima(105) considered a thin film model where the penetration of the electrolyte in the central area of the pore is hindered by the repellence of PTFE. This is schematically shown in Fig. 2.9. The current potential relation derived was of the following form :

$$i = \frac{e_0}{\sqrt{\rho k}} \tanh \frac{\sqrt{\rho}}{k} l \qquad [2.14]$$

where e_o is the IR corrected voltage drop, i is the current density, l is the thickness of the catalyst layer, ρ is the resistivity of the electrolyte film per unit working area, k is the impedance per unit thickness of the catalyst layer.

B. The Meniscus Model

A meniscus model (91) is proposed as a combination of the physical pictures of the simple pore and thin film models.

A schematic representation of the flow of current through the solution of a porous gas diffusion electrode for the finite contact angle meniscus model is shown in Fig. 2.10.

Theoretical analysis leads to a differential equation which has the form of Eqn. [2.9] with the following boundary conditions :

$$\eta = \eta_o \qquad \text{at} \quad z = 0 \qquad [2.15]$$

$$\frac{d\eta}{dz} = 0 \qquad \text{at} \quad z=0 \qquad [2.16]$$

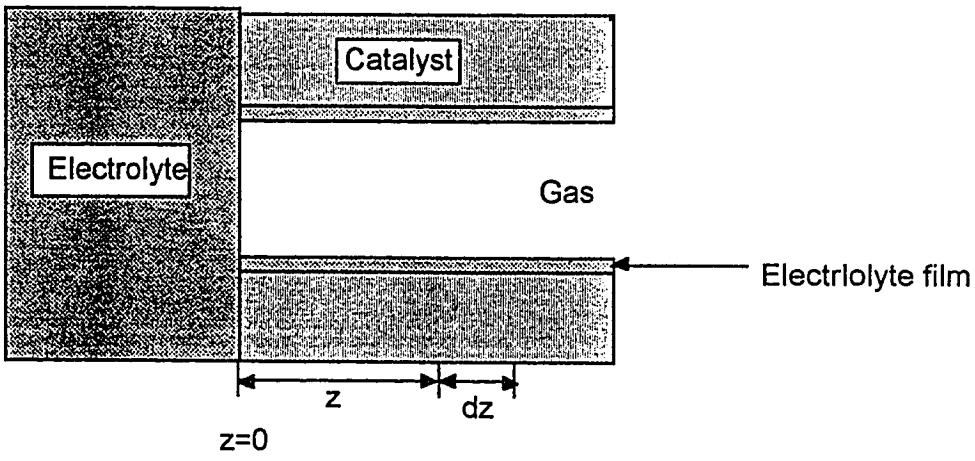

Fig. 2.9 : The Thin Film Model by Kenjo et al. (105)

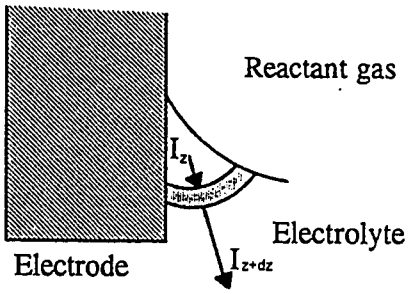

Fig. 2.10 : The Meniscus Model (91)

The equations are solved numerically as it is not possible to obtain analytical solution .

Rockett and Brown(99) proposed a meniscus model to account for the polarization mechanism in a porous electrode. The analysis accounted for the polarization associated with transport of electrolyte species, transport of dissolved gas, chemical reaction at the solid-liquid interface and ohmic loses in the electrolyte. Chen et al.(106) treated electrolyte meniscus geometry as a wedge and presented analytical solutions for constant overpotential case and numerical solutions for all forms of polarization

2.5.4. Hydrophobic Electrode Models

Several models have been proposed for this purpose and they could be classified into three basic types (107).

Type 1: Hydrophobic gas pores are formed by agglomerates PTFE in a hydrophilic medium consisting of catalyst particles separated by the electrolyte.

Type 2: Hydrophobic pores are formed by agglomerates of catalyst located in a hydrophobic medium consisting of PTFE particles with the space occupied by the gas.

Type 3: A material whose activity is proportional to the specific surface of the catalyst per unit volume-the contact angle at the boundary of the liquid being determined by PTFE concentration at the surface of gas pores.

The activity of hydrophobic electrodes is determined not only by the pressure difference, but by the hydrophobizer concentration. For hydrophobic electrodes, it is necessary to determine the pore distribution in terms of radii and also in terms of effective angle of wetting by the electrolyte of the hydrophilic-hydrophobic pore walls(108). The polarization distribution in the electrode is found by solving differential equations which involve a probability factor of the position of PTFE grains in crystal lattice.

2.5.5. Hydrophilic Electrode Models

The leading models of this kind are the dual porosity model and the model of intersecting capillaries. The dual porosity model treats a porous electrode as containing both wide and narrow pores (109). The wide ones are filled with gas but their walls are covered with an electrolyte film, and the narrow ones are flooded. According to this model,

$$I\alpha\sqrt{(p\phi)}$$

where p is the total perimeter of the gas filled areas and ϕ refers to the total cross-section of the solution filled pores. The parameters p and ϕ vary with gas pressure such that an increase in gas pressure leads to an increase in ϕ and a decrease in p.

On the other hand, model of intersecting capillaries assumes that the current generation is localized in the neighborhood of intersections of liquid pores with gaseous ones. In this case, the equation for the potential distribution is given as:

$$K\frac{d^2\eta}{dx^2} = \iint N(r_i, r_k) I(\eta r_i, r_k) dr_i dr_k \qquad [2.17]$$

where $N(r_i, r_k)$ is the number of intersections between the gaseous pores of radius r_i and the liquid pores of radius r_k in a unit volume of the electrode, and $I(r_i, r_k)$ is the current generated by single intersection.

2.5.6. Cylindrical Gas Pore Model

The main parameter determining the distribution of gas and liquid and the electrochemical activity of hydrophobic electrodes is the pressure difference between the gas and the electrolyte. However, in the case of hydrophobized electrodes, the performance characteristics depend on the degree of hydrophobization. Thus, as the Teflon concentration is increased, the electrochemical activity goes through a maximum.

Burshtein et al.(110) and Chirkov(111) suggested a model to explain the above observation by proposing gas filled cylinders of radius r, arranged in a regular manner, with walls composed of a mixture of PTFE and catalyst, moistened with the electrolyte. The polarization distribution equation was solved for the total current density :

$$i_t = \left[\frac{4RT\bar{x}\nu_1}{F^{1/2} r} \left(\eta \bar{D} C_0 S_c V_c\right)^{1/2} \int_{\bar{\eta}\Delta}^{\bar{\eta}_a} \exp\left(\bar{\eta}/2\right) \psi\left(\bar{\eta}\right) d\bar{\eta} \right] \qquad [2.18]$$

where,

$$\bar{\eta} = \frac{\eta F}{RT} \qquad [2.19]$$

and

$$\psi = \frac{I_1(l'/l_d)K_1(r/l_d) - K_1(l'/l_d)I_1(r/l_d)}{I_1(l/l_d)K_0(r/l_d) - K_1(l'/l_d)I_0(r/l_d)} \qquad [2.20]$$

2.5.7. Models Based on Macrokinetics and Electrode Effectiveness

These models are developed and used to calculate the macrokinetic characteristics of the gas diffusion electrodes which utilize the interfacial area between the liquid and gas filled pores as the main structural parameter (112-114). The gas diffusion electrode is considered as a system of doubly distributed parameters, first, along a coordinate which is normal to the interface (in the microstructure) and, second, along a coordinate which is normal to the external surface of the electrode (in the macrostructure). The micro kinetic expressions and macrokinetic parameters (effective electrical conductivity, interfacial surface per unit volume, effective diffusion coefficient) and processes are solved simultaneously to describe the performance of the electrodes. Efficiency factors are used to describe the non-uniformity of processes throughout the porous electrode which gives the utilization of the surface of catalyst. This is the ratio of the observed current to the maximum possible current which would be obtained if the electrode is operated under intrinsic kinetic conditions.

2.5.8. Flooded Agglomerate Models

The first flooded agglomerate model was proposed by Giner (115,116). This model is based on more realistic assumptions about the structure of the

porous bonded-electrodes. According to this model the electrode is composed of agglomerates of catalyst and PTFE(binder). The catalyst particles are microporous. The idealization is in assuming that these agglomerates are cylindrical. Being hydrophilic the catalyst particle pore in the agglomerates get flooded with the electrolyte as soon as the electrode comes in contact with the electrolyte. The space between these parallel cylindrical agglomerates forms macroporous structure is used for reactant gas diffusion. In this model the agglomerates are assumed as a continuum. A schematic sketch of this model is shown in Fig. 2.11.

Iczkowski and Cutlip(117) proposed an flooded agglomerate model for PTFE bonded platinum-on carbon electrode. In addition to Giner's model a thin film of electrolyte is assumed covering the agglomerate in this model as shown in Fig. 2.12. This film adds an extra diffusion resistance in the system.

Pehr Bjornbom(118) used the assumption of flooded agglomerate in the modeling of double layered PTFE bonded electrode. This effort mainly was to relate limiting current density with the model parameters in addition to the current-density overpotential relationship. Vitanen and Lampinen(119) modified the original model for two-layer porous air electrode by incorporating the resistance in gas diffusion and overpotential due to ionic mobility.

A new approach was proposed in the agglomerate model by Celiker et al.(120,121) by the assumption of spherical agglomerates instead of conventional cylindrical geometry. The electrode is assumed to be composed of identical spherical particles of PTFE bonded catalyst particles. This model

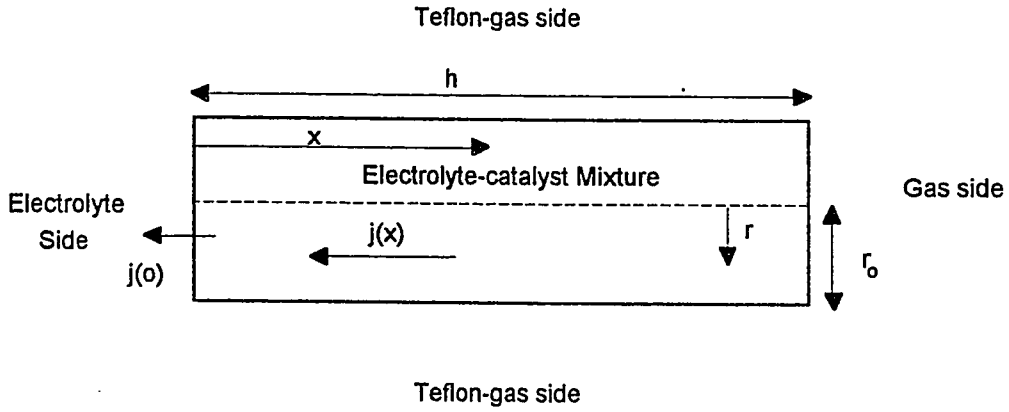

Fig. 2.11 : Flooded Agglomerate Model (115)

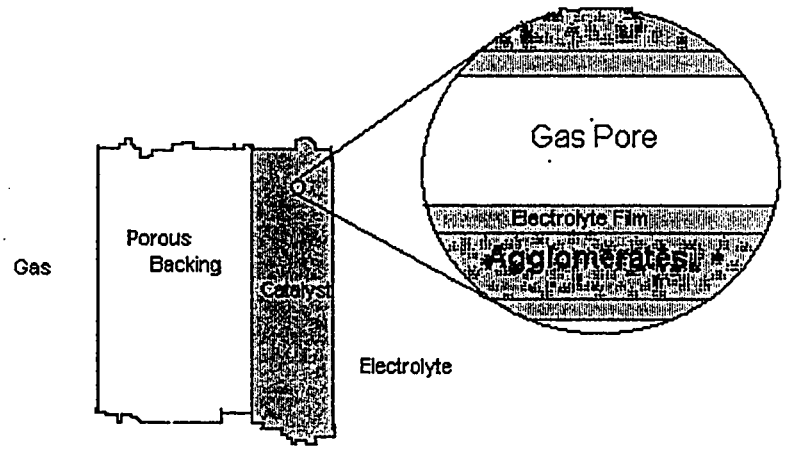

Fig. 2.12 : Flooded Agglomerate Model (117)

is used for Raney-Ni gas diffusion single-layer electrodes. This model is discussed in detail in Chapter 7 of this dissertation.

Kimble and White(122,123,124) used the basis of flooded agglomerate model to model the entire alkaline fuel cell. This includes anode, cathode, separator and gas diffusion layers etc. A detailed schematic three-phase region in AFC as assumed in this model is shown in Fig. 2.13. Yang and Bjornbom (125) proposed a model using the concentrated electrolyte solution theory.

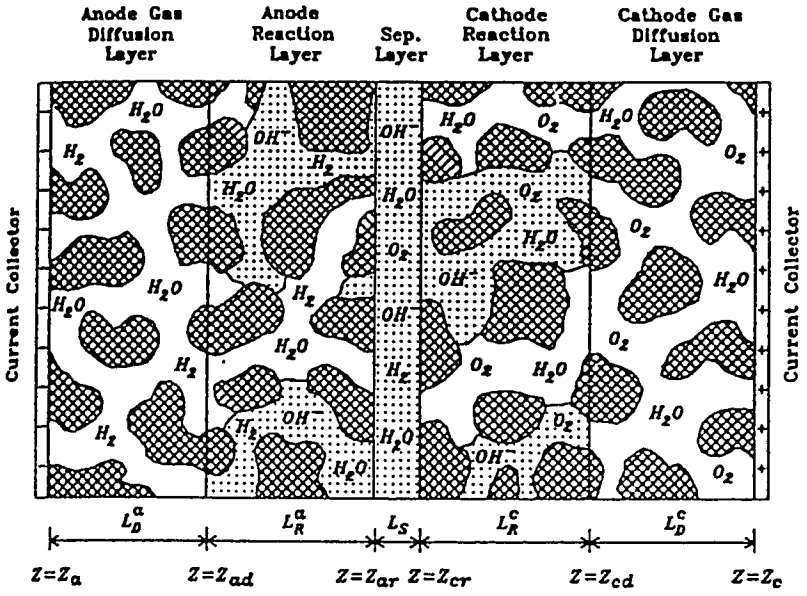

Fig. 2.13 : Schematic Diagram of the Model of a Complete Fuel-cell (123)

References

1. Appleby, A.J., in *Comprehensive Treatise of Electrochemistry*, Vol 7, Editors : B.E. Conway, J. O. M. Bockris, S.U.M. Khan and R.E. White, Plenum, New York, 173 (1983)

2. Appleby, A.J., G. Bronoel, M. Chelma and H. Kita in *Encyclopedea of the Electrochemistry of Elements*, Vol. IX, Part A., Editor: A.J. Bard, Dekker, New York, 383 (1983).

3. Pourbaix, M., *Atlus d'Equilbres Electrochimiques*, Gautier-Villars, Paris, 449(1963).

4. Ross, P.N., *Proceedings of Workshop Electrocatalysis Fuel Cell Reactions*, Brookhaven National Lab., 169(1978).

5. Christner, L. and P.N. Ross, *Proceedings of Workshop Electrocatalysis Fuel Cell Reactions*, Brookhaven National Lab., 40(1978)

6. Rolla, A., A. Sadkowski, J. Wild and P. Zoltowski, *J. of Power Sources*, **5**, 189 (1980).

7. Ewe, H. H., E.W. Justi and A. Schmitt, *Electrochim. Acta*, **19**, 799(1974).

8. Visscher, W. and E. Barendrecht, *J. Applied Electrochem.*,**10**,269(1980).

9. Bacon, F.T., *Fuel Cell symposium, A.C.S. Meeting*, Atlantic City, (1959).

10. Korovin, N.V., O.N. Saveleva and N.I. Kozlova, *Elektrokhimiya*, **16**, 585 (1980).

11. Jasinski, R.J., *Electrochem. Tech.*, **3**, 129 (1965).

12. Meibuhr, S.G., *Electrochim Acta*, **21**, 1059 (1967).

13. Meibuhr, S.G., J. Electrochm Soc., **121**, 11264 (1974).

14. Vallet, C. E., and Braunstein, *J. Electrochem. Soc.*, **125**, 1193(1978).

15. Sepa, D.B., M.V. Vojnovic, D.S. Ovcin and N.D. Pavlovic, *J. of Electroanalytic Chemistry*, **51**, 99 (1974).

16. Hobbs, B.S., A.C.C. Tseung, *J. Electrochem. Soc.*, **119**, 580 (1972).

17. Binder, H., W.H. Kuhn, W. Linder and G. Sandstede, *U.S. Patent No.* **3,708,342** (1973).

18. Sandstede, G., in *From Electrocatalysis to Fuel Cells*, Editor: G. sandstede, Univ. of washington Press, Seatle 87(1972).

19. Yeager, E., *Electrochemicia Acta*, **29**, 11, 1527 (1984).

20. Hyde, P.J., K.Hordesch, L.Oporto, A. Reid and S. Srinivasan, *Electrochemical Society Extended Abstracts*, Abstract # **646**, 904 (1982).

21. Brodd, R.J., A. Kozawa and K.V.Kordesch, Journal of the Electrochemical Society,125, 271c (1978).

22. Manoharan, R. and A.K. Shukla, *Journal of Power Sources*, **10,** 333 (1983).

23. Manoharan, R., D. D. Sarma and A.K. Shukla, *Journal of Power Sources*, **10,** 273(1984).

24. Vasudevan, P. and Neelammann, *Journal of Power Sources* , **28** 317 (1989).

25. Ramesh, K.V. and A.K.Shukla, *Journal of Power Sources*, **19**,279 (1987).

26. Shukla, A.K. and R. Manoharan, *Journal of Applied Electrochemistry*, **18,** 774(1985).

27. Kunz, R. and G. Gruver, *Journal of Electrochemical Society*, **122**, 1279 (1975).

28. Jalan, V.M. and D.A. Landsman, *U.S. Patent* **4,186,110** (1977).

29. Jalan, V.M. *U.S. Patent* **4,202,934** (1980).

30. Landsman, D.A. and F.S. Luczak, *U.S. Patent* **4,316,944** (1982).

31. Luczak, F.S. and D.A.Lndsman, *U.S.Patent* **4,447,506** (1984).

32. Beard, B. and Ross P. , *Journal of Electrochemical Society* ,**133**, 1839 (1986).

33. Paffet, M., K. Daube and S. Gottesfeld, *Journal of Electroanalytical Chemistry*, 220, 269 (1987).

34. Beard, B. C., *Journal of Electrochemical Society,* 137, 11, 3368 (1990).

35. Ewe,H., E.W.Justi and A. Schimidt, *Energy Conversion and Management*, **14**, 34(1975).

36. Kirchenmann, M., D. Whorle and Vielatich, W., *Ber, Bunsenges (Physical Chemistry)*, **92**, 1403 (1988).

37. Kivisaari, J., J.Lamminen and M.J.Lampinenn, *Journal of Power Sources*, **32**, 233(1990).

38. Lessner, P. and S. Sarangpani, *Journal of Power Sources*, **29**, 437 (1990).

39. Carbonio, R.E., D.Tryk and E.Yeager, *Journal of Power Sources*, **22**, 387 (1988).

40. Shimizu, Y., K. Uemura and N.Miura, *Chemical Society of Japan*, 1979 (1988).

41. Anderson, E.B., E.J. Taylor and G.A. Moniz, *IECEC conference*, **3**,125 (1989).

42. Grove, W.R., *Phil Mag., S. 3*, **14**, 127 (1839).

43. Grove, *W.R., Phil. Mag, S.3*, **21**, 417 (1842).

44. Mond, L. and Langer, *Proc. Roy. Soc. (London)*, **46**, 296 (1889).

45. Haber, F. and A.Moser, *Z. Electrochem*, **11**, 593 (1905).

46. Baur, E., W.D.Treadwell and G.Trumpler, *Z.Electrochem*, 27, 199 (1921).

47. Jung, M., and H. vanDohren, *5th Intern. Symp. Batteries*, Paper # 23, Bringhton (1966).

48. Tobler, J., *Z. Electrochem*, **39**, 180 (1933).

49. Vielstich, W., *Fuel Cells*, Wiley-InterScience (1965).

50. Justi, E. and A. Winsel, *Journal of the Electrochemical Society*,**108**,1075 (1961).

51. Krupp, H., R. McJones, H. Robenhorst, G. Sandstede and D. Walter, *Journal of the Electrochemical Society*, **109**, 553 (1962).

52. Dousek, F.P., J. Jansta and J.Riha, *Coll. Czech. Chem. Comm.*, **31**, 457 (1966).

53. Jung, M., and H. vanDohren, *5th Intern. Symp. Batteries*, Paper # 23, Bringhton (1966).

54. Liebhafsky, H.A. and J.Cairns, *Fuel Cells and Fuel Batteries*, John Wiley and Sons (1968).

55. Despic, A.R., D.M. Drazic, C.B. Petrovic and V. Lj. Vulcic, *Journal of the Electrochemical Society*, **111**, 1109 (1964).

56. Williams, K.R., D.P. Gregery, *British Patent* **874,283** (1961).

57. Niedrach, L.W. and H.R. Alford, *Journal of the Electrochemical Society*, 112, **117** (1965).

58. Clark, M.B., W.G. Darland and K.V. Kordesch, *Proc. of 18th Ann. Power Source Conf, Paper # 11*, DSC Publicatio Committee, Red Bank, N.J. (1964).

59. Bacon, F.T., *British Patent* **667,296** (1952).

60. Winsel, A., *German Patent* **D.E.-O.S. 3710168** (1987).

61. Kordesch, K, S.Jahangir and M.Sachautz, *Workshop on the Electrochemistry of Carbon*, Cleveland, 17-19 August (1983).

62. Motoo, S., M. Watanabe and N. Furuya, *Journal of Electroanalytical Chemistry*, **160**, 351 (1984).

63. Tomida, T. and I. Nkabayashi, *Journal of the Electrochemical Society*, **136**,11,3296 (1989).

64. Mund, K., G.Ritcher and F. vanSturn, *Journal of the Electrochemical Society*, **124**, 1,1 (1977).

65. Kenjo, T., *Bulletin of Chemical Society of Japan*, **54**, 2553 (1981).

66. Justi, E. and A. Winsel, *Journal of the Electrochemical Society*,**108**,1075 (1961).

67. Ewe, H., E.Justi and H.J. Selbach, *Energy Conversion and Management*, **23**, 42, 245 (1983).

68. Ewe, H., E.Justi and H.J. Selbach, *Energy Conversion and Management*, **24**, 1, 89 (1984).

69. Ewe, H., E.Justi and A. Schimit, *Energy Conversion and Management*, **14**, 35 (1983).

70. Mund, K., G.Ritcher and F. vanSturn, *Journal of the Electrochemical Society*, **124**, 1,1 (1977).

71. Ewe, H., E.Justi and H.J. Selbach, *Energy Conversion and Management*, **20**, 1, 97 (1983).

72. Tarabic, M.M., I. Onaca and I. Solacolu, *Journal of the Electrochemical Society*, **6**,135 (1976).

73. Mitchel, *Fuel Cells*, Academic Press , New York (1963).

74. Jensiet, W., A.Khalil and H.Wendt, *Journal of Applied Electrochemisty*, **20**,893 (1990).

75. Kenjo, T., *Journal of the Electrochemical Society*,**132**, 2, 383 (1985).

76. Sauer, H. *German Patent* **D.E-O.S. 2941774** (1979).

77. Bolvin, K., E.Gulzow and W. Schnurnberger, *Fuel Cells Seminar Abstract*, Long Beach, California, 1964 (1988).

78. Winsel, A., O. Fuhrer, K. Ruthling and C. Fischer, *Ber. Bunsenges. Phys. Chem.*, **94**,926 (1990).

79. Schautz, M., *Doctoral Dissertation at The Technical University Graz*, Austria (1984).

80. Jahangir, S., M., *Doctoral Dissertation at The Technical University Graz*, Austria (1984).

81. Clark, M.B., W.G. Darland and K.V. Kordesch, *18th Ann Power Sources Cof.*, Atlantic City, 11 (1964).

82. Kordesch, K.D. , *18th Ann Power Sources Cof.*, Atlantic City, 17 (1965).

83. Watanabe, M., M. Tomikawa and S.Motoo, *Journal of Electroanalytical Chemistry*, **182**, 193 (1985).

84. Watanabe, M., M.Tozawa and S.Motoo, *Journal of Electroanalytical Society*, **183**, 391 (1985).

85. Watanabe, M., K.Makita and S.Motoo, *Journal of Electroanlytical Chemistry*, **197**, 195 (1986).

86. Rangarajan, S.K., *Curr. Sci.*, **40**, No. 8,175 (1971).

87. Tilak, B.V., Yeo, R.S., Srinivasan., Comprehensive Treatise of Electrochemistry, Plenum Press, 3, 39 (1981).

88. Austin, L.G., Ariet, M., Walker, R.D., Wood, G.B., Comyn, R.H., *IEC Fundamentals*, **4**, 321 (1965).

89. Srinivasan, S., Hurwitz, N.D., Bockris, J.O.M., *J. Chem.* **12**, 46, 3108 (1967).

90. Srinivasan, S., Hurwitz, *Electrochim. Acta*, **12**,495 (1967).

91. Bockris, J.O.M., Cahan, B.D., *J. Chem. Phys.*, **50**, 1307 (1969).

92. Grens, E.A., Turner, R.M., Katan, T., *Adv. Energy Conv.*, **4**,109 (1964).

93. Ruetschi, P., Ockerman, J.B., *J. Electrochem. Soc.*, **116**, No. 9, 1222 (1969).

94. Will, F.G., Ben, D. D. J., *J. Electrochem. Soc.*, **116**, No. 7, 933 (1969).

95. Moren, C., *J. Electrochem. Soc.*, **122**, No. 4, 500 (1975).

96. Will, F.G., *J. Electrochem. Soc.*, **110**, 145 (1963).

97. Will, F.G., *J. Electrochem. Soc.*, **110**, 152 (1963).

98. Iczkowski, R.P., *J. Electrochem. Soc.*, **111**, 1078 (1964).

99. Rockett, J.A., Brown R., *J. Electrochem. Soc.*, **113**, 207 (1966).

100. Lindstrom, O., *Tek. Tidskr*, **23**,593 (1963).

101. Lindstrom, O., *Meeting American Chemical Society, De. Fuel Chemistry*, Sept (1967).

102. Bennion, D.N., Tobias, C.W., *J. Electrochem. Soc.*, **113**, 593 (1966).

103. Mund, K., *Siemens Forsch, Entwicklungsbu*, **4**, 1 (1975).

104. Mund, K., Ritcher, G., Von Sturm, F., *J. Electrochem. Soc.*, **124**, 1 (1977).

105. Kenjo, T., Nakajima, N., *Bull. Chem. Soc. Jpn*, **56**, (1983).

106. Chan, K.Y., Efthymiou, G.S., Cochetto, J.F., *Electrochim. Acta.*, **32**, 1227 (1987).

107. Chirkov, Y.G., *Sov. Electrochem.*, **8**, 358 (1972).

108. Pshenichnikov, A.G., Kruyukov, Y.K., Burshtein, R. K., Astakhov, I.I., Surikov, V.V., *Sov. Electrochem*, **12**, 1183 (1976).

109. Pshenichnikov, A.G., *Sov. Electrochem.*, **6**, 644 (1970).

110. Burshtein, R.K., Dribinskii, A.V., Tarasevich, M.R., Chizmadzhev, Y.A., Chirkov, Y.G., *Sov. Electrochem.*, **7**, 1762 (1971).

111. Chirkov, Y.G., *Sov. Electrochem.*, **11**, 36 (1975).

112. Vol'fkovich, Y. M., *Electrokhimiya*, **19**, 237 (1983).

113. Vol'fkovich, Y.M., Shkol'nikov, E.K., *Sov. Electrochem.*, 19, 586 (1983).

114. Sakellarapoulos, G.P., Langer, S.H., *AIChE J.*, **24**, 1115 (1978).

115. Giner, J., Hunter, C., *J. Electrochem Soc.*, **116**, 1124 (1969).

116. Giner, J. in *"From Electrocatalysis to Fuel Cells"*, Ed. G. Sandstede, Univ. of Washington Press, Seattle (1972).

117. Iczkowskii, R.P., Cutlip, M.B., *J. Electrochem Soc.*, **127**, 1433 (1980).

118. Bjornbom, P., *Electrochim. Acta*, **32**, 115 (1987).

119. Vitanen, M., and M.J. Lampinen, *J. Power Sources*, **32**, 207 (1990).

120. Celiker, H., *Ph.D. Thesis, King Fahd University of Petroleum and Minerals*, 1990.

121. Celiker, H., M.A.Al-Saleh, S.Gultekin and A.S.Al-Zakri, *Journal of the Electrochemical Society*, **138**, 6, 1991.

122. Kimble, M.C., *Ph.D. Thesis, Texas A & M University*, 1991.

123. Kimble, M.C., R.E. White, *J. Electrochem. Soc.*, **138**, 3370 (1991).

124. Kimble, M.C., R.E. White, *J. Electrochem. Soc.*, **139**, 478 (1992).

125. Yang, S.C. and P. Bjornbom, Eletrochim. Acta, 37, 1831 (1992).

3

Electrode Preparation by Filtration Method

3.1. Introduction

There are essentially two methods of making single-layered, hydrophobic, PTFE-bonded gas diffusion electrodes, namely; 'wet method' and 'dry method'. The electrodes made according to the dry method are thin and inexpensive. In this method, expensive PTFE emulsion is not used. On the other hand the activity of the electrodes is somewhat lower than those of made by the wet method (1). As both of the methods use the same catalyst this difference in the apparent activity is due to the structure of the electrode. In this work, a novel method which is called Filtration Method, is introduced which eliminates the problem of the structure to certain extent.

Another problem identified in the electrode preparation is related to the passivation of the freshly leached Raney-Ni catalyst. The conventional method of the passivation has some demerits. In order to deal with these problems, a treatment with H_2O_2 is proposed in this work for passivation.

3.2. Dry Method

The dry method was proposed by Sauer(2). and improved by Winsel(3,4). In this method the passivated catalyst is milled with PTFE in a high speed mixer having sharp knives. In this process PTFE particles fragment into tiny particles, which partially coat the catalyst particles. Cooling of the catalyst while milling further assists in this process(5). As a result of this process which is known as *reactive mixing*, a fluffy mass of the powder is produced. This fluffy powder is rolled to obtain a catalyst tape. In a subsequent step the catalyst tape is rolled with nickel screen which works as charge collector and provides mechanical strength. The methods suffers from following disadvantages:

1. While rolling the dry powder, high rolling pressure is required which results into higher diaphragm resistance and builds up a diffusion barrier for the reactant gas (6).
2. Powder rolling is not well understood.
3. While rolling the fluffy mass of powder, control on the flow rate of the powder into nip of the rolls is difficult and subjective. The varying flow rate results into uneven electrode morphology.
4. Rolling of the powder can take place successfully at a narrow range of the parameters. As contraints on the parameters are increased the optimization becomes difficult.
5. The reproducibility is not ensured as uncontrollable variables come into the picture.
6. It involves wastage of catalyst.

3.3. The Filtration Method

In order to take care of the disadvantages of the dry method a new method called *"Filtration Method"* is introduced and tested in this work. Until the fluffy powder of catalyst and PTFE from the reactive mixing is produced the steps are similar to those of dry method. Instead of making catalyst tape by cold rolling of the dry powder, a slurry of the milled catalyst is made using a suitable surfactant. When foams are broken, this slurry is filtered on a filter paper by the application of regulated vacuum. This results into a uniform filter-cake. The filter-cake with the filter paper is air dried. After drying the filter cake is rolled with the nickel screen. In this step the catalyst web is transferred to the nickel mesh from the filter paper. Some traces of the surfactant are present in the electrode. This is removed by boiling in acetone to get the final electrode.

3.4. Advantages of the Filtration Method

The newly developed method in this work has the following advantages :

1. The uniformity in the thickness of the electrode is ensured.
2. The macroporosity of the electrode can be controlled.
3. High compaction pressure is not required therefore the diaphragm resistance in the electrode is low.
4. The preparation parameters e.g. PTFE content can be varied in a wider range.
5. Mass production of the electrodes is easily possible and can be controlled.
6. Filtration is a well understood process to the chemical engineers.

3.5. Passivation of the Raney-Ni Catalyst

3.5.1. Conventional Method

During leaching of Raney-Ni, due to its very fine microporous structure and adsorption of hydrogen produced in the reaction, the catalyst becomes pyrophoric and therefore not stable in air. For making electrode, it has to be passivated. In the conventional method which is described in detail in an article by Ewe et al.(7), the catalyst is oxidized in a controlled and slow process in presence of oxygen gas. To carry out passivation as a first step, freshly leached catalyst is repetitively washed with distilled water till all the aluminum salts produced are removed. The washed catalyst is dried under vacuum at low temperatures (20 -40°C). When the catalyst is dry a small volume of oxygen is introduced. As a result the adsorbed hydrogen is oxidized to form water. By this gradual addition of oxygen, a water film is formed over the catalyst surface if the catalyst is not heated. This film retards the process of oxidation due to diffusion resistance. Further addition of the gas results into partial oxidation of Ni surface to NiO and $Ni(OH)_2$. The Kinetics of nickel oxidation depend significantly on the water film.

This is performed in an apparatus as show in Fig 3.1. The reaction chamber is made of quartz tube which is connected in a ground quartz plug. It is connected to the vacuum pump via two valves; SV1 (a solenoid valve) and NV1 (a needle valve). A thermocouple which is right in the catalyst is connected to temperature controller which operetes SV1 and SV2. A U-tube manometer, with two contacts placed between the inlet values and the reaction chamber, is used as pressure controlling device.

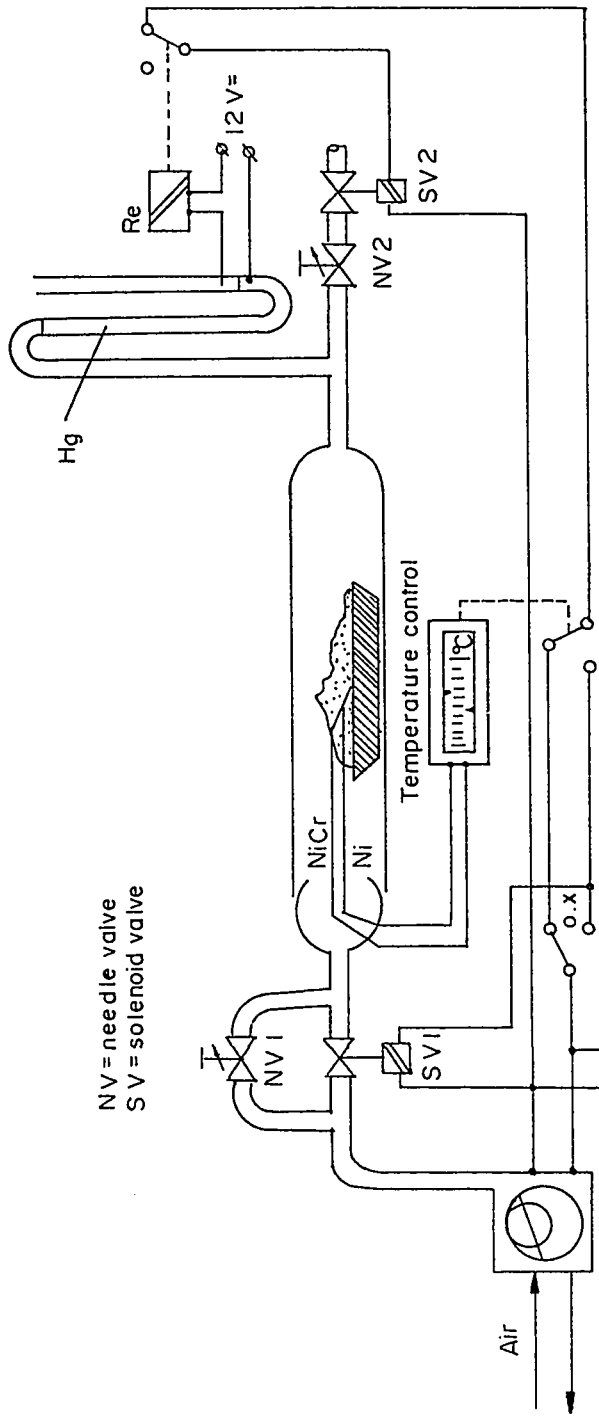

Fig. 3.1 : Apparatus for Passivation by Conventional Method (7)

It is found that this method is slow, tedious, and involves expensive equipment e.g. vacuum pump, vacuum chamber, controllers etc. Moreover any accidental leak of air in the system will suddenly raise the temperature and cause catalyst sintering.

3.5.2. Passivation by H_2O_2 Treatment

H_2O_2 treatment for the passivation of Raney-Ni catalyst is introduced in this work. A diluted solution of H_2O_2 is added to the freshly leached and washed catalyst. When H_2O_2 comes in contact with Ni particles it decomposes and the following exothermic reaction takes place:

$$2H_2O_2 \rightarrow O_2 + 2H_2O$$

There are two possibilities of oxidation of hydrogen adsorbed on Ni, in this situation. The first one is that the hydrogen may directly react with H_2O_2 as per following reaction

$$2H_2O_2 + H_2 \rightarrow 2H_2O$$

Another possibility is that the oxygen produced by decomposition of H_2O_2 in the presence of Ni oxidize the hydrogen :

$$2H_2 + O_2 \rightarrow 2H_2O$$

All of these reactions are exothermic and generate considerable heat. As the reaction is taking place in aqueous medium, the heat generated will be taken away by water. This avoids excessive heating of the catalyst. Therefore sintering in this

method is highly unlikely. Moreover the temperature of the reaction mixture can be controlled by putting the reactor in a cold water / ice bath.

An apparatus as shown in Fig. 3.2 is made for H_2O_2 treatment. The reactor has three necks which accommodate a thermometer, a stirrer and a funnel. The whole assembly is kept in water bath. A known volume of H_2O_2 solution with known concentration is poured into the reactor. Subsequently the catalyst is added and stirring is started. A vigorous reaction takes place with bubbling and effervescence. The reaction is allowed to go on till visible bubbling and effervescence is stopped.

The catalyst is filtered and dried in vacuum under nitrogen atmosphere. After drying the catalyst is taken out in air and is observed carefully. If the catalyst is successfully passivated no visual burning or rise in temperature should take place. Some preliminary runs using these methods have been performed. The results are discussed in Chapter 8. This method has several advantages over the conventional method. Among these advantages are :

1. Fast passivation
2. Simple apparatus is required
3. Expensive equipment are not used.
4. Vacuum is not used.
5. Catalyst sintering is highly unlikely.

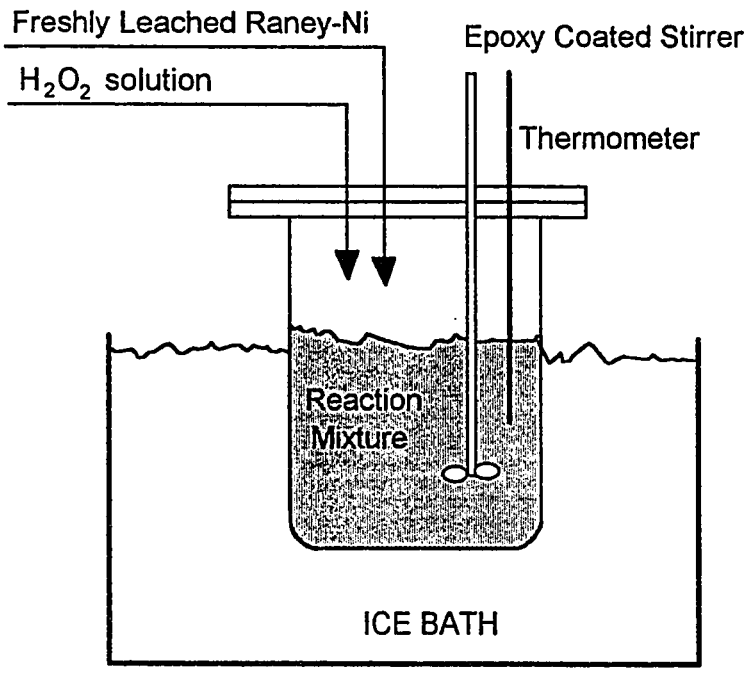

Fig. 3.2 : Apparatus for Passivation by H_2O_2 Treatment

References

1. Jensiet, W., A.Khalil and H.Wendt, *Journal of Applied Electrochemisty*, **20**,893 (1990).

2. Sauer, H. *German Patent* **D.E-O.S. 2941774** (1979).

3. Winsel, A., *German Patent* **D.E.-O.S. 3710168** (1987).

4. Winsel, A., O. Fuhrer, K. Ruthling and C. Fischer, *Ber. Bunsenges. Phys. Chem.*, 94,926 (1990).

5. Bolvin, K., E.Gulzow and W. Schnurnberger, *Fuel Cells Seminar Abstract*, Long Beach, California, 1964 (1988).

6. Kohler, B. and A. Winsel, *Z. Naturforsch.*, **19a**, 602 (1964).

7. Ewe, H., E.W. Justi and H.J. Sebach, *Energy Conversion and Management*, **23**, No. 4, 245 (1983).

4

Experimental Procedure and the Set-Up

4.1. Preparation of the Gas Diffusion Electrodes

4.1.1. Introduction

The proposed 'Filtration method' is used to make gas diffusion electrode. The principle of this method is discussed in Chapter 3. It involves making a slurry of the catalyst which is already milled with a suitable binder. The resultant slurry is subsequently filtered with the help of vacuum. A uniform filter cake is produced which is rolled with a metallic mesh followed by removal of the surfactant. A flow-diagram of the electrode preparations indicating the major steps is given in Fig 4.1. The detailed procedure is described in the following sections.

4.1.2. Materials Used

A. Raney Ni- Al alloy

This is the starting material for making the catalyst. The alloy contains equal mass of nickel and aluminum. The alloy is virtually non-porous. Some of its properties are listed in Table 4.1. The material was procured from Merch-schuchardt, Germany (Art. # 820875).

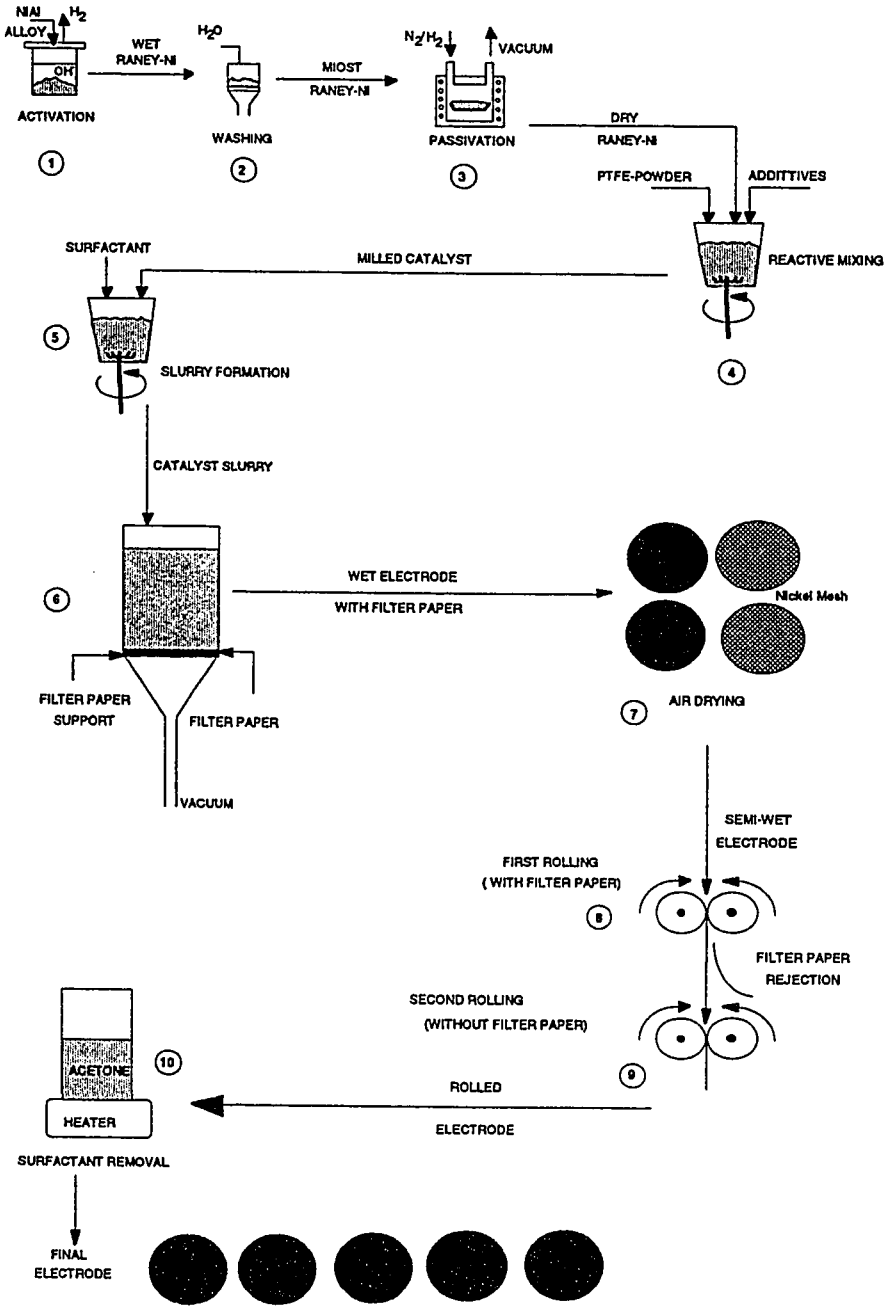

Fig. 4.1 : Flow-diagram of Electrode Preparation by Filtration Method

Table 4.1: Properties of Raney-Ni-Al Alloy

Chemical Composition	
• Ni Content	50.0 wt %
• Al Content	50.0 wt %
Solid Phase Density	4.1 g/cm^3
Particle Density	3.99g/cm^3
Porosity	0.027
Pore Volume	0.007cm$^{3/g}$

B. Nickel Mesh

A metallic wire mesh is used as current collector and to provide mechanical strength. For making Ni electrodes a nickel mesh was used. It has mesh size equivalent to 40 wires per inch. The diameter of the wires is 0.013mm.

C. The PTFE Powder

The Polytetrafluoroethylene (PTFE or Teflon) is used in the powder form under the trade name Hostaflon TF 2053 manufactured by Hoechst, Germany. The powder was made by pulverization. In Fig. 4.2 an SEM micrograph of this powder is shown.

D. Potassium Hydroxide

The potassium hydroxide was chosen as electrolyte due to its high electrical conductivity. The material was obtained from BDH (AnalaR, CAS # 130-58-3). The conductivity of the KOH solution depends on its concentration and temperature. An empirical relationship between these variables is available (1). The optimum concentration at any temperature from this relation can easily be estimated. At room temperature it comes out to be 30%.

E. Surfactants

Following two commercially available surfactant were used to make the catalyst slurry.

1. Brij 96 (Polyoxyethylene{10} olyl ether)
2. Triton X-100 (iso-octylphenoxypolyethoxyethanol, a nonionic surfactant, CAS # 9002-93-1)

Fig. 4.2 : SEM Micrograph of PTFE Particles

4.1.3. Prepration of the catalyst

A. Leaching of Raney-Ni-Al Alloy

The starting material for making the catalyst is alloy of Nickel and aluminum 50-50 % by weight. The material is a finely ground powder. In order to make catalyst, aluminum is to be removed which results into a microporous structure. This is done by leaching with 25% NaOH solution. Following chemical reaction takes place in this process :

$$Al + 3NaOH \rightarrow Na_3AlO_3 + \frac{3}{2}H_2$$

The parameters used in this experiment were chosen on the basis of experimental study done by Choudhary and Choudhary (2). These parameters are listed in Table 4.2. An apparatus as shown in Fig. 4.3 was made to carry out the leaching of Ranny-Ni alloy. As a result a fine black powder is produced. Part of the hydrogen produced in the reaction is adsorbed on freshly available nickel sites. This nascent hydrogen makes the catalyst highly pyrophoric.

B. Washing of the catalyst

The aluminum compounds produced during the leaching process may plug the microporous structure of the catalyst. It is therefore deemed necessary to remove these soluble salts. It is done by washing the catalyst with distilled water. It is done in a continuously stirred glass vessel as shown in Fig 4.4. The bottom is made of fritted glass. To remove the wash water, vacuum is applied intermittently and pH is measured with the help of a pH meter. It was observed that when pH is reached near neutral, most of the aluminum salt was removed. Therefore washing was stopped when the pH has reached neutral.

Table 4.2: Parameters of Leaching.

Parameter	Value
Temperature, K	343
Concentration of NaOH, mmol/cm^3	6.25
Time, minutes	80
Speed of the stirrer, RPM	1000

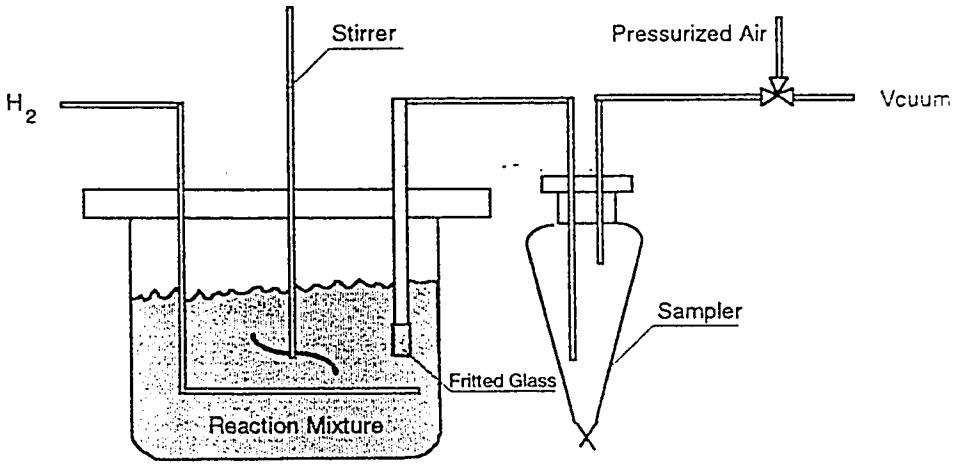

Fig. 4.3 : Apparatus for Leaching of Raney-Ni Alloy

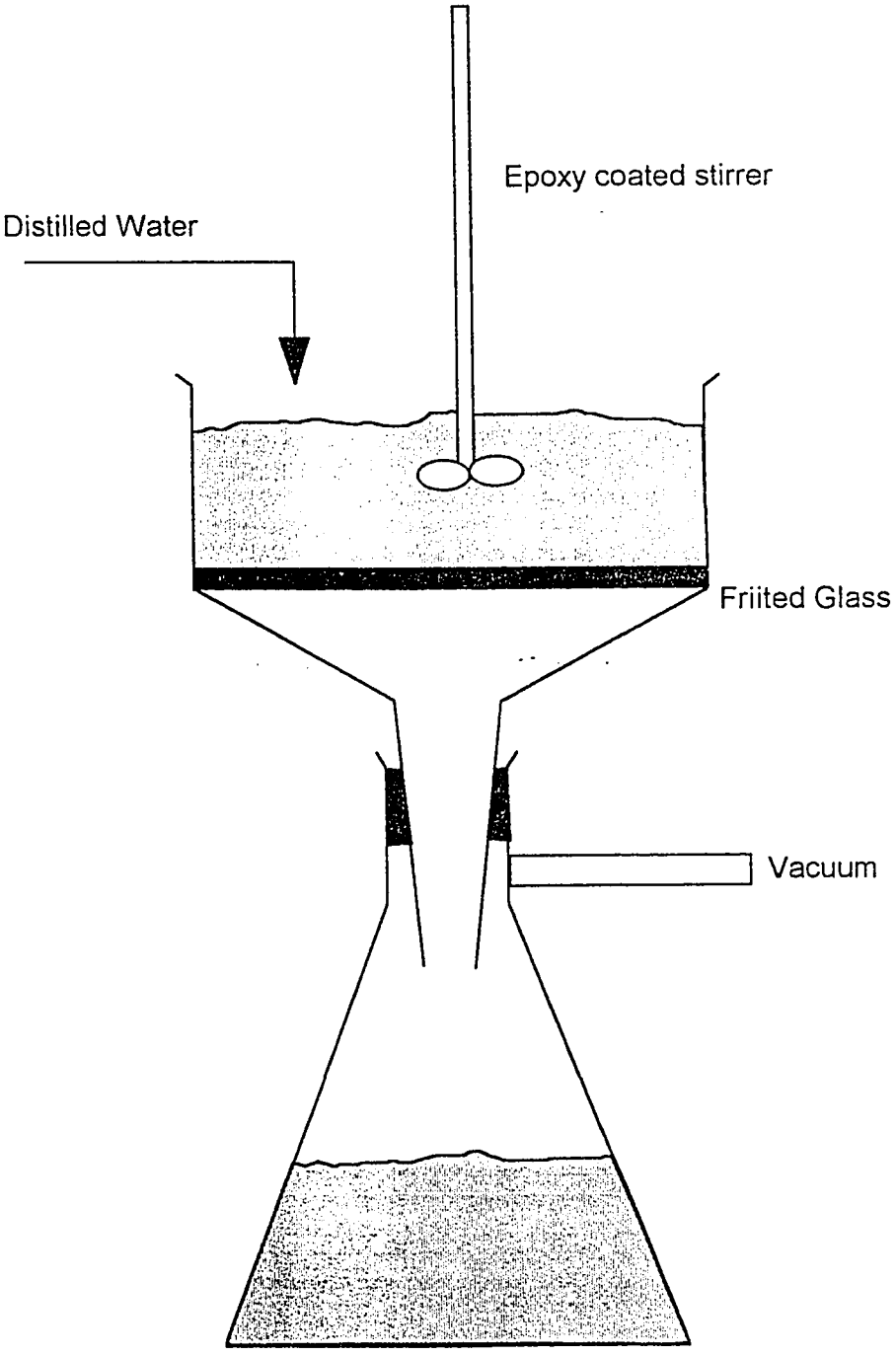

Fig. 4.4 : Apparatus for Washing the Leached Raney-Ni

C. Passivation of Raney- Ni catalyst

In the process of leaching the hydrogen gas evolves. This nascent hydrogen adsorbs on Ni-sites. The amount of this hydrogen is sufficient to make the catalyst highly pyrophoric. It burns as soon as it comes in direct contact with air or oxygen. This makes handling of catalyst very difficult. Therefore the catalyst has to be stabilized or passivated before making the electrodes. The passivation is done by controlled oxidation of the catalyst. A special apparatus is made for this purpose. A schematic diagram is shown in Fig. 4.5. A known mass of washed catalyst, which is still wet, is placed into a vacuum oven, using a stainless steel dish. Approximately 300 mbar pressure is maintained in the oven. Nitrogen gas is introduced into the oven till the pressure is atmospheric. The pressure is reduced to 300 mbar again by applying vacuum. This process is repeated 6-7 times to ensure the inert atmosphere. The temperature in the oven is maintain at 40 °C. The catalyst is left in this condition for several hours. The changes in the catalyst is observed intermittently through the viewing window of the oven. Once the catalyst powder looks dried, a small dose of oxygen is introduced into the oven till the pressure is 400 mbar. While doing this, the temperature of the catalyst is observed carefully. If the temperature rises sharply the nitrogen gas is purged into the oven. After waiting approximately half an hour this process is repeated. The introduction of small doses is continued till atmospheric pressure is reached. A small sample of dry catalyst is kept in a watch-glass and observed carefully. If the catalyst is successfully passivated, no visual burning should occur. As a final check the catalyst is characterized for BET surface area and XRD. A sample is observed though scanning electron microscope to observe any accidental burning.

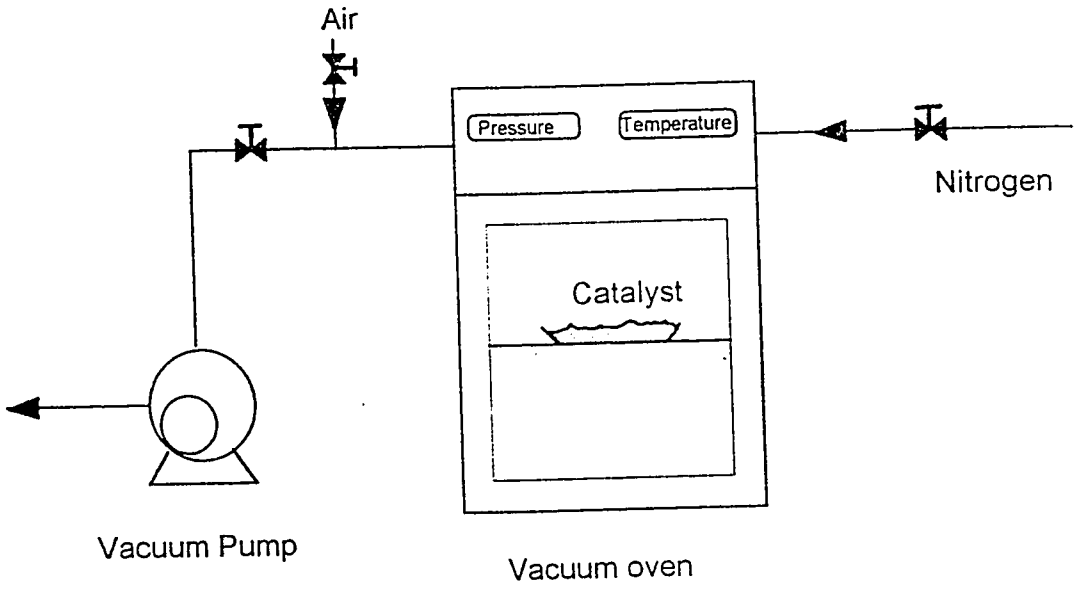

Fig. 4.5 : Apparatus for Conventional Controlled Surface Oxidation

4.1.4. Reactive Mixing

To incorporate hydrophobicity in the electrode and to provide required bonding for mechanical strength, a binder is added to the catalyst. In this work PTFE is selected for this purpose. It is mixed with the catalyst by a method purposed by Winsel et al.(3) which is known as reactive mixing. In this method a predetermined quantity is blended with the catalyst. The mixture is mixed with the help of a glass rod till PTFE particles are apparently disappeared. This mixture is transferred into a special high speed (20000 RPM) grinder. This grinder has two sharp knives and has provision of cold water circulation for cooling the catalyst. The catalyst is milled in this grinder for a required time period. While milling, the mixer is vigorously tumbled to avoid dead zones in the mixer. A photograph of this mixer is shown in Fig. 4.6.

4.1.5. Preparation of Slurry

The most important step in making the slurry is the selection of surfactant. As very stable suspension is not required, the main function of the surfactant is wetting. The surfactant must not generate too much foams, as it affects the formation of the filter-cake. Considering these requirements two surfactant were selected, namely Brij-96 and Triton X-100. A predetermined quantity of milled catalyst required for the desired catalyst loading is transferred to the mixer. Before pouring the water into the mixer, surfactant is added. This mixture is blended till visual dispersion is achieved. The foams and surds are broken by air to achieve foam-free slurry. This slurry is transferred to a beaker.

4.1.6. Formation of the Filter-cake

In this method filtration is used to form a uniform filter-cake of catalyst to obtain a uniform electrode. This is done in a vacuum filtration apparatus. This apparatus is

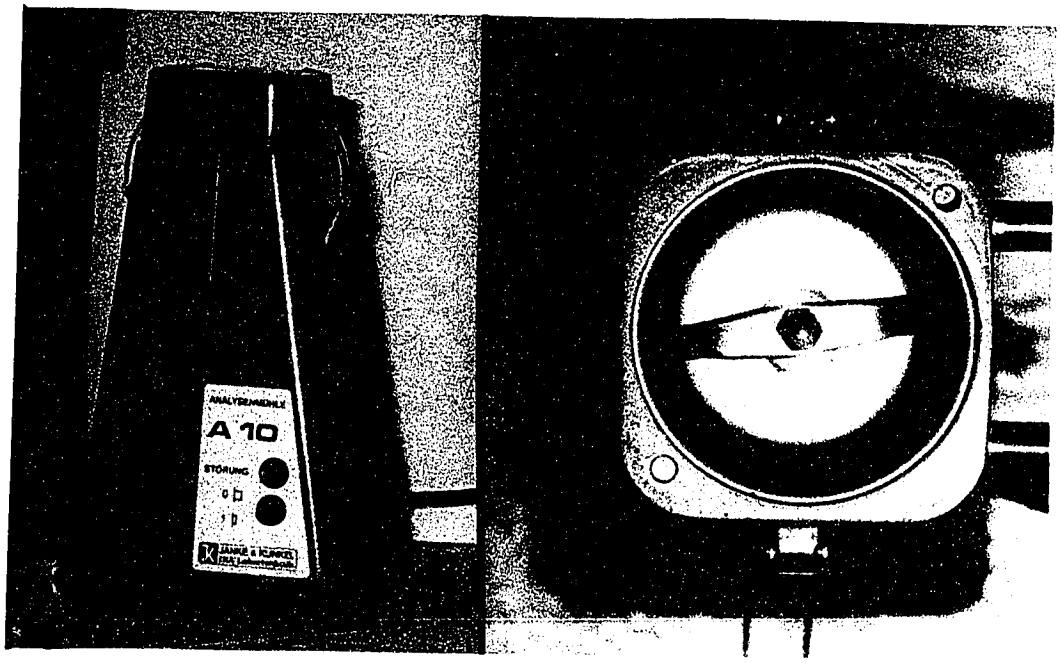

Fig. 4.6 : High Speed Mill for Reactive Mixing

shown in Fig. 4.7. A Whatman filter paper No. 42 is used for filtration. The filter paper is wetted with the water prior to transferring into Buchner Funnel. The Buckner Funnel is mounted on a conical flask. The conical flask is connected to a vacuum pump via a vacuum regulator. Before decanting the catalyst slurry into the Buchner funnel apparatus is leveled with the help of a spirit level. The vacuum maintained in this step is approximately 500 mbar. After some time the vacuum is increased to 300 mbar. At this vacuum level all of the slurry water is allowed to filter out. As a result of this process, a uniform filter cake is formed on the filter paper. This filter cake with the filter paper is carefully removed from the Buchner Funnel. The cake is allowed to dry in air for the couple of hours. Special care must be taken while handling this cake because it is fragile as catalyst particles did not form bonds.

4.1.7. Cold Rolling

A pre-cut and pre-rolled metallic mesh is placed over the air dried filter cake. A filter paper is placed over the metallic mesh. This whole assembly is to be rolled at room temperature in a rolling machine. While rolling, the clearance between the rolling machine rolls is maintained as desired. A photograph of the rolling machine used in this work is shown in Fig. 4.8. The filter papers from the rolled assembly are carefully removed. As the result of this step the catalyst web is transferred onto the metallic mesh. This web with the mesh is rolled again without filter paper to incorporate strength. This is done by second cold rolling while maintaining a desired clearance. The clearance in the second rolling must be lesser then that of first rolling.

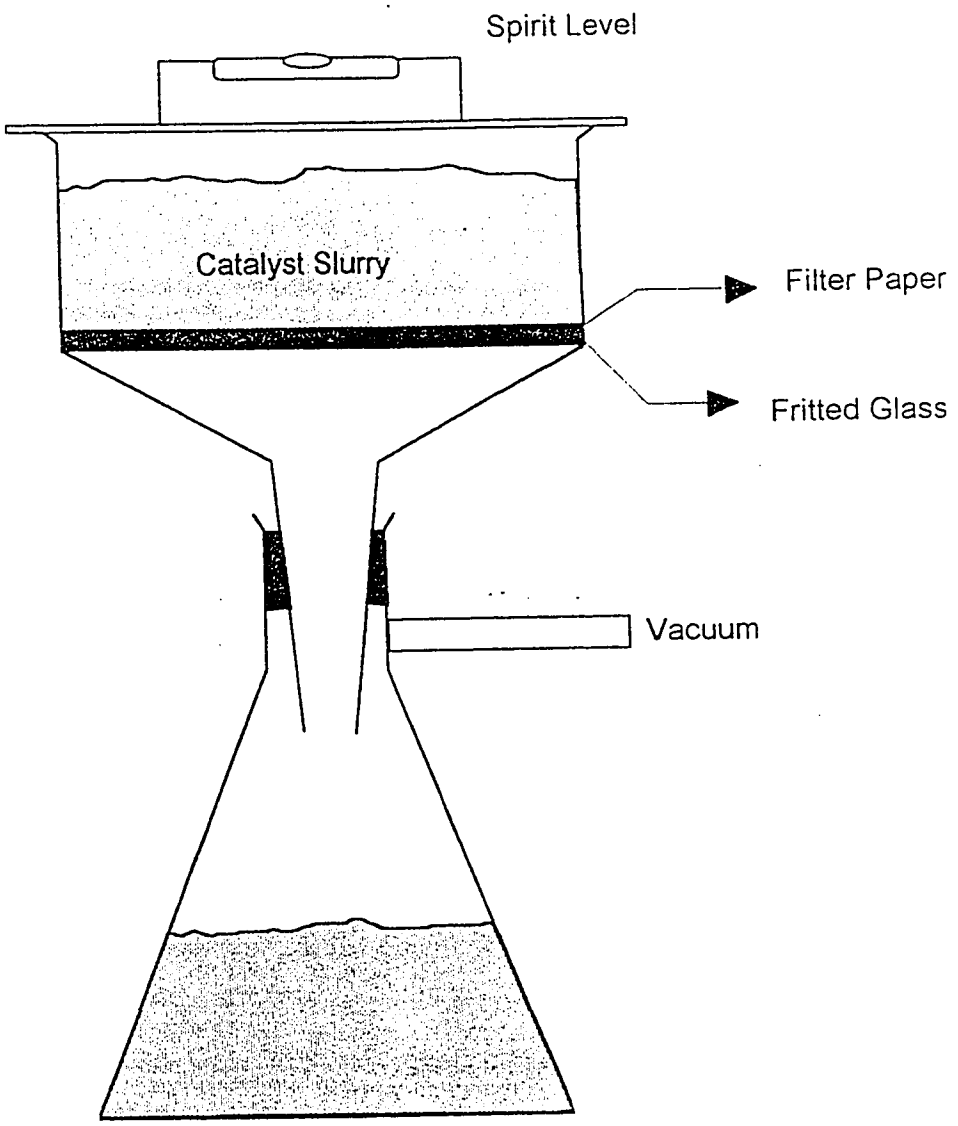

Fig. 4.7 : Apparatus for Electrode Formation by filtration Method

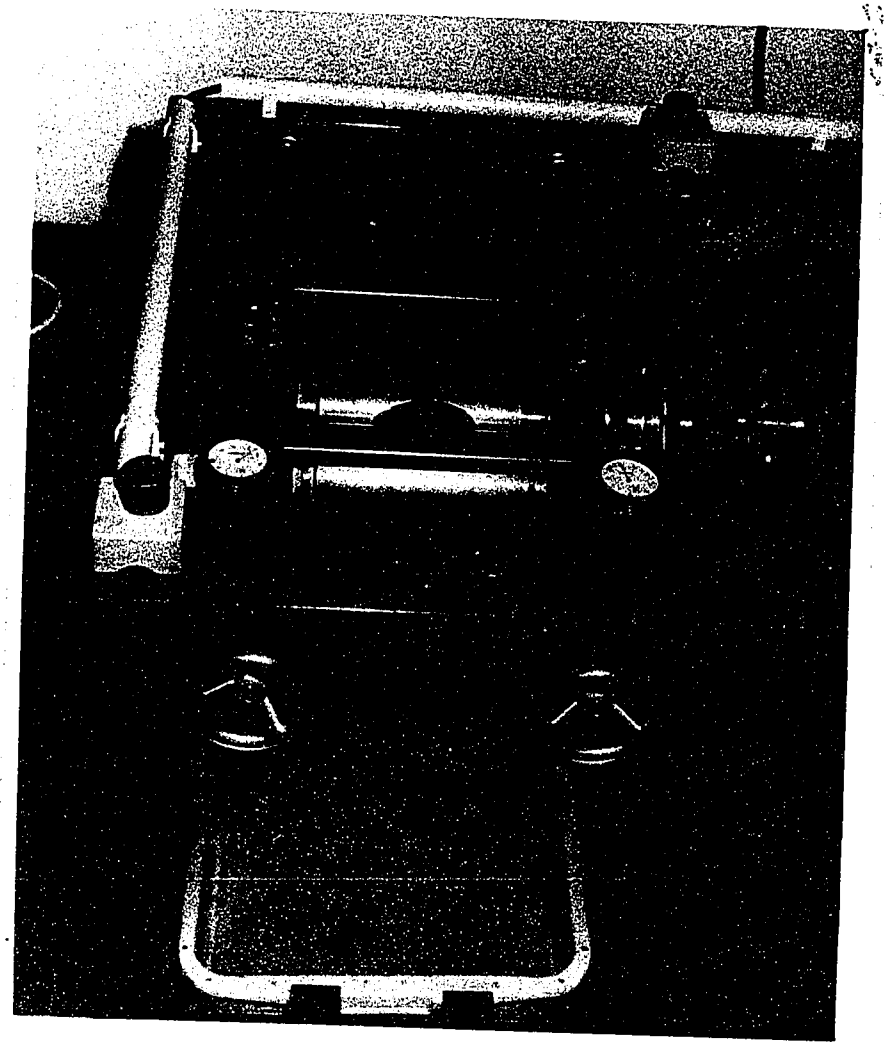

Fig. 4.8 : The Rolling machine

4.1.8. Removal of the Surfactant

While making slurry, a surfactant is added. The traces of this surfactant are present in the freshly made electrode. The presence of surfactant traces is detrimental to the performance of the electrode. Therefore the removal of surfactant is imperative. Through some preliminary trials, it was found that the surfactant is easily soluble in acetone. Considering this, the freshly made electrode is boiled in acetone for 5 minutes to remove the surfactant.

4.2. Testing of the Electrode Performance

4.2.1. Introduction

The electrode produced by conventional dry method and the filtration method are tested for the performance. For this purpose, polarization curves were obtained for the electrodes using a half-cell. The half-cell set-up, instrumentation, procedure for activation of hydrogen electrode and procedure of obtaining polarization data are discussed in this section. A general view of the testing facility is shown in Fig. 4.8.

4.2.2. The Half-cell Set-up

A schematic diagram of the half-cell assembly used is show in Fig. 4.9. The half-cell used in these experiments was fabricated from Plexi-Glass and consisted of a gas chamber and a rectangular piece which housed the gas diffusion electrode, a ring shaped sheet of PTFE sealing and a pair of nickel wire current collectors. The rectangular piece is screwed to the gas chamber with stainless steel screws. The half-cell is mounted into a PTFE container which is filled with the electrolyte such that the electrode was completely submerged. A 2.5x2.5 cm^2 nickel foil which is welded on a nickel rod, worked as a counter electrode. This counter electrode is mounted onto the Plexi-glass lid of the half-cell container made of PTFE. The

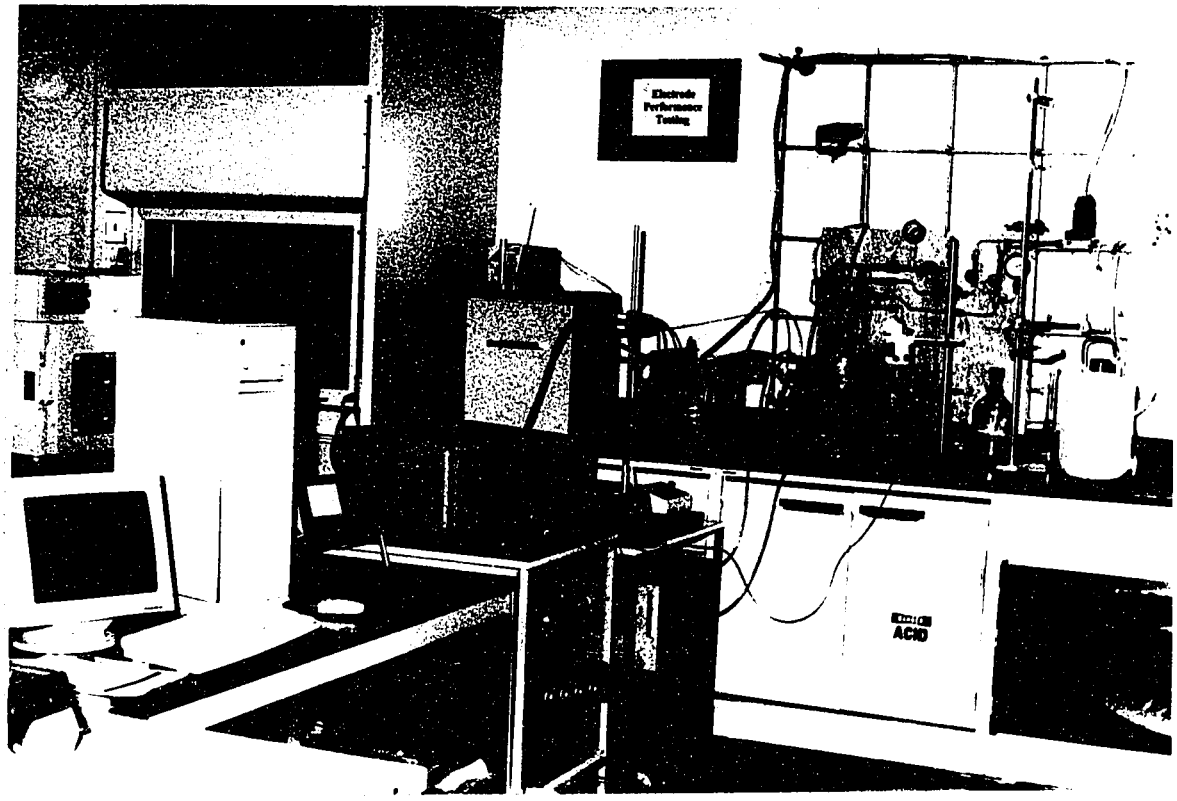

Fig. 4.9 : General View of the Performance Testing Set-up

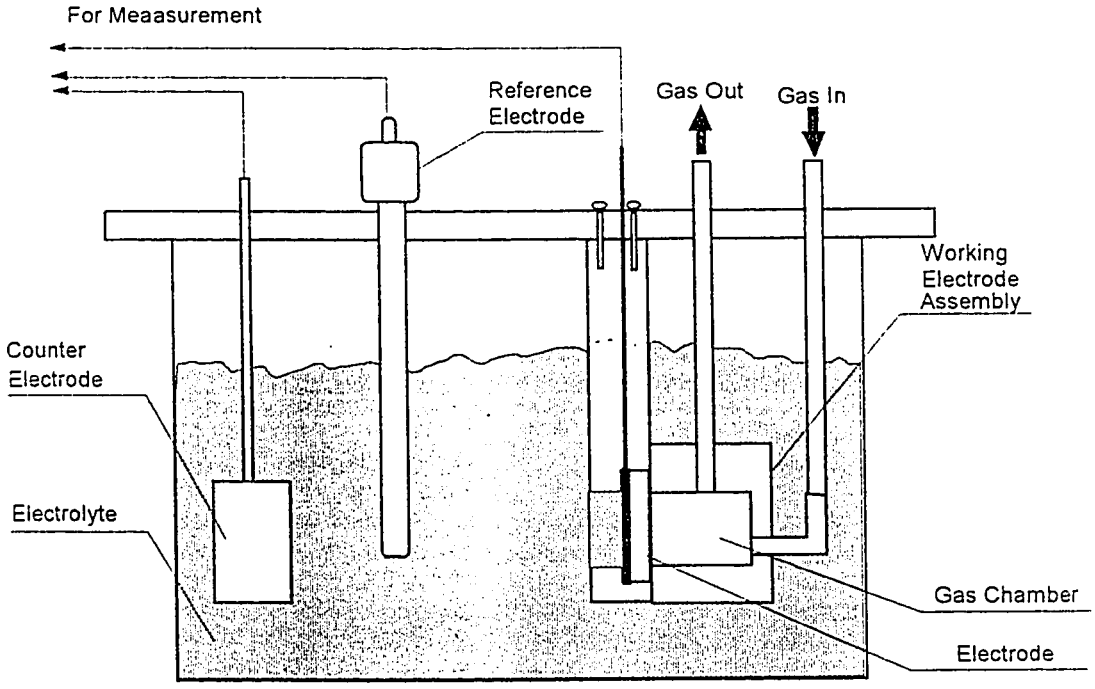

Fig. 4.10 : Schematic Diagram of the Half-cell Assembly

reference electrode used is a commercially available Hg/HgO electrode filled with the 25% KOH solution. It is fixed in the electrolyte near the working electrode through an opening on the lid of PTFE container. The gas chamber of the half cell has inlet and outlet via PTFE fittings which were sealed properly with Teflon tape. The inlet gas is introduced through the side of the gas chamber while the outlet gas leaves through the top of the gas chamber. The gas cylinder is connected to the half-cell inlet via a regulator, Brooks controller, and a pressure gauge as shown in the Fig. 4.10. The outlet gas tubing has control valve to apply required back pressure. The outlet tubing is left in an exhaust gas hood. The flow rate of the gas is calibrated with the help of soap bubble to standardized the Brook controller.

4.2.3. Procedure of Activation and Measurement of Polarization

A. Potentiostat and Related Circuit

A potentiostat/galvanostat is used for controlling and measuring current and potential of the working electrode in the half cell against a reference electrode (an Hg/HgO electrode) as well as the IR drop in the electrolyte. The potentiostat used was Model-273A manufactured by EG & G Princeton Applied Research, Princeton, New Jersey, USA. The equipment has in-built IR compensation facility using two methods; positive feedback and current interruption. The potentiostat has two computer interfaces the RS232-C and IEEE-488 (for General purpose Interface Board).

The potentiostat has its own microprocessor. The microprocessor recognizes a set of commands. These commands are described in Model 273A manual(4). These commands can be given through a computer. This can be done by connecting a computer to either RS-232C or GPIB interface available in the potentiostat. In the absence of a GPIB card, the potentiostat was connected to the serial port of the

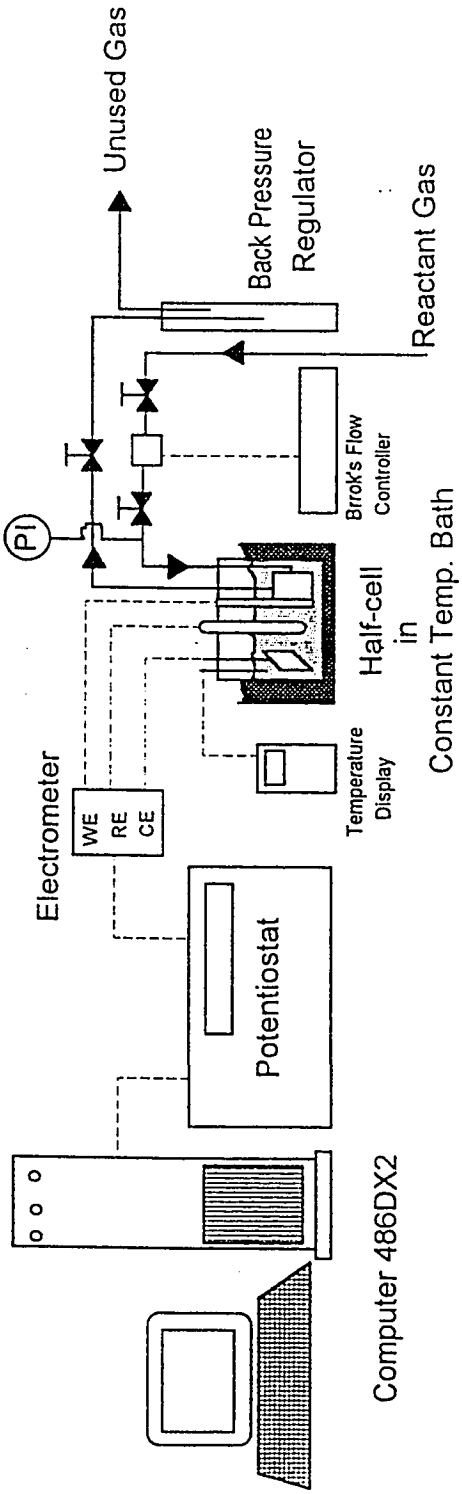

Fig. 4.11 : Schematic Diagram of the Set-up for Performance Testing

computer via RS-232C interface with the help of a null modem cable. For this purpose a Gateway-2000, IBM -486/DX2 personal computer was utilized. In order to check the current and potential from the potentiostat additional voltammeters were connected to the equipment. The circuit diagram with equipment is shown in Fig. 4.10.

B. IR-drop Compensation

In the half-cell set-up, the working electrode is away from the reference electrode. When current is passed in the cell, there will be potential drop due to the resistance of the electrolyte present between these two electrodes. The electrode potential read with respect to the reference electrode incorporates this potential. The actual electrode potential is obtained by subtracting IR drop from this value. There are two methods for estimation of IR-drop namely; positive feed back and current interruption. Both of these methods are available in Model 273A potentiostat.

In the positive feedback technique, and analog positive feedback loop is established from the output of the current measurement circuit to the control amplifier input. The loop gain is set to exactly the value required for compensation. In this method the compensation is continuous i.e. the IR-drop values are continuously generated. The main disadvantages are its tediousness and subjectiveness. It also reduces the stability of the potentiostat. This method is not available when potentiostat is operating in galvanostatic mode.

In the current interruption technique, the current is periodically interrupted and a correction factor is developed based on the potential versus time change that occurs at the moment of an interrupt. The current is interrupted in less than 1

microsecond for approximately 190 microseconds at periodic intervals. When the circuit interrupts, the potential of the electrode drops by a value equal to the IR-drop. As the interrupts are taking place at different points in time, the IR values at different points in the scan are available. This method requires no adjustment in contrast to the positive feedback technique.

However there are strengths an weaknesses of both of the methods. Depending on the use a suitable technique is selected. Table 4.3 gives a quick comparison of these methods. In the present work, as galvanostatic mode is used, IR-drop was compensated using current interruption method.

C. Activation of Passivated Raney-Ni Electrode.

The passivated electrode was activated by reduction with hydrogen gas while a cathodic current of 25 mA was passed into the working electrode. It is observed that the electrodes gain their full activity if activation is done for 48 hours at 25 ° C or 25 hours at 60 °C. In this work activation was done at 60 °C for 25 hours. The hydrogen gas pressure in the electrode chamber is maintained at 6 psig.

For carrying out the activation, a set of commands was to send to the potentiostat microprocessor. This is performed with the help of a computer program written in 'C'. The program is known as ACTIV. This program generates a file ACTIVE.DAT where the data are stored. An executable file was made which enables running this program from the DOS prompt. The program is shown in Appendix-A.

After 25 hours, activation is automatically stopped. It was made sure that activation was complete. It is done by passing 350 mA anodic current and

Parameter	Positive Feedback	Current Interruption
Speed	Fast	Slow
Ease of use	More difficult	Very simple
Resistance tracking	Does not track	Tracks
Stability	Critical	Very stable
Artifacts	None	Some
E monitoring Compensated	Yes	Yes
Galvanostatic Mode	Not available	Available

Table 4.3 : Comparison of Positive Feedback and Current Interruption

observing potential for ten minutes. If the electrode potential is steady, the activation was deemed completed. This is done by a computer program called TEST as shown in Appendix A.

D. Polarization of Activated Electrodes.

The polarization data of the activated electrodes in the half-cell assembly were obtained galvanostatically. At one point of time a negative current (anodic) was passed into the cell. The potential of the electrode and the IR-drop was measured for ten minutes. During this time, the system goes to steady state and the potential does not change with time. At this point the data for the current, potential and IR-drop were obtained. The whole process is repeated for several currents namely 0 ,5 ,10 ,25 ,50 ,100 ,250, 350, 500, 600, 750, 900 and 1000 mA. It is done with the help a computer program POLA shown in Appendix-A. This program enables the data to store in a file called POLA.DAT. The data from this file are transferred subsequently to LOTUS-123 for plotting.

References

1. A.L.Horwarth, *Handbook of Aqueous Electrolyte Solutions, Physical Properties*, Estimation and Correlations, Ellis Horwood Ltd., England, 252(1985)

2. Winsel, A., *German Patent* **D.E.-O.S. 3710168** (1987).

3. Choudhary, V.R., Chaudhari, S.K. and Gokarn, A.K., *Ind. Eng. Chem. Res.* , **28**, 33-37 (1989).

4. *Model 273A Potentiostat/Galvanostat: Command Handbook*, EG & G Instruments Corporation (1990).

5

Parametric Study of Electrode Preparation by Filtration Method

5.1. Introduction

This chapter essentially has two parts. In the first part an experimental design is utilized to find out the significantly important parameters of electrode preparation by Filtration Method. In the second part effects of various parameters on the electrode performance are presented.

5.2. Experimental Design

During the preliminary experiments of preparing electrodes with filtration method, it was observed that even minor variations in the various parameters affect the performance of the electrodes significantly. In order to get best performance, the parameters which are significantly important are to be recognized. In this context statistical method have been found useful. Among these factorial design is most common in use. Factorial designs have their advantages. The most obvious is that these are more efficient then one-factor-at-a-time experiments. In this regard, the

estimation of relative efficiencies is a good measure of the ease of experimentation. This is defined as number of experiment needed in one-factor-at-a-time method divided by number of experiments in a particular design required to obtain same information. The relative efficiencies are calculated and plotted in Fig. 5.1 (1) for full factorial design. It can be seen that the relative efficiency increases as number of factors are increased.

Another important advantage of using factorial design is that it gives information about the interactions of the parameters. A factorial design is necessary when interactions between the parameter are significant to avoid misleading results. Besides these, factorial designs allow the effects of a factor to be estimated at several levels of the other factors, yielding conclusions that are valid over a range of experimental conditions.

As the number of the factors in full factorial design increases, the number of runs required grow rapidly. In order to keep the number of runs in the pragmatic range, a fraction of the factorial design may be used. This is done by assuming that the high-order interactions are negligible

5.2.1. Parameters Affecting the Performance

A number of the parameters in the preparation of the electrodes by filtration method are identified which affect the performance of the final electrodes. As described elsewhere in this dissertation, the performance of the electrode can be quantified in terms of total IR-free overpotential at certain current density. For this statistical analysis, the response variables chosen therefore are overpotential at 100 mA/cm^2 and 150 mA/cm^2. The overpotential of the electrode at a given current density depends on following parameters :

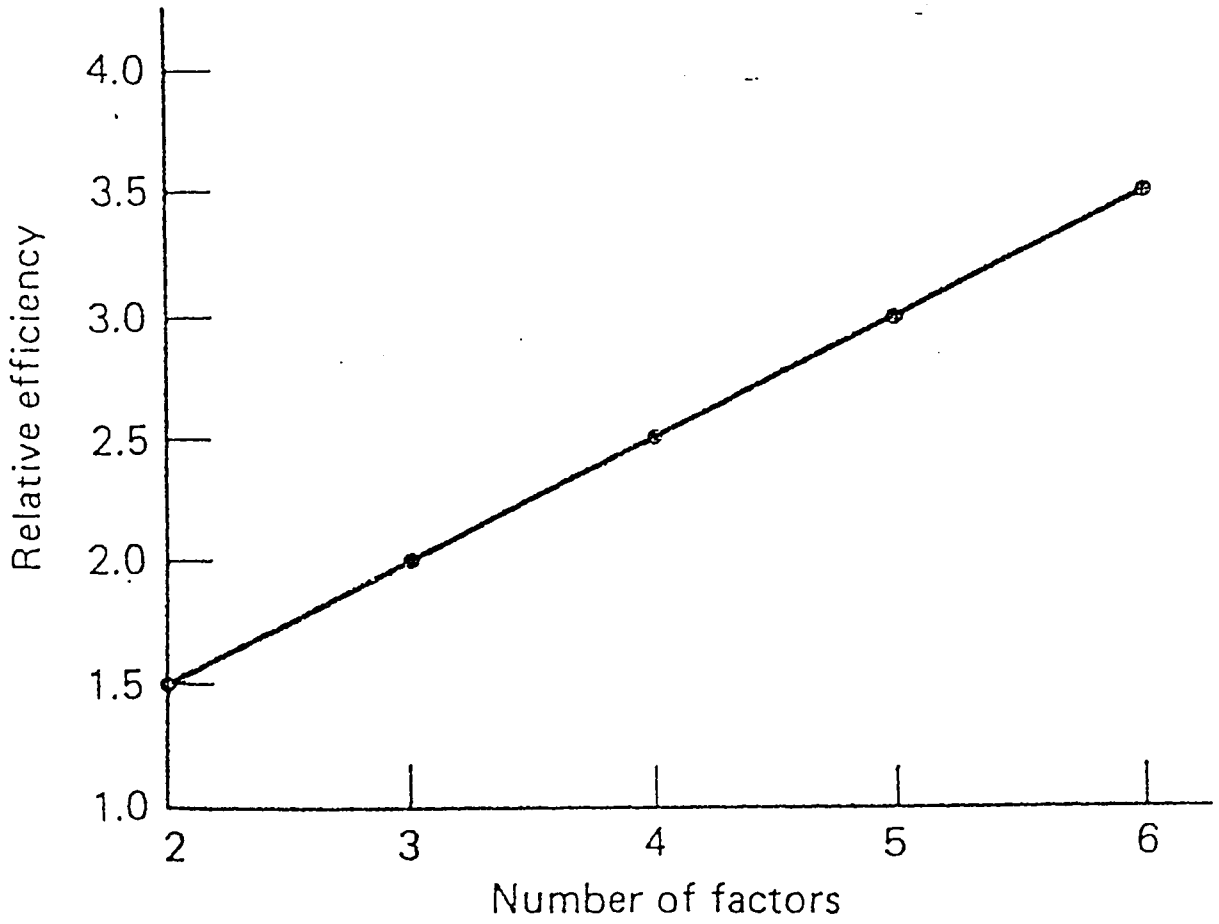

Fig. 5.1: Relative Effectiveness of the Designs (1)

1. Loading of catalyst : Total mass of the catalyst per unit geometric area of the electrode.

2. PTFE content : Mass percent content of PTFE in the electrode.

3. Milling time : The time period for which the catalyst and PTFE were milled.

4. Cooling (On/Off) : Whether the catalyst was cooled with circulating water while milling.

5. Type of surfactant

6. Amount of surfactant : Amount of the surfactant per unit volume of the slurry.

7. Vacuum applied while filtration

8. Clearance of the rolls : Distance between the rolls of the calendar at second rolling of the electrode.

9. Removal of the surfactant :Number of times surfactant was removed from the finished electrode by fresh boiling acetone.

10. Activation time: Time period for which cathodic current was passed in the presence of hydrogen into the electrode for activation.

11. Activation temperature: Temperature at which activation took place.

12. KOH concentration

13. Temperature of the polarization

14. Reactant gas pressure

Out of the fourteen parameters mentioned, first nine are in the electrode preparation. The later five parameters (10 through 14) are not varied to ensure that the response variable is affected by preparation parameters only. The values of these parameters are fixed as follows:

Activation time = 25 hrs.

Activation temperature = 65 °C

KOH concentration = 25 %

Temperature of Polarization = 25 °C

H_2 gas pressure = 6 psig

The amount of total catalyst in the electrode is obviously going to effect the performance. The higher the catalyst loading, the better should be the performance, for this reason the loading of catalyst was not included in the factorial design. The PTFE content, milling time, cooling ON/OFF, clearance of the rolls and surfactant removal were considered in this statistical analysis. The higher and lower levels of these variables are listed in Table 5.1.

5.2.2. The Partial Factorial Design

As described in previous section, there are five variables. A full factorial design of two levels will require 2^5= 32 runs. The number of the runs were decreased due to two reasons. The first one is that the high-order interaction are not important. The second reason is the material constraint. A batch of conventionally passivated Raney-Ni is approximately 300 gm. As the performance of the electrodes depends on the passivation also, to avoid the variation due to passivation one batch is used for making all the electrodes of all runs. Due to these reasons half of 2^5 design was selected. Such a design is called 2^{5-1} partial factorial design. In this scheme 16 runs are required.

The construction of 2^{5-1} design is shown in Table 5.2. The design was constructed by writing down the basic design having 16 runs. Such a design is known as 2^4 design in A, B, C, D. In the table the effect E column was made with generator E = -ABCD. Therefore the defining relation for the design is I=-ABCDE. This indicates that every main effect is aliased with a four factor interaction. For

Table 5.1: Higher and Lower Levels of Parameter Values.

Parameters	A	B	C	D	E
	PTFE Content, %	Milling Time, sec.	Cooling on/off	Clearance μm	Number of Removals
Lower Level (-)	8	30	off	200	once
Higher Level (+)	11	120	on	400	thrice

Table 5.2 : Construction of 2^{5-1} Factorial Design

RUN #	PARAMETERS				
	A	B	C	D	E
1	-	-	-	-	+
2	+	-	-	-	-
3	-	+	-	-	-
4	+	+	-	-	+
5	-	-	+	-	-
6	+	-	+	-	+
7	-	+	+	-	+
8	+	+	+	-	-
9	-	-	-	+	-
10	+	-	-	+	+
11	-	+	-	+	+
12	+	+	-	+	-
13	-	-	+	+	+
14	+	-	+	+	-
15	-	+	+	+	-
16	+	+	+	+	+

example, A is aliased with - BCDE. Further more all two effects interactions are aliased with three effects interactions. This makes this design, a V resolution design. Due to high resolution, it is expected that this design will provide excellent information about main effects and two-factor interactions.

5.2.3. Result and Discussion

The plan of the experimental runs is shown in Table 5.3 Electrodes are made with each set of parameters while the rest of the parameters were fixed at particulars values. The polarization curves were obtained at constant temperature (298 K). The complete set of data is given in Appendix-B. The overpotentials are given with respects to Hg/HgO reference electrode. For statistical analysis overpotential values at 100 mA/cm^2 and 150 mA/cm^2 were taken from the data set. These data are listed in Table 5.4.

The statistical analyses were performed using a personal computer software called STATGRAPHICS. developed by Statistical Graphics Corporation, USA(2).

A. Analysis of Data at 100 mA/cm^2

The estimated effects and Analysis of Variance Table (ANOVA) are shown in Table 5.5 and Table 5.6 respectively. These include all two-effect interactions except those which involve roll clearance (D) and surfactant removal (E). These interactions are eliminated because they do not have physical significance. The pictorial representation of the estimated effects is given in Fig. 5.2 and Fig. 5.3. From these figures and Table 5.5 it can be conveniently concluded that important variables are PTFE content (A), milling time(B), and the cooling(C). The interaction of PTFE content and milling time is also important. The ANOVA table also indicates the similar results. The F-ratio for PTFE, milling-time, cooling and

Table 5.3 : Plan of the Experiments

FOR 2^5-1 FACTORIAL DESIGN						
RUN	PTFE, %	PTFE gm	MILL_TIME	COOLIN	CLEARANC	REMOVAL
1	8	1.6	30	ON	200	1
2	11	2.2	30	ON	200	3
3	8	1.6	120	ON	200	3
4	11	2.2	120	ON	200	1
5	8	1.6	30	OFF	200	3
6	11	2.2	30	OFF	200	1
7	8	1.6	120	OFF	200	1
8	11	2.2	120	OFF	200	3
9	8	1.6	30	ON	400	3
10	11	2.2	30	ON	400	1
11	8	1.6	120	ON	400	1
12	11	2.2	120	ON	400	3
13	8	1.6	30	OFF	400	1
14	11	2.2	30	OFF	400	3
15	8	1.6	120	OFF	400	3
16	11	2.2	120	OFF	400	1

Table 5.4 : Overpotentials at 100 mA/cm^2 and 150 mA/cm^2

	Overpotential (mV) at	
Run #	100 mA/cm2	150 mA/cm2
1	145	203
2	123	185
3	161	242
4	139	209
5	148	222
6	128	192
7	172	258
8	130	195
9	152	228
10	121	182
11	155	233
12	126	189
13	160	240
14	143	215
15	166	249
16	129	194

Table 5.5: Estimated Effects at 100 mA/cm^2

Parameters and Interactions	Estimated Effects
Average	143.625
A:PTFE	-27.5
B:Milling Time	-7.25
C:Clooling	6.75
D:Clearance	0.75
E:Removal	0
AB	-5
BC	-2.75

Table 5.6 : ANOVA at 100 mA/cm²

Effects	Sum of Sq	DF	Mean Squa	F-Ratio	P-value
A:PTFE	3025	1	3025	46.98	0.0002
B:Milling T	210.25	1	210.25	3.27	0.1137
C:Clooling	182.25	1	182.25	2.83	0.1364
D:Clearanc	2.25	1	2.25	0.03	0.8589
E:Removal	0	1	0	0	1
AB	100	1	100	1.55	0.2528
AC	9	1	9	0.14	0.7234
BC	30.25	1	30.25	0.47	0.5222
Total Error	450.75	7	64.3929		
Total	4009.75	15			

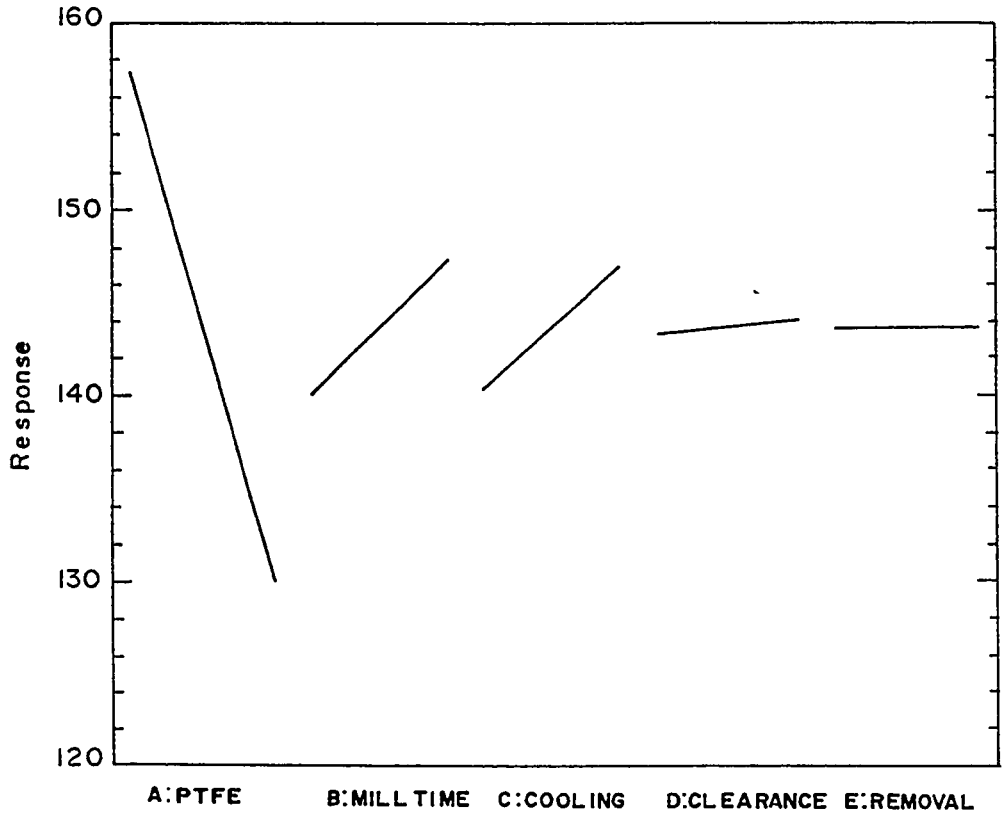

Fig. 5.2 : Plot of Main Effects for 100 mA/cm^2.

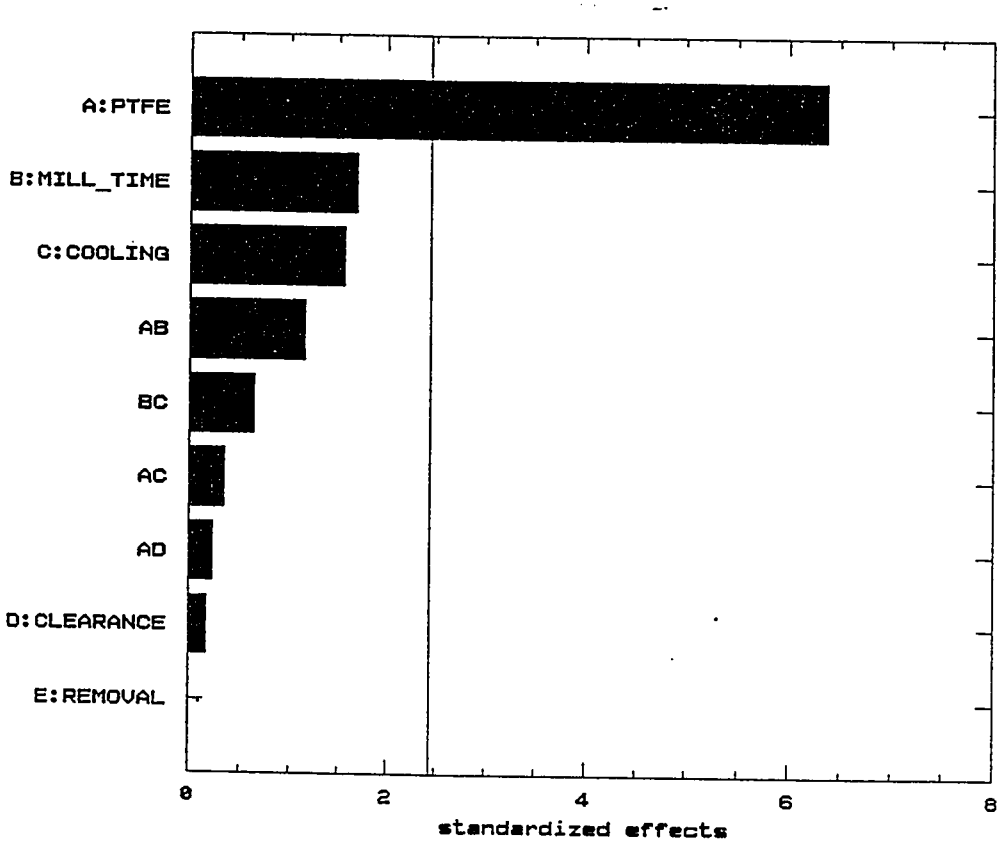

Fig. 5.3 : Standardized Pareto Chart for 100 mA/cm^2.

A-B are higher then their corresponding P-values. Fig. 5.4. shows standard normal probability plot. It can be seen that PTFE, Milling time, cooling and AB is away from the rest indicating that these effects are large Fig. 5.5 shows the plot of residuals with respect to the run number. The plots is satisfactory as no apparent pattern is formed.

B. Analysis of Data at 150 mA / cm^2

The estimated effects and analysis of variance are shown respectively in Table 5.7. and Table 5.8. The estimated effect are shown in Fig. 5.6. and Fig. 5.7. These tables and plots clearly indicated that the important parameters are PTFE content, milling time and cooling and interaction of PTFE content and milling time. From the ANOVA table also similar results are concluded because for these effects F-ratio is higher then P-value and from the normal probability plot in Fig. 5.8. The dispersed residual versus. run number shown in Fig. 5.9 is also satisfactory.

From the analyses of data at both current densities, it can safely be concluded that following are the important effect:

1. PTFE content
2. Milling time
3. Cooling
4. Interaction of PTFE content and milling time

As an attempt to optimize these parameters can be adjusted according to the effect values in Table 5.5 and Table 5.7. To obtain the optimum performance, a parameter must be shifted to the upper limit from the average for positive values

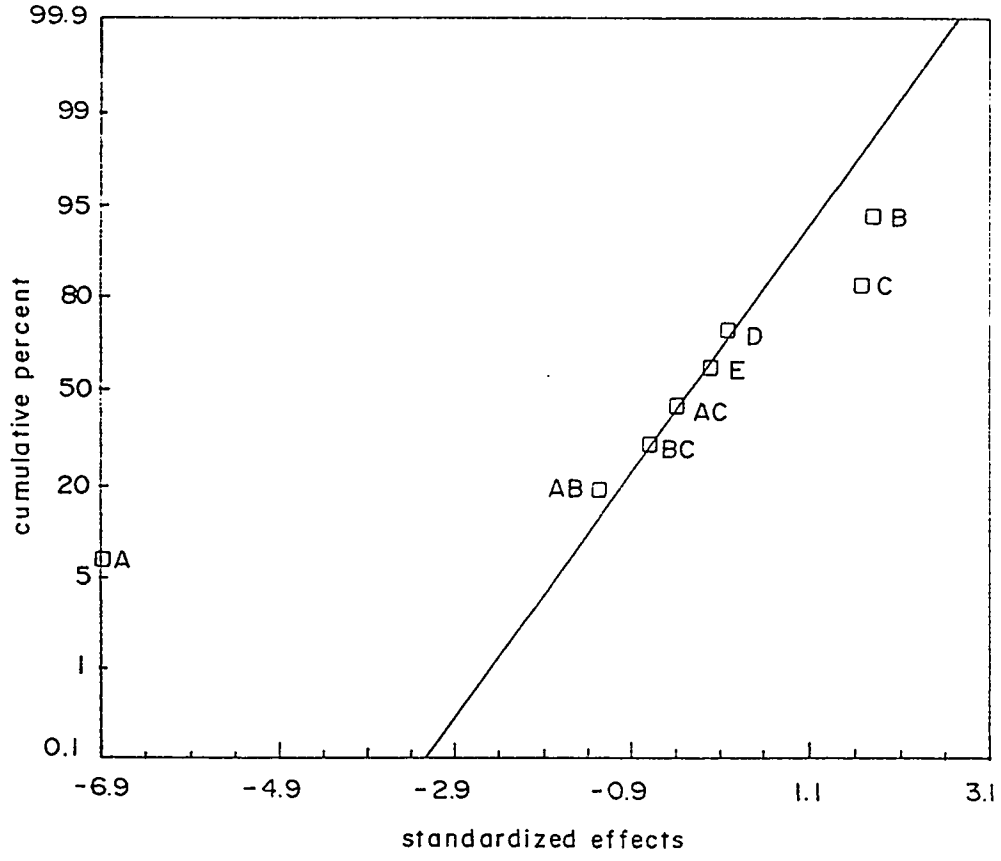

Fig. 5.4 : Standard Probability Plot 100 mA/cm^2.

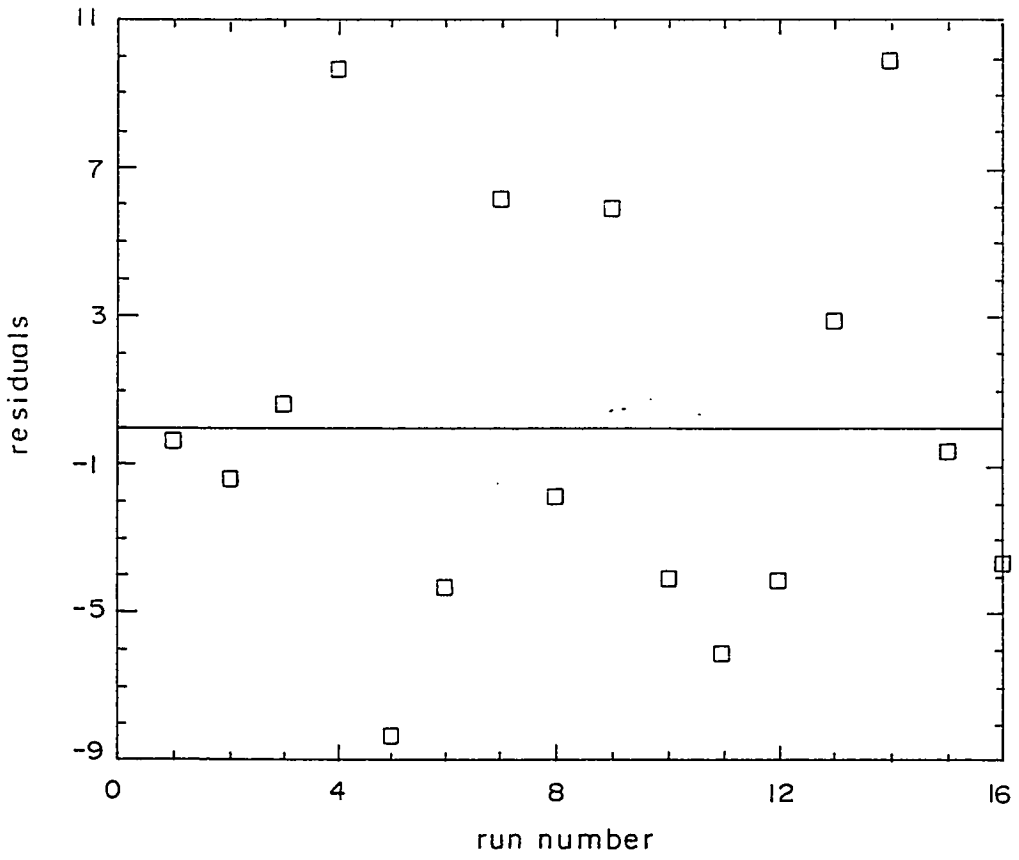

Fig. 5.5 : Plot of the Residuals w.r.t. run number 100 mA/cm^2.

Table 5.7 : Estimated Effects at 150 mA/cm^2

Parameters and Interactions	Estimated Effects
Average	214.75
A:PTFE	-39.25
B:Milling Time	-12.75
C:Clooling	11.75
D:Clearance	3
E:Removal	1.75
AB	-9.5
AC	-4
BC	-6

Table 5.8 : ANOVA at 150 mA/cm²

Effects	Sum of Sq	DF	Mean Squa	F-Ratio	P-value
A:PTFE	6162.25	1	6162.25	38.07	0.0005
B:Milling T	650.25	1	650.25	4.02	0.0851
C:Clooling	552.25	1	552.25	3.41	0.1072
D:Clearanc	36	1	36	0.22	0.6564
E:Removal	12.25	1	12.25	0.08	0.794
AB	361	1	361	2.23	0.179
AC	64	1	64	0.4	0.5559
BC	144	1	144	0.89	0.3867
Total Error	1133	7	161.8571		
Total	9115	15			

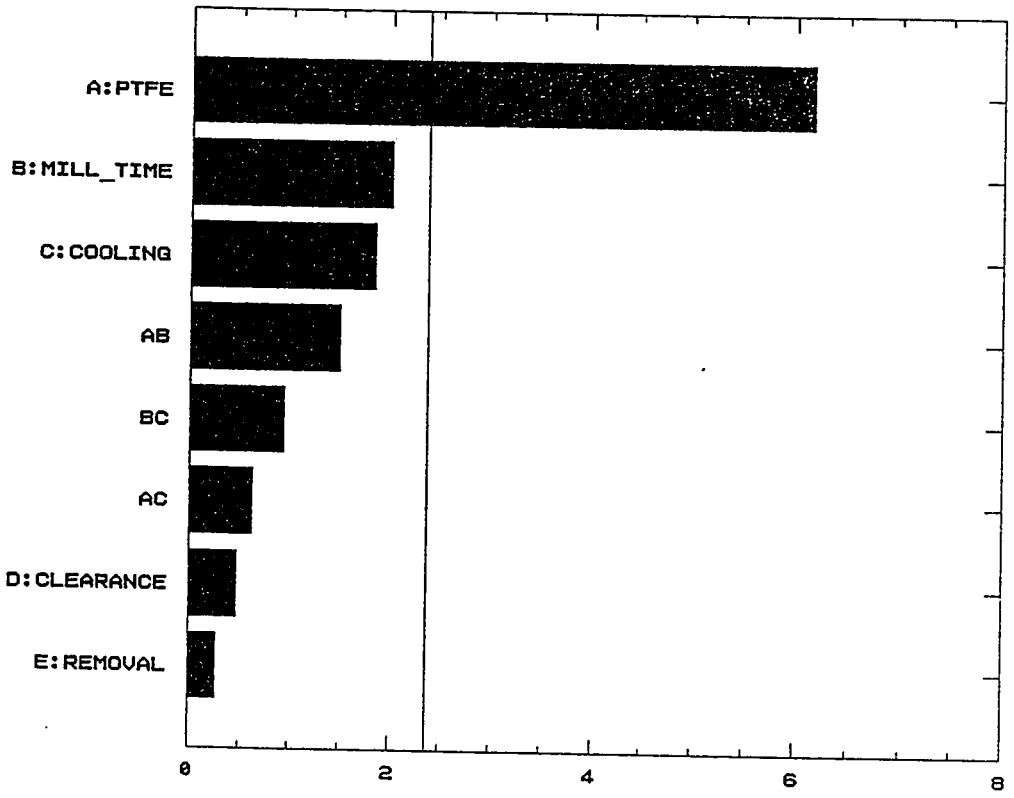

Fig. 5.6 : Standardized Pareto Chart for 150 mA/cm^2.

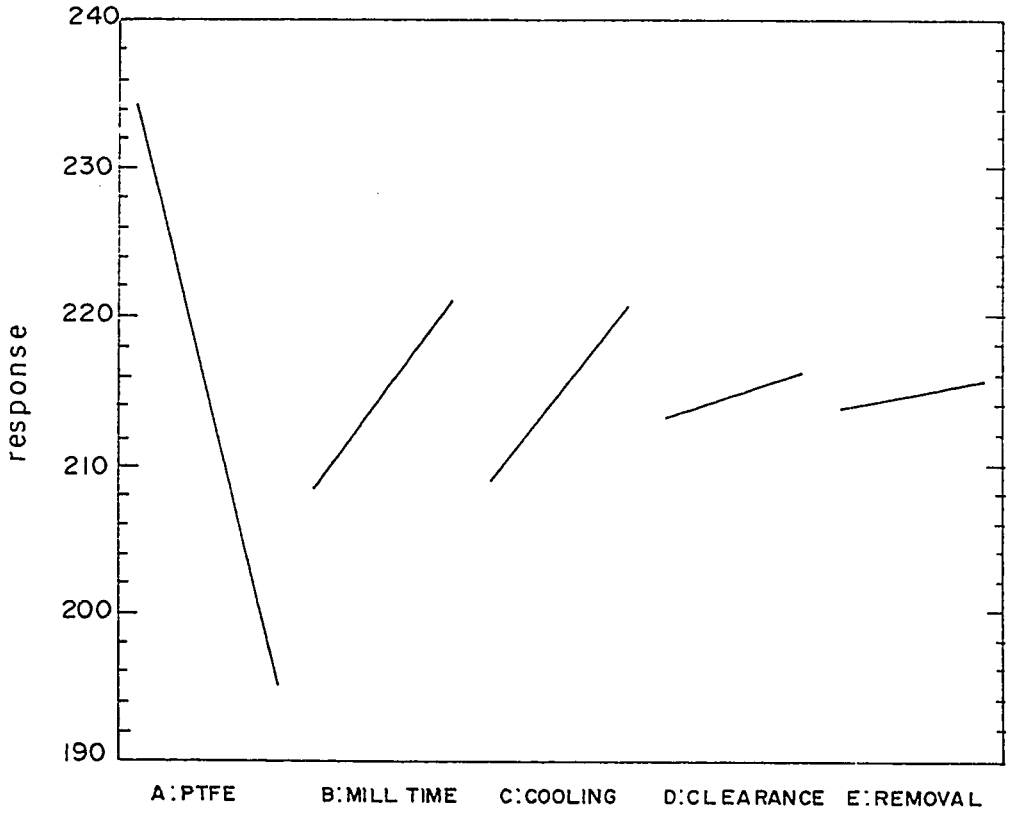

Fig. 5.7 : Plot of Main Effects for 150 mA/cm^2.

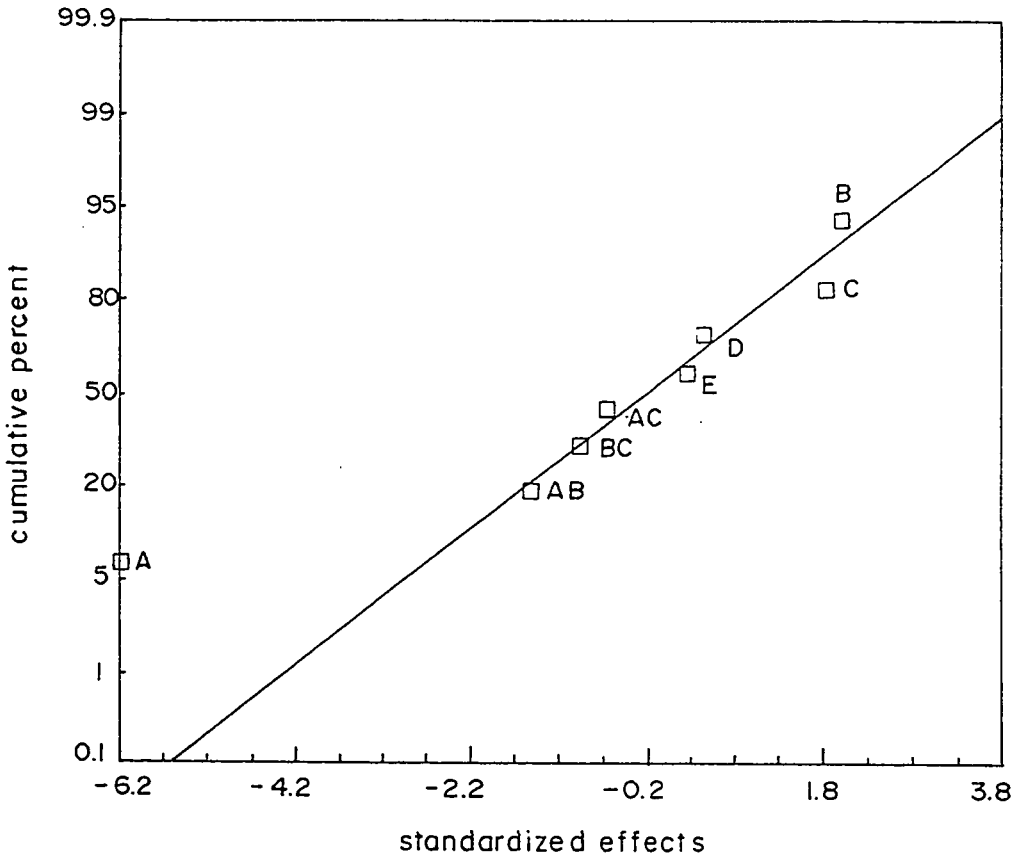

Fig. 5.8 : Standard Probability Plot 150 mA/cm^2

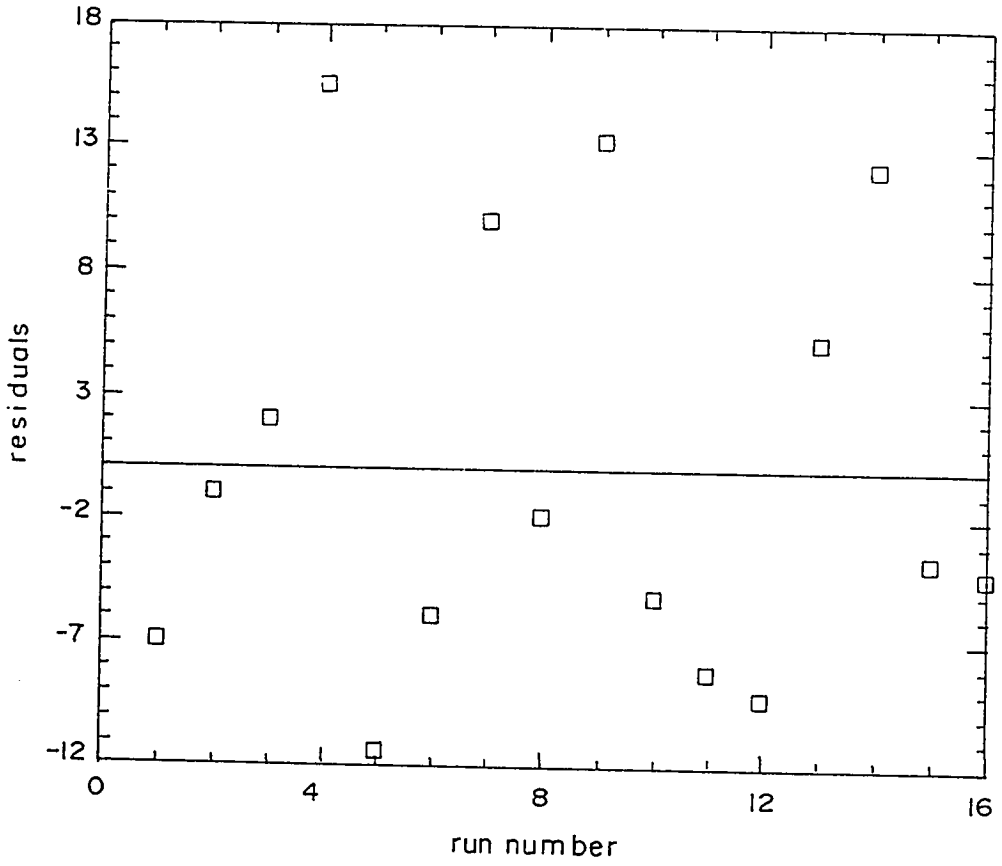

Fig. 5.9 : Plot of the Residuals w.r.t. run number 150 mA/cm^2.

and to the lower limit for negative values. Therefore the optimum performance can be obtained in the following range.

PTFE	= 8 to 9.5%
Milling time	= 30 to 75 seconds.
Clearance between the rolls	= 300 microns
Cooling while milling	= ON
Surfactant Removal	= Once

5.3. Effects of Parameters on Electrode Performance

In the previous sections of this chapter, using 2^{5-1} factorial design, it was found out that the significant parameters of the electrode preparation process are PTFE content, milling time and cooling during reactive mixing. In this section effects of these parameters on the electrode performance are studied. One parameter at a time is varied while keeping other parameters at a predetermined base value. The base values of these parameters are given in Table 5.9 with other parameters.

5.3.1. Effect of PTFE Content

To study the effect of PTFE content on the performance, the electrodes were made with 2, 5, 8, 11 and 14 % PTFE contents while keeping other parameters at base value. The polarization data at 298 K were obtained. These data are tabulated in Appendix-C. The overpotential values at 100 mA/cm^2 are plotted against the PTFE content in Fig. 5.10. It is obvious that the minimum overpotential is at 8% PTFE.

Table 5.9 : Base values of various parameters affecting the electrode performance

Parameters	Value
PTFE Content	8 %
Milling Time	60 second
Cooling	ON
Clearance between Rolls	400 μ
Surfactant Removal	Once
Activation Time	25 hrs
Activation Temperature	65°C
KOH Concentration	25% wt
Polarization Temperature	25°C
Gas pressure	6psig
Catalyst loading	120mg/cm^2
Filtration Vacuum	300/500 mbar

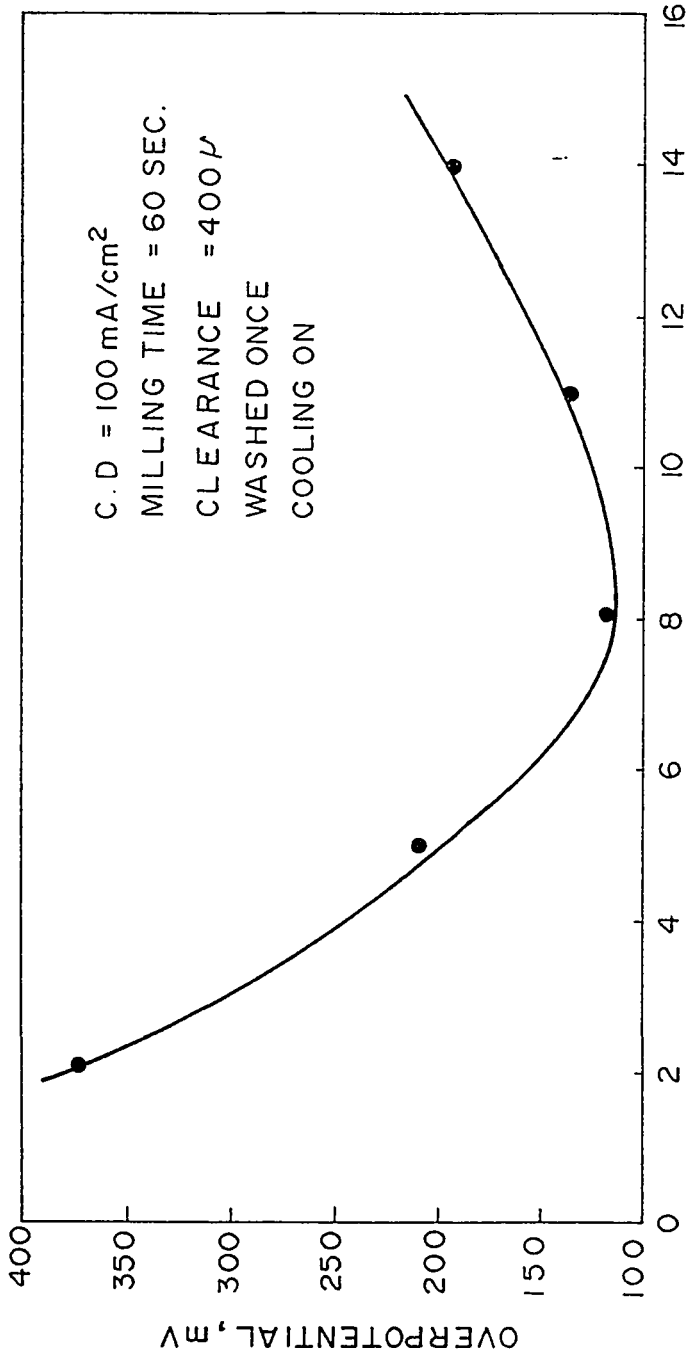

Fig. 5.10 : Effect of PTFE Content on the Electrode Performance

5.3.2. Effect of Milling Time

The polarization data were obtained for electrodes using catalyst milled for 30, 60, 90, 120, 150, and 200 seconds. The polarization experiments were repeated. These data are listed in Appendix-D. The overpotential values at 100 mA/cm^2 are plotted against milling time in Fig. 5.11. It is observed that the best performance was at 60 seconds milling.

5.3.3. Effect of Cooling while Reactive Mixing

The electrode performance curves obtained for electrodes using catalysts with reactive mixing while cooling was ON and OFF respectively. The rest of the parameters were at the base values given in Table 5.9. The data are plotted in Fig. 5.12.

After obtaining the value of the parameters at which the overpotential were lowest, an electrode was prepared using these values. The electrode was tested at diffrent temperatures. The polarization data obtained are tabulated in Appendix-E.

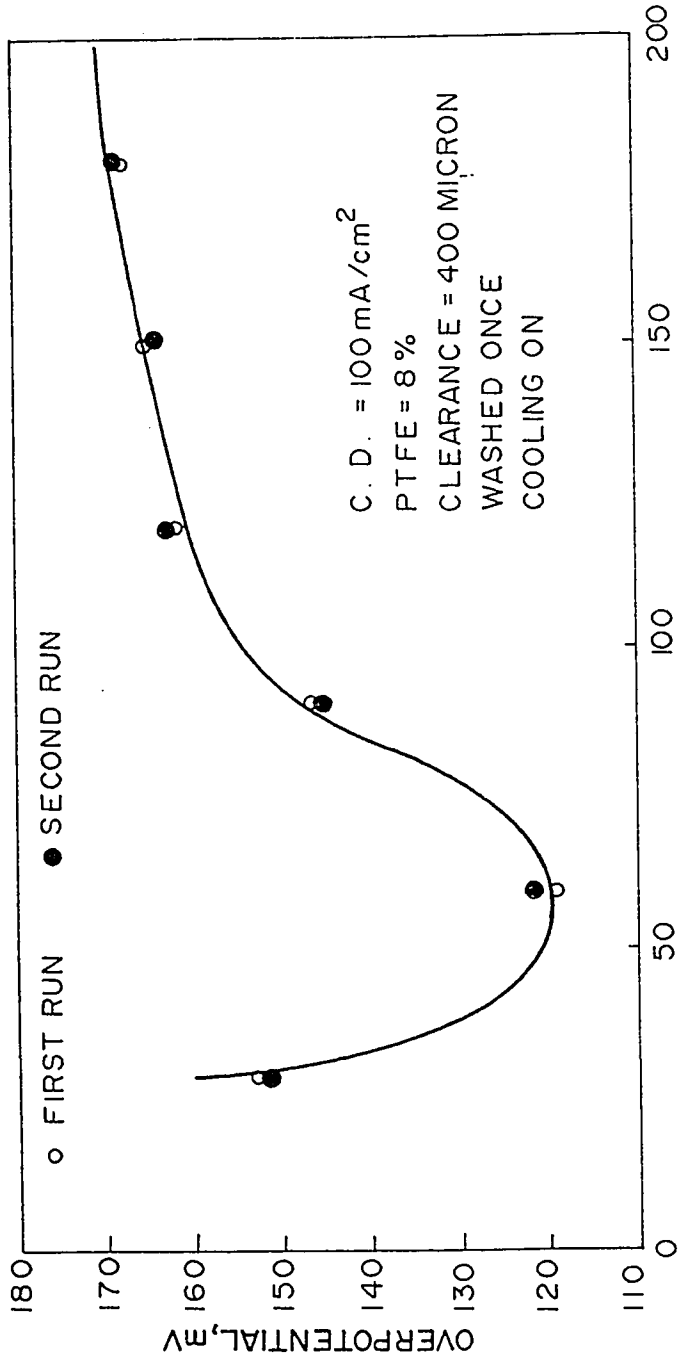

Fig. 5.11 : Effect of Milling Time on the Electrode Performance

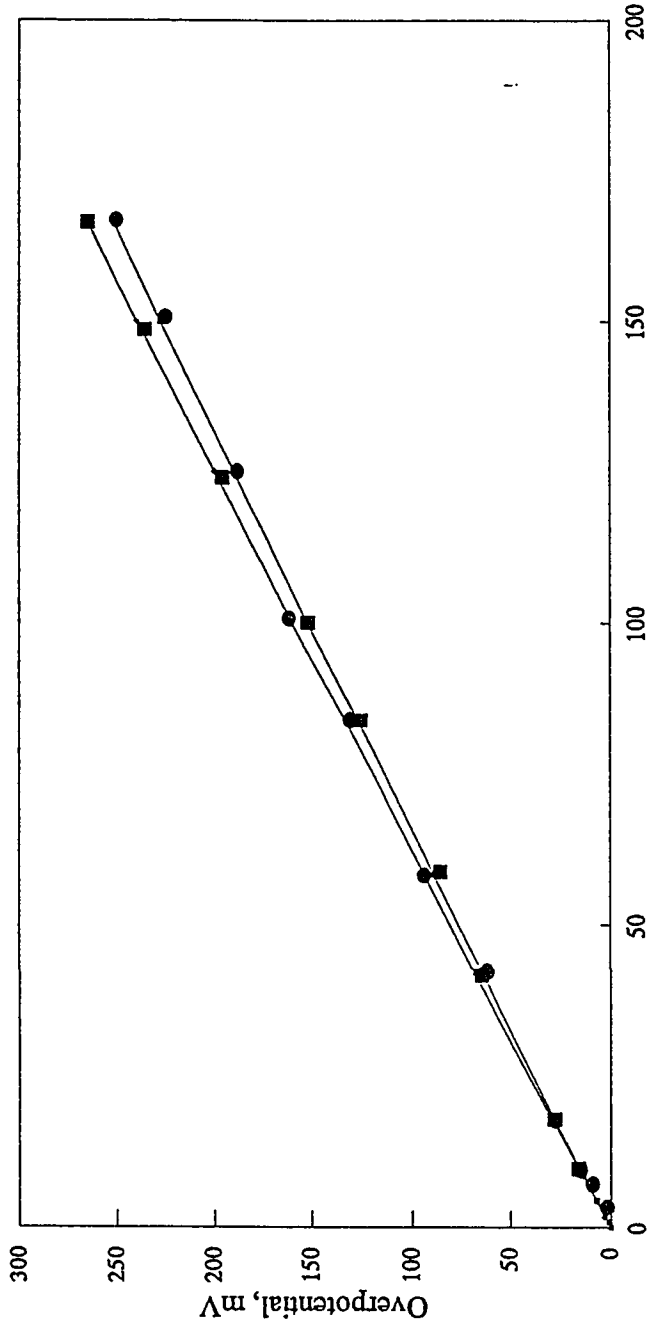

Fig. 5.12 : Effect of Cooling During Reactive Mixing on the Electrode Performance

References

1. Montgomerry, D.C., *'Design and Analysis of Experiments'*, Third Ed., John Wiley, New York (1991).

2. *'Users' Manual: Statgraphics'*, Statistical Graphics Corporation, USA (1989).

6

Characterization of the Materials and the Electrode

6.1. Introduction

The characterization of the starting materials, intermediate materials and the final electrode was done to study the structure and to obtain the parameters to be used in the mathematical model developed in Chapter 7. The electrode and the milled catalyst sample were prepared by using the optimum parameter i.e. 8% PTFE, 60 seconds milling time, 400 microns clearance between the rolls and surface removal once. Following techniques have been used for characterization :

1. BET surface area
2. Mercury Intrusion Porosimetery
3. Scanning Electron Microscopy
4. X-ray Diffraction
5. Density by Helium Displacement
6. Particle Size Analysis

6.2. BET Surface Area

In this method, the amount of nitrogen at the equilibrium and at the normal boiling point (-195.8 C) is measured over a range of nitrogen pressures below one atmosphere.

In essence, the Langmuir adsorption isotherm is extended to apply to multilayer adsorption, arriving at the following equation:

$$\frac{p}{v(p_0 - p)} = \frac{1}{V_m c} + \frac{(c-1)p}{cV_m p_0} \qquad [6.1]$$

where P_o is the saturation or vapor pressure and c is a constant for the particular temperature and gas-solid system. A plot of $P/v(P_o-P)$ versus P/P_o should give a straight line, which can be extrapolated to $P/P_o=0$. From the intercept I and the slope S of this line, the volume of the adsorbed gas V_m corresponding to the monolayer can be obtained using the relation:

$$V_m = \frac{I}{(I+S)} \qquad [6.2]$$

The volume V_m can be converted to the surface area. For nitrogen at -195.8 C. the surface area (m^2/g) is equal to V_m*4.35X10^4.

The equipment used was a SORPTOMATIC in which the volume of the gas adsorbed was obtained by measuring the decrease in the pressure resulting from the adsorption of a portion of a known gas volume. Known and constant volumes were introduced into an evacuated empty burette and kept at liquid nitrogen

temperature. The corresponding equilibrium pressures were recorded. When the test was repeated with the sample, part of the nitrogen introduced was adsorbed and the pressures of the gas in equilibrium with the portion adsorbed, were recorded. Comparing with the values of the pressures with empty burette, the gas volume adsorbed at the various equilibrium pressures and hence the isotherm could be calculated.

The BET surface area were measured for the electrode, passivated Raney-Ni and the milled Raney-Ni. The obtained results are tabulated in Table 6.1. and the isotherms corresponding each sample are shown in Fig.6.1 through 6.3.

6.3. Mercury Intrusion Porosimetery

Mercury intrusion porosimetery was used to measure the porosity of the passivated Raney-Ni, milled Raney-Ni and the finished electrode.

In this method, the porous sample was kept in a cell and evacuated. Mercury was then injected into the pores at various pressures and the volume of the mercury taken up was measured as a function of pressure. If the radius of a pore is r, mercury will enter this pore when the pressure is equal to or greater than that expressed by:

$$p = \frac{2\sigma\cos\theta}{r} \qquad [6.3]$$

where σ and θ are the surface tension and the contact angle for the mercury-solid interface respectively.

Table 6.1 : The BET surface area of various samples

	BET surface Area, m^2/g	BET surface area after correcting for Ni-mesh, m^2/g	Pore volume, cm^3/g
Passivated Raney-Ni	72	---	0.293
Milled Raney-Ni	62	---	0.205
Electrode	39	64	0.050 (with Ni-mesh)

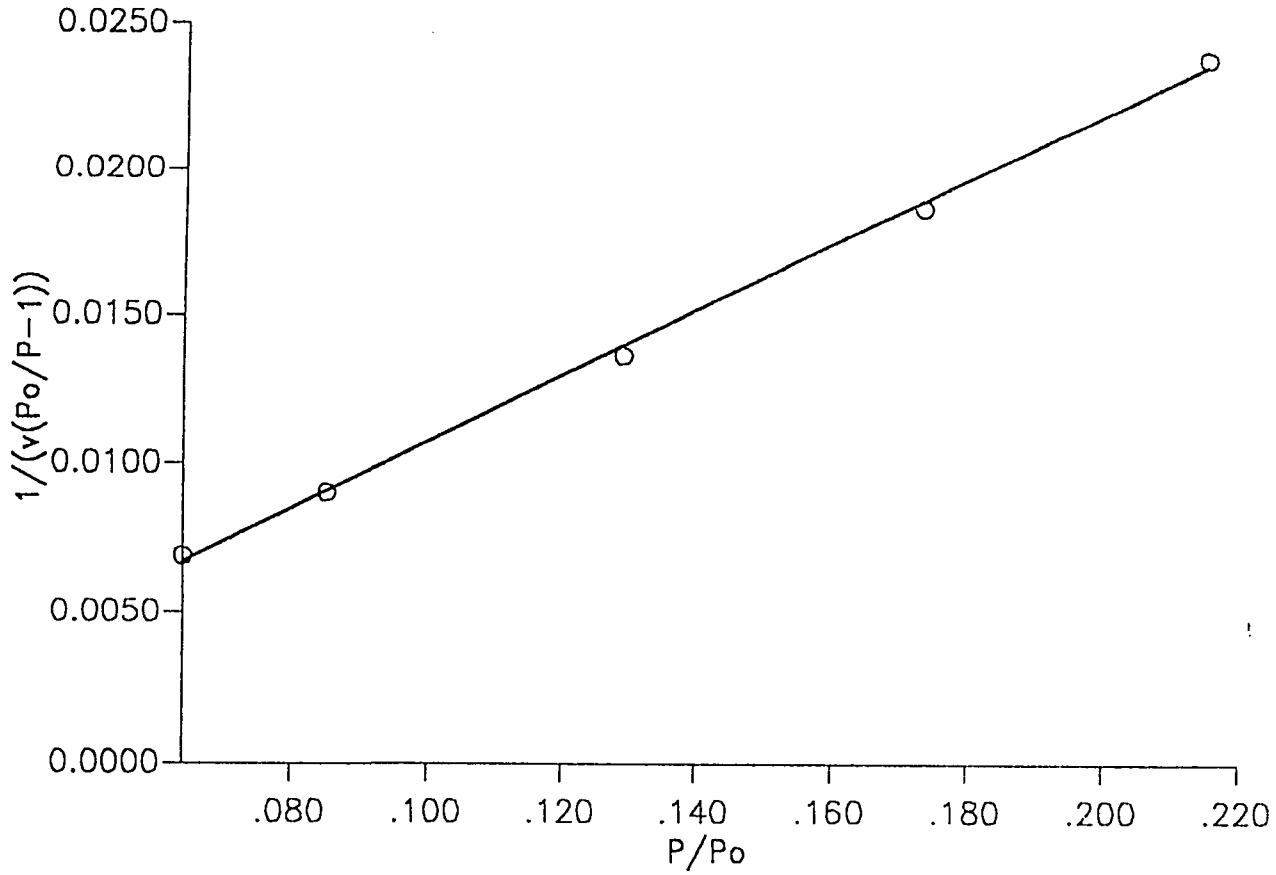

Fig. 6.1. : BET Isotherm for the Passivated Raney-Ni.

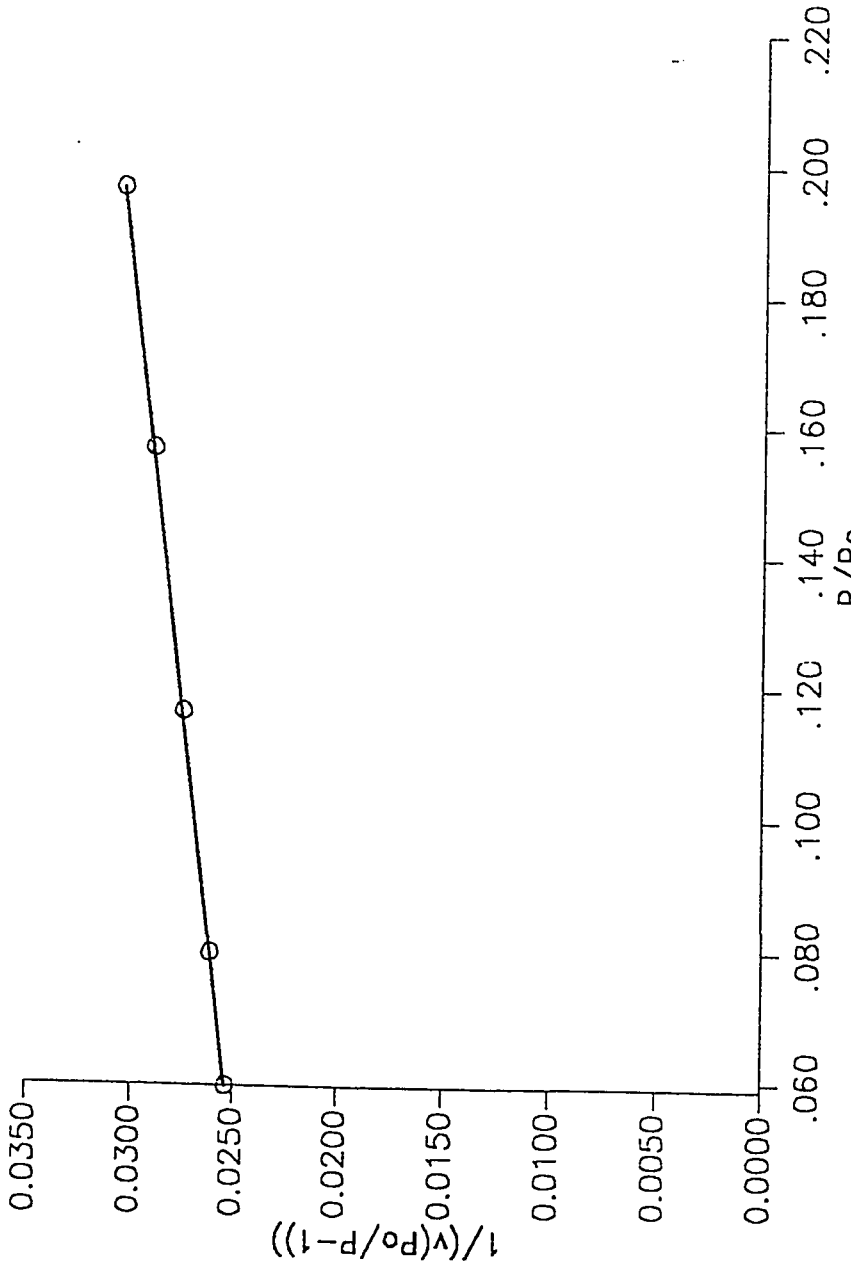

Fig. 6.2. : BET Isotherm for the Milled Raney-Ni.

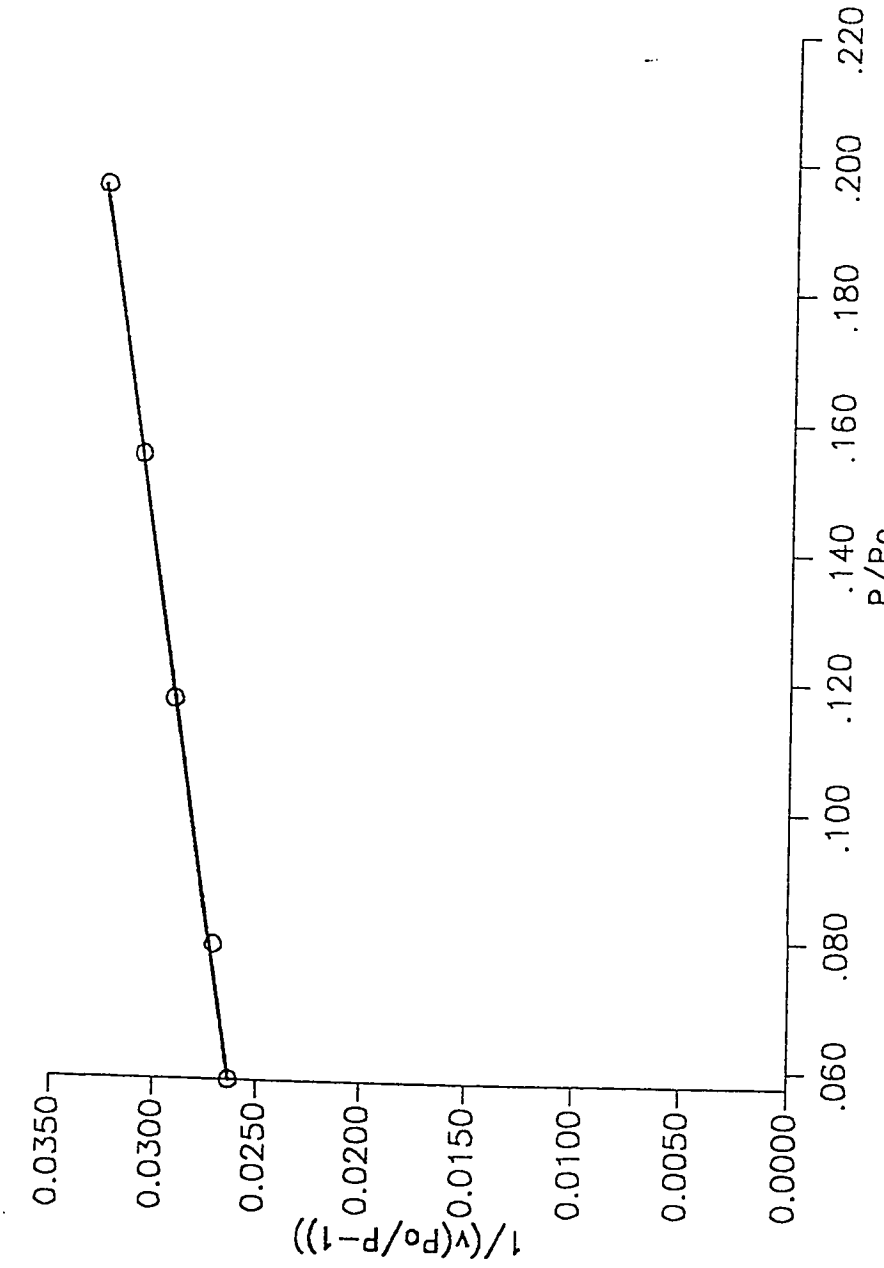

Fig. 6.3. : BET Isotherm for the Electrode.

Cumulative void volume distributions as a function of pore size for different samples are given in Fig. 6.4 through 6.6. The total pore volumes were estimated and are listed in Table 6.1. The porosity of the electrode calculated by eliminating the Ni-mesh is 0.31.

6.4. Scanning Electron Microscopy (SEM)

In this method, an electron spot of 5 nm diameter minimum, focused on the sample, is moved over a small area by means of a set of deflecting coils. This area is displayed highly magnified on a cathode ray tube(CRT) by focusing the current passing through the scanning coils to pass through the corresponding deflecting coils. The CRT image can be transferred to the photographic paper. The sample is mounted on a sample holder by means of a double sided adhesive tape and conducting black carbon paint. In order to facilitate charge transfer, a thin gold film is deposited on the sample using plasma deposition. The SEM analysis was done to study the structure and morphology of the catalyst particles.

SEM micrographs of PTFE powder, passivated Raney-Ni by conventional method and by H_2O_2 treatment, and the finished electrode were obtained at various magnification. The micrograph of the finished electrode is shown in Fig 6.7 through 6.9. Other micrographs are shown in appropriate places in this dissertation. The SEM micrographs of the surface and the cross-section of the electrode show that although the catalyst particles are well compacted to form bonds, considerable porous structure exists. Fig. 6.9 shows an SEM of the surface of the electrode from the mesh-side. The nickel wires are well embeded into the

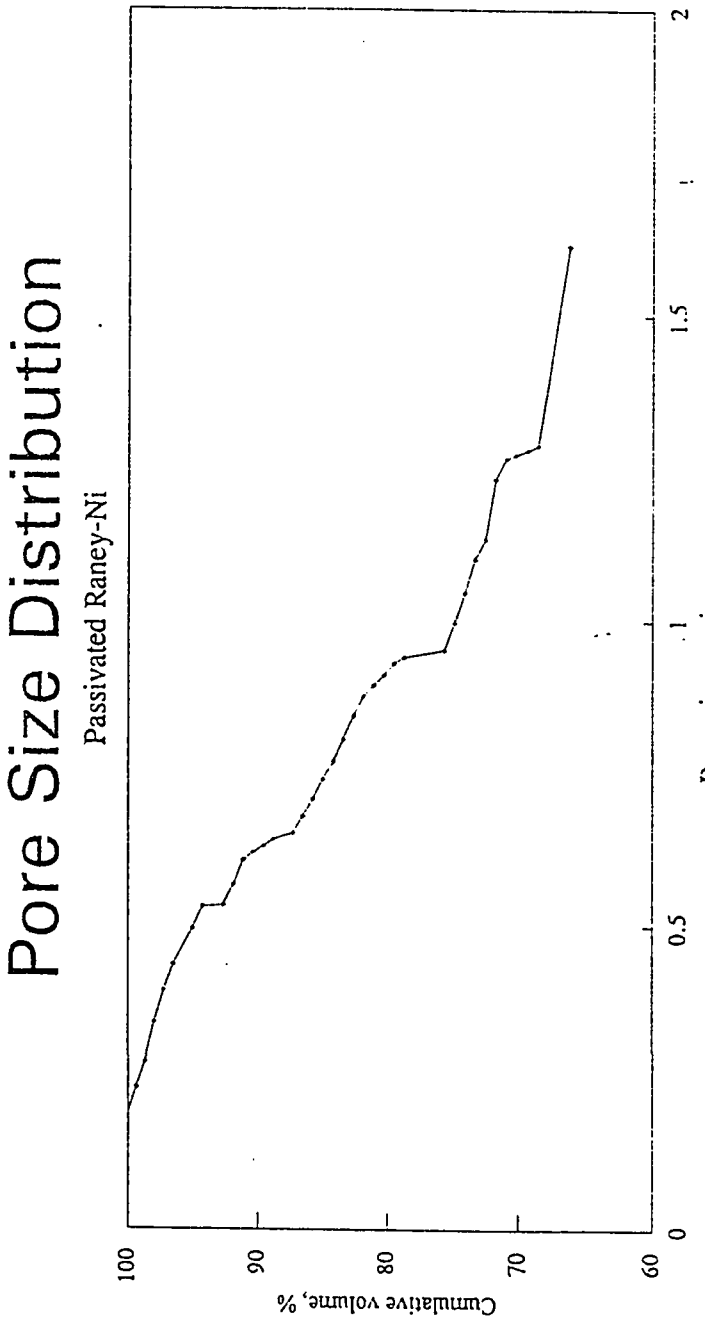

Fig. 6.4. : Cumulative Void Volume Distribution for the Passivated Raney-Ni.

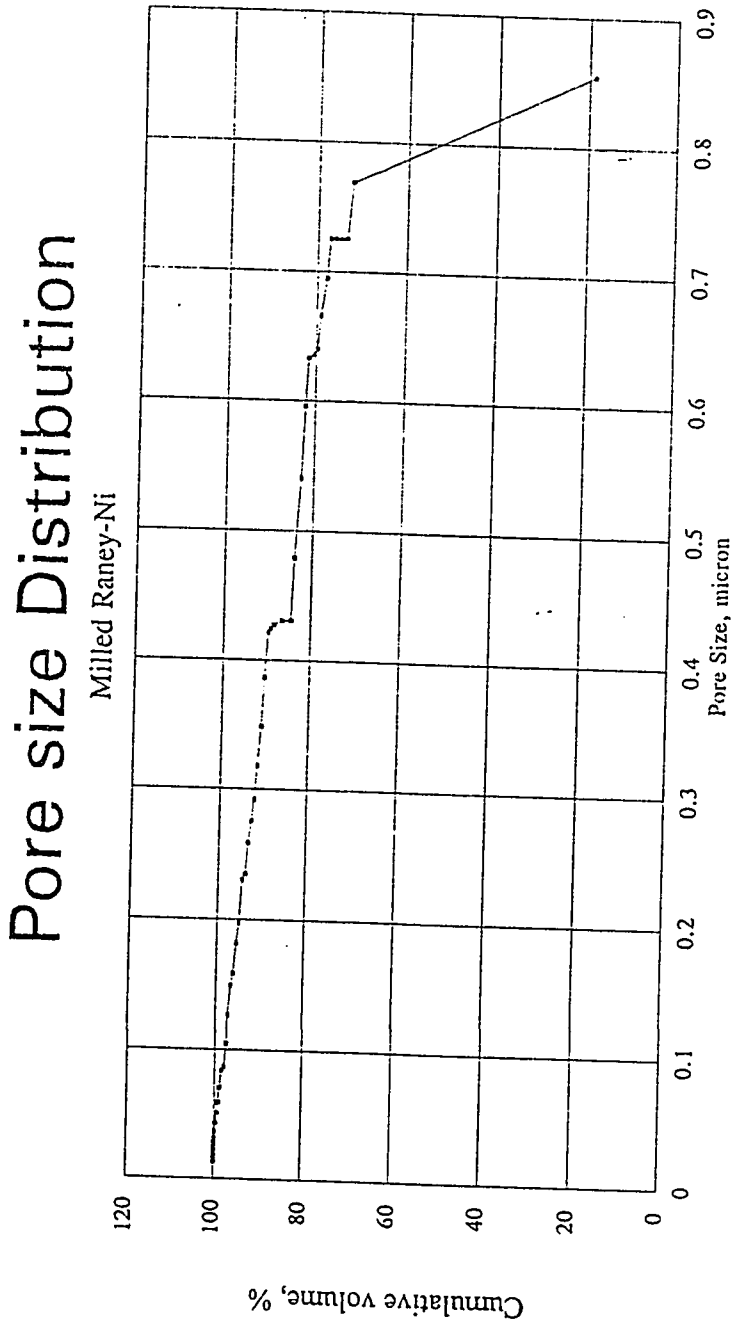

Fig. 6.5. : Cumulative Void Volume Distribution for the Milled Raney-Ni.

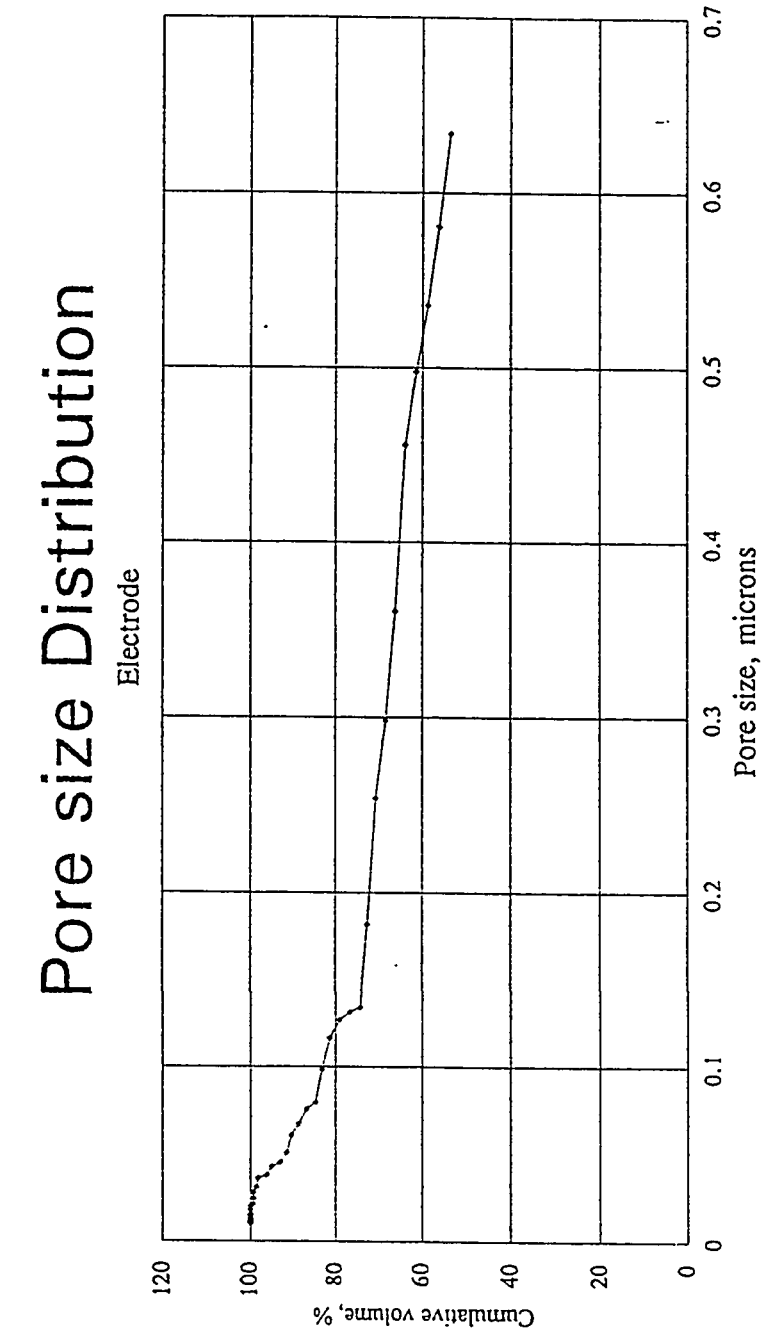

Fig. 6.6. : Cumulative Void Volume Distribution for the Electrode.

Fig. 6.7. : Micrograph of the Cross-section of the Electrode

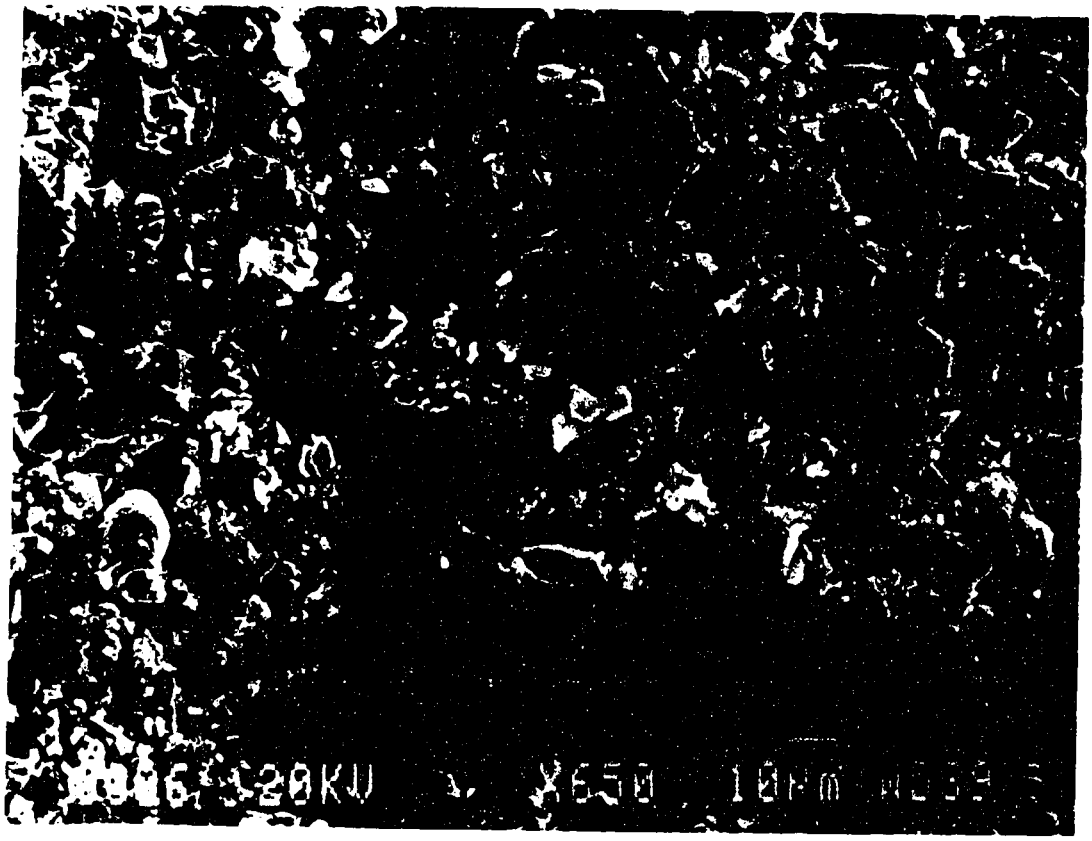

Fig. 6.8. : Micrograph of the of Catalyst Side of the Electrode

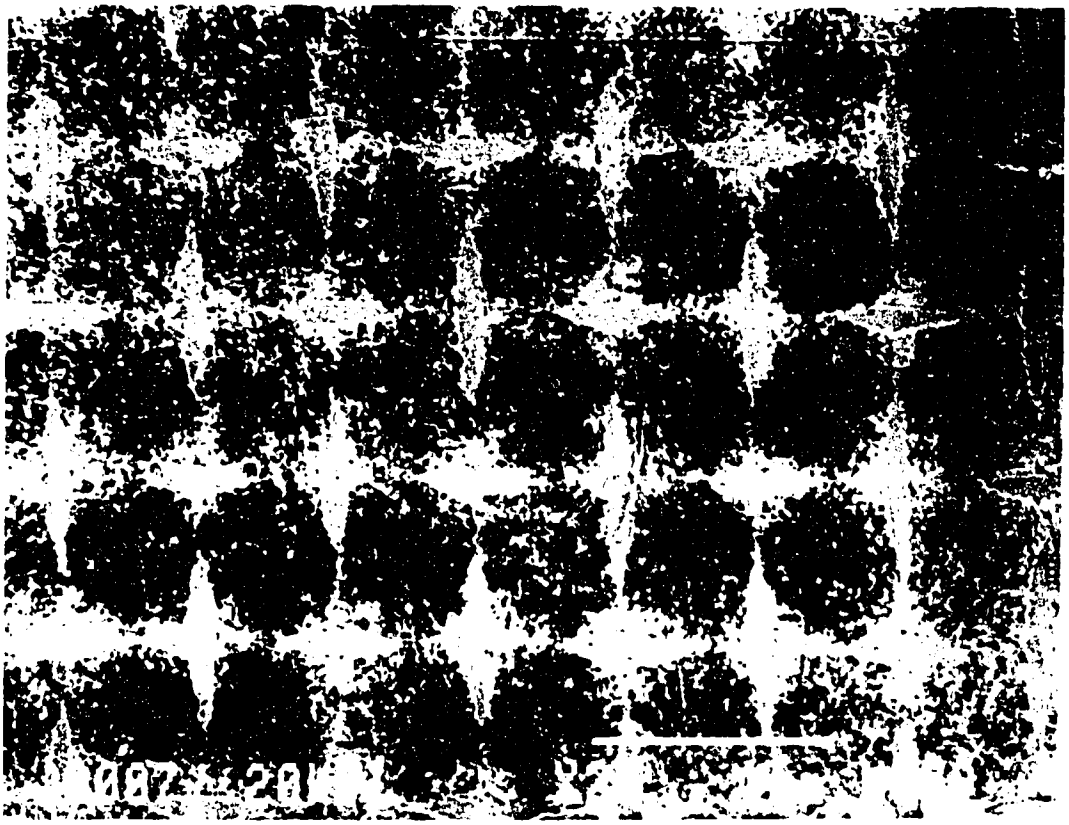

Fig. 6.9. : Micrograph of the of Mesh-side of the Electrode

catalyst. Fig. 6.10 shows similar SEM of a electrode made by dry procedure (1). The current colleector mesh, in this case is just touching the catalyst.

6.5. X-ray Diffraction

X-ray diffraction is mainly used to obtain information about the structure and composition of the crystalline material. Higher amount of crystalline material usually mean higher active surface area and thus the catalytic activity. The technique is used to identify and compare the crystalline Ni, NiO and NiH_2 in the passivated Raney-Ni samples. The XRD patterns were obtained by using a Theta-2-theta scanning diffractometer. It scanned from 4 to 80 degree two theta. The obtained XRD patterns were compared with standard Ni and NiO patterns of Joint Committee of Powder Diffraction Services(JCPDS). The JCPDS phase No. 4-850 (Ni) and 4-835(NiO) were used. The XRD patterns for passivated Raney-Ni by conventional method and by H_2O_2 treatment are shown in Chapter 8 with the discussion of the relevant results.

6.6. Density of the Powder by Helium Displacement

The density of the passivated Raney-Ni and Milled Raney Ni is required for the particle size analysis. In the Helium displacement method the volume occupied by the known mass of a powder sample is measured. This is done by measuring the volume and the pressure of the displaced Helium in a Helium Displacement Pycnometer. This method gives the actual density of the particles excluding the effect of the pores where gas can diffuse. Following results were obtained :

Passivated Raney-Ni = 5.212 g/cm^3

Milled Raney-Ni = 4.126 g/cm^3

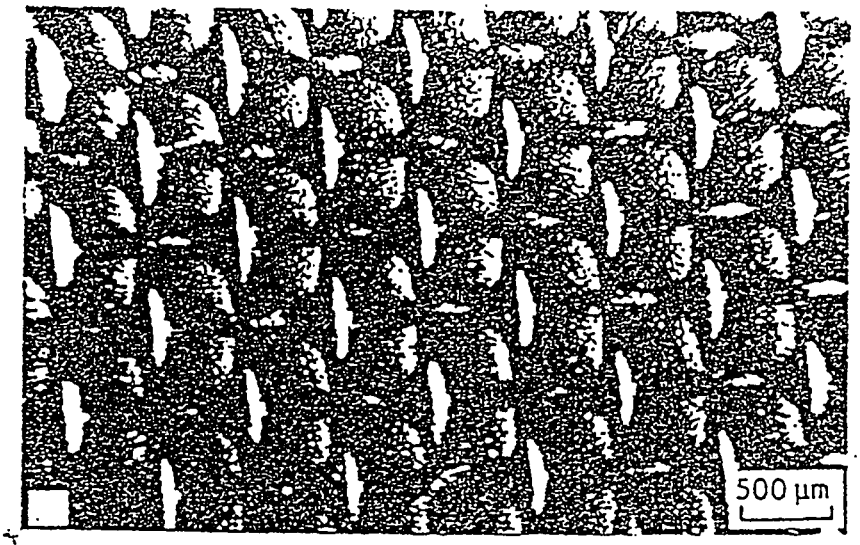

Fig. 6.10 : Micrograph of the Mesh-side of the Electrode Produced by Dry Method (1).

6.7. Particle Size Distribution

The particle size distribution of the milled Raney-Ni sample was obtained using Quantachrome Microscan Particle Size Analyzer. In this equipment the sample particles are sedimented in an appropriate liquid. For milled Raney-Ni particles water was used. The absorption of the falling particle in the liquid is measured and converted into the particle size using sample density, liquid viscosity and temperature. A histogram of the sample is shown in Fig. 6.11. The average particle diameter is 25.06 micron.

KFUPM/RI-ELPAR III PROJECT
Quantachrome Microscan Particle Size Analyzer Data Report
Version 1.10

File Name..... PASRANI.MRD
Operator..... Mohammed Sumani
Sample ID..... SA4C1401
Sample Description.. Passivated Raney-Nikel

Data Type..... Raw
Moving Point Avg.... 5
Sample Density..... 5.21[illegible] g/

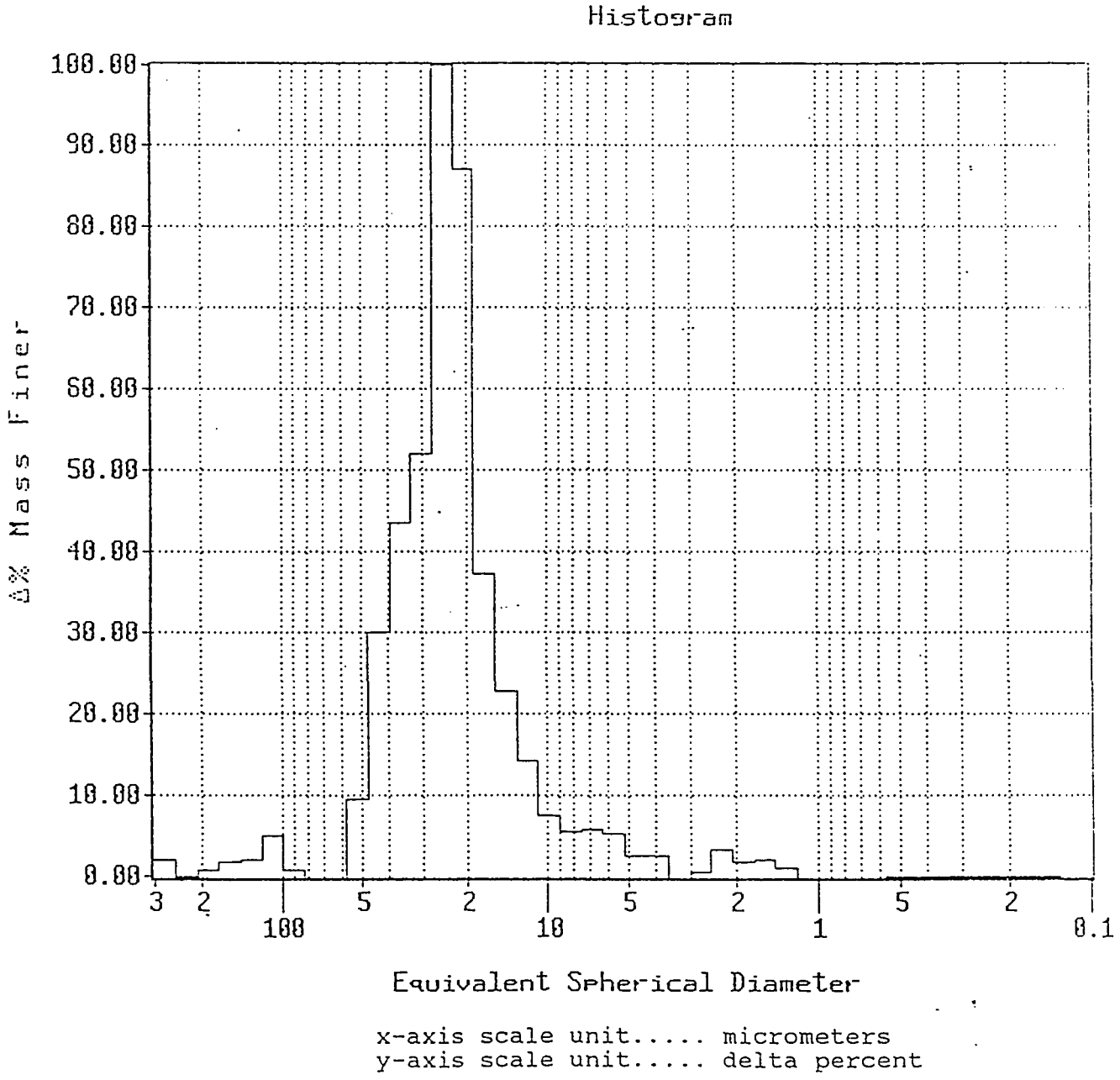

Fig. 6.11. : Histogram for the Particle Size Distribution of the Milled

Reference

1. Jensiet, W., A.Khalil and H.Wendt, *Journal of Applied Electrochemisty*, **20**,893 (1990).

7

Mathematical Model for the Performance of the Fuel Cell Electrode

7.1 The Flooded Spherical Agglomerate Model

A mathematical model was proposed by Celiker et al.(1,2) with the assumption of uniform spherical agglomerates distributed homogeneously through out the electrode. the structure of the Raney Catalyst Gas Diffusion Electrode is extensively studied by various investigators, e.g. Mund et al. (3), Vielstich (4), F. von Sturm et al.(5) and Ewe et al.(6,7,8). A typical micrograph of Raney Silver Electrode is shown in Fig 7.1. This shows actual distribution of irregularly shaped agglomerates. In fact, these Raney Metal grains are entangled between the fine strands of the PTFE. These PTFE strands provide hydrophobicity to the outer surface of the agglomerates. The porous structure of the agglomerate itself remains intact and thus hydrophilic. This PTFE-catalyst structure provide the macroporosity to the electrode. The inherent porosity of the

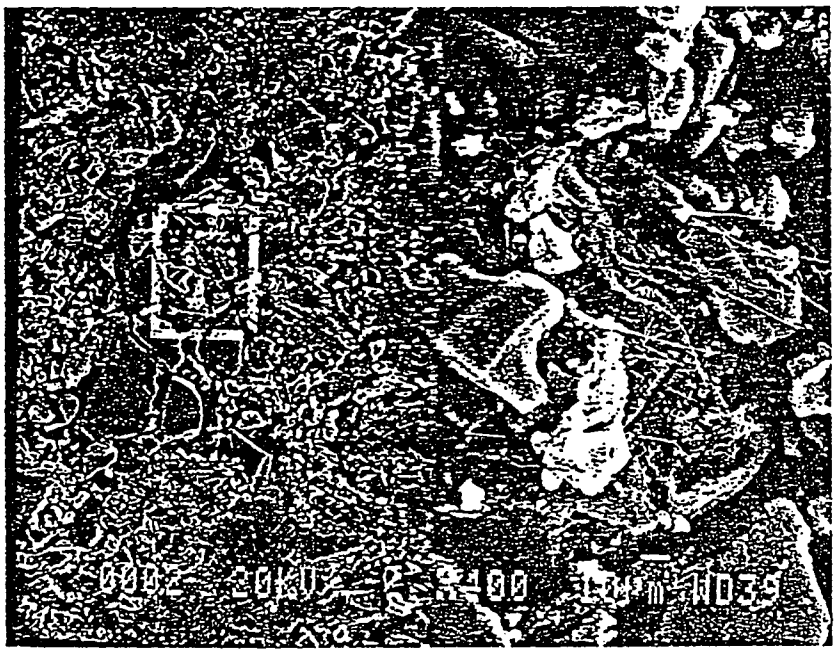

Fig. 7.1 : Micrograph of the Ni/PTFE electrode from mesh side (Magnification =400x) (1)

catalyst constitutes microporosity to the electrode. The model is based on the following assumed mechanism for the working of the electrode.

The catalyst agglomerates are touching one another which helps in electrical conductance across the length of the electrode. The electrolyte filling the micropores of the agglomerates provide ionic conductivity path from the gas side to the electrolyte side. Electrolyte in the porous structure of the electrode is stagnant and remains mainly inside the micropores of the agglomerates. The macropores are filled with the reactant gas . There are narrow electrolyte bridges among the grains. These bridges make ionic conductive paths between the agglomerates. As current is withdrawn from the electrode, the reactant gas diffuses into the macropores. The gas gets dissolved at the outer surface of the agglomerate as soon as it comes in contact with the electrolyte. This happens without any kinetic limitation. The dissolved gas, then diffuses into the microporous structure of the catalyst. The gas reacts simultaneously at the active sites, as it diffuses. The mechanism is illustrated in Fig 7.2.

The mathematical treatment of the model necessitates following assumptions :

1. Raney catalyst grains in the electrode are spherical in shape and have the same average size.
2. Spheres of the catalyst grains are distributed homogeneously in the electrode and are touching one another.
3. The porous Raney catalyst grains are flooded with electrolyte.
4. There are relatively narrow electrolyte bridges among the neighboring grains helping the ionic transport across the electrode.

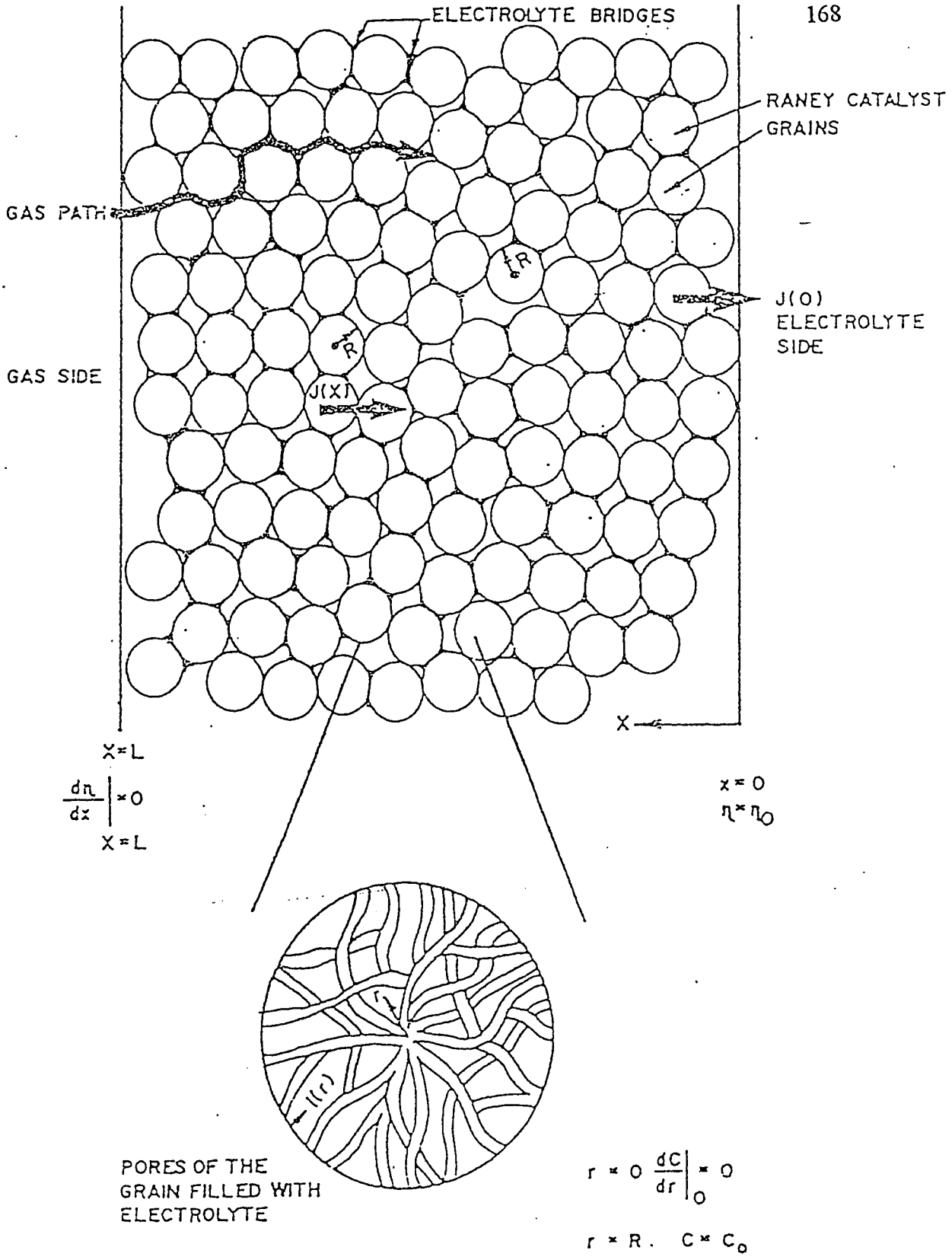

Fig. 7.2 : Schematic diagram of spherical grain model

5. The local current density in the grain is directly proportional to the local reactant concentration.

6. The potential of a single catalyst grain is uniform (isopotential grains). The potential changes in the axial direction only.

7. Diffusion of the dissolved gas in the grain occurs in the radial direction.

8. Diffusion of the gases in the macropores occurs only across the length of the electrode.

9. Electrocatalytic activity of spherical grains do not change in the radial direction.

10. There are no transport limitations in the gas macropores with pure gasses.

11. There are no kinetic limitations on the dissolution of the gas in the electrolyte.

12. The ionic concentration equilibration along the electrode is achieved by an evaporation -condensation mechanism.

The final equations of this model are as follows :

$$\left(\frac{\partial C}{\partial r}\right)_{r=R} = C_0\left(1-\frac{A_3}{A_2}\right)\left[\sqrt{\frac{A_1 A_2}{C_0}}\coth\left(R\sqrt{\frac{A_1 A_2}{C_0}}\right)-\frac{1}{R}\right] \qquad [7.1]$$

where,

$$A_1 = \frac{i_0 a}{nFD_{le}} \qquad [7.2]$$

$$A_2 = \exp\left[\frac{\alpha z F \eta(x)}{R_g T}\right] \qquad [7.3]$$

$$A_3 = \exp\left[\frac{-(1-\alpha)\,z\,F\,\eta(x)}{R_g\,T}\right] \qquad [7.4]$$

The distribution of the overpotential is given by

$$\frac{d^2\eta}{dx^2} = \frac{2nFD_{le}}{k_e R}\left(\frac{dC}{dr}\right)_{r=R} \qquad [7.5]$$

with following boundary conditions

$$\text{at } x = 0 \qquad \eta = \eta_0, \qquad \text{at} \qquad x = L, \frac{d\eta}{dx} = 0$$

These equations are solved numerically using finite difference method. An IMSL library routine called BVPFD was used to solve this boundary value problem. The results are plotted in Fig. 7.3 with experimental polarization curves obtained with Raney Ni-PTFE electrode and hydrogen gas (1).

7.2 The Modified Flooded Spherical Agglomerate Model

The flooded agglomerate model was found to be in good agreement with the experimental data at lower values of the overpotential and temperature. At higher values of these variables, the deviation is large enough to suggest that there is something missing, although the assumption of the spherical; and homogeneously distributed grain is much more realistic than the conventional assumption of straight cylindrical pores and agglomerates (9,10). The polarization curve of this model shows monotonous linear trend even at high temperatures. The obvious reason for this discrepancy is the assumption of absence of mass transfer resistances in the macropores. In this modified model this resistance has been

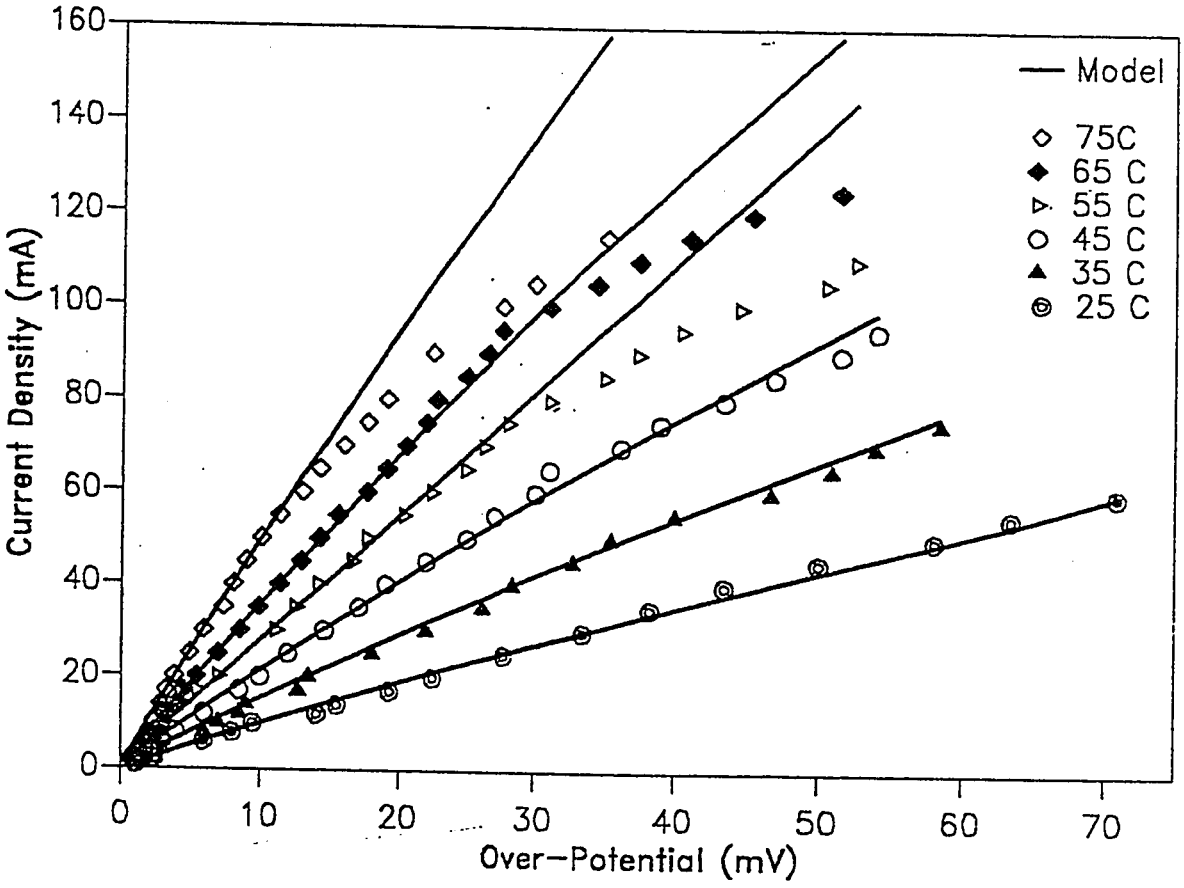

Fig. 7.3 : Polarization curves obtained from the spherical grain model and experimental data (2)

included. Besides, it is proposed that the hydrophilic grain is surrounded by a stagnant film of electrolyte of constant thickness. The reactant gas gets dissolved at outer surface. The dissolved molecules then diffuse into the stagnant film to reach the surface of the flooded catalyst grain. Further diffusion of these molecules takes place into the grain itself where the actual reaction takes place. The ionic conductivity path which was explained with the help of narrow electrolyte bridges among the grains in the previous model is more convincing now with the electrolyte film around the grain. The working mechanism and the structure of the electrode is shown in a schematic diagram in Fig. 7.4 The resistances in the different section of diffusion path of the gas are also shown.

For the mathematical development of this model, it is necessary to make the following assumptions :

1. Raney catalyst- PTFE grains are spherical, identical in size, structure and activity, isopotential, distributed homogeneously in the electrode, flooded with electrolyte and touching one another.
2. There exists a thin layer of the electrolyte on the surface of each agglomerates. This film helps in the ionic and electronic transport across the dissolved gas.
3. The local current density in the grain is given by Butler-Volmer Equation.
4. Diffusion of the dissolved gas in the grain and in the film occurs in the radial direction only while in macropores diffusion is in axial direction only.
5. The potential changes only across the thickness of the electrode.
6. There is no kinetic limitation on the dissolution of gas in the electrolyte.
7. The ionic concentration equilibration along the electrode is achieved by an evaporation condensation mechanism.

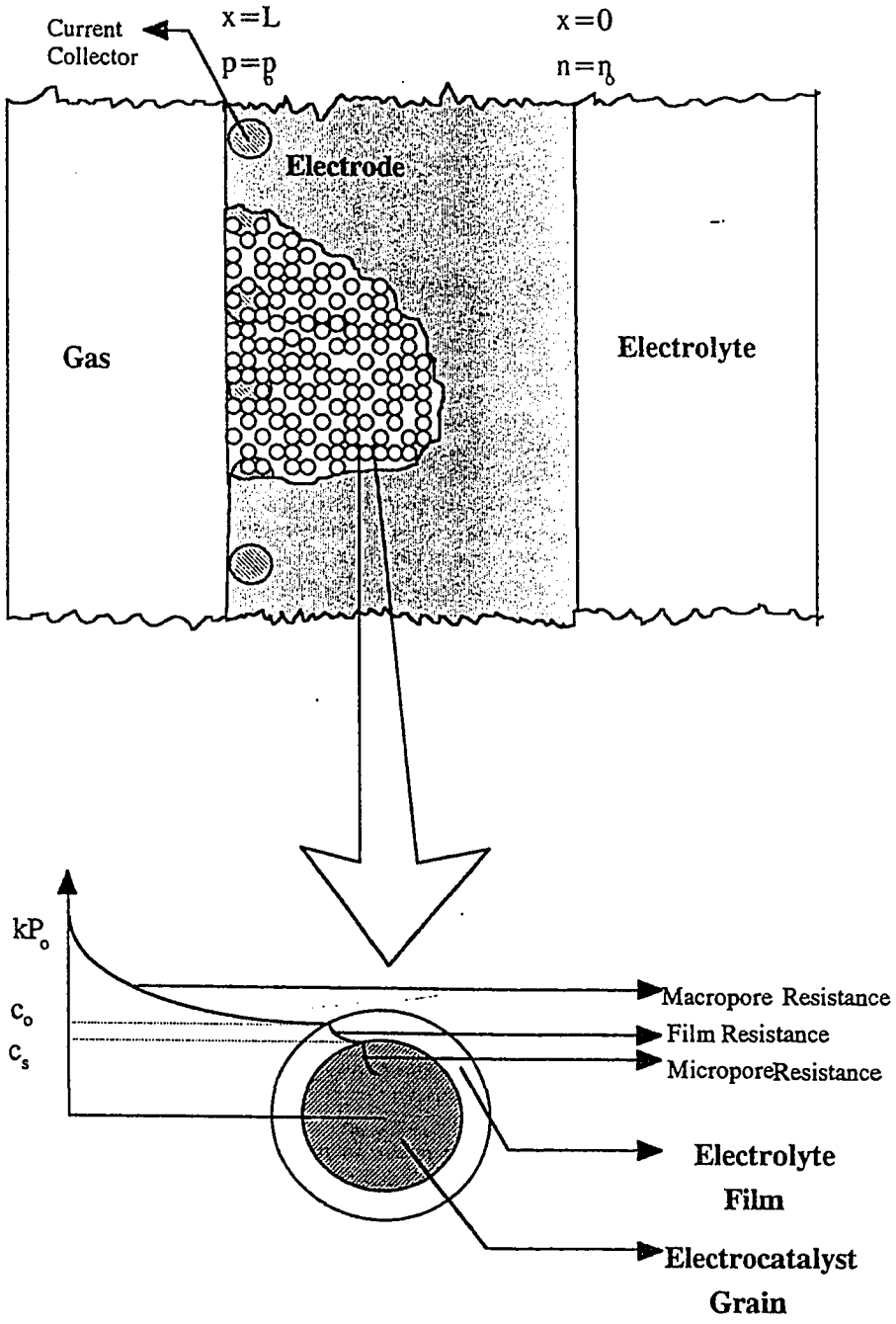

Fig.7.4: Schematic diagram of the fuel cell electrode and Raney Ni- PTFE grain

The modified model is based on the analyses of the grain, the film and the macropores. Then these analyses will be used with Ohm's law to describe the relationship between current density and overpotential.

7.2.1. The Grain

In the grain, the dissolved reactant gas is diffusing radially and reacting simultaneously. The local current density in the grain at a plane x in the electrode is given by Butler-Vohmer equation :

$$i = i_0\left[\frac{C}{C_0}\exp\left(\frac{\alpha zF\eta(x)}{R_gT}\right) - \exp\left(\frac{-(1-\alpha)zF\eta(x)}{R_gT}\right)\right] \qquad [7.6]$$

The rate of consumption of the reactant gas in the grain in terms of mol/cm^3 s, is given by :

$$r_{gas} = \frac{ia}{nF} \qquad [7.7]$$

The following equation is the mass conservation equation with simultaneous diffusion and reaction under steady state conditions in the grain assuming diffusion in radial direction only.

$$\frac{D_{le}}{r^2}\frac{\partial}{\partial r}\left[r^2\frac{\partial C(x,r)}{\partial r}\right] - r_{gas} = 0 \qquad [7.8]$$

Combining Eq. [7.6], [7.7]and [7.8] with necessary rearrangements to get :

$$\frac{1}{r^2}\frac{\partial}{\partial r}\left[r^2\frac{\partial C(x,r)}{\partial r}\right] = A_1\left\{\frac{C(x,r)}{C_0}A_2 - A_3\right\} \qquad [7.9]$$

with,

$$r = R \qquad C = C_s$$

$$r = 0 \qquad \frac{\partial C}{\partial r} = 0$$

Where A_1, A_2 and A_3 are given by Eqns. [7.2],[7.3] and [7.4] respectively.

The analytical solutions of Eq. [7.9] are:

$$\frac{C(x,r)}{C_0} = \left[\frac{C_s}{C_0} - \frac{A_3}{A_2}\right]\frac{R\sinh\left(r\sqrt{A_1A_2/C_0}\right)}{r\sinh\left(R\sqrt{A_1A_2/C_0}\right)} + \frac{A_3}{A_2} \qquad [7.10]$$

and

$$\left(\frac{dC(x,r)}{dr}\right)_{r=R} = C_0\left[\frac{C_s}{C_0} - \frac{A_3}{A_2}\right]\left[\sqrt{\frac{A_1A_2}{C_0}}\coth\left(R\sqrt{\frac{A_1A_2}{C_0}}\right) - \frac{1}{R}\right] \qquad [7.11]$$

7.2.2. The film

The dissolved gas must diffuse first into the film surrounding the spherical grain. The concentration at the outer surface is kp(x) while at the interface of film and grain, concentration is C_S. The continuity equation for this diffusing system at steady state is given by :

$$D_l\left[\frac{1}{r^2}\frac{\partial}{\partial r}\left(r^2\frac{\partial C_f}{\partial r}\right)\right] = 0 \qquad [7.12]$$

with the boundary conditions,

$$r = R \qquad C_f = C_s$$

$$r = R + \delta \qquad C_f = kp(x)$$

The solution of Eq. [7.12] is:

$$\left(\frac{\partial C_f}{\partial r}\right)_{r=R+\delta} = \frac{R(kp(x)-C_s)}{\delta(R+\delta)} \qquad [7.13]$$

At the interface between the film and the grain, following mass balance holds,

$$4\pi(R+\delta)^2 D_l\left(\frac{\partial C_f}{\partial r}\right)_{r=R+\delta} = 4\pi R^2 D_{le}\left(\frac{\partial C}{\partial r}\right)_{r=R} \qquad [7.14]$$

Substituting $\frac{\partial C}{\partial r}_{r=R}$ and $\frac{\partial C_f}{\partial r}_{r=R+\delta}$ from Eq [7.11] and [7.13] ,into Eq [7.14] to get:

$$C_s = \frac{kp(x) + \frac{R\delta D_{le} C_0 A_3}{(R+\delta)D_l A_2}\left[\sqrt{\frac{A_1 A_2}{C_0}}\coth\left(R\sqrt{\frac{A_1 A_2}{C_0}}\right) - \frac{1}{R}\right]}{1 + \frac{R\delta D_{le}}{(R+\delta)D_l}\left[\sqrt{\frac{A_1 A_2}{C_0}}\coth\left(R\sqrt{\frac{A_1 A_2}{C_0}}\right) - \frac{1}{R}\right]} \qquad [7.15]$$

7.2.3. The Macropores

In the hydrophobic macropores, the reactant gas is diffusing and is being consumed simultaneously with the following mass conservation equation :

$$D_g \frac{d^2 p}{dx^2} - R^* = 0 \qquad [7.16]$$

Here Dg is the effective diffusivity of the gas in the macropores. The consumption term R* is the rate of consumption per unit volume of the electrode, and is given by :

$$R^* = \left[4\pi R^2 D_{le} \left(\frac{\partial C}{\partial r} \right)_{r=R} \right] \left[\frac{N_1}{L} \right] \qquad [7.17]$$

Where, $$N_1 = \frac{(1-\varepsilon)}{\pi R^2} \qquad [7.18]$$

Combining Eq.[7.16],[7.17],[7.18] to get :

$$D_g \frac{dp}{dx^2} - \frac{4 D_{le} (1-\varepsilon)}{L} \left. \frac{\partial C}{\partial r} \right|_{r=R} = 0 \qquad [7.19]$$

with the following boundary conditions

$$x = 0 \qquad \frac{dp}{dx} = 0$$

$$x = L \qquad p = p_0$$

7.2.4. Ionic Overpotential

The overpotential inside the electrode varies in the axial direction. The current density and overpotential are related by Ohm's Law:

$$\frac{d\eta}{dx} = \frac{-j(x)}{\pi R^2 \kappa_e N_1} \qquad [7.20]$$

The differential current density generated in the differential axial distance dx is given as :

$$-dj(x) = 2\pi R N_1 n F D_{le}\left(\frac{dC}{dr}\right)_{r=R} dx \qquad [7.21]$$

Differentiating Eq. [7.20] and substituting N1 from Eq. [7.18] to get :

$$\frac{d^2\eta}{dx^2} = -\frac{1}{k_e(1-\varepsilon)}\left(\frac{dj(x)}{dx}\right) \qquad [7.22]$$

Substituting $\frac{dj(x)}{dx}$ from Eq.[7.21] into [7.22] to get :

$$\frac{d^2\eta}{dx^2} = \frac{2nFD_{le}}{k_e R}\left(\frac{dC}{dr}\right)_{r=R} \qquad [7.23]$$

with,

$$x = 0 \qquad \eta = \eta_0$$

$$x = L \qquad \frac{d\eta}{dx} = 0$$

The term $\left.\frac{dC}{dr}\right|_{r=R}$ is given by Eqn [7.11].

The final form of the equation is :

$$\frac{d^2\eta}{dx^2} = \frac{2nFD_{le}C_0}{k_e R}\left[\frac{C_s}{C_0} - \frac{A_3}{A_2}\right]\left[\sqrt{\frac{A_1A_2}{C_0}}\coth\left(R\sqrt{\frac{A_1A_2}{C_0}}\right) - \frac{1}{R}\right] \qquad [7.24]$$

7.3. Solution of Model Equations

In order to get polarization data for the electrode, Eq. [7.19] and [7.24] have to be solved simultaneously. Analytical solution of these equations is not possible. A numerical technique is used . In this technique, the given boundary problem is converted into initial value problem (IVP) by guessing the initial conditions where they are not given. Other sets of initial value problems are generated by differentiating the first set with respect to the assumed values of initial conditions. These sets are solved simultaneously using a suitable subroutine. The assumed initial conditions are corrected using the solution of IVP's. The procedure is repeated with new corrected initial conditions, till the calculated boundary conditions and given boundary conditions are almost same. (11).

The first set of IVP for Eq. [7.19] and [7.23] is as follows :

$$
\begin{aligned}
y'_1 &= y_2 \\
y'_2 &= AW1 * DECR \\
y'_3 &= y_4 \\
y'_4 &= AW2 * DECR
\end{aligned}
\qquad [7.25]
$$

$$
\begin{aligned}
y_1(0) &= \eta_0 \\
y_2(0) &= a, (assumed) \\
y_3(0) &= b, (assumed) \\
y_4(0) &= 0
\end{aligned}
\qquad [7.26]
$$

Here, a and b are the first guess for the initial conditions. Following abbreviations are used for the sake brevity.

$$y_1 = \eta, y_2 = \frac{d\eta}{dx}, y_3 = p, y_4 = \frac{dp}{dx}$$

$$AW_1 = \frac{2nFD_{le}}{\kappa_e R},\ AW = \frac{4D_{le}(1-e)}{D_g L} \text{ and } DECR = \frac{\partial C}{\partial r}$$

In order to find out the second set of the IVP's Eq. [7.25] and [7.26] are differentiated with respect to a . This results into :

$$\begin{aligned} y'_5 &= y_6 \\ y'_6 &= AW1 * DECRA \\ y'_7 &= y_8 \\ y'_8 &= AW2 * DECRA \end{aligned} \qquad [7.27]$$

$$\begin{aligned} y_5(0) &= 0 \\ y_6(0) &= 1 \\ y_7(0) &= 0 \\ y_8(0) &= 0 \end{aligned} \qquad [7.28]$$

Where,

$$y_5 = \frac{dy_1}{da}, y_6 = \frac{dy_2}{da}, y_7 = \frac{dy_3}{da}, y_8 = \frac{dy_4}{da}$$

$$DECRA = \frac{dDECR}{da}$$

In the same way third set of IVP's are generated by differentiating Eq.[7.25] and [7.26] with respect to b :

$$\begin{aligned} y'_9 &= y_{10} \\ y'_{10} &= AW1 * DECRB \\ y'_{11} &= y_{12} \\ y'_{12} &= AW2 * DECRB \end{aligned} \qquad [7.29]$$

$$\begin{aligned} y_9(0) &= 0 \\ y_{10}(0) &= 0 \\ y_{11}(0) &= 1 \\ y_{12}(0) &= 0 \end{aligned} \qquad [7.30]$$

Where,

$$y_9 = \frac{dy_1}{db}, y_{10} = \frac{dy_2}{db}, y_{11} = \frac{dy_3}{db}, y_{12} = \frac{dy_4}{db}$$

$$DECRB = \frac{dDECR}{db}$$

These three sets of IVP's have been solved numerically by using a FORTRAN subroutine called RKGS. RKGS uses Runge Kutta method with adjustable step size according to the error. Once these IVP's are solved, the correction in a and b, denoted by da and db are estimated using the solution. Following calculations are performed before da and db :

$$\delta y_2 = (y_2|_{x=L})_{estimated} - (y_2|_{x=L})_{given}$$
$$\delta y_2 = (y_2|_{x=L})_{estimated} - (y_2|_{x=L})_{given} \quad [7.31]$$

Then da and db are estimated by solving following two simultaneous linear equations :

$$\delta y_2 = y_6 da + y_{10} db$$
$$\delta y_3 = y_7 da + y_{11} db \quad [7.32]$$

The error is estimated by:

$$SS = \sqrt{\delta y_2^2 + \delta y_3^2} \quad [7.33]$$

After that new guesses for the initial conditions are estimated.

$$a = a|_{initial} + da \quad [7.34]$$

$$b = b|_{initial} + db \quad [7.35]$$

The flowchart of the logic used in the development of FORTRAN code to solve this problem is shown in Fig. 7.5. The FORTRAN program is given in Appendix-F.

7.4. Result and Discussion

The model equations have been solved using the estimated parameters of hydrogen, Raney Ni-PTFE electrode using 25% KOH electrolyte. This system has been studied extensively by Celiker (1). Parameters related to the electrode were

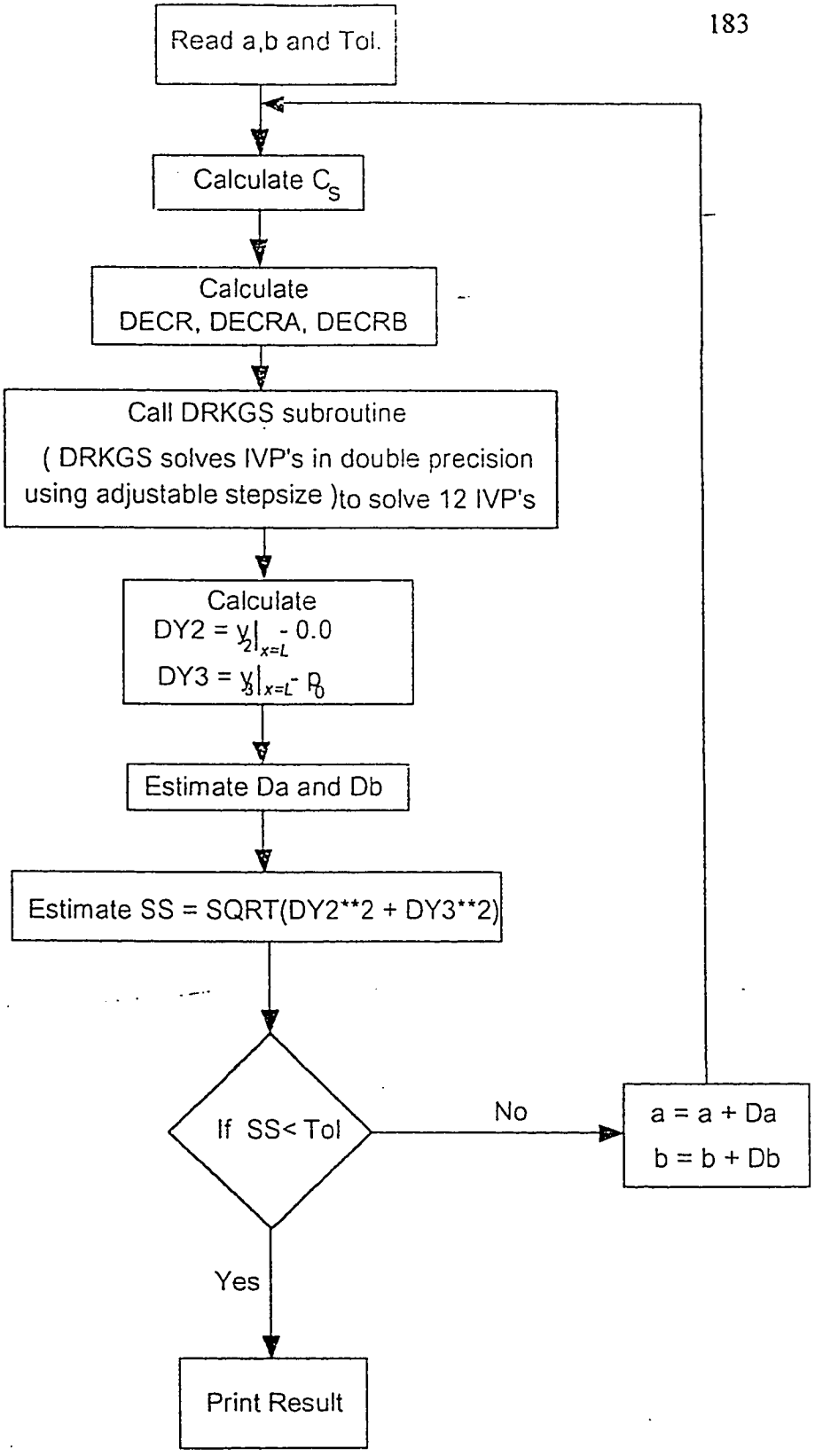

Fig. 7.5 : Flow chart for the FORTRAN program to solve model equations

deduced from the characterization of the electrode. The rest of the parameters have been estimated using empirical relationships and published data. Using these parameters at various temperatures namely; 25,35,45,55,65 and 75°C, polarization data were generated and fitted into the experimentally obtained curves. Fitted parameters were estimated from these curves.

7.4.1. Estimation of the Model Parameters

A. Conductivity of the Electrolyte:

Conductivity of KOH solution depends upon its concentration and the temperature. In this calculation an empirical relation proposed by Kirkpatric et al. (12) is used. The general form of this equation is:

$$\kappa = 0.0262W + 6.7\times10^{-4}Wt - 4.8\times10^{-4}W^2 - 8.8\times10^{-6}W^2t$$

where,

κ= conductivity, $\Omega^{-1}cm^{-1}$

W= concentration of KOH solution, wt %

t= temperature , °C

The values of conductivity are estimated at all desired temperatures . They are listed in Table 7.1. The path of the ionic conductivity is considered through the flooded agglomerates. Therefore model requires effective conductivity . The effective conductivity can be written as

$$\kappa_e = \frac{\kappa\varepsilon_{mic}}{\tau_{mic}}$$

Here,

κ_e= effective conductivity

Table 7.1 : Estimated and Fitted Parameters for the modified Model at Different Temperatures

	Estimated Parameters from Literature				Parameters found from this Model		
Temp °C	κ $\Omega^{-1}cm^{-1}$	$k.10^9$ $mol/cm^3\ kPa$	$D_g.10^{11}$ $mol/cm.kPa.s$	$D_l.10^5$ cm^2/s	α	$\delta.10^5$ cm	$i_0.10^6$ mA/cm^2
25	0.254	1.449	4.589	1.515	0.59	7.0	11
35	0.300	1.230	4.097	1.938	0.59	7.0	26
45	0.344	1.0145	3.540	2.625	0.59	7.0	85
55	0.390	0.8696	3.182	3.931	0.59	8.0	160
65	0.434	0.6667	2.551	7.404	0.59	8.0	300
75	0.464	0.5070	2.279	9.529	0.59	8.0	1000

ε_{mic} = micropore porosity

τ_{mic} = micropore tortuosity

B. Estimation of Henry's Constant

Henry's constant for Oxygen and Hydrogen are estimated from the solubility and activity data given by Shoor *et al.*(13) Solubility of these gases in pure water at atmospheric pressure is taken from the same source. Solubility in 25% KOH is calculated by dividing these values by the activity at the corresponding temperature. The data are available at 25°C,40°C,60°C, 80°C, and 100°C and at concentration from 0N to 50.65N. Required data are extra or interpolated from these values. The estimated values for hydrogen gas are listed in Table 7.1.

C. Diffusion Coefficients in Macropores:

The molecular diffusivities of Oxygen and Hydrogen are calculated according to equation proposed by Hirchfelder *et al.* (14). The equation is as follows ;

where,

D_{AB} = diffusivity of A in B , m^2/s

M_A= molecular wt of A

M_B= molecular wt of B

P_t= pressure, Pa

r_{AB} and $f(kT / \varepsilon_{AB})$ are parameters which depend upon diffusing gases and the temperature. Diffusivity calculated in this way has to be corrected for the porous structure of the electrode. This is done according to the following equation;

$$D_e = \frac{D\varepsilon_{mac}}{\tau_{mac}}$$

where,

D_e= effective diffusivity

ε_{mac}= porosity due to macropores = 0.21 (from the characterization of the electrode)

τ_{mac}= tortuosity of the macropores = 6 (assumed in order to check the validity of the model)

As the concentration in the macropores is considered in terms of pressure, the diffusivity must be multiplied with Henry's constant. As a result the dimensions of diffusivity becomes mol/cm kPa s. Estimated values for Oxygen and Hydrogen are shown in Table 7.1.

D. Diffusivities in KOH Solution

Estimation of diffusivities in the liquid is not as reliable as that of the gases. Following expression can be used for estimation of diffusivity of Hydrogen in the electrolyte (15).

$$D_l \mu = 7.4\text{X } 10^{-8} \frac{(xM)^{0.5}}{(v_b)^{0.6}}$$

where,

D_l = diffusivity, cm^2/s

μ = viscosity of liquid, cp

M = average molecular weight of the liquid

x and v_b are constant listed in Ref (15).

Values of diffusivity and effective diffusivities are estimated at required temperatures and listed in Table 7.1.

E. Other Parameters and Constants

Other parameters and constants required in the model are listed below :

z.= 1.0

n = 2.0

F = 96484.56

R = 2.0x10-3 cm (from characterization of the electrode)

L = 0.032 cm (from characterization of the electrode)

R_g = 8.31

ε_{mac} = 0.21

7.4.2. Effects of Various Parameters on the Polarization Behavior

In order to see the effect of the parameters on the polarization behavior, a base set of estimated and fitted parameters is arbitrarily fixed. The estimated temperature dependent parameters were fixed at 75°C. A set calculated in this way is as follows :

κ_e= 0.464 $\Omega^{-1}cm^{-1}$

k= 0.507x10^{-9} mol/cm^3 kPa

D_g= 2.279x10^{-11} mol/cm kPa s

d_{le}= 9.529x10^{-5} cm^2/s

δ= 8.0x10^{-5} cm

i_0= 1000 mA/cm^2

P_0= 138 kPa

One parameter is varied while keeping all other at the base value. Fig.7.6 shows effect of the film thickness (δ). This is varied from 0.5x10^{-5} cm to 10.0x10^{-5} cm. It can be seen that with low values of δ, the current generated for a given value of the overpotential is high. It is obvious that with thinner film, diffusion will be higher resulting into relatively higher supply of the reactant gas to the catalytic sites. At higher values of δ, current becomes almost constant at overpotential more than 100 mV. This shows the limiting current of the electrode. The previous model failed to show the limiting current.

In Fig 7.7 effect of exchange current density is shown. Exchange current density is the electrochemical counterpart of the rate constant of the chemical reaction. The current generated must increase with increased values of the exchange current density. This result is shown in Fig. 7.7, where exchange current density varies from 50X10-6 to 1000X10-6 mA/cm2.

The grain radius (R) affects the polarization performance of the electrode as shown in Fig. 7.8. in which R is varied from 1.5x10^{-3} to 3.0x10^{-3} cm. The larger the grain radius, the less current is generated.

Effect of diffusivities of reactant gas into the electrolyte is shown in Fig.7.9. D_{le} has been varied from the 5.0x10^{-5} to 20x10^{-5} cm^2/sec. As D_{le} increases the current density increases for each value of the overpotential. This trend is expected because as D_{le} increases, more reactant is available for the reaction.

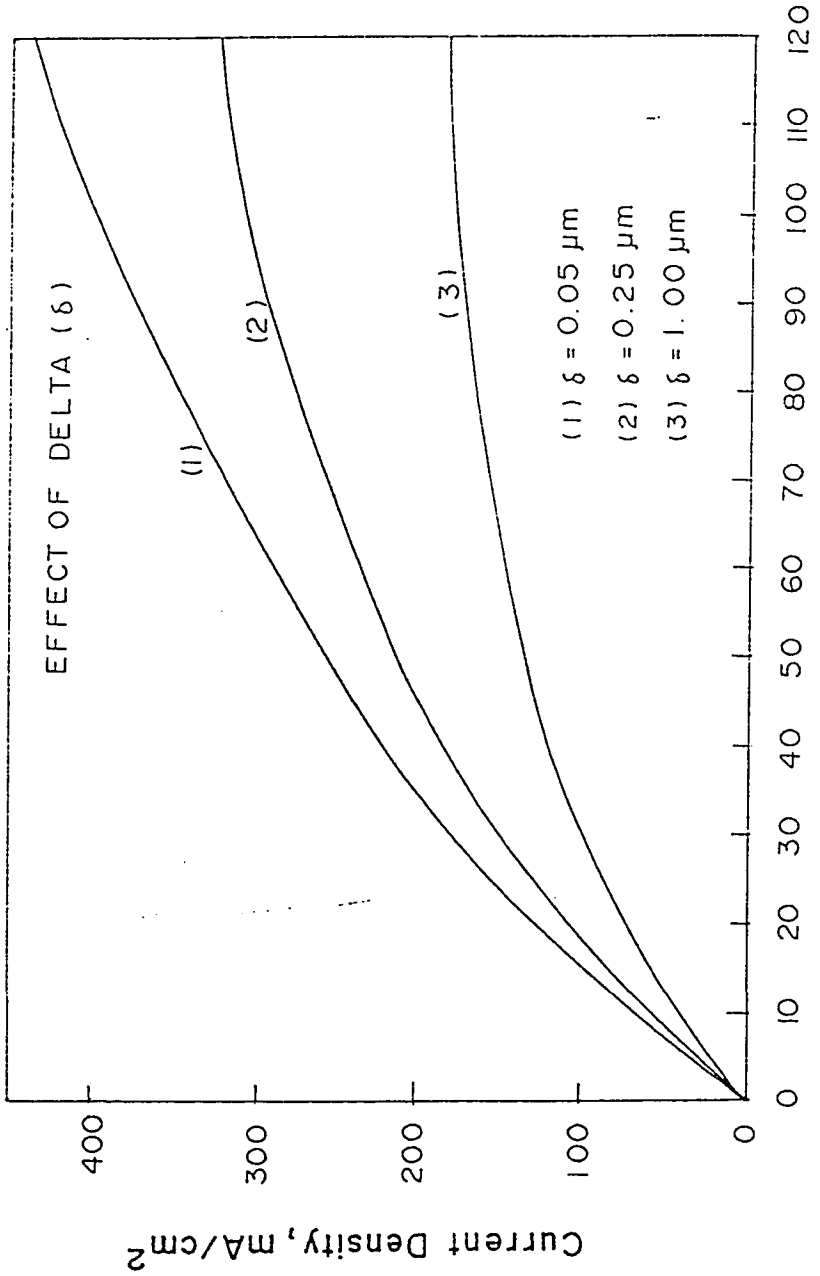

Fig. 7.6 : Effect of film thickness on Polarization of electrode using parameters at 348 K

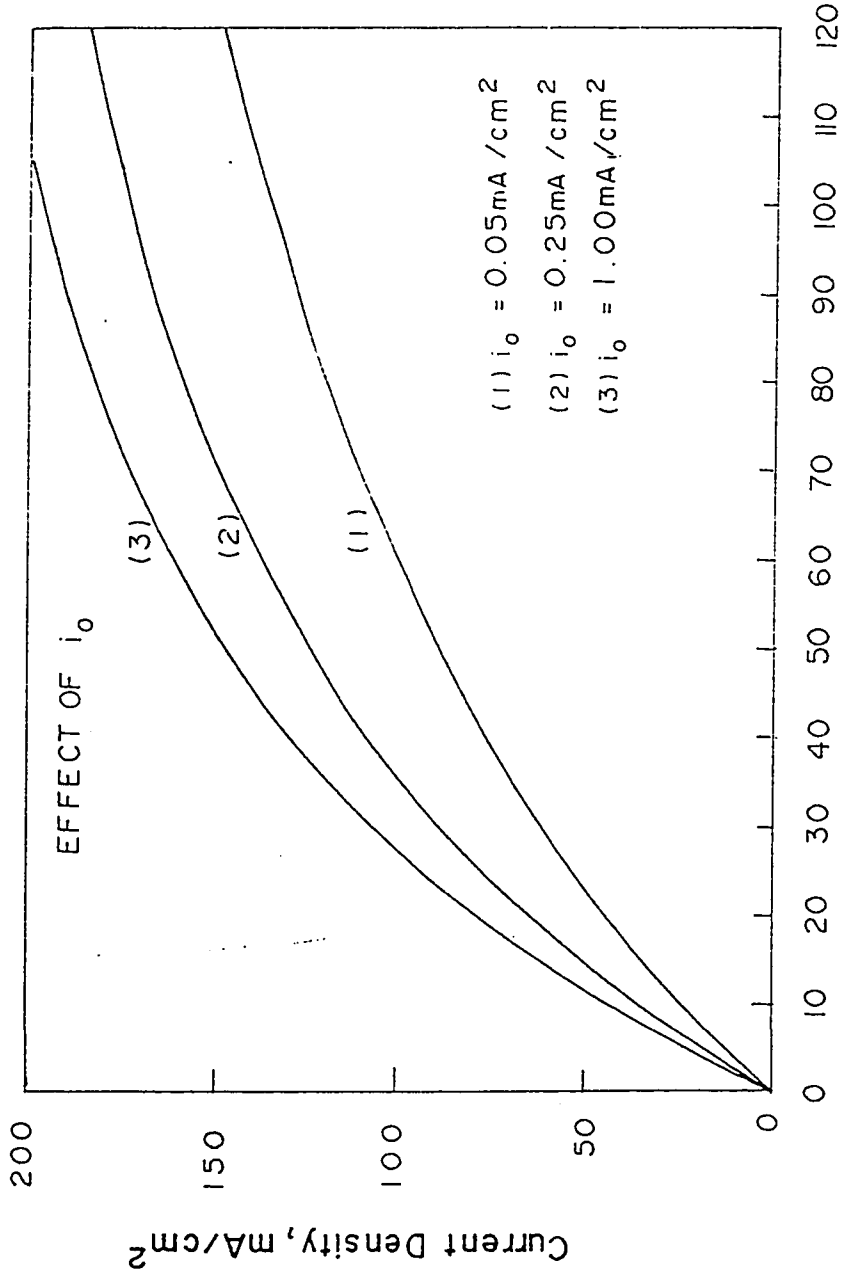

Fig. 7.7 : Effect of exchange current density on polarization of electrode using parameters at 348 K

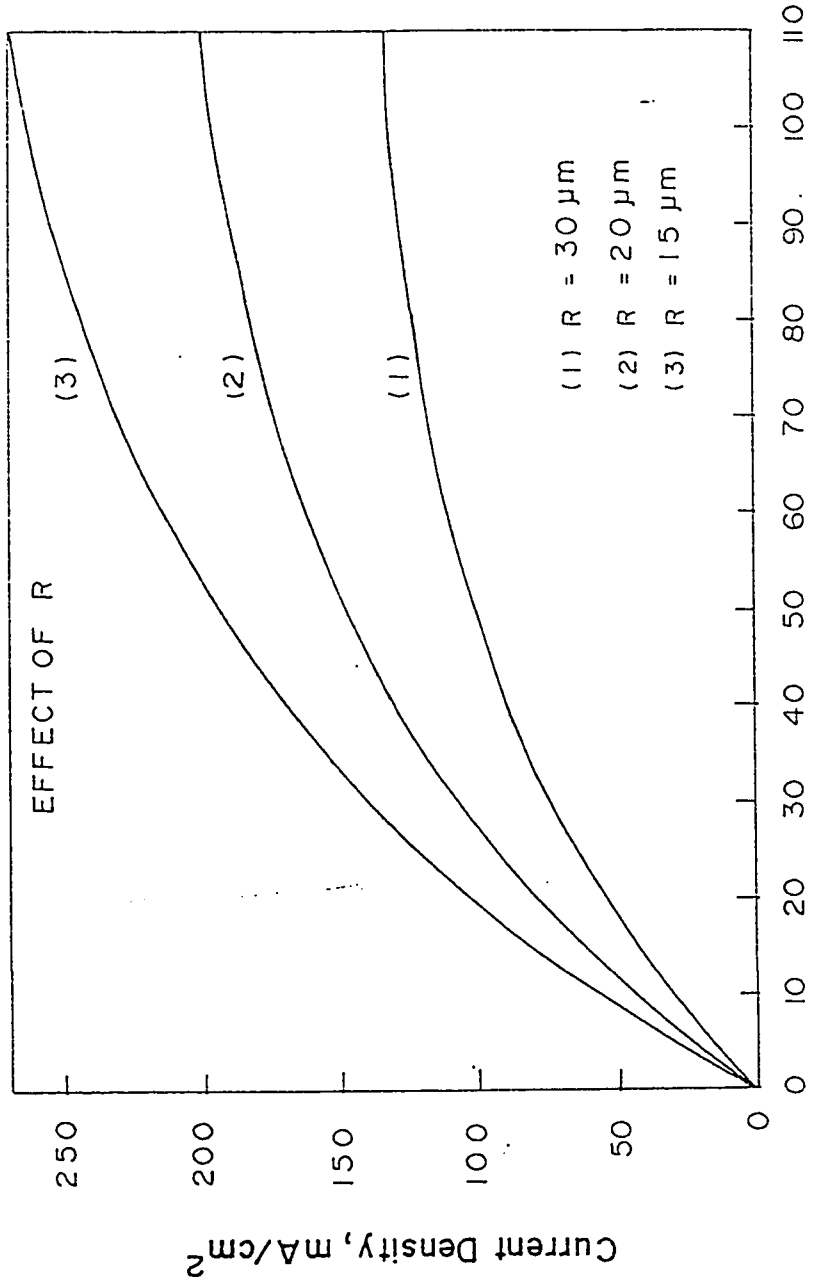

Fig. 7.8 : Effect of grain radius on polarization of electrode using parameters at 348 K

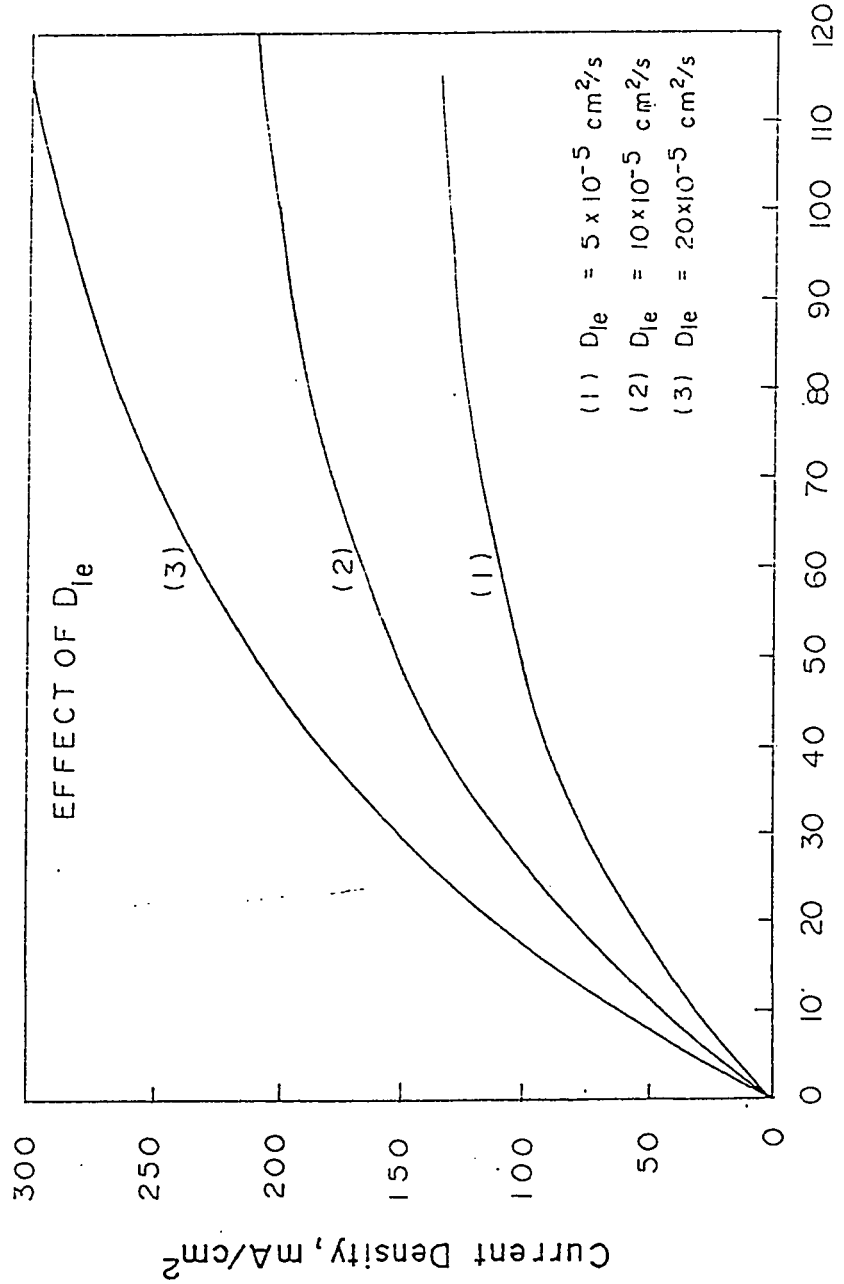

Fig. 7.9 : Effect of diffusivity of H_2 in the electrolyte on polarization of electrode using parameters at 348 K

In Fig. 7.10, effect of D_g is shown. Higher D_g means higher reactant supply to the catalyst. Therefore the current density for higher D_g should be higher. This is coherent with the plotted results.

In Fig 7.11 , profiles of the reactant concentration across the electrode are plotted. The data are generated at measurable overpotential of 55 mV. It is clear from the plot that at higher values of D_g, the pressure in the macropores remains almost constant. At this situation, macropore diffusion resistance is negligible and the overall reaction is controlled by the electrochemical reaction and/or micropore diffusion. At lower values of D_g the overall reaction will be macropore diffusion controlled. At extremely low values there will be very little reactant available for the reaction. This explains the dip to zero current after the limiting current.

7.5.3 Polarization Curves at Different Temperatures

Polarization curves obtained from this modified model, previous model and experiments are plotted in Fig.7.12 and 7.13 for temperature 35 & 45 and 55 & 75 °C. It can be seen that the modified model fits very well into the experimental data. It can be inferred from the fitted data that film thickness remains constant with temperature while exchange current density varies. The exchange current density in fact is electrochemical counterpart of the rate constant for the chemical reactions. Therefore an Arhenious type of temperature dependence is expected. Logarithm of i_0 is plotted against the inverse of the absolute temperature. Fig. 7.14 shows that this plot is linear and the estimated value of the activation energy is 75.2 kJ/mol. This value is about twice that of predicted by the spherical grain model. This indicates that the hydrogen oxidation on Ni-PTFE electrode is, in fact,

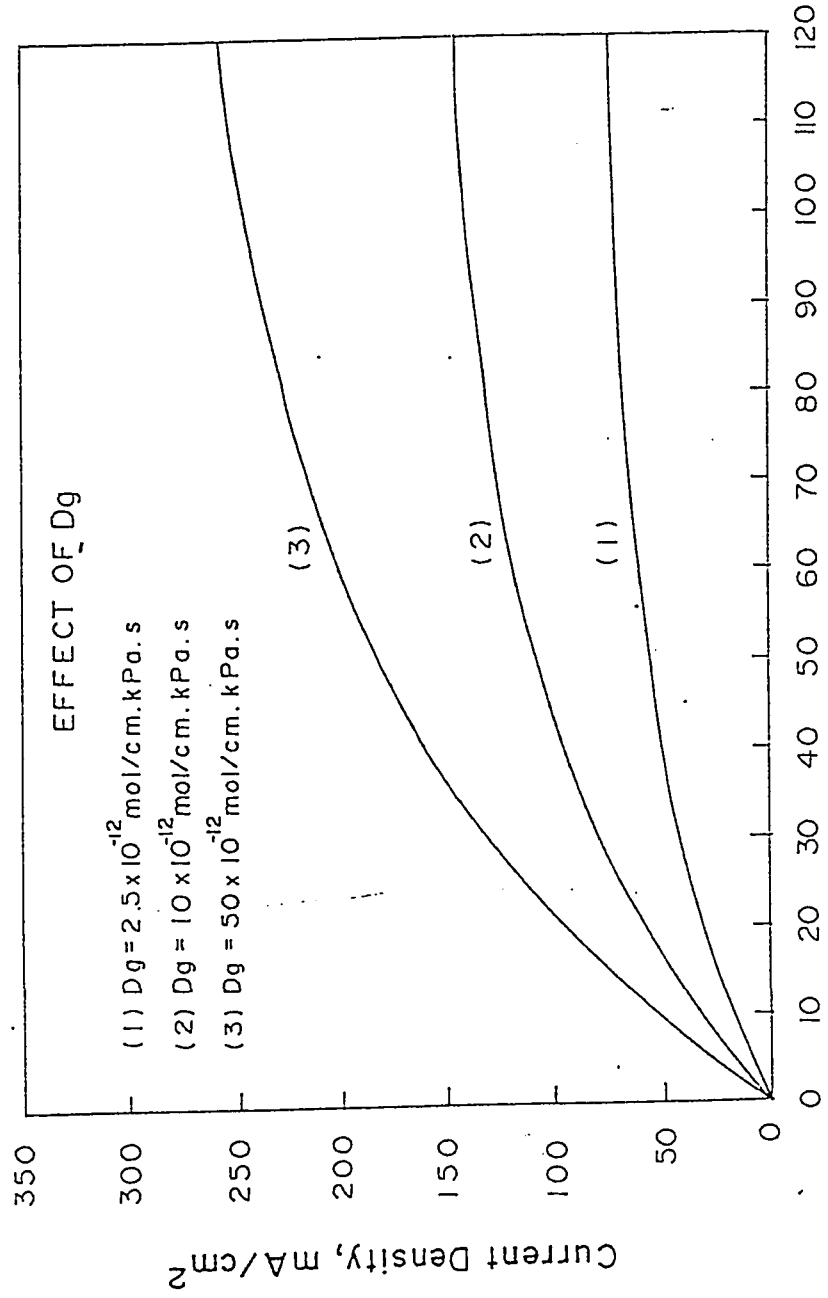

Fig. 7.10 : Effect of diffusivity of H_2 in the macropores on polarization of electrode using parameters at 348 K

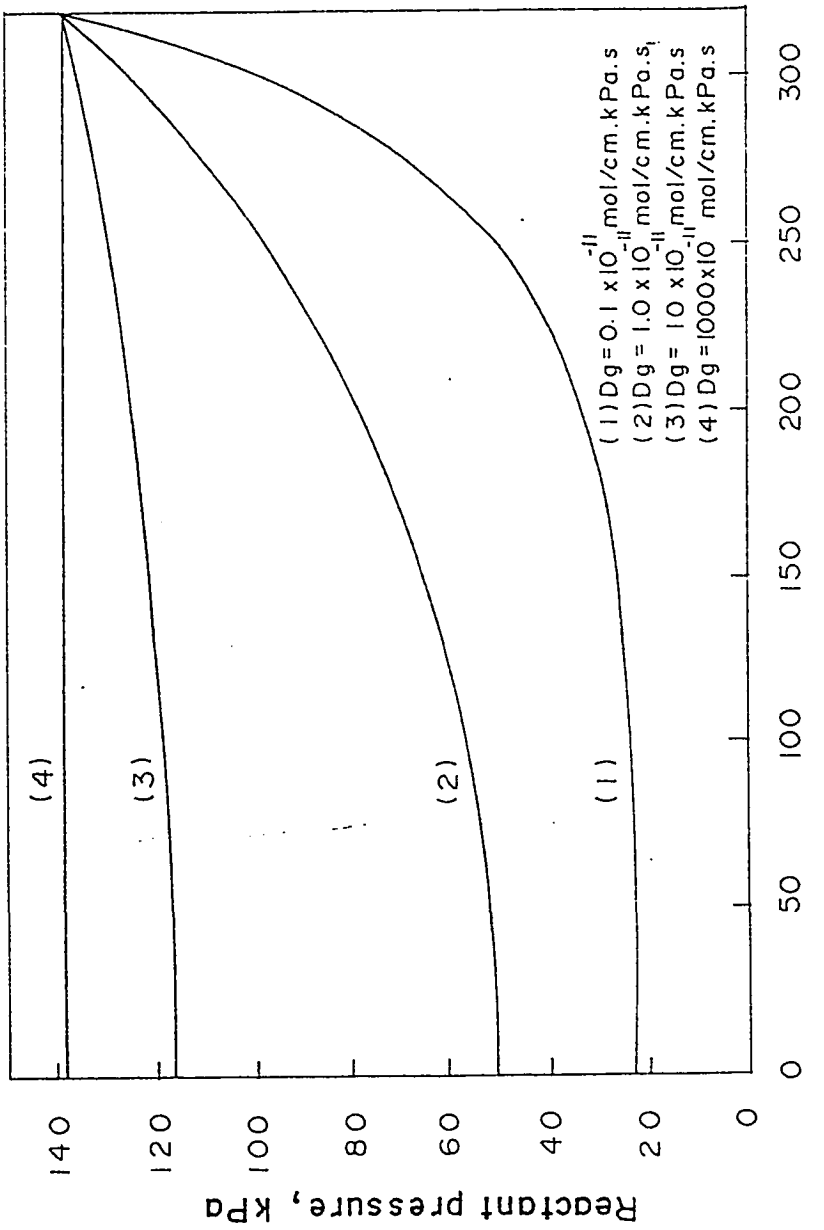

Fig. 7.11 : Reactant pressure profiles in the electrode at different macropore diffusivities at η_0 = 44 mV and other parameters at 348 K

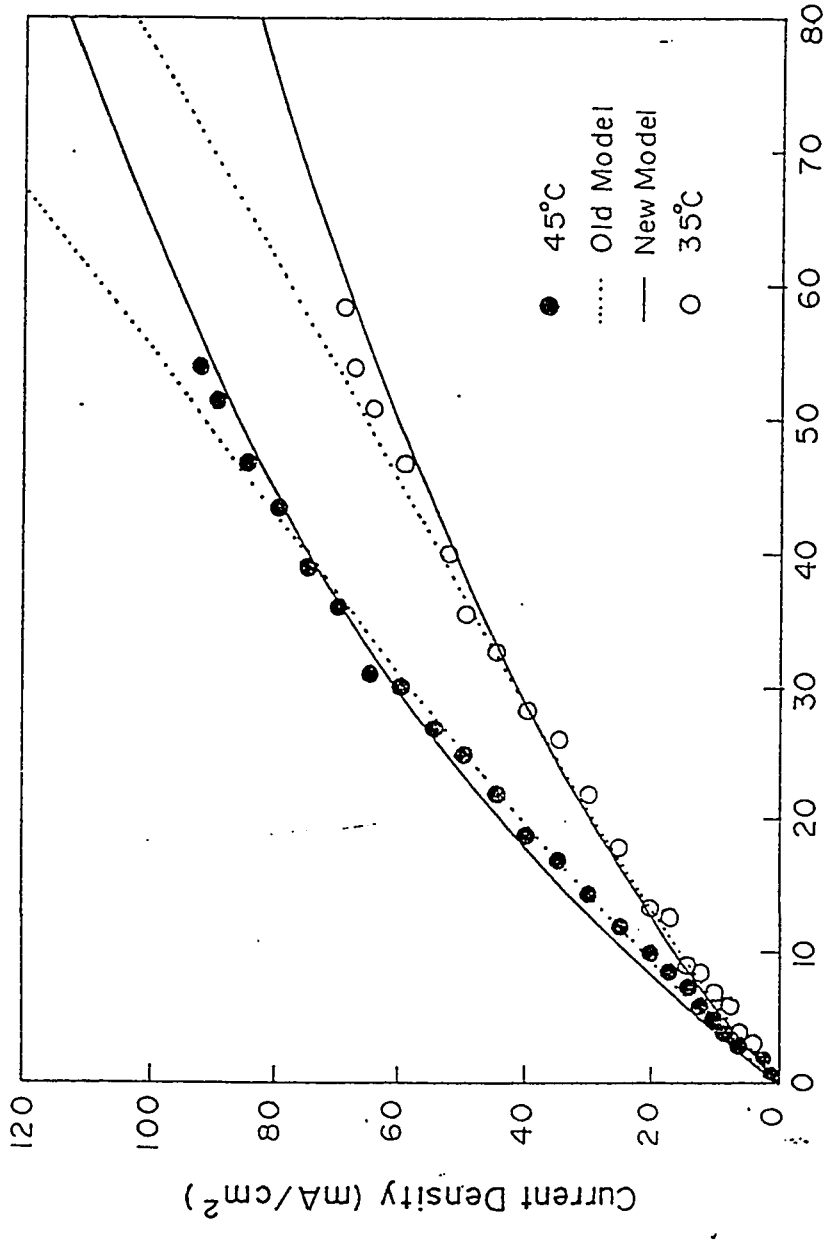

Fig. 7.12 : Comparison of the experimental data with old and modified model (T= 308 and 318 K)

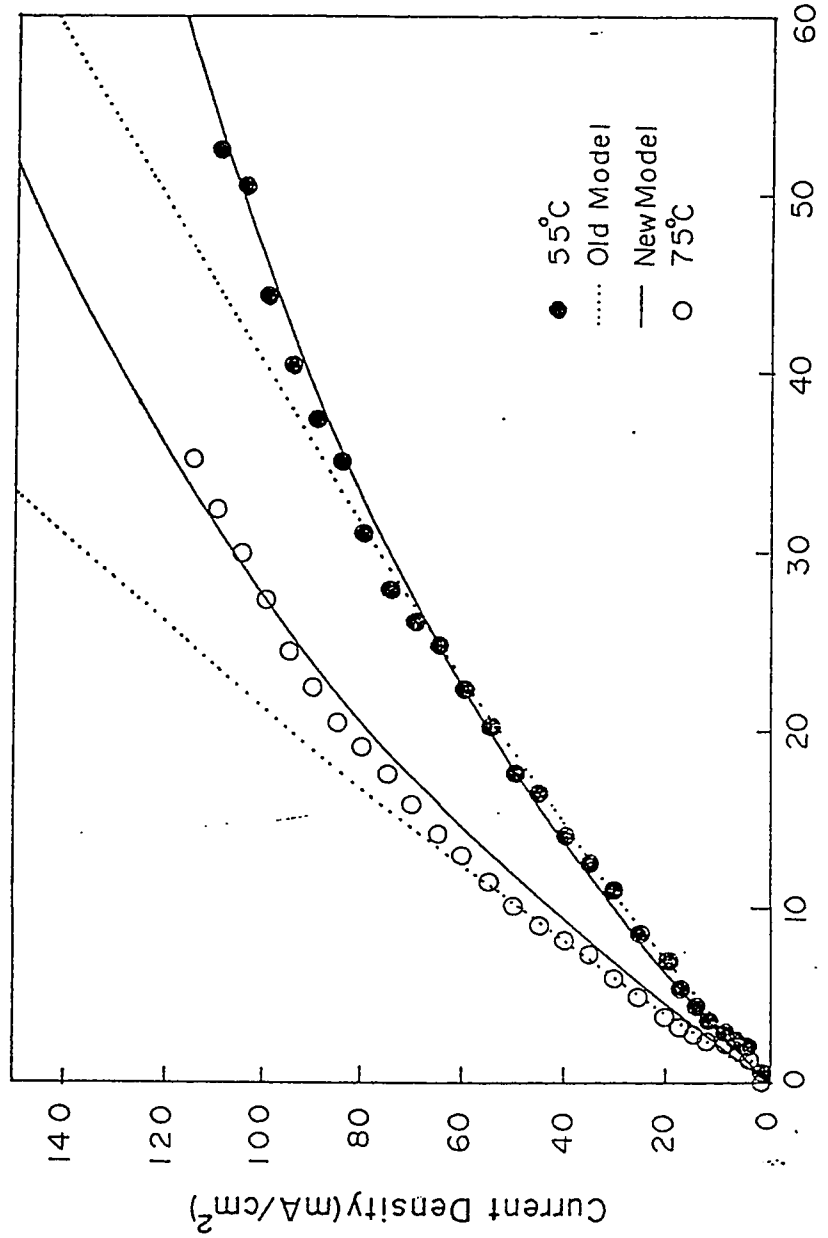

Fig. 7.13 : Comparison of the experimental data with old and modified model (T=328 and 348 K)

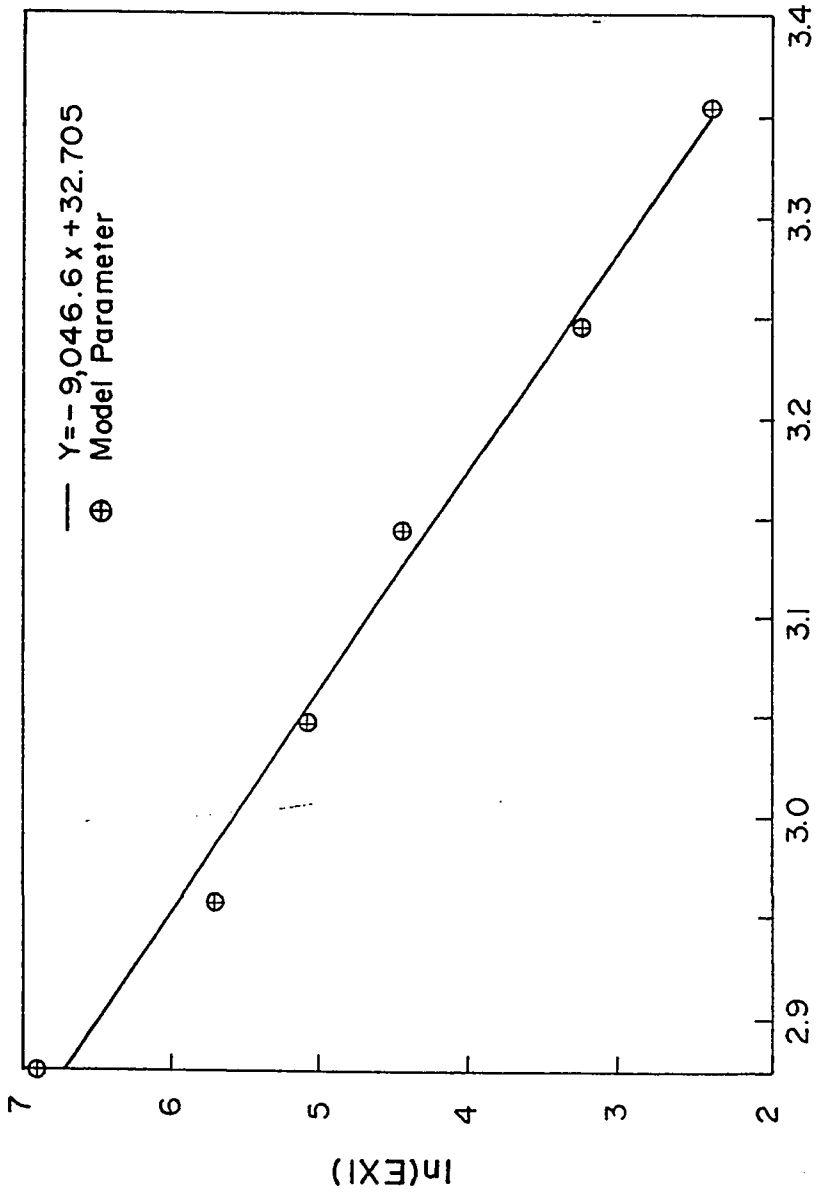

Fig. 7.14 : Exchange current density vs. 1/T (Arrhenious Plot)

mass transfer limited. Therefore the activation energy predicted by the original model gave a lower value.

References

1. Celiker, H., *Ph.D. Thesis, King Fahd University of Petroleum and Minerals*, 1990.

2. Celiker, H., M.A.Al-Saleh, S.Gultekin and A.S.Al-Zakri, *Journal of the Electrochemical Society*, **138**, 6, 1991.

3. Mund, K., G. and F. von Sturm, *Journal of Proceedings of the Workshop on the Electrocatalysis of Fuel Cell Reactions*, **79-2**,Ed. W.E. O'Grady, S. Srinivasan, R.F. Dudley, Brookhaven National Laboratory, Upton, New York, pp 47-66. May 15-16 (1978).

4. Vielstich, W., *Journal of Proceedings of the Workshop on the electrocatalysis of Fuel Cell Reactions*, Vol. **79-2**, Ed. W.E. O'Grady, S. Srinivasan, R.F. Dudley, Brookhaven National Laboratory, Upton, New York, pp 67-83,May 15-16, (1978).

5. F. von Sturm, H. Nischik and E. Weidlich, *Ing. Dig.*, **5**, 2 ,1966.

6. Bacon, F.T., *British Patent* **667,296** (1952).

7. Ewe, H., E.Justi and H.J. Selbach, *Energy Conversion and Management*, **23**, 42, 245 (1983).

8. Ewe, H.H., E.W.Justi and H.J. Selbach, *Energy Conv. & Mgmt.*, **20**, 75, 1980.

9. Giner, J. and C. Hunter, *Journal of the Electrochemical Society*, **116,** 1124, 1969.

10. Will, F.G., *Journal of the Electrochemical Society*, **110**, 145, 1963.

11. Fox, L., *Numerical Solution of Ordinary and Partial Differential equations*, Pegamon Press, Oxford, 1961.

12. A.L.Horwarth, *Handbook of Aqueous Electrolyte Solutions, Physical Properties*, Estimation and Correlations, Ellis Horwood Ltd., England, 252(1985)

13. S.K.Shoor, R.Duklaker and K.E.Gubbins, *Journal of Phy. Chem*, **175,** 312 (1969).

14. J.Hircheflder, R.B.Bird and E.L.Spotz, *Trans. ASME*, **71,** 921(1949)

15. R.H.Perry, and C.H. Chilton, *Chemical Engineers' Handbook*, Fifth Ed., McGraw Hill International Book Co., (1982).

8

Results and Discussions

8.1. Introduction

The gas diffusion electrodes are prepared using the filtration Method. In this method, the passivated Raney-Ni is milled with PTFE powder. A slurry of the milled powder is made using a suitable surfactant. This slurry is filtered on a filter paper. Subsequent rolling of nickel mesh and the filter cake produced in the previous step, results into the electrode. There are a number of parameters which may affect the performance of the electrode. Out of these parameters, five parameters are selected for further investigation. A number of electrodes are prepared, tested and characterized for this purpose. Galvanostatic polarization data were obtained to assess the performance of the electrodes. In this chapter, the mechanism of important steps in the formation of the electrodes are discussed. In the subsequent section, the effect of various parameters on the performance is discussed. Using the optimum parameters, electrodes are made and tested at various temperatures. These results are compared with similar electrodes prepared by other research groups. The long term performance of the optimum electrode was tested under an external load. The results are included in this chapter.

8.2. Passivation of the Raney-Ni Catalyst

All the electrodes prepared by filtration method utilized Raney-Ni passivated by conventional method as discussed in Chapter 4. The passivated catalyst was characterized by XRD, BET surface area and SEM. The XRD pattern shown in Fig 8.1. has three prominent peaks which correspond to (1,1,1), (2,0,0) and (2,2,0) of the standard nickel XRD pattern. The peaks are sharp and pointed indicating the presence of considerable crystalline nickel. This is a harbinger of high active surface area. The peaks corresponding to NiO are very shallow and small suggesting that little NiO is present in the sample. This may be hypothesized to be present on the surface as a result of slow oxidation of Ni along with the adsorbed hydrogen.

The BET surface area is $72.27 m^2/g$. The external surface area of the Raney Ni powder which has average particle size of 25 micron and density equals to 5.212 g/cm^3 can be calculated theoretically assuming spherical particles. This comes out to be $1.51*10^{-2} m^2/g$. From the comparison of the BET surface area and the external surface area, it can be easily deduced that the particles posses considerable micropores.

In Fig 8.2 two SEM micrographs of Raney-Ni samples passivated with conventional method are shown. They are magnified to 500 and 5000 times respectively. The particles are of irregular shapes and have different size varying from submicron to 50 microns. The SEM with 5000 magnification shows clearly that the particles have sharp edges and are not fused into one another. This suggests that virtually no sintering took place. However, the sintering in the microporous structure having pores of less than 100 °A in each particle, can not be

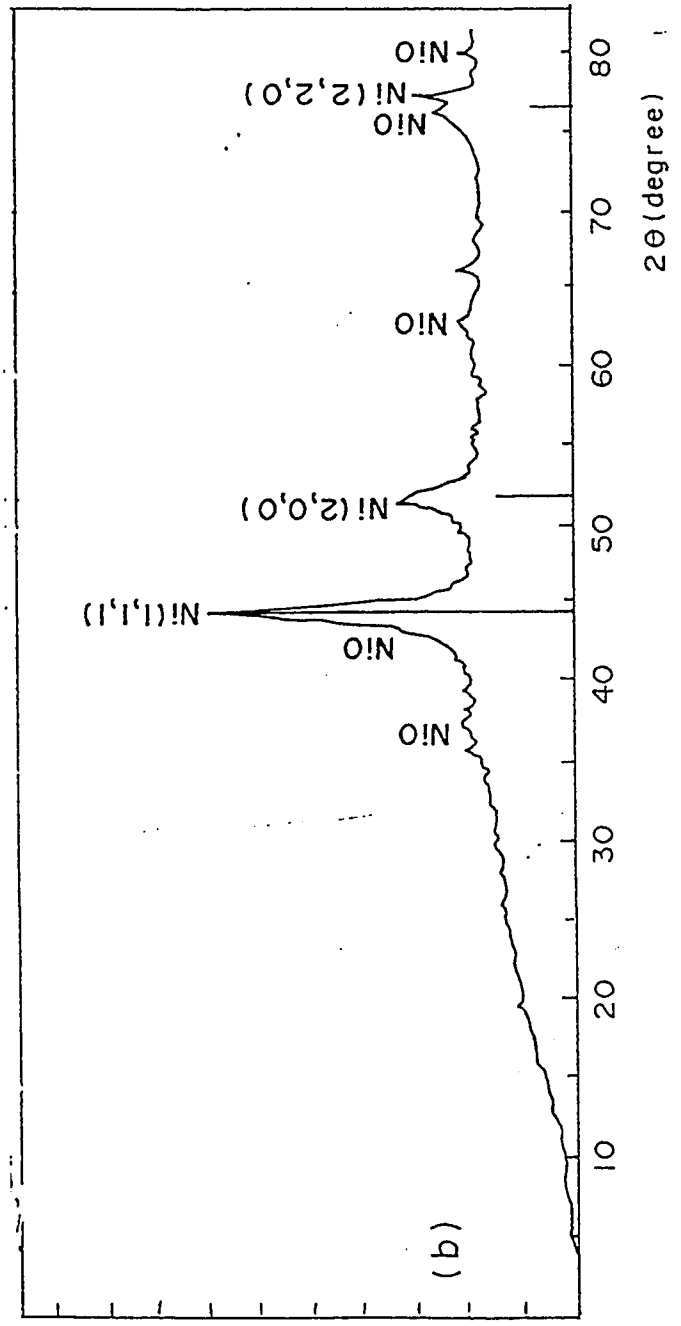

Fig. 8.1 : XRD Pattern of the Raney-Ni Sample Passivated by Conventional Method

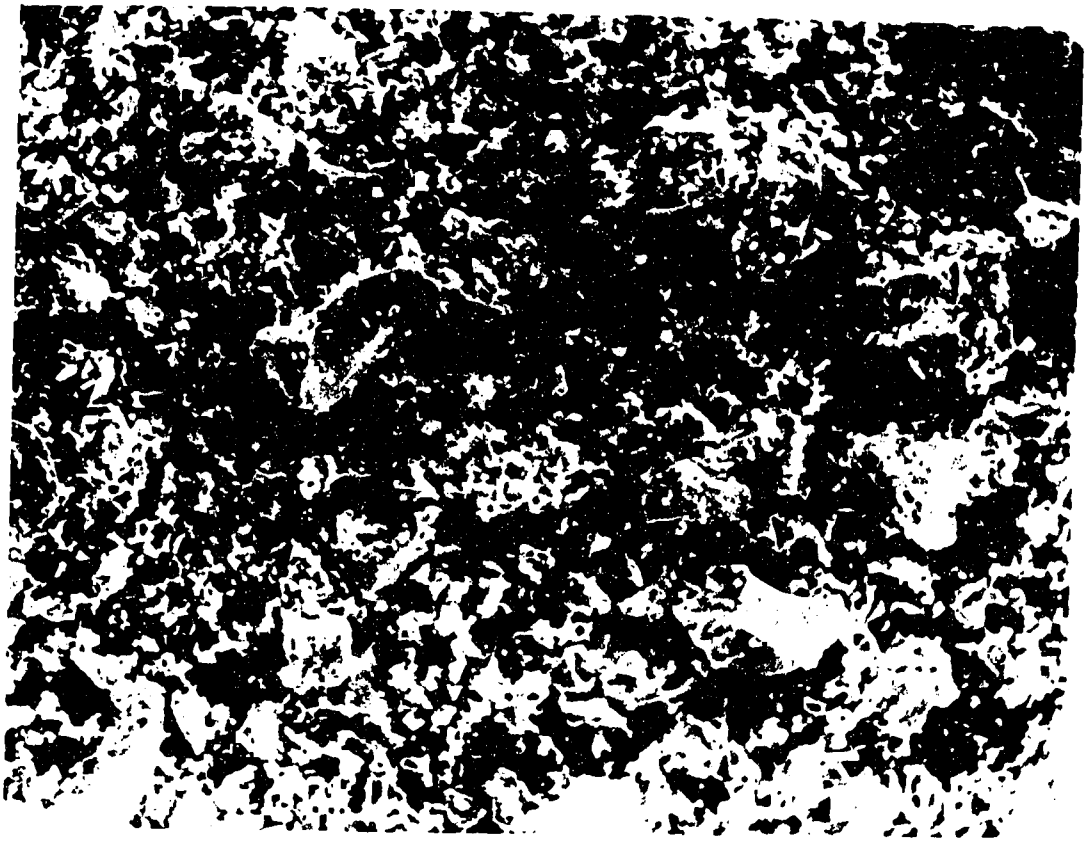

Fig. 8.2.a : SEM Micrograph of the Conventionally Passivated Raney-Ni (500X magnification)

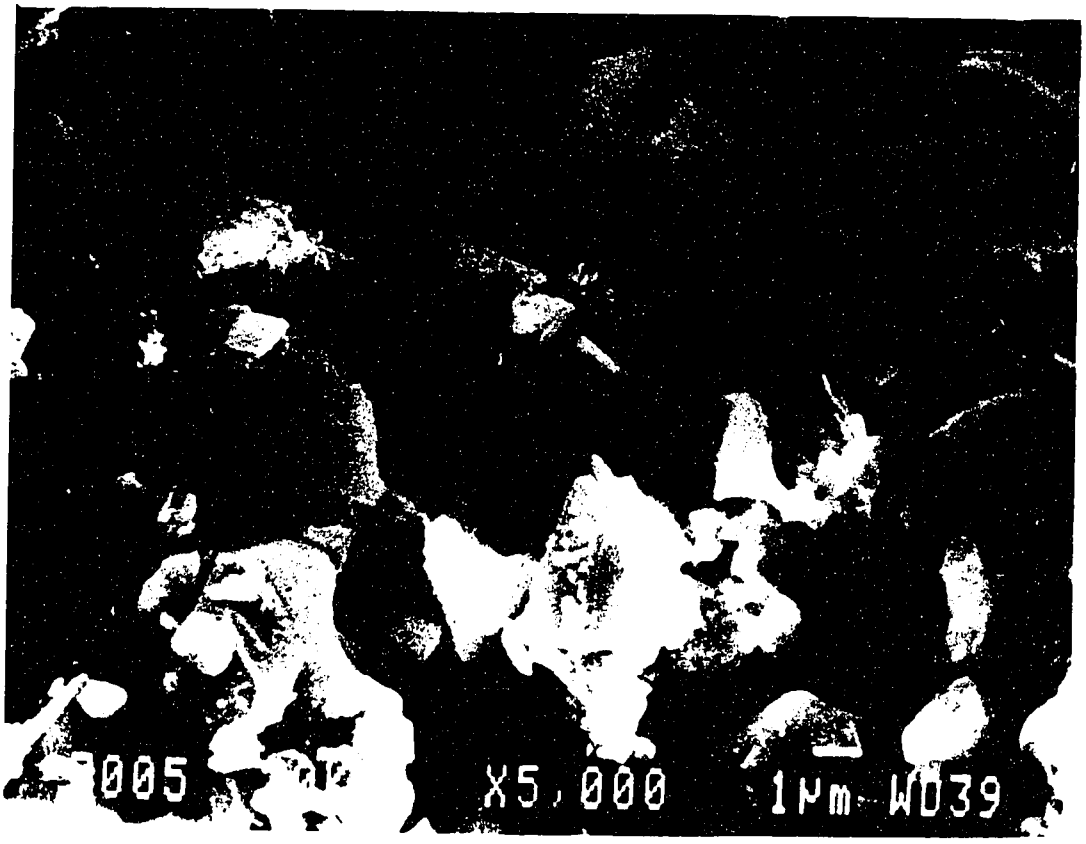

Fig. 8.2.b : SEM Micrograph of the Conventionally Passivated Raney-Ni (5000X magnification)

identified in these micrographs. Nevertheless, the information derived from XRD, SEM and BET surface area put together establishes that sintering did not take place and the catalyst samples can be successfully activated.

Freshly leached Raney-Ni catalyst was treated with 30% H_2O_2 solution at room temperature as described in Chapter 3. The passivated samples were characterized using XRD and SEM. The results of this characterizations are shown in Fig. 8.3 and 8.4. The XRD pattern shows sharp peaks of Ni corresponding to (1,1,1) , (2,0,0) and (2,2,0). This pattern is similar to the one for the conventionally passivated sample as shown in Fig. 8.1. It indicates the presence of considerable crystalline Ni. The smaller and shallow peaks for NiO indicate that small quantity of NiO is also present. The SEM micrograph shows particles with sharp edges, suggesting no apparent sintering took place. This can be concluded that the samples treated with H_2O_2 passivated successfully without sintering. However, more detailed investigation is needed to verify this approach of passivation and compare it with the conventional method.

8.3. Reactive Mixing.

Reactive mixing is the main step of this method which makes it better than 'The Wet Method', in which a PTFE dispersion is mixed with the catalyst powder to make electrodes. In the process of reactive mixing, the catalyst particles are milled with PTFE powder. The PTFE powder consists of amorphous particles of size ranging between 20 microns to 600 microns. As evident from the SEM in Fig. 4.1, each particle has some cracks. When these particles are milled with Raney-Ni, they fragment into small pieces of lesser than one micron. The fragmentation of these particles may take place in two ways. Firstly, these particles come in contact

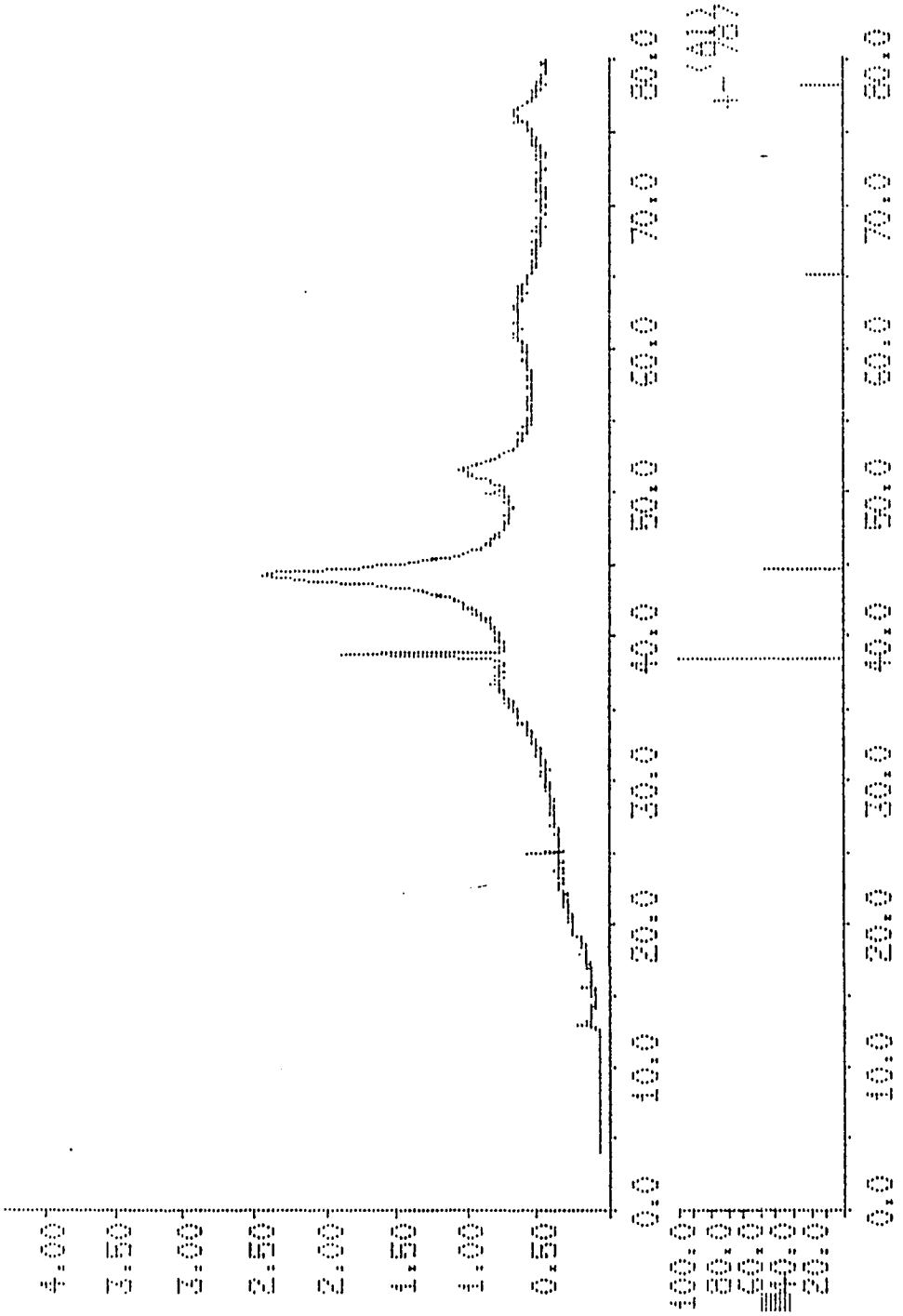

Fig. 8.3. : XRD Pattern for the Raney-Ni Sample Passivated by H_2O_2 Treatment.

Fig. 8.4. : SEM Micrograph for the Raney-Ni Sample Passivated by H_2O_2 Treatment.

with the sharp knives of the mill rotating at high speed. Secondly, the metallic catalyst particles which are moving at high speed result into shearing action on the PTFE particles. The shear force is considerable as all particles are not moving at the same speed.

The fragmented particles adhere on the surface of the catalyst particles as shown in SEM with 500x and 5000x magnifications, given in Fig 8.5. These fine fragment work as binder when certain pressure is applied on the milled powder. Beside its function as binder, the PTFE fines on the catalyst surface incorporate required hydrophobicity. When an electrode made with the milled particles is dipped into the electrolyte, only a very small quantity of the electrolyte can stay in the space between the catalyst particles. This space is therefore available to reactant gas diffusion. Albeit, the electrolyte has chance to get into the microporous structure of the individual particle hence flood them. The electrolyte flooding is basically due to capillary action. As PTFE does not get into the micropores, they are still hydrophilic and assist in electrolyte flooding. These micropores filled with electrolyte work as immobilized phase.

8.4 Performance Testing and Reproducibility

The performance of the electrodes was tested by obtaining the galvanostatic polarization data. For this purpose, a piece of the electrode was mounted in the working electrode assembly of the half-cell as described in Chapter 4. The electrodes were activated by passing 25mA cathodic current for 25 hours at 60°C. Hydrogen gas pressure was 148 kPa. These parameters were selected on the basis of literature recommendation (1). The electrode potential change with time for the optimum electrode is shown in Fig. 8.6 which is a typical plot. The initial drop in

Fig. 8.5.a : SEM Micrographs of Milled Raney-Ni (Magnification 500x)

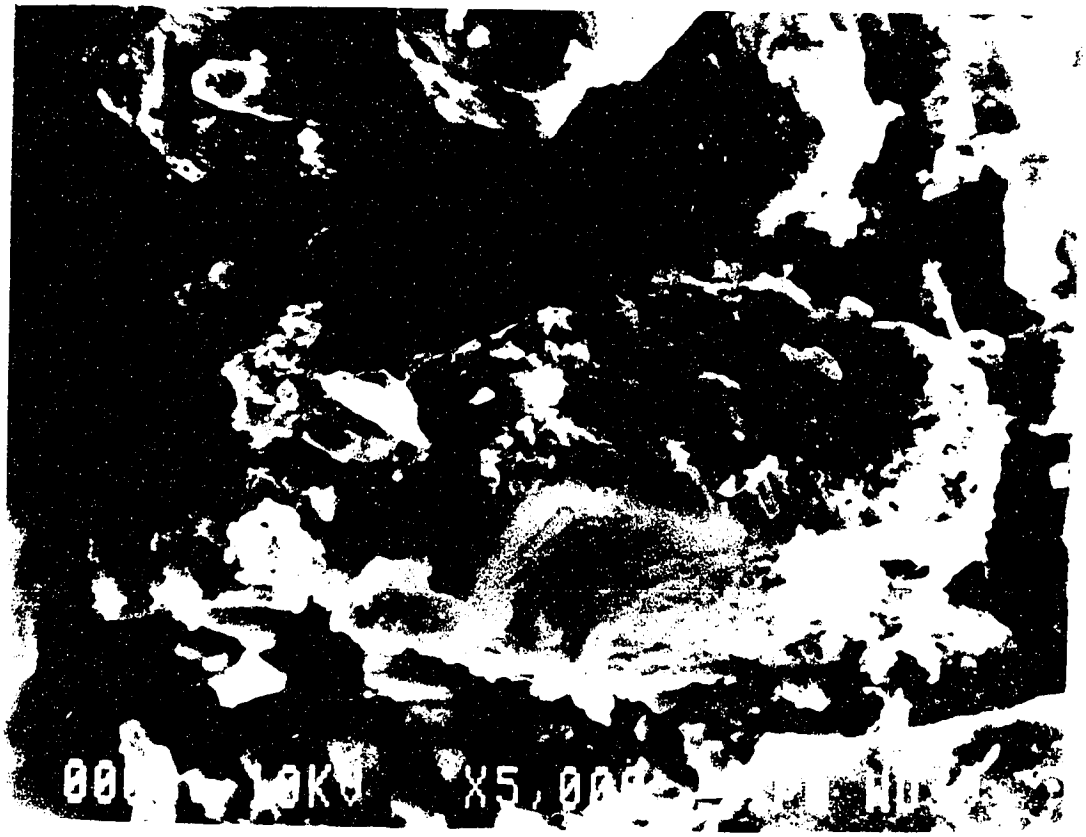

Fig. 8.5.b : SEM Micrographs of Milled Raney-Ni (Magnification 5,000x)

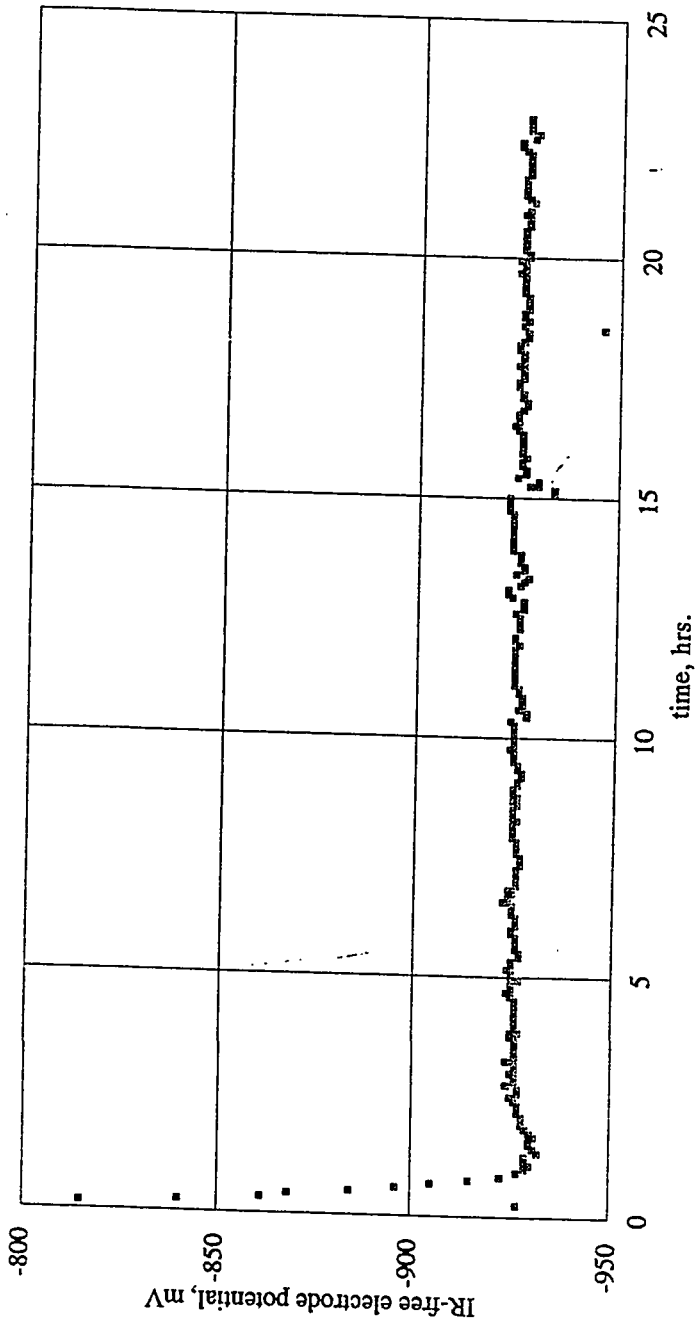

Fig. 8.6 : A typical Activation Plot

the electrode potential is associated with temperature rise. After the completion of the activation, 350 mA anodic current was passed to check whether the activation was sufficient. The activation can be considered completed, if there is no appreciable change in potential with time at an external load of 350 mA. A test plot for the optimum electrode is shown in Fig. 8.7, which is typical.

After the successful activation, the temperature of the electrolyte is brought to 25 ° C. A known anodic current is passed and the electrode potential is recorded. The overpotential is estimated by eliminating the IR-drop of the electrolyte. The IR-drop was measured by current interruption method. The current is converted into the current density by dividing it by the geometrical area of the electrode exposed to the gas and the electrolyte.

To establish the reproducibility of the performance testing set-up, a typical electrode was subjected to the polarization. The process was repeated twice. These data are shown in Table 8.1. The difference between these values is within ±2mV.

8.5. Effect of Various Parameters on the Performance of the Electrodes

Using 2^{5-1} partial factorial experimental design, it is shown in Chapter 5 that three parameters namely; PTFE content, milling time and cooling during milling are significantly important in a given range. The other two parameters namely; clearance between the calender rolls and the removal of the surfactant are significant in a wider range only. For studying the effect of each parameter electrodes were made from a single batch of passivated Raney-Ni. The BET

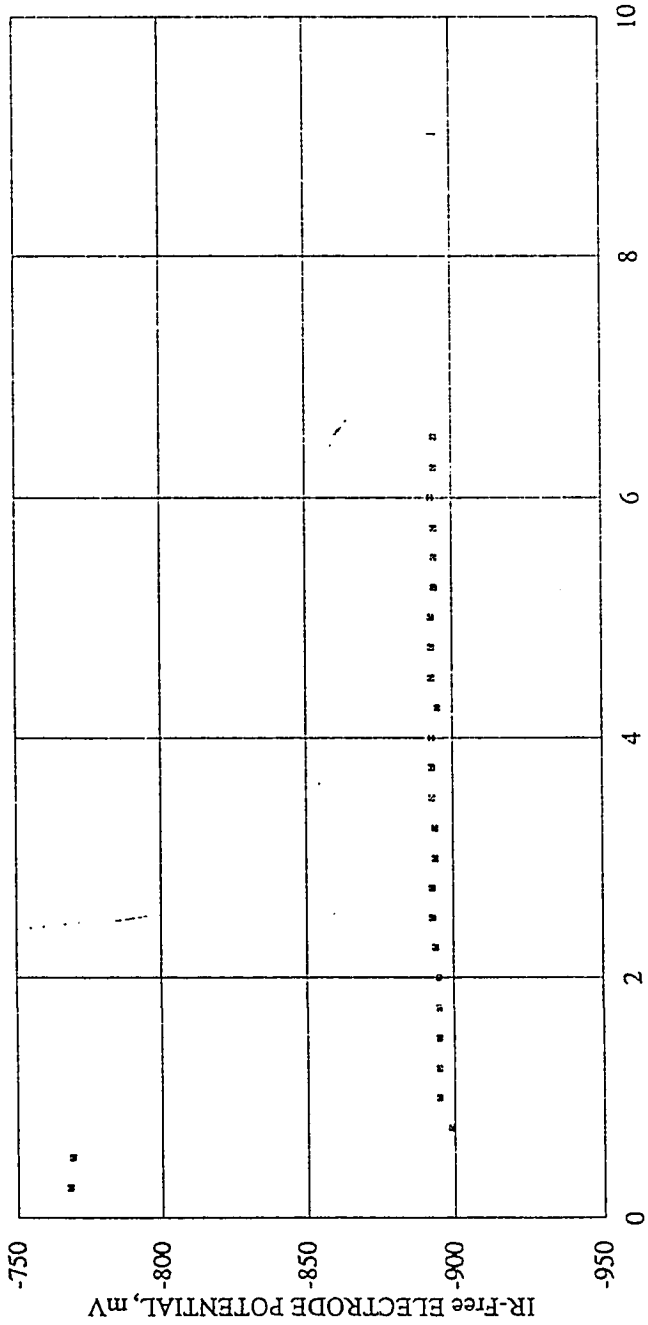

Fig. 8.7 : A Typical Plot for Test of Activation

Table 8.1 : Reproducibility of the Half-cell Set-up

Current Density, mA/cm^2	Overpotential at 25 °C		Difference, mV
	First Run, mV	Second Run, mV	
0.00	0	0	0
0.83	1	1	0
1.67	1	2	+1
4.17	3	4	+1
8.33	6	6	0
16.67	13	13	0
41.67	36	37	+1
58.33	53	54	+1
83.33	77	76	-1
100.00	90	92	+2
125.00	112	112	0
150.00	132	134	+2
166.67	141	143	+2

surface area of this batch was 60.6m^2/g. The polarization of these electrodes was measured in a half-cell with 25 % KOH solution at 25 °C.

A. PTFE Content

It can be observed from the results of the partial factorial design analysis that the PTFE content has the most pronounced effect on the performance. In order to find out the optimum amount of the PTFE, electrodes using 1, 2, 5, 8, 10, 12 and 15% PTFE were made The catalyst was milled for 60 seconds while the cooling was on. The clearance between the calendar rolls was 400 micron while rolling. The prepared electrode was washed once with boiling acetone for five minutes. The polarization data of these electrodes were obtained. These are tabulated in Appendix C.

The overpotential at 100 mA/cm^2 is plotted against the PTFE content in Fig. 8.8. The overpotential first decreases with increasing PTFE content until it reaches a minimum. After the minimum point the overpotential increases with a smaller gradient. From this plot it is evident that the optimum PTFE content is 8%.

The higher overpotential of electrodes having lesser PTFE is mainly due to the poor binding and lack of hydrophobicity of the catalyst particles. It was observed that at 1% PTFE the electrode was highly fragile and it broke while cutting for polarization. Due to poor binding the electrode made with 2% PTFE also disintegrated to some extent. Lack of hydrophobicity apparently permitted the introduction of electrolyte between the space among the catalyst particles. The diffusion of the dissolved gas into the electrolyte is much slower than that in the

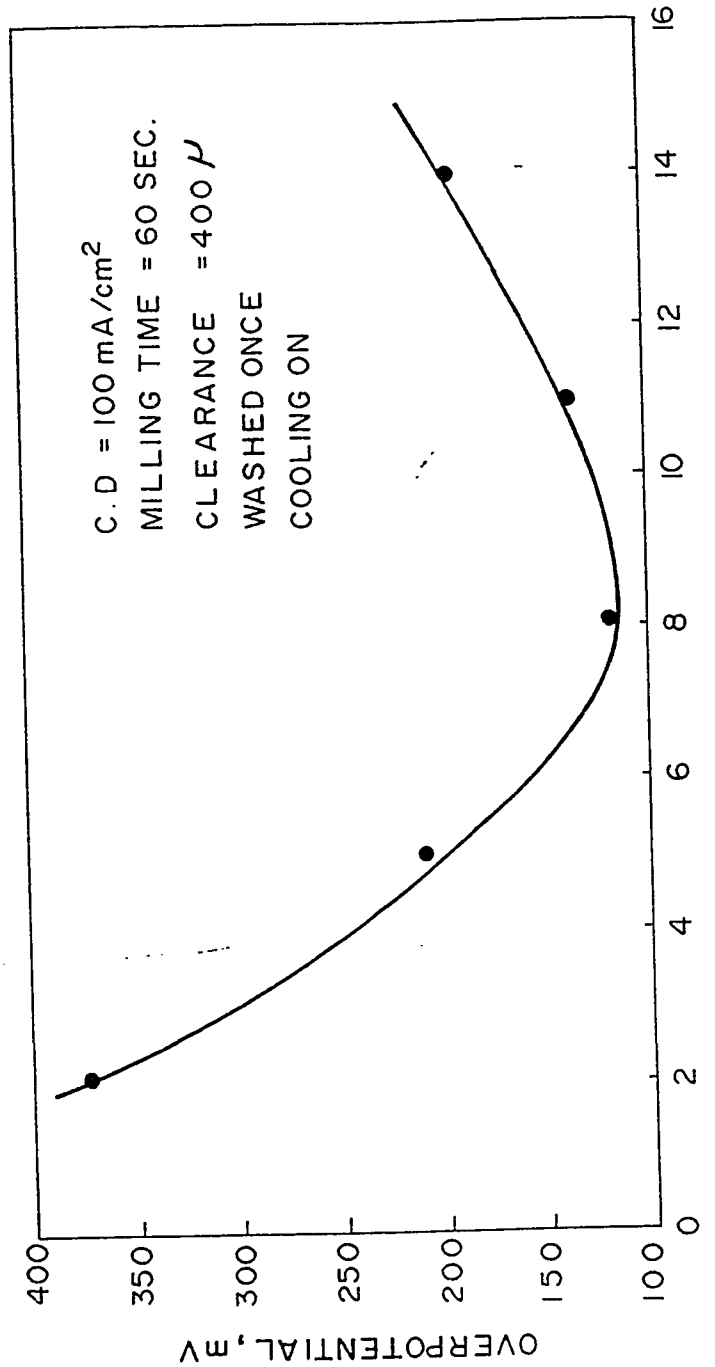

Fig. 8.8 : Effect of the PTFE Content on the Performance of the Electrode

empty pores. This incorporates extra resistance and therefore higher overpotential in the electrodes with low PTFE contents were observed.

At the optimum PTFE content, the PTFE fragments should cover only a partial external area of the catalyst particle to facilitate the introduction of the electrolyte and diffusion of the reactant gas. As the PTFE content exceeds the optimum value, uncovered area starts decreasing. Due to this reason lesser micropores are available for gas diffusion and reaction. This leads to decreased activity of the catalyst and the overpotential increases.

The optimum PTFE content for these electrodes is 8 %. This is in coherence with the optimum value for the Wet Method electrodes obtained by Jenseit et al. (4) as shown in Fig. 8.9.

B. Milling Time

To investigate the effect of the milling time on the performance, the electrodes were made with catalyst which was milled for 30, 60, 90, 120, 150 and 180 seconds while cooling was on. The PTFE content was 8% and rolling was done at 400 microns clearance between the rolls. The electrodes were washed once with boiling acetone for five minutes. The polarization data were obtained and are tabulated in appendix-D.

The overpotential at 100mA/cm^2 is plotted against milling time in Fig. 8.10. Two sets of data were obtained to establish the reproducibility of the data. The overpotential of the electrode made with catalyst milled for 30 second is relatively high. The over potential comes to a minimum at 60 seconds before it again starts

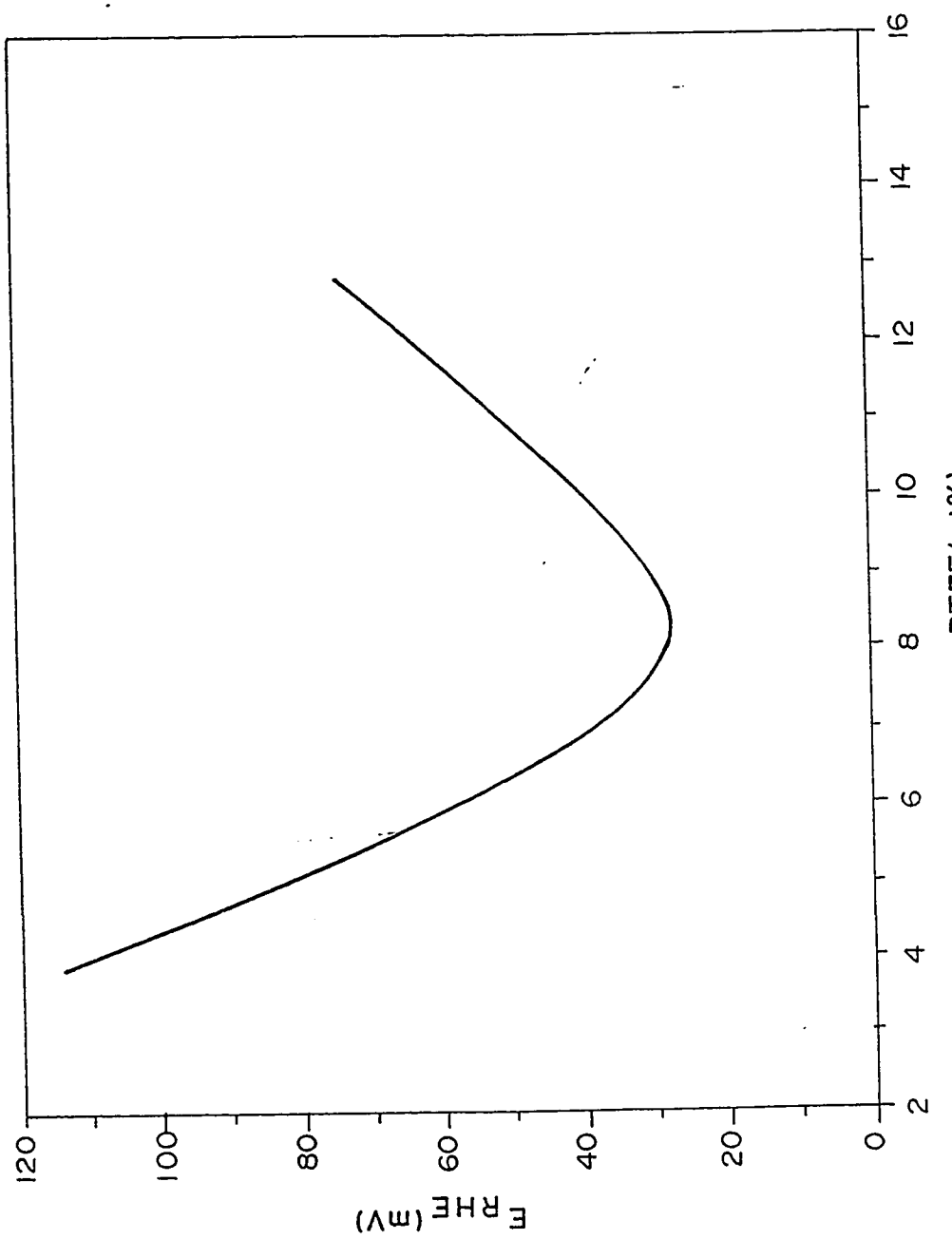

Fig. 8.9 : Effect of the PTFE Content on the Performance of the Electrode made by Wet Method (4)

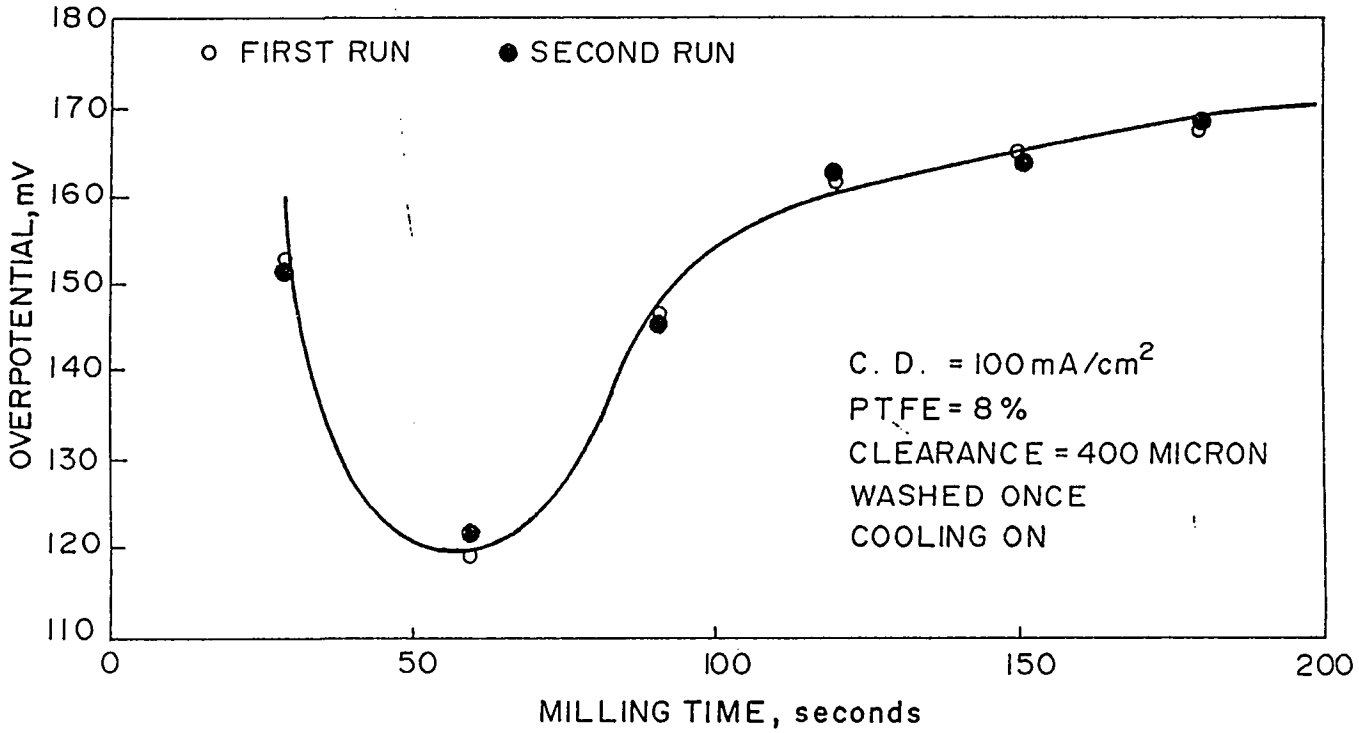

Fig. 8.10 : Effect of the Milling Time on the Performance of the Electrode

increasing. There is little variation in the overpotential of the electrodes which used catalyst milled for more than 120 seconds.

At very little milling time, all PTFE particles apparently did not have the chance to fragment completely into small fines and adhere to Raney-Ni particles. This results into poor binding and lack of hydrophobicity. In this condition the electrolyte has chance to fill the macropores which poses resistance in the diffusion. This is the reason of high overpotential at 30 second milling. At optimum milling time, the hydrophobicity is such that the most of the macropores are empty and are available for the gas diffusion. The catalyst particle is not considerably covered with PTFE fragments and diffusion and reaction in the micropores of the catalyst particle is relatively easy.

When milling is done for longer periods, the PTFE particles becomes very fine and heat is generated due to the friction among the catalyst particles. This heat softens the PTFE fines. As a result of these facts, the PTFE fines cover considerable external area of the catalyst particle. This increases the hydrophobicity of the particles. In this situation, although the gas is available in the macropores, further diffusion into the micropores becomes difficult due blockage of micropore mouths at external surface area. This leads to high overpotentials. After a certain milling time, the rise in the overpotential is not appreciable. This is because the further coating with PTFE is relatively unlikely.

C. Cooling while Milling

In the process of reactive mixing due to the friction among the moving metallic catalyst particles considerable heat is generated. If this heat is not removed, the

PTFE fines will soften. This leads to coating of PTFE on the catalyst particles resulting into blockage of the micropore mouths at the external surface area. Particularly when milling for longer periods the effect is much more pronounced. On the other hand when the generated heat is removed continuously with the help of circulating cold water, excessive covering of the catalyst particles is unlikely as little softening takes place. This is the reason of marginally higher overpotential when cooling was OFF. The polarization curves of the electrodes produced with 60 second milling, 8% PTFE, 400 micron clearance is shown in Fig 8.11. The overpotentials, in the electrode which used catalyst milled without cooling, are slightly higher than those in electrodes with cooling ON.

D. Clearance between the Rolls

The inter-particle porosity of the electrodes can be controlled by varying compaction. This is performed by rolling the electrodes while maintaining desired clearance. For the same catalyst loading and the current collector mesh the macroporosity changes depending on the clearance between the calender rolls. The macroporosity affects the diffusion in the inter-particle space and in turn into the micostructure. The higher clearance will result into higher porosity and therefore into lesser diffusional resistance. This will lead to less overpotential. On the other hand less clearance will result into higher overpotential due

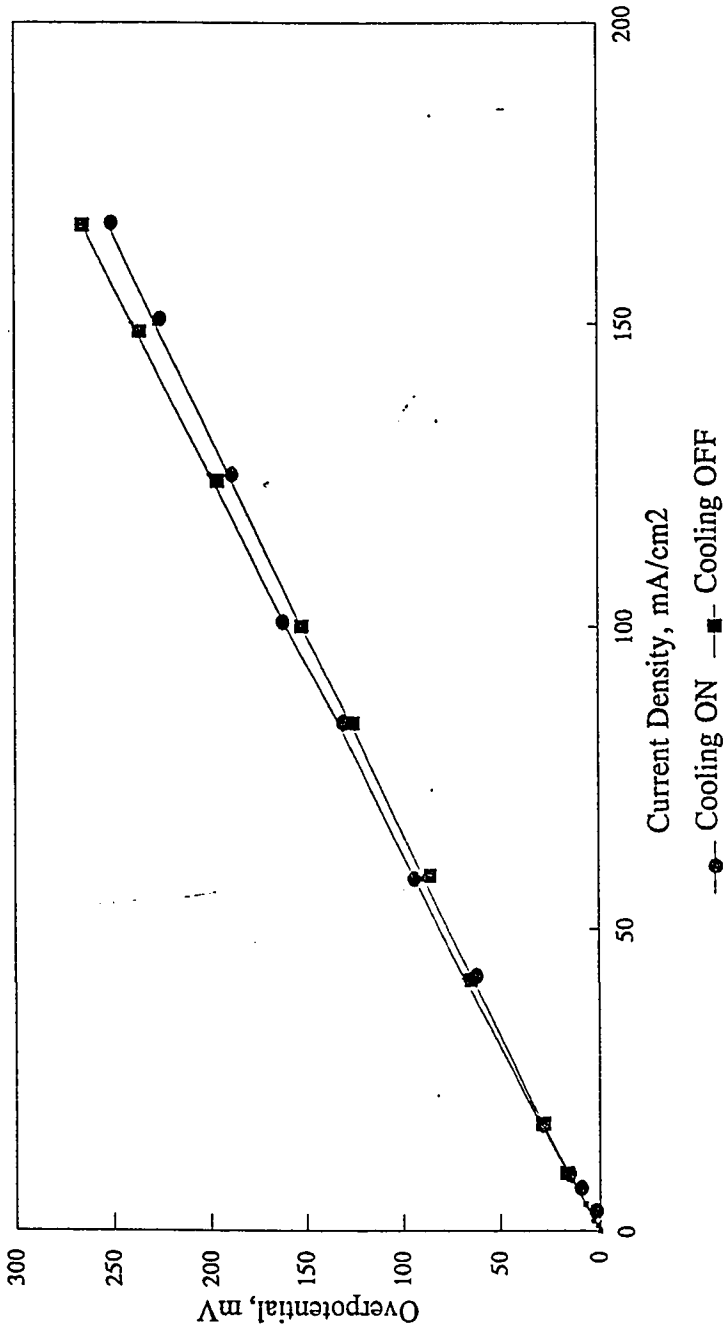

Fig. 8.11 : Effect of the Cooling while Milling on the Performance of the Electrode

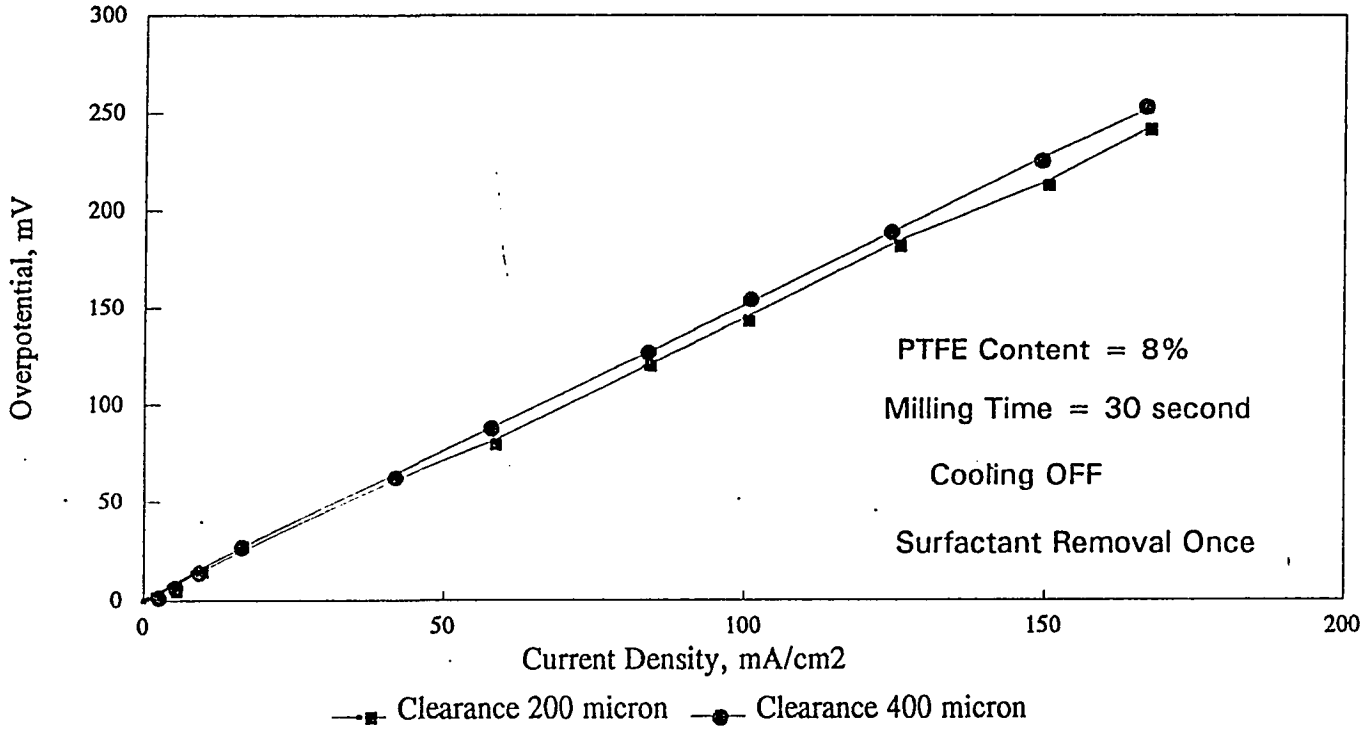

Fig. 8.12 : Effect of the Clearance between the Calender Rolls on the Performance of the Electrode

E. Removal of the Surfactant

The polarization curves shown in Fig. 8.13 were obtained from two samples of one electrode. One sample was washed with boiling acetone for five minutes while other was not washed. The sample which was not washed has unusually higher overpotentials. It can be inferred that the removal of the surfactant is extremely important. The surfactant used to make the electrode was Brij-96 which is chemically Poly oxy ethylene{10}oleyl ether. It is hypothesized that the surfactant adhere on the catalyst surface. This forbids the reactant gas from reaching the active sites. Due to this blockage the performance of the electrode drastically drops down. Although the removal of the surfactant is extremely important, the results of partial factorial design in Chapter 5 show that removing it once is sufficient.

8.6. Comparison of the Electrode Performance

The performance of the optimum electrode produced by Filtration Method is compared with the similar electrodes made by other research groups. Electrodes used by Celiker (1) are Raney-Ni electrodes made by Dry Method in DLR, Germany. The polarization data of this electrode obtained at temperature 25, 35, 45, 55, 65 and 75 °C are compared with those obtained with electrodes by Filtration Method at the same conditions. The mathematical model developed in Chapter 7 was used to predict the data for both electrodes. These results are shown in Fig. 8.14 through 8.19. The parameters used in the model for the filtration method electrode are listed in Table 8.2 and 8.3.

It is observed that the performance at all temperatures is comparable to that of DLR electrodes used by Celiker (1). The exchange current density and charge

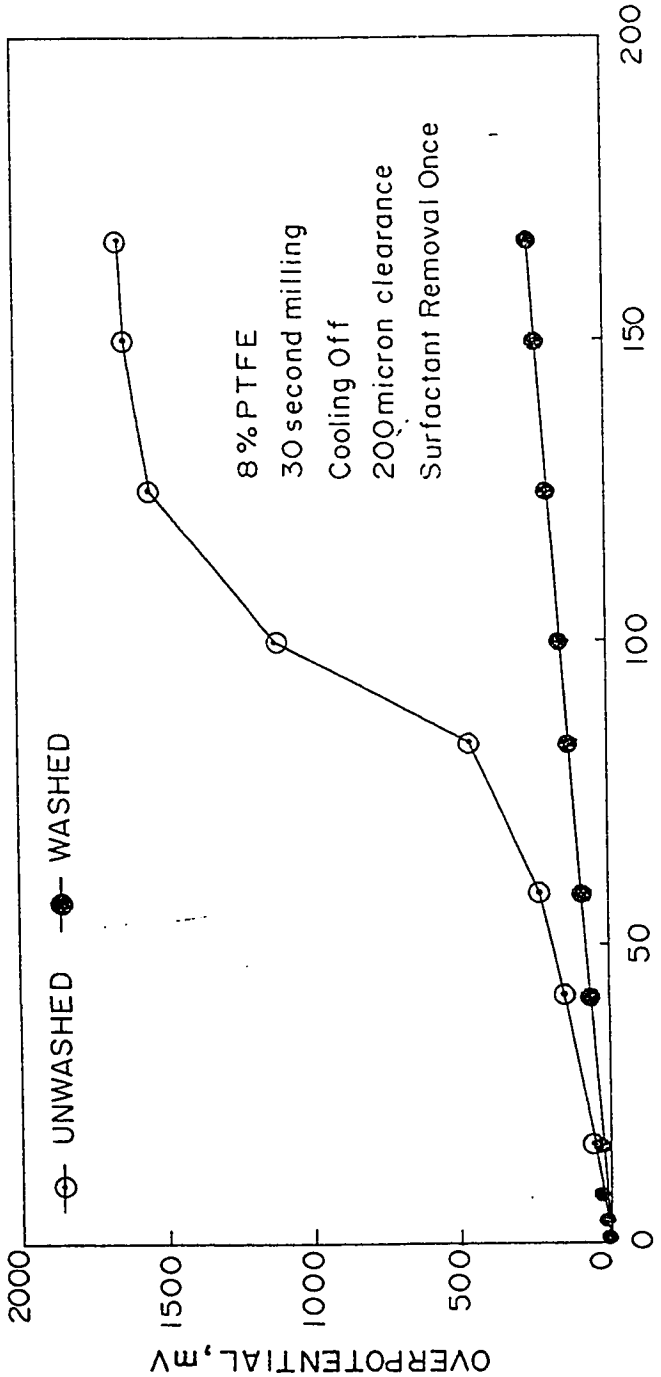

Fig. 8.13 : Effect of the Surfactant Removal on the Performance of the Electrode

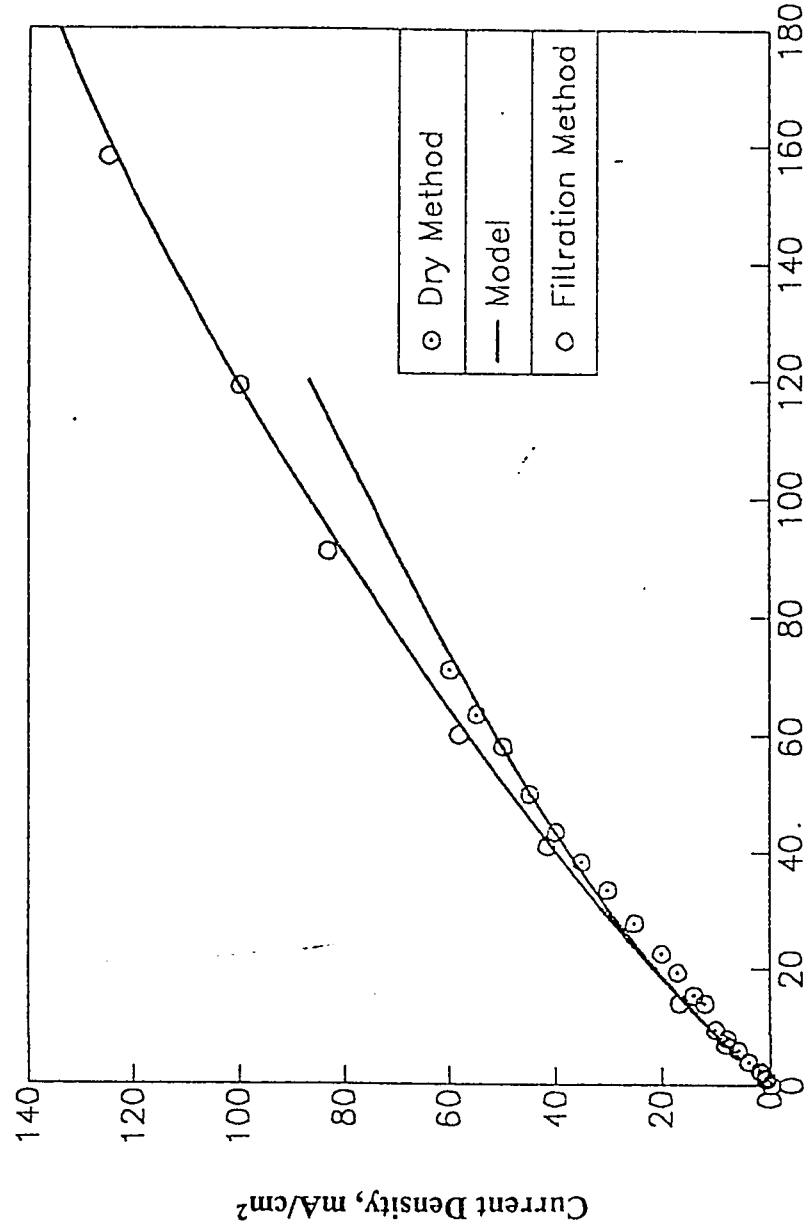

Fig. 8.14 : Polarization of Electrode at 25°C

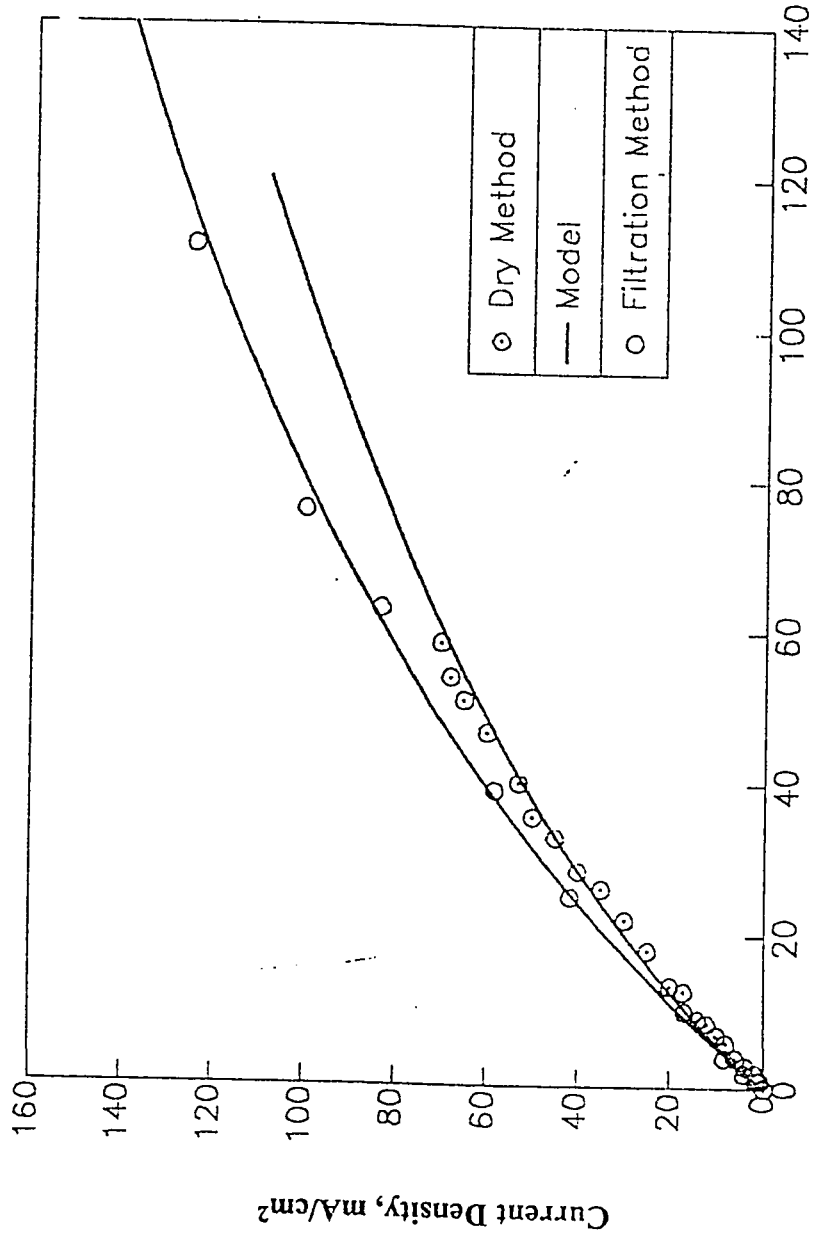

Fig. 8.15 : Polarization of Electrode at 35°C

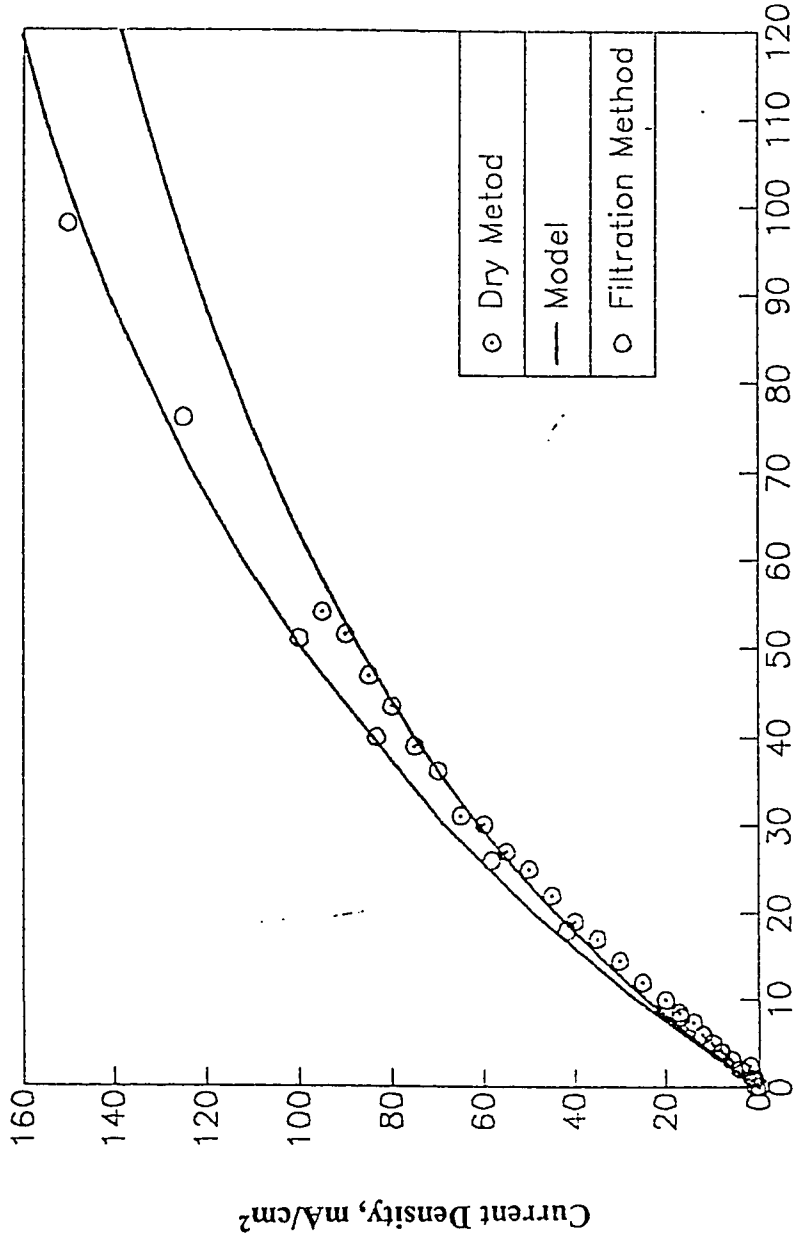

Fig. 8.16 : Polarization of Electrode at 45°C

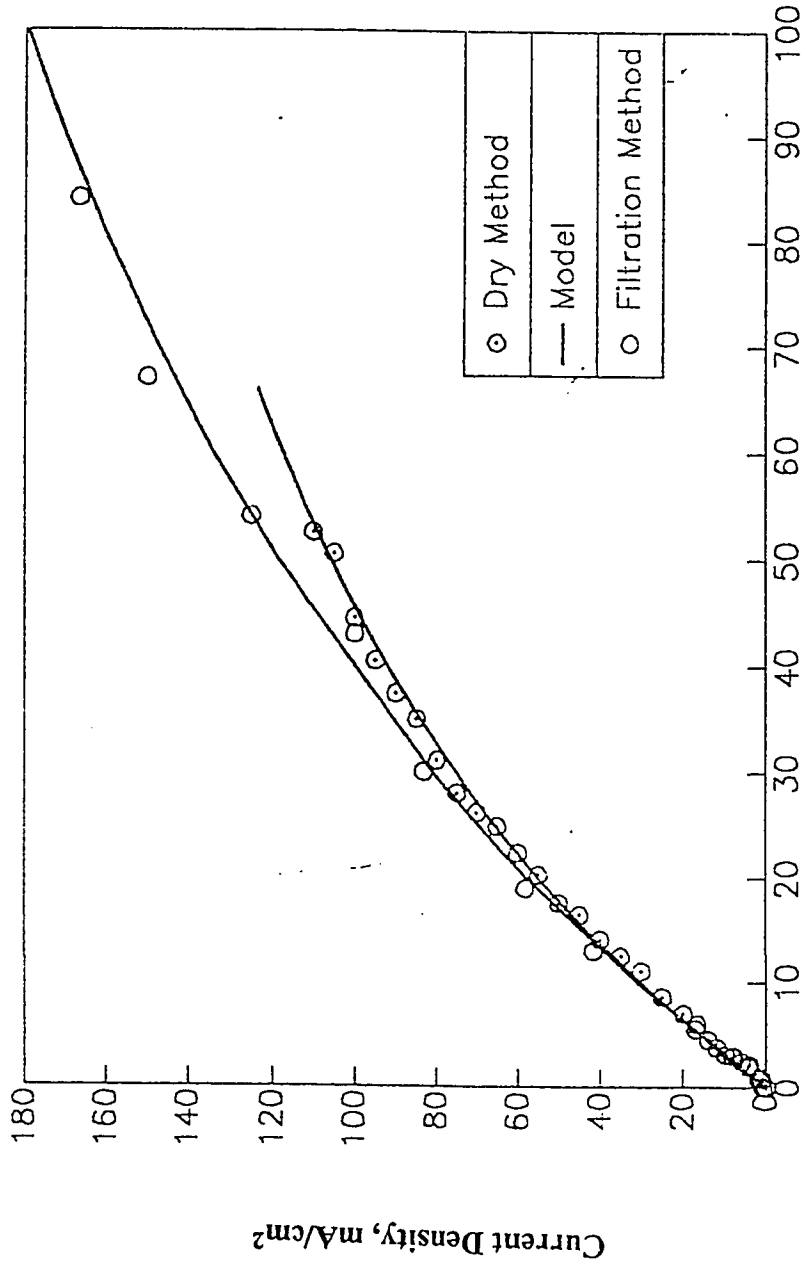

Fig. 8.17 : Polarization of Electrode at 55°C

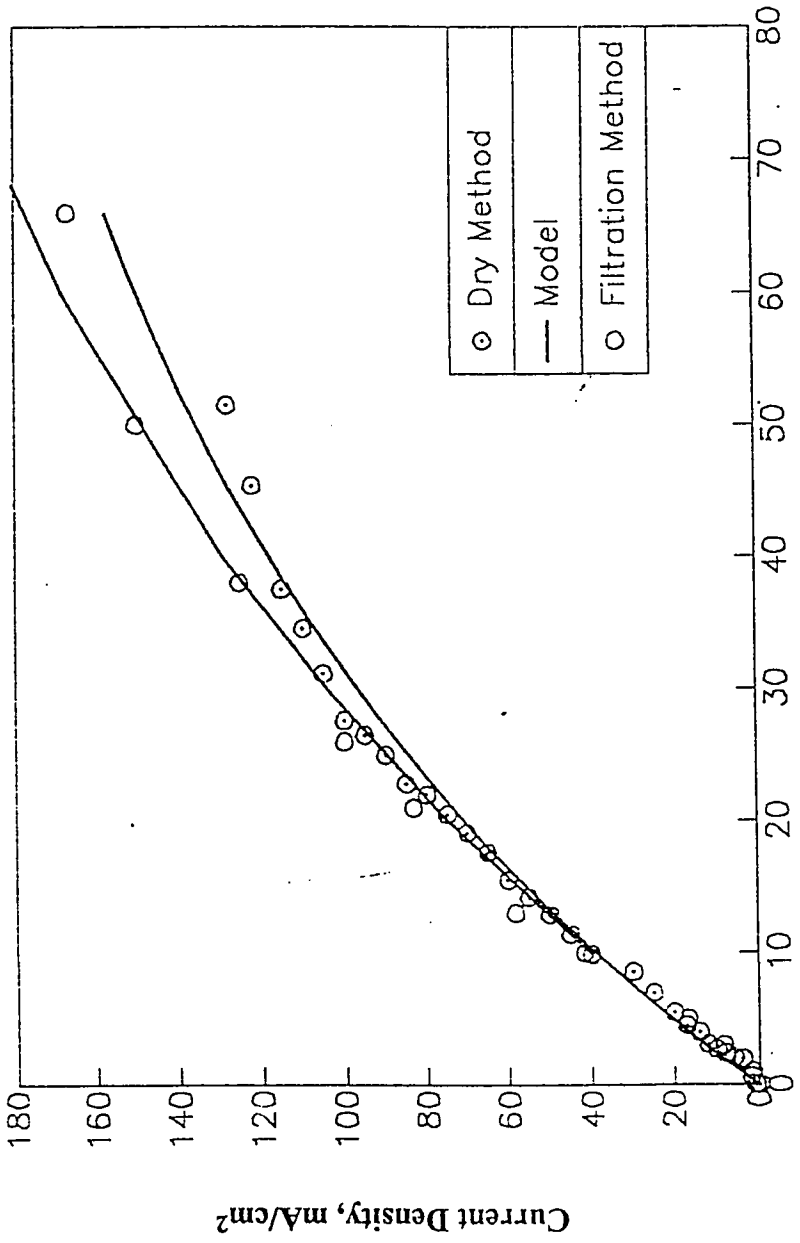

Fig. 8.18 : Polarization of Electrode at 65°C

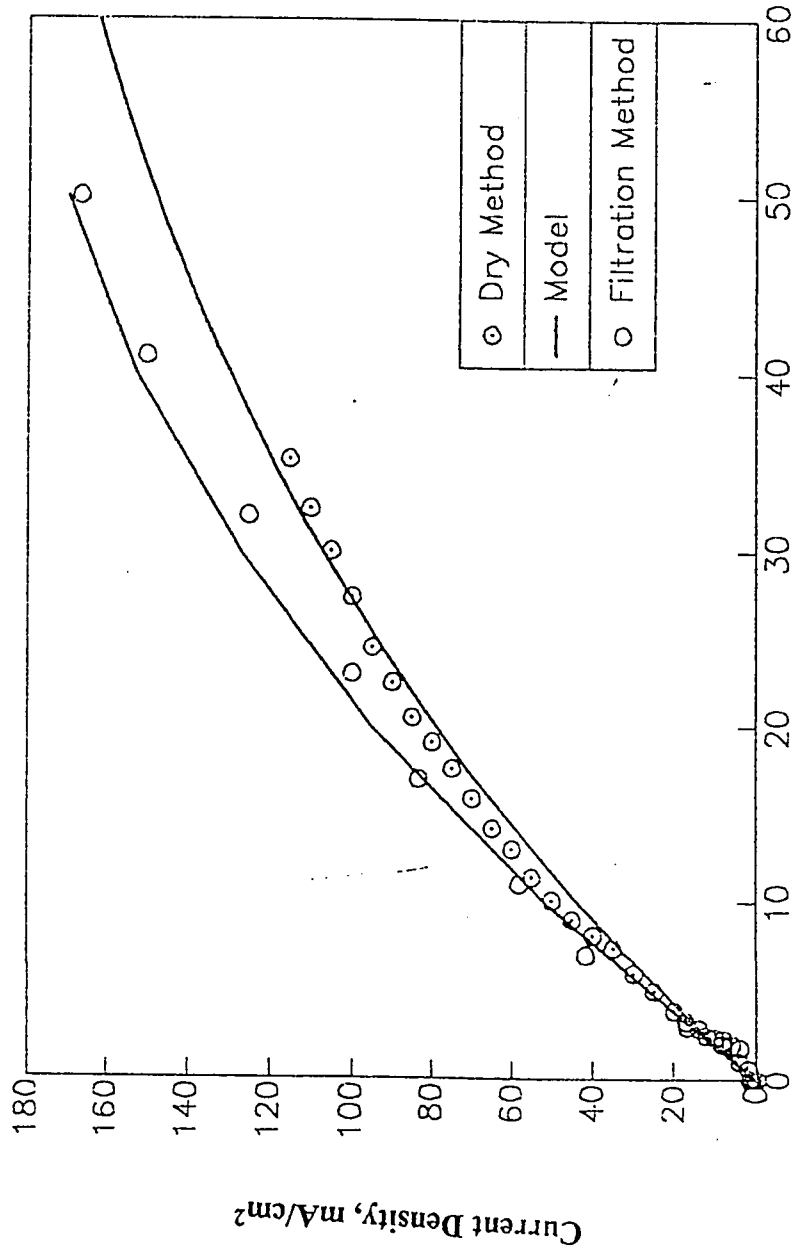

Fig. 8.19 : Polarization of Electrode at 75°C

Table 8.2 : Estimated and Fitted Parameters for the modified Model at Different Temperatures (Filtration Method)

	Estimated Parameters from Literature				Parameters found from this Model		
Temp °C	κ $\Omega^{-1}cm^{-1}$	$k.10^9$ $mol/cm^3\ kPa$	$D_g.10^{11}$ $mol/cm.kPa.s$	$D_l.10^5$ cm^2/s	α	$\delta.10^5$ cm	$i_0.10^6$ mA/cm^2
25	0.254	1.449	4.589	1.515	0.62	6.0	24
35	0.300	1.230	4.097	1.938	0.63	6.0	66
45	0.344	1.0145	3.540	2.625	0.65	6.0	164
55	0.390	0.8696	3.182	3.931	0.67	6.0	379
65	0.434	0.6667	2.551	7.404	0.71	6.0	836
75	0.464	0.5070	2.279	9.529	0.74	6.0	1763

Table 8.3 : Other Parameters for the Model (Electrode Prepared by Filtration Method)

Parameter	Value
z, Stoichiometric number	1.0
n, number of electrons transferred	2
F, Faradays Constant	96484.56
R_g, Gas Constant	8.31 kJ/kmol K
L, Electrode thickness	380μ, (from Electrode Characterization)
R, Average Radius of the Catalyst Particles	12.5μ, (from Electrode Characterization)
Porosity of the Electrode	0.31, (from Electrode Characterization)

transfer coefficients were higher. The apparent activation energy estimated from the Arrhenious plot of the exchange current density shown in Fig. 8.20 is 73.9 kJ/mol. This is comparable to the activation energy for DLR electrode which is 75.9 kJ/mol.

Mund et al. (2) prepared supported Raney-Ni electrodes. The Raney-Ni electrode contained 2% titanium to enhance the catalytic activity. The polarization curves were obtained at various temperatures using 6M KOH. The extrapolated data for 55 °C are plotted with those obtained from the filtration method electrode. This is shown in Fig. 8.21. Although the catalyst and the experimental parameters are not same as used in this study, it is evident that the performance of the filtration method is comparable. Similar conclusions can be drawn from the comparison of the data obtained by Kenjo(3) with PTFE bonded Raney-Ni electrode and by Jenseit et al.(4) with PTFE bonded Raney-Ni electrodes using dry method. These data are compared in Table 8.4.

8.7. Long Term Performance Test

The electrode made with optimum parameters was subjected to a constant load of 100 mA/cm^2 anodic. The potential change with respect to time was recorded. The results are plotted in Fig. 8.22. The electrode potential remained almost constant for 180 hours. The test was discontinued due to the limited time. This result is encouraging but to establish the commercial utility of the electrode long term performance test for more than 1000 hours is required .

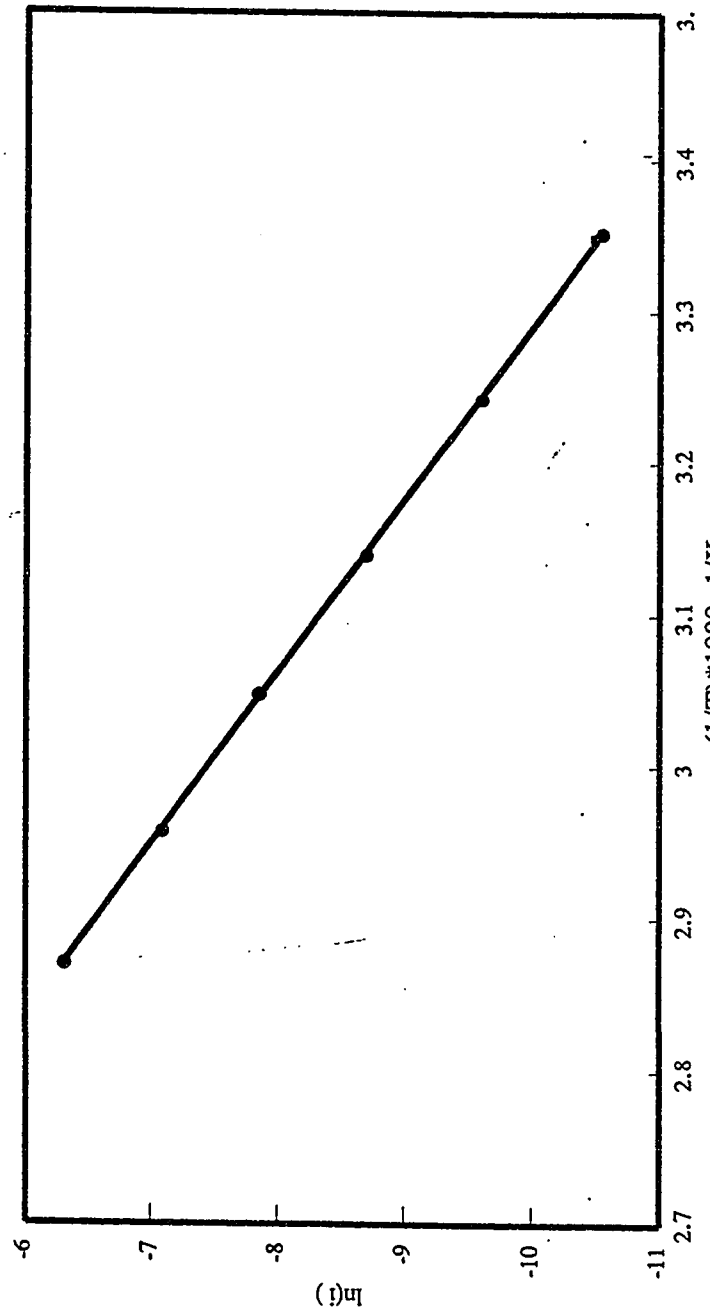

Fig. 8.20 : Arrhenious Plot of Exchange Current Density for Electrode Made by Filtration Method

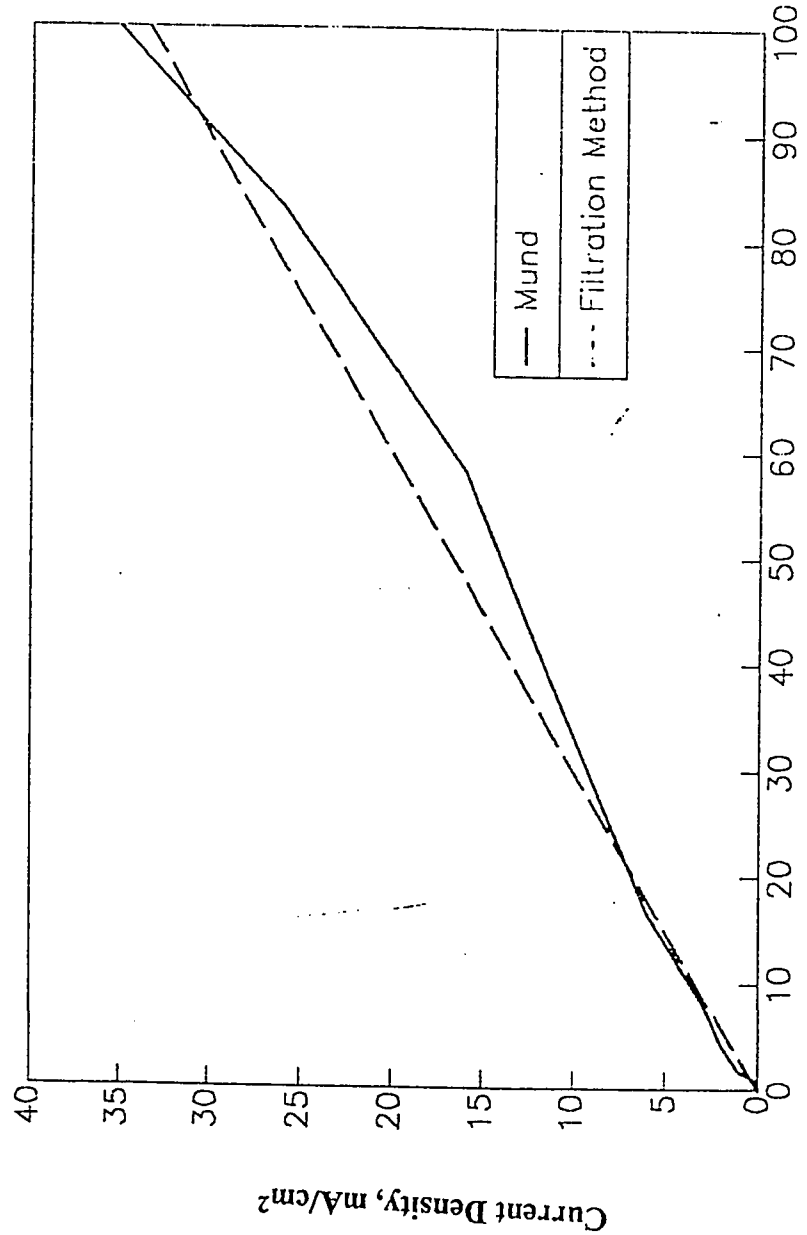

Fig. 8.21 : Comparision of the Polarization with Electrode Prepared by Mund et al. (2)

Table 8.4 : Comparison of the Performance of Various Electrodes

	Overpotential (mV) *			
Current density, mA/cm^2	Filtration Method	Jenseit et al (4)	Mund et al.(2)	Kenlo et al. (3)
0	0.0	0.0	0.0	0.0
20	6.8	6.7	8.0	10.0
40	11.6	13.3	14.0	20.0
80	24.2	26.7	32.0	47.5
100	35.0	33.3	43.0	64.0
150	49.0	50.0	70.5	105.4
* interpolated values				

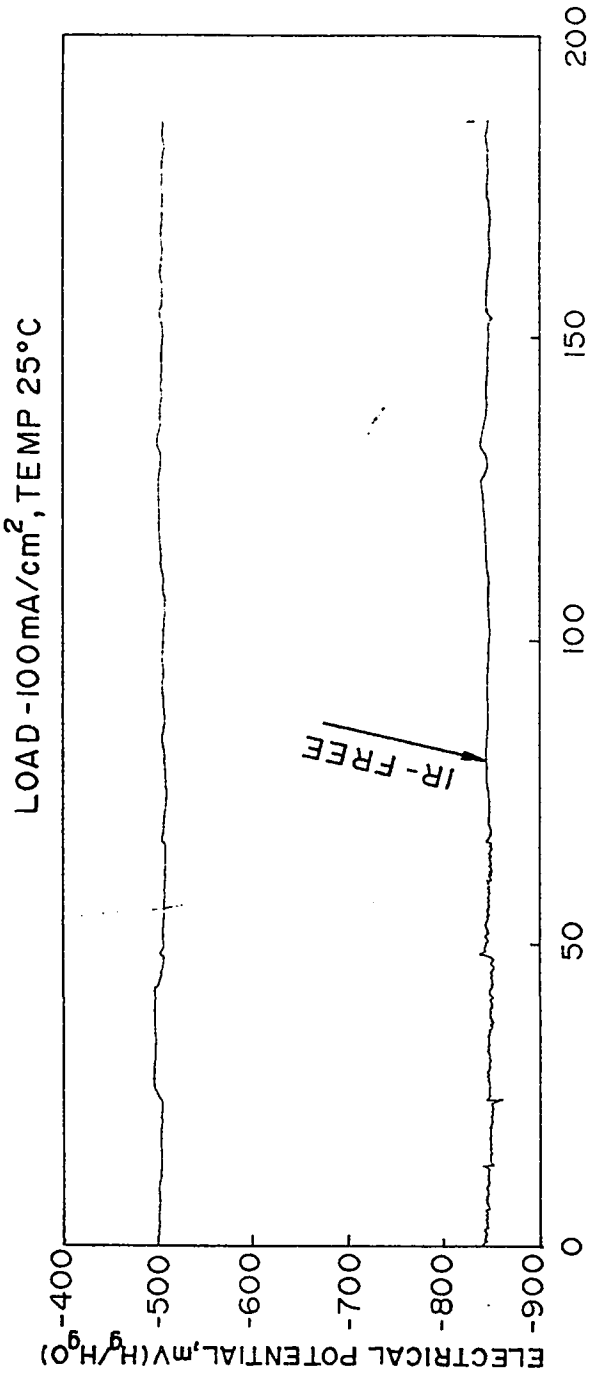

Fig. 8.22 : Long Term Performance of the Filtration Method Electrode

Reference

1. Celiker, H., Ph.D. *Thesis, King Fahd University of Petroleum and Minerals,* 1990.

2. Mund, K., G. Ritcher and F. von Sturm, *Journal of the Electrochemical Society,* **124**, 1, 1(1977).

3. Kenjo, T., *Bulletin of Chemical Society of Japan,* **54**,2553(1981).

4. Jenseit, W., A. Khalil and H. Wendt, *Journal of Applied Electrochemistry,* **20**, 893 (1990).

9

Conclusions and Recommendations

9.1. Conclusions

A. Electrode Preparation

1. A novel method namely; the 'Filtration Method', of making the gas diffusion electrodes for fuel-cells is proposed. A number of Raney-Ni/PTFE gas diffusion electrodes were prepared to study the effects of the parameters of the new method on the performance.

2. Experimental galvanostatic polarization curves for the electrodes were obtained by using a half-cell set-up and EG & PARC potentiostat 273A with computer interface.

3. By utilizing a 2^{5-1} partial factorial experimental design, it was found that the PTFE content, milling time and cooling while reactive mixing were the most significant parameters in the preparation of the electrodes.

4. The effect of the PTFE content on the overpotential of the electrode at a certain current density was studied. The PTFE content was varied between 1% to 14%. It was observed that with increasing PTFE content the overpotential first decreases to reach a minimum value at 8% before again increasing.

5. The effect of milling time in the reactive mixing on the performance of the electrode was studied in a range between 30 and 180 seconds. The overpotential first decreases with increasing milling time. After reaching a minimum at 60 seconds, it again starts increasing.

6. The cooling while reactive mixing is important. The overpotential with electrodes made with catalyst which was milled with cooling ON was lower.

7. The clearance between the calendar rolls controlled the macroporosity. Higher clearance results into better performance of the electrode.

8. The removal of the surfactant from the finished electrode is extremely important. But washing with boiling acetone once is sufficient.

9. The polarization data of an electrode prepared using the optimum parameters were obtained at temperature between 25 to 75 °C.

10. The polarization of the optimum electrode was compared with similar electrodes produced by other research groups including DLR, Germany. The electrodes prepared with the new method had slightly lower overpotentials at all temperature.

11. The polarization data obtained for the optimum electrode at different temperatures were used with the modified mathematical model to obtain Tafel parameters i.e. exchange current density(i_0) and the charge transfer coefficient (α). At 25°C, the values of these parameters are 24.0×10^{-6} mA/cm^2 and 0.62 respectively.

12. The exchange current density was a strong function of the temperature. The obtained values were plotted as Arrehenius plot to determine the apparent activation energy. The apparent activation energy (E) for the electrode was 73.9 kJ/mol while E for DLR electrode was 75.2 kJ/mol.

B. Mathematical Model

1. The mathematical model to describe the physical and electrochemical phenomena in the gas diffusion electrodes proposed by Celiker et al. was modified. The previous model failed to predict overpotential-current density relation at higher overpotential and higher temperatures.

2. The modified model incudes the external mass transfer resistance in the macropores carrying the reactant gas and in the electrolyte film surrounding the individual catalyst particle.

3. The validity of the modified model was tested and verified by using typical physical and electrochemical parameters.

4. The intrinsic parameters of the Hydrogen PTFE bonded Raney-Ni electrodes produced in this study and in DLR, Germany were obtained using the modified model.

C. Passivation of Raney-Ni

1. Anew method of passivating Raney-Ni catalyst for making fuel-cell gas diffusion electrodes was proposed. In this method the catalyst is treated with diluted H_2O_2 solution. This method eliminates the possibility of accidental catalyst sintering and the instrumentation required in the convention controlled slow oxidation with gaseous oxygen. The new method is less time consuming.

2. The preliminary study using XRD shows H_2O_2 treated passivated catalyst is more crystalline than that of convention method.

9.2. Recommendations

1. The filtration method should be used to make PTFE bonded Raney-Ag cathodes for alkaline fuel-cells (AFC).

2. Electrodes for Phosphoric Acid Fuel-cells (PAFC) should be prepared using platinum loaded carbon catalyst utilizing the new method.

3. The filtration method can be used for mass production of the electrodes. A prototype of an electrode making machine on the basis of drawings shown in Fig. 9.1 and 9.2 should be fabricated and optimized.

4. Complete fuel-cells using Raney-Ni and Raney-Ag electrodes should be fabricated and studied. A fuel-cell stack may also be considered.

5. The effect of loading of different amount of the catalyst should be studied and optimum value if any should be found out.

6. The electrodes and the complete cells should be tested under load for more than 1000 hours.

7. The H_2O_2 treatment for the passivation of Raney-Ni catalyst should be studied in detail. The parameters e.g. H_2O_2 concentration, reaction temperature and time should be identified.

8. Experiments should be performed for passivating Raney-Ni by bubbling oxygen in the slurry of Raney-Ni particles. Preliminary experiments were encouraging.

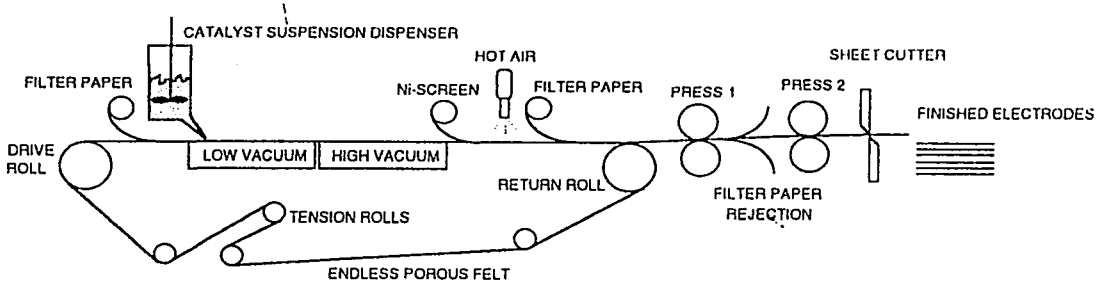

Fig. 9.1 : PROPOSED CONTINUOUS PRODUCTION OF THE GAS DIFFUSION ELECTRODES

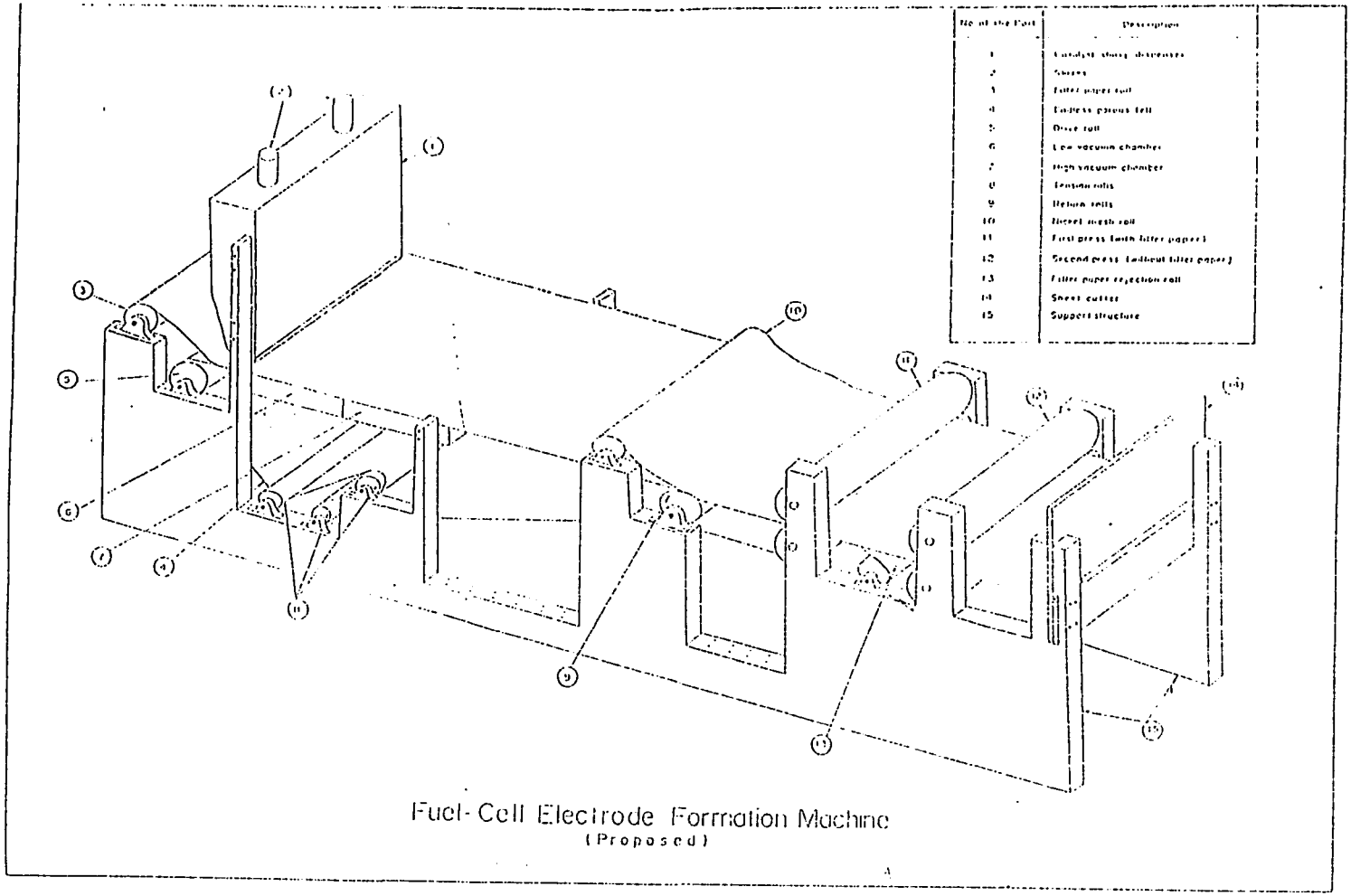

Fig. 9.2. : Proposed Machine for Electrode Production.

Nomenclature

a = surface area of the porous grain per unit volume, cm^{-1}.

A_1, A_2, A_3 = terms define by Eons. 7.2, 7.3 and 7.4.

C = reactant gas concentration, mol/cm^3.

C_0 = solubility of the reactant gas into the electrolyte, mol/cm^3.

C_f = reactant gas concentration in the electrolyte film, mol/cm^3.

C_s = concentration of the reactant gas at the surface of the catalyst grain, mol/cm^3.

D_g = reactant gas diffusivity in the empty macropores of the electrode, mol/cm^3.

D_l = Diffusivity of the reactant gas into KOH solution, mol/cm^3.

D_{le} = effective diffusivity of the reactant gas into the porous catalyst filled with electrolyte, cm^2/sec.

F = Faraday constant.

i_0 = exchange current density, mA/cm^2.

j(x) = current flowing through any plane x per unit geometric area, mA/cm^2.

k = Henry's constant.

L = thickness of the electrode, cm.

n = number of electrons involved in the reaction.

N1 = number of grains per unit geometric surface area, cm^{-2}.

p = reactant gas pressure, kPa.

p_0 = measurable reactant gas pressure in the gas chamber, kPa.

R * = term defined by Eqn. 7.17.

R = average radius of the catalyst grain, cm.

r = radial distance in the catalyst grain, cm.

Rg = Gas constant.

r_{gas} = term defined by Eqn. 7.7.

T = absolute temperature, K.

t = temperature, °C.

W = concentration of KOH solution, wt%.

x = axial distance in the electrode, cm.

z = stoichiometric number.

Greek Letters

α = charge transfer coefficient.

η = overpotential, volt.

η_0 = measurable overpotential on the electrolyte side, volt.

κ_e = effective conductivity of the pores catalyst, Ω^{-1} cm^{-1}.

κ = conductivity of KOH solution, Ω^{-1} cm^{-1}.

δ = thickness of the electrolyte film, cm.

ε = porosity of the catalyst.

ε_{mic} = micro porosity.

ε_{mac} = macroporosity

τ = tortuosity of the pores.

τ_{mic} = tortuosity of the micropores.

τ_{mac} = tortuosity of the macropores.

μ = viscosity of KOH solution.

APPENDICES

APPENDIX-A

Computer programs for running the experiments

Program #1

Name : ACTIV

```
#include <bios.h>
#include <stdio.h>
#define  DATA_READY 0x0100;

unsigned int _bios_serialcom(unsigned int, unsigned int, unsigned int);
void main()
{

FILE *fpw;      /*pointer for the write file*/

char command1[]="DCL;SIE 15;CELL 1;MODE 1;S/P 6000;TMB 50000\n";
char *ptr1 ;
char command2[]="PAM 1;IRMODE 3;SETI 25 -3;DO 150;TP;RUERR;LOOP\n";
char *ptr2 ;
char command3[]="DO 150;TP;RUERR;LOOP\n";
char *ptr3 ;
char command4[]="CELL 0\n";
char *ptr4 ;
unsigned int r;
unsigned int com_status;
int i;
   fpw=fopen("aCTIV.dat","w");
   ptr1=command1;
   ptr2=command2;
   ptr3=command3;
   ptr4=command4;
   com_status=_bios_serialcom(_COM_STATUS,1,0);
   printf("COM2 Status:0x% .4x \n", com_status);
   _bios_serialcom(_COM_INIT,1,_COM_CHR8 |
                              _COM_STOP1 | _COM_NOPARITY |
                              _COM_300);

   while (*ptr1 != NULL) {
  _bios_serialcom(_COM_SEND,1,*ptr1);
   ptr1++;
  }
```

```
i=0;
r=' ';
while(r  != '*') {
   com_status= _bios_serialcom(_COM_STATUS,1,0);
   printf("COM2 Status:0x% .4x \n", com_status);

      r=_bios_serialcom(_COM_RECEIVE,1,0);
  fwrite(&r,1,1,fpw);

}
while (*ptr2 != NULL) {
_bios_serialcom(_COM_SEND,1,*ptr2);
 ptr2++;
}

 r=' ';
while(r  != '*') {
   com_status= _bios_serialcom(_COM_STATUS,1,0);
   printf("COM2 Status:0x% .4x \n", com_status);

      r=_bios_serialcom(_COM_RECEIVE,1,0);
  fwrite(&r,1,1,fpw);

}
while (*ptr3 != NULL) {
_bios_serialcom(_COM_SEND,1,*ptr3);
 ptr3++;
}

 r=' ';
while(r  != '*') {
   com_status= _bios_serialcom(_COM_STATUS,1,0);
   printf("COM2 Status:0x% .4x \n", com_status);

      r=_bios_serialcom(_COM_RECEIVE,1,0);
  fwrite(&r,1,1,fpw);

}

 while (*ptr4 != NULL) {
_bios_serialcom(_COM_SEND,1,*ptr4);
 ptr4++;
```

```
  }

   r=' ';
  while(r  != '*') {
     com_status= _bios_serialcom(_COM_STATUS,1,0);
     printf("COM2 Status:0x% .4x \n", com_status);

        r=_bios_serialcom(_COM_RECEIVE,1,0);
    fwrite(&r,1,1,fpw);

  }
     fcloseall();
}
```

Program # 2

Name : TEST

```
#include <bios.h>
#include <stdio.h>
#define  DATA_READY 0x0100;

unsigned int _bios_serialcom(unsigned int, unsigned int, unsigned int);
void main()
{

FILE *fpw;      /*pointer for the write file*/

char command1[]="DCL;SIE 15;CELL 1;MODE 1;S/P 300; TMB 50000\n";
char *ptr1 ;
char command2[]="PAM 1;IRMODE 3;SETI -350 -3;TP;DO
25;TP;RUERR;LOOP\n";
char *ptr2 ;
char command3[]="CELL 0\n";
char *ptr3 ;

unsigned int r;
unsigned int com_status;
int i;
   fpw=fopen("TEST.dat","w");
   ptr1=command1;
```

```
ptr2=command2;
ptr3=command3;
com_status=_bios_serialcom(_COM_STATUS,1,0);
printf("COM2 Status:0x% .4x \n", com_status);
_bios_serialcom(_COM_INIT,1,_COM_CHR8 |
                        _COM_STOP1 | _COM_NOPARITY |
                        _COM_300);

while (*ptr1 != NULL) {
_bios_serialcom(_COM_SEND,1,*ptr1);
ptr1++;
}

i=0;
r=' ';
while(r  != '*') {
   com_status= _bios_serialcom(_COM_STATUS,1,0);
   printf("COM2 Status:0x%..4x \n", com_status);

     r=_bios_serialcom(_COM_RECEIVE,1,0);
  fwrite(&r,1,1,fpw);

}
while (*ptr2 != NULL) {
_bios_serialcom(_COM_SEND,1,*ptr2);
ptr2++;
}
```

```
 r=' ';
while(r  != '*') {
   com_status= _bios_serialcom(_COM_STATUS,1,0);
   printf("COM2 Status:0x% .4x \n", com_status);

      r=_bios_serialcom(_COM_RECEIVE,1,0);
  fwrite(&r,1,1,fpw);

}
while (*ptr3 != NULL) {
_bios_serialcom(_COM_SEND,1,*ptr3);
 ptr3++;
}

 r=' ';
while(r  != '*') {
   com_status= _bios_serialcom(_COM_STATUS,1,0);
   printf("COM2 Status:0x% .4x \n", com_status);

      r=_bios_serialcom(_COM_RECEIVE,1,0);
  fwrite(&r,1,1,fpw);

}
    fcloseall();
}
```

Program # 3

Name : POLA

```
#include <bios.h>
#include <stdio.h>
#define  DATA_READY 0x0100;

unsigned int _bios_serialcom(unsigned int, unsigned int, unsigned int);
void main()
{

FILE *fpw;      /*pointer for the write file*/

char command1[]="DCL;SIE 15;CELL 1;MODE 1;S/P 600; TMB 50000\n";
char *ptr1 ;
char command2[]="PAM 1;IRMODE 3;SETI -0 -3;TP;DO 5;TP;RUERR;LOOP\n";
char *ptr2 ;
char command3[]="SETI -5 -3;TP;DO 10;TP;RUERR;LOOP\n";
char *ptr3 ;
char command4[]="SETI -10 -3;TP;DO 10;TP;RUERR;LOOP\n";
char *ptr4 ;
char command5[]="SETI -25 -3;TP;DO 10;TP;RUERR;LOOP\n";
char *ptr5 ;
char command6[]="SETI -50 -3;TP;DO 10;TP;RUERR;LOOP\n";
char *ptr6 ;
char command7[]="SETI -100 -3;TP;DO 15;TP;RUERR;LOOP\n";
char *ptr7 ;
char command8[]="SETI -250 -3;TP;DO 15;TP;RUERR;LOOP\n";
char *ptr8 ;
char command9[]="SETI -350 -3;TP;DO 15;TP;RUERR;LOOP\n";
char *ptr9 ;
char command10[]="SETI -500 -3;TP;DO 15;TP;RUERR;LOOP\n";
char *ptr10 ;
char command11[]="SETI -600 -3;TP;DO 15;TP;RUERR;LOOP\n";
char *ptr11 ;
char command12[]="SETI -750 -3;TP;DO 15;TP;RUERR;LOOP\n";
char *ptr12 ;
char command13[]="SETI -900 -3;TP;DO 15;TP;RUERR;LOOP\n";
char *ptr13 ;
```

```
char command14[]="SETI -1000 -3;TP;DO 15;TP;RUERR;LOOP;CELL 0\n";
char *ptr14 ;
unsigned int r;
unsigned int com_status;
int i;
   fpw=fopen("pola.dat","w");
   ptr1=command1;
   ptr2=command2;
   ptr3=command3;
   ptr4=command4;
   ptr5=command5;
   ptr6=command6;
   ptr7=command7;
   ptr8=command8;
   ptr9=command9;
   ptr10=command10;
   ptr11=command11;
   ptr12=command12;
   ptr13=command13;
   ptr14=command14;

   com_status=_bios_serialcom(_COM_STATUS,1,0);
   printf("COM2 Status:0x% .4x \n", com_status);
   _bios_serialcom(_COM_INIT,1,_COM_CHR8 |
                              _COM_STOP1 | _COM_NOPARITY |
                              _COM_300);

   while (*ptr1 != NULL) {
  _bios_serialcom(_COM_SEND,1,*ptr1);
   ptr1++;
  }

  i=0;
  r=' ';
  while(r  != '*') {
     com_status= _bios_serialcom(_COM_STATUS,1,0);
     printf("COM2 Status:0x% .4x \n", com_status);

        r=_bios_serialcom(_COM_RECEIVE,1,0);
    fwrite(&r,1,1,fpw);

  }
```

```
while (*ptr2 != NULL) {
_bios_serialcom(_COM_SEND,1,*ptr2);
 ptr2++;
}

 r=' ';
while(r  != '*') {
   com_status= _bios_serialcom(_COM_STATUS,1,0);
   printf("COM2 Status:0x% .4x \n", com_status);

      r=_bios_serialcom(_COM_RECEIVE,1,0);
  fwrite(&r,1,1,fpw);

}
while (*ptr3 != NULL) {
_bios_serialcom(_COM_SEND,1,*ptr3);
 ptr3++;
}

 r=' ';
while(r  != '*') {
   com_status= _bios_serialcom(_COM_STATUS,1,0);
   printf("COM2 Status:0x% .4x \n", com_status);

      r=_bios_serialcom(_COM_RECEIVE,1,0);
  fwrite(&r,1,1,fpw);

}

 while (*ptr4 != NULL) {
_bios_serialcom(_COM_SEND,1,*ptr4);
 ptr4++;
}

 r=' ';
while(r  != '*') {
   com_status= _bios_serialcom(_COM_STATUS,1,0);
   printf("COM2 Status:0x% .4x \n", com_status);

      r=_bios_serialcom(_COM_RECEIVE,1,0);
  fwrite(&r,1,1,fpw);
```

```
}

while (*ptr5 != NULL) {
_bios_serialcom(_COM_SEND,1,*ptr5);
 ptr5++;
}

 r=' ';
while(r  != '*') {
   com_status= _bios_serialcom(_COM_STATUS,1,0);
   printf("COM2 Status:0x% .4x \n", com_status);

      r=_bios_serialcom(_COM_RECEIVE,1,0);
  fwrite(&r,1,1,fpw);

}
while (*ptr6 != NULL) {
_bios_serialcom(_COM_SEND,1,*ptr6);
 ptr6++;
}

 r=' ';
while(r  != '*') {
   com_status= _bios_serialcom(_COM_STATUS,1,0);
   printf("COM2 Status:0x% .4x \n", com_status);

      r=_bios_serialcom(_COM_RECEIVE,1,0);
  fwrite(&r,1,1,fpw);

}
while (*ptr7 != NULL) {
_bios_serialcom(_COM_SEND,1,*ptr7);
 ptr7++;
}

 r=' ';
while(r  != '*') {
   com_status= _bios_serialcom(_COM_STATUS,1,0);
   printf("COM2 Status:0x% .4x \n", com_status);

      r=_bios_serialcom(_COM_RECEIVE,1,0);
  fwrite(&r,1,1,fpw);
```

```
}
while (*ptr8 != NULL) {
_bios_serialcom(_COM_SEND,1,*ptr8);
 ptr8++;
}

 r=' ';
while(r  != '*') {
   com_status= _bios_serialcom(_COM_STATUS,1,0);
   printf("COM2 Status:0x% .4x \n", com_status);

      r=_bios_serialcom(_COM_RECEIVE,1,0);
  fwrite(&r,1,1,fpw);


}
while (*ptr9 != NULL) {
_bios_serialcom(_COM_SEND,1,*ptr9);
 ptr9++;
}

 r=' ';
while(r  != '*') {
   com_status= _bios_serialcom(_COM_STATUS,1,0);
   printf("COM2 Status:0x% .4x \n", com_status);

      r=_bios_serialcom(_COM_RECEIVE,1,0);
  fwrite(&r,1,1,fpw);

}
while (*ptr10 != NULL) {
_bios_serialcom(_COM_SEND,1,*ptr10);
 ptr10++;
}

r=' ';
while(r  != '*') {
   com_status= _bios_serialcom(_COM_STATUS,1,0);
   printf("COM2 Status:0x% .4x \n", com_status);

      r=_bios_serialcom(_COM_RECEIVE,1,0);
  fwrite(&r,1,1,fpw);
```

```
}
while (*ptr11 != NULL) {
_bios_serialcom(_COM_SEND,1,*ptr11);
 ptr11++;
}

 r=' ';
while(r  != '*') {
   com_status= _bios_serialcom(_COM_STATUS,1,0);
   printf("COM2 Status:0x% .4x \n", com_status);

      r=_bios_serialcom(_COM_RECEIVE,1,0);
  fwrite(&r,1,1,fpw);

}
while (*ptr12 != NULL) {
_bios_serialcom(_COM_SEND,1,*ptr12);
 ptr12++;
}

 r=' ';
while(r  != '*') {
   com_status= _bios_serialcom(_COM_STATUS,1,0);
   printf("COM2 Status:0x% .4x \n", com_status);

      r=_bios_serialcom(_COM_RECEIVE,1,0);
  fwrite(&r,1,1,fpw);

}
while (*ptr13 != NULL) {
_bios_serialcom(_COM_SEND,1,*ptr13);
 ptr13++;
}

 r=' ';
while(r  != '*') {
   com_status= _bios_serialcom(_COM_STATUS,1,0);
   printf("COM2 Status:0x% .4x \n", com_status);

      r=_bios_serialcom(_COM_RECEIVE,1,0);
  fwrite(&r,1,1,fpw);
```

```
 }
 while (*ptr14 != NULL) {
 _bios_serialcom(_COM_SEND,1,*ptr14);
  ptr14++;
 }

   r=' ';
 while(r  != '*') {
     com_status= _bios_serialcom(_COM_STATUS,1,0);
     printf("COM2 Status:0x% .4x \n", com_status);

        r=_bios_serialcom(_COM_RECEIVE,1,0);
    fwrite(&r,1,1,fpw);

 }
     fcloseall();
}
```

APPENDIX-B

Electrode Polarization Data for Experimental Design

Abbrevation:

C.D.	: Current density, mA/cm^2
CURR	: Current drawn from the electrode, mA/cm^2
POT	: Electrode Potential, mV(Hg/HgO)
IR	: Ohmic Potential Drop in the Cell, mV
RESIST	: Resistance of the Cell, ohms
IR-FREE	: Electrode Porential after IR-elimination, mV
OVER	: Overpotential of the Electrode

RUN#1

C.D.	CURR	POT	IR	RESIST	IR-FREE	OVER
0	0	-934	0	0	-934	0
0.83	-5	-930	3	0.6	-933	1
1.67	-10	-926	6	0.6	-932	2
4.17	-25	-914	15	0.6	-929	5
8.33	-50	-892	29	0.58	-921	13
16.67	-100	-852	56	0.56	-908	26
41.67	-250	-730	142	0.57	-872	62
58.33	-350	-657	199	0.57	-856	78
83.33	-500	-530	286	0.57	-816	118
100	-600	-447	342	0.57	-789	145
125	-750	-332	429	0.57	-761	173
150	-900	-216	515	0.57	-731	203
166.67	-1000	-143	573	0.57	-716	218

RUN#2

C.D.	CURR	POT	IR	RESIST	IR-FREE	OVER
0	0	-932	0	0	-932	0
0.83	-5	-928	3	0.6	-931	1
1.67	-10	-924	6	0.6	-930	2
4.17	-25	-912	15	0.6	-927	5
8.33	-50	-891	28	0.56	-919	13
16.67	-100	-852	57	0.57	-909	23
41.67	-250	-735	142	0.57	-877	55
58.33	-350	-659	201	0.57	-860	72
83.33	-500	-545	287	0.57	-832	100
100	-600	-467	342	0.57	-809	123
125	-750	-347	431	0.57	-778	154
150	-900	-232	515	0.57	-747	185
166.67	-1000	-153	574	0.57	-727	205

RUN#3

C.D.	CURR	POT	IR	RESIST	IR-FREE	OVER
0	0	-921	0	0	-921	0
0.83	-5	-917	3	0.6	-920	1
1.67	-10	-912	6	0.6	-918	3
4.17	-25	-900	14	0.56	-914	7
8.33	-50	-877	29	0.58	-906	15
16.67	-100	-835	57	0.57	-892	29
41.67	-250	-708	144	0.58	-852	69
58.33	-350	-627	201	0.57	-828	93
83.33	-500	-500	287	0.57	-787	134
100	-600	-415	345	0.58	-760	161
125	-750	-289	431	0.57	-720	201
150	-900	-162	517	0.57	-679	242
166.67	-1000	-79	574	0.57	-653	268

RUN#4

C.D.	CURR	POT	IR	RESIST	IR-FREE	OVER
0	0	-924	0	0	-924	0
0.83	-5	-920	3	0.6	-923	1
1.67	-10	-916	6	0.6	-922	2
4.17	-25	-903	14	0.56	-917	7
8.33	-50	-883	29	0.58	-912	12
16.67	-100	-835	60	0.6	-895	29
41.67	-250	-723	142	0.57	-865	59
58.33	-350	-643	203	0.58	-846	78
83.33	-500	-523	288	0.58	-811	113
100	-600	-440	345	0.58	-785	139
125	-750	-320	431	0.57	-751	173
150	-900	-198	517	0.57	-715	209
166.67	-1000	-119	574	0.57	-693	231

RUN#5

C.D.	CURR	POT	IR	RESIST	IR-FREE	OVER
0	0	-933	0	0	-933	0
0.83	-5	-929	3	0.6	-932	1
1.67	-10	-925	6	0.6	-931	2
4.17	-25	-912	14	0.56	-926	7
8.33	-50	-891	29	0.58	-920	13
16.67	-100	-850	57	0.57	-907	26
41.67	-250	-728	143	0.57	-871	62
58.33	-350	-647	200	0.57	-847	86
83.33	-500	-526	286	0.57	-812	121
100	-600	-442	343	0.57	-785	148
125	-750	-319	429	0.57	-748	185
150	-900	-196	515	0.57	-711	222
166.67	-1000	-116	572	0.57	-688	245

RUN#6

C.D.	CURR	POT	IR	RESIST	IR-FREE	OVER
0	0	-931	0	0	-931	0
0.83	-5	-927	3	0.6	-930	1
1.67	-10	-923	6	0.6	-929	2
4.17	-25	-910	14	0.56	-924	7
8.33	-50	-891	29	0.58	-920	11
16.67	-100	-852	57	0.57	-909	22
41.67	-250	-734	143	0.57	-877	54
58.33	-350	-657	200	0.57	-857	74
83.33	-500	-540	286	0.57	-826	105
100	-600	-460	343	0.57	-803	128
125	-750	-343	429	0.57	-772	159
150	-900	-224	515	0.57	-739	192
166.67	-1000	-147	571	0.57	-718	213

RUN#7

C.D.	CURR	POT	IR	RESIST	IR-FREE	OVER
0	0	-923	0	0	-923	0
0.83	-5	-919	3	0.6	-922	1
1.67	-10	-914	6	0.6	-920	3
4.17	-25	-901	14	0.56	-915	8
8.33	-50	-880	28	0.56	-908	15
16.67	-100	-836	57	0.57	-893	30
41.67	-250	-706	143	0.57	-849	74
58.33	-350	-621	200	0.57	-821	102
83.33	-500	-494	286	0.57	-780	143
100	-600	-408	343	0.57	-751	172
125	-750	-279	429	0.57	-708	215
150	-900	-151	514	0.57	-665	258
166.67	-1000	-66	572	0.57	-638	285

RUN#8

C.D.	CURR	POT	IR	RESIST	IR-FREE	OVER
0	0	-925	0	0	-925	0
0.83	-5	-921	3	0.6	-924	1
1.67	-10	-917	6	0.6	-923	2
4.17	-25	-904	14	0.56	-918	7
8.33	-50	-885	28	0.56	-913	12
16.67	-100	-846	57	0.57	-903	22
41.67	-250	-727	143	0.57	-870	55
58.33	-350	-650	200	0.57	-850	75
83.33	-500	-533	286	0.57	-819	106
100	-600	-451	344	0.57	-795	130
125	-750	-334	429	0.57	-763	162
150	-900	-215	515	0.57	-730	195
166.67	-1000	-136	573	0.57	-709	216

RUN#9

C.D.	CURR	POT	IR	RESIST	IR-FREE	OVER
0	0	-932	0	0	-932	0
0.83	-5	-928	3	0.6	-931	1
1.67	-10	-923	6	0.6	-929	3
4.17	-25	-911	14	0.56	-925	7
8.33	-50	-890	28	0.56	-918	14
16.67	-100	-848	57	0.57	-905	27
41.67	-250	-725	143	0.57	-868	64
58.33	-350	-643	200	0.57	-843	89
83.33	-500	-520	286	0.57	-806	126
100	-600	-437	343	0.57	-780	152
125	-750	-313	429	0.57	-742	190
150	-900	-190	514	0.57	-704	228
166.67	-1000	-108	572	0.57	-680	252

RUN#10

C.D.	CURR	POT	IR	RESIST	IR-FREE	OVER
0	0	-930	0	0	-930	0
0.83	-5	-926	3	0.6	-929	1
1.67	-10	-922	6	0.6	-928	2
4.17	-25	-910	14	0.56	-924	6
8.33	-50	-891	28	0.56	-919	11
16.67	-100	-852	57	0.57	-909	21
41.67	-250	-736	143	0.57	-879	51
58.33	-350	-660	200	0.57	-860	70
83.33	-500	-545	286	0.57	-831	99
100	-600	-466	343	0.57	-809	121
125	-750	-349	430	0.57	-779	151
150	-900	-232	516	0.57	-748	182
166.67	-1000	-154	574	0.57	-728	202

RUN#11

C.D.	CURR	POT	IR	RESIST	IR-FREE	OVER
0	0	-926	0	0	-926	0
0.83	-5	-922	3	0.6	-925	1
1.67	-10	-918	6	0.6	-924	2
4.17	-25	-905	14	0.56	-919	7
8.33	-50	-883	28	0.56	-911	15
16.67	-100	-842	57	0.57	-899	27
41.67	-250	-717	143	0.57	-860	66
58.33	-350	-636	200	0.57	-836	90
83.33	-500	-512	286	0.57	-798	128
100	-600	-427	344	0.57	-771	155
125	-750	-303	429	0.57	-732	194
150	-900	-178	515	0.57	-693	233
166.67	-1000	-95	573	0.57	-668	258

RUN#12

C.D.	CURR	POT	IR	RESIST	IR-FREE	OVER
0	0	-924	0	0	-924	0
0.83	-5	-920	3	0.6	-923	1
1.67	-10	-916	6	0.6	-922	2
4.17	-25	-904	15	0.6	-919	5
8.33	-50	-884	28	0.56	-912	12
16.67	-100	-845	57	0.57	-902	22
41.67	-250	-729	142	0.57	-871	53
58.33	-350	-659	201	0.57	-860	64
83.33	-500	-534	287	0.57	-821	103
100	-600	-456	342	0.57	-798	126
125	-750	-337	431	0.57	-768	156
150	-900	-220	515	0.57	-735	189
166.67	-1000	-141	574	0.57	-715	209

RUN#13

C.D.	CURR	POT	IR	RESIST	IR-FREE	OVER
0	0	-934	0	0	-934	0
0.83	-5	-930	3	0.6	-933	1
1.67	-10	-925	6	0.6	-931	3
4.17	-25	-913	14	0.56	-927	7
8.33	-50	-891	29	0.58	-920	14
16.67	-100	-849	57	0.57	-906	28
41.67	-250	-722	144	0.58	-866	68
58.33	-350	-639	201	0.57	-840	94
83.33	-500	-515	287	0.57	-802	132
100	-600	-429	345	0.58	-774	160
125	-750	-303	431	0.57	-734	200
150	-900	-177	517	0.57	-694	240
166.67	-1000	-94	574	0.57	-668	266

RUN#14

C.D.	CURR	POT	IR	RESIST	IR-FREE	OVER
0	0	-933	0	0	-933	0
0.83	-5	-929	3	0.6	-932	1
1.67	-10	-925	6	0.6	-931	2
4.17	-25	-913	14	0.56	-927	6
8.33	-50	-891	28	0.56	-919	14
16.67	-100	-851	57	0.57	-908	25
41.67	-250	-729	143	0.57	-872	61
58.33	-350	-660	200	0.57	-860	73
83.33	-500	-530	286	0.57	-816	117
100	-600	-447	343	0.57	-790	143
125	-750	-326	429	0.57	-755	178
150	-900	-204	514	0.57	-718	215
166.67	-1000	-123	572	0.57	-695	238

RUN#15

C.D.	CURR	POT	IR	RESIST	IR-FREE	OVER
0	0	-925	0	0	-925	0
0.83	-5	-921	3	0.6	-924	1
1.67	-10	-916	6	0.6	-922	3
4.17	-25	-903	15	0.6	-918	7
8.33	-50	-883	28	0.56	-911	14
16.67	-100	-839	57	0.57	-896	29
41.67	-250	-711	142	0.57	-853	72
58.33	-350	-627	201	0.57	-828	97
83.33	-500	-501	287	0.57	-788	137
100	-600	-417	342	0.57	-759	166
125	-750	-287	431	0.57	-718	207
150	-900	-161	515	0.57	-676	249
166.67	-1000	-76	574	0.57	-650	275

RUN#16

C.D.	CURR	POT	IR	RESIST	IR-FREE	OVER
0	0	-924	0	0	-924	0
0.83	-5	-920	3	0.6	-923	1
1.67	-10	-916	6	0.6	-922	2
4.17	-25	-904	14	0.56	-918	6
8.33	-50	-884	28	0.56	-912	12
16.67	-100	-844	57	0.57	-901	23
41.67	-250	-726	143	0.57	-869	55
58.33	-350	-649	200	0.57	-849	75
83.33	-500	-532	286	0.57	-818	106
100	-600	-451	344	0.57	-795	129
125	-750	-334	429	0.57	-763	161
150	-900	-215	515	0.57	-730	194
166.67	-1000	-137	573	0.57	-710	214

APPENDIX-C

Electrode Polarization Data for the Effect of PTFE Content

Abbrevation:

C.D.	: Current density, mA/cm^2
CURR	: Current drawn from the electrode, mA/cm^2
POT	: Electrode Potential, mV(Hg/HgO)
IR	: Ohmic Potential Drop in the Cell, mV
RESIST	: Resistance of the Cell, ohms
IR-FREE	: Electrode Porential after IR-elimination, mV
OVER	: Overpotential of the Electrode

PTFE = 2%

C.D.	CURR	POT	IR	RESIST	IR-FREE	OVER
0.17	-1	-933	0	0	-933	0
0.83	-5	-924	3	-0.6	-927	6
1.83	-11	-916	6	-0.55	-922	11
4.33	-26	-899	15	-0.58	-914	19
8.5	-51	-878	29	-0.57	-907	26
16.67	-100	-818	58	-0.58	-876	57
41.83	-251	-692	143	-0.57	-835	98
58.5	-351	-576	199	-0.57	-775	158
83.33	-500	-394	287	-0.57	-681	252
100.17	-601	-209	347	-0.58	-556	377
125	-750	148	428	-0.57	-280	653
150	-900	612	514	-0.57	98	1031
166.67	-1000	767	579	-0.58	188	1121

PTFE = 5%

C.D.	CURR	POT	IR	RESIST	IR-FREE	OVER
0	0	-928	0	0	-928	0
1	-6	-924	4	-0.67	-928	0
1.83	-11	-920	7	-0.64	-927	1
4.33	-26	-907	18	-0.69	-925	3
8.5	-51	-884	31	-0.61	-915	13
16.83	-101	-837	62	-0.61	-899	29
41.83	-251	-699	146	-0.58	-845	83
58.5	-351	-609	201	-0.57	-810	118
83.33	-500	-462	291	-0.58	-753	175
100	-600	-363	354	-0.59	-717	211
125	-750	-145	443	-0.59	-588	340
150	-900	119	536	-0.6	-417	511
166.67	-1000	366	571	-0.57	-205	723

PTFE = 8%

C.D	CURR	POT	IR	RESIST	IR-FREE	OVER
0	0	-934	0	0	-934	0
0.83	-5	-930	3	0.6	-933	1
1.67	-10	-926	6	0.6	-932	2
4.33	-26	-914	15	0.58	-929	5
8.33	-50	-896	29	0.58	-925	9
16.67	-100	-855	59	0.59	-914	20
41.67	-250	-737	145	0.58	-882	52
58.33	-350	-660	202	0.58	-862	72
83.33	-500	-551	284	0.57	-835	99
100	-600	-470	342	0.57	-812	122
125	-750	-350	429	0.57	-779	155
150	-900	-223	520	0.58	-743	191
166.67	-1000	-140	578	0.58	-718	216

PTFE = 11%

C.D.	CURR	POT	IR	RESIST	IR-FREE	OVER
0.17	-1	-931	0	0	-931	0
0.83	-5	-927	3	-0.6	-930	1
1.83	-11	-923	7	-0.64	-930	1
4.33	-26	-909	16	-0.62	-925	6
8.5	-51	-891	30	-0.59	-921	10
16.67	-100	-849	61	-0.61	-910	21
41.83	-251	-734	146	-0.58	-880	51
58.5	-351	-645	205	-0.58	-850	81
83.33	-500	-522	293	-0.59	-815	116
100.17	-601	-442	351	-0.58	-793	138
125	-750	-302	439	-0.59	-741	190
150	-900	-149	532	-0.59	-681	250
166.67	-1000	-42	591	-0.59	-633	298

PTFE = 14%

C.D.	CURR	POT	IR	RESIST	IR-FREE	OVER
0.17	-1	-931	0	0	-931	0
0.83	-5	-927	3	-0.6	-930	1
1.83	-11	-921	6	-0.55	-927	4
4.33	-26	-907	15	-0.58	-922	9
8.5	-51	-881	30	-0.59	-911	20
16.67	-100	-843	59	-0.59	-902	29
41.83	-251	-709	148	-0.59	-857	74
58.5	-351	-624	207	-0.59	-831	100
83.33	-500	-478	293	-0.59	-771	160
100.17	-601	-390	349	-0.58	-739	192
125	-750	-220	441	-0.59	-661	270
150	-900	-52	529	-0.59	-581	350
166.67	-1000	51	581	-0.58	-530	401

APPENDIX-D

Electrode Polarization Data for the Effect of Milling Time

Abbrevation:

C.D.	: Current density, mA/cm^2
CURR	: Current drawn from the electrode, mA/cm^2
POT	: Electrode Potential, mV(Hg/HgO)
IR	: Ohmic Potential Drop in the Cell, mV
RESIST	: Resistance of the Cell, ohms
IR-FREE	: Electrode Porential after IR-elimination, mV
OVER	: Overpotential of the Electrode

MILL-TIME = 30 SECOND

C.D	CURR	POT	IR	RESIST	IR-FREE	OVER
0	0	-934	0	0	-934	0
0.83	-5	-930	3	0.6	-933	1
1.67	-10	-925	6	0.6	-931	3
4.33	-26	-912	15	0.58	-927	7
8.33	-50	-894	29	0.58	-923	11
16.67	-100	-858	57	0.57	-915	19
41.67	-250	-727	145	0.58	-872	62
58.33	-350	-646	203	0.58	-849	85
83.33	-500	-527	284	0.57	-811	123
100	-600	-440	343	0.57	-783	122
125	-750	-313	429	0.57	-742	192
150	-900	-178	522	0.58	-700	234
166.67	-1000	-71	581	0.58	-652	282

MILL-TIME = 60 SECOND

C.D	CURR	POT	IR	RESIST	IR-FREE	OVER
0	0	-934	0	0	-934	0
0.83	-5	-930	3	0.6	-933	1
1.67	-10	-926	6	0.6	-932	2
4.33	-26	-914	15	0.58	-929	5
8.33	-50	-896	29	0.58	-925	9
16.67	-100	-855	59	0.59	-914	20
41.67	-250	-737	145	0.58	-882	52
58.33	-350	-660	202	0.58	-862	72
83.33	-500	-551	284	0.57	-835	99
100	-600	-470	342	0.57	-812	122
125	-750	-350	429	0.57	-779	155
150	-900	-223	520	0.58	-743	191
166.67	-1000	-140	578	0.58	-718	216

MILL-TIME = 90 SECOND

C.D	CURR	POT	IR	RESIST	IR-FREE	OVER
0	0	-933	0	0	-933	0
0.83	-5	-929	3	0.6	-932	1
1.67	-10	-924	6	0.6	-930	3
4.33	-26	-911	15	0.58	-926	7
8.33	-50	-893	29	0.58	-922	11
16.67	-100	-856	57	0.57	-913	20
41.67	-250	-730	143	0.57	-873	60
58.33	-350	-951	200	0.57	-1151	-218
83.33	-500	-528	285	0.57	-813	120
100	-600	-445	342	0.57	-787	146
125	-750	-321	428	0.57	-749	184
150	-900	-181	513	0.57	-694	239
166.67	-1000	-87	570	0.57	-657	276

MILL-TIME = 120 SECOND

C.D	CURR	POT	IR	RESIST	IR-FREE	OVER
0	0	-932	0	0	-932	0
0.83	-5	-927	3	0.6	-930	2
1.67	-10	-923	6	0.6	-929	3
4.33	-26	-910	14	0.54	-924	8
8.33	-50	-891	28	0.56	-919	13
16.67	-100	-852	55	0.55	-907	25
41.67	-250	-727	138	0.55	-865	67
58.33	-350	-641	193	0.55	-834	98
83.33	-500	-525	275	0.55	-800	132
100	-600	-440	330	0.55	-770	162
125	-750	-308	413	0.55	-721	211
150	-900	-178	495	0.55	-673	259
166.67	-1000	-96	550	0.55	-646	286

MILL-TIME = 150 SECOND

C.D.	CURR	POT	IR	RESIST		
0	0	-935	0	0	-935	0
0.83	-5	-931	3	-0.6	-934	1
1.83	-11	-926	6	-0.55	-932	3
4.33	-26	-914	14	-0.54	-928	7
8.5	-51	-893	28	-0.55	-921	14
16.83	-101	-851	57	-0.56	-908	27
41.83	-251	-726	141	-0.56	-867	68
58.5	-351	-639	198	-0.56	-837	98
83.33	-500	-519	281	-0.56	-800	135
100.17	-601	-436	334	-0.56	-770	165
125	-750	-310	419	-0.56	-729	206
150	-900	-172	501	-0.56	-673	262
166.67	-1000	-85	559	-0.56	-644	291

MILL-TIME = 180 SECOND

C.D	CURR	POT	IR	RESIST	IR-FREE	OVER
0	0	-933	0	0	-933	0
0.83	-5	-928	3	0.6	-931	2
1.67	-10	-924	6	0.6	-930	3
4.33	-26	-913	14	0.54	-927	6
8.33	-50	-892	29	0.58	-921	12
16.67	-100	-851	57	0.57	-908	25
41.67	-250	-717	144	0.58	-861	72
58.33	-350	-631	201	0.57	-832	101
83.33	-500	-501	291	0.58	-792	141
100	-600	-421	344	0.57	-765	168
125	-750	-289	429	0.57	-718	215
150	-900	-148	513	0.57	-661	272
166.67	-1000	-66	566	0.57	-632	301

APPENDIX-E

Electrode Polarization Data for at Different Temperatures

Abbrevation:

C.D.	: Current density, mA/cm^2
CURR	: Current drawn from the electrode, mA/cm^2
POT	: Electrode Potential, mV(Hg/HgO)
IR	: Ohmic Potential Drop in the Cell, mV
RESIST	: Resistance of the Cell, ohms
IR-FREE	: Electrode Porential after IR-elimination, mV
OVER	: Overpotential of the Electrode

TEMP = 25 C

C.D.	CURR	POT	IR	RESIST	IR-FREE	OVER
0	0	-924	0	0	-924	0
0.83	-5	-920	3	0.6	-923	1
1.67	-10	-916	6	0.6	-922	2
4.17	-25	-905	15	0.6	-920	4
8.33	-50	-889	28	0.56	-917	7
16.67	-100	-853	57	0.57	-910	14
41.67	-250	-739	144	0.58	-883	41
58.33	-350	-664	200	0.57	-864	60
83.33	-500	-547	286	0.57	-833	91
100	-600	-461	344	0.57	-805	119
125	-750	-335	431	0.57	-766	158
150	-900	-209	515	0.57	-724	200
166.67	-1000	-124	575	0.58	-699	225

TEMP = 35 C

C.D.	CURR	POT	IR	RESIST	IR-FREE	OVER
0	0	-922	0	0	-922	0
0.83	-5	-918	3	0.6	-921	1
1.67	-10	-916	5	0.5	-921	1
4.17	-25	-908	12	0.48	-920	2
8.33	-50	-894	24	0.48	-918	4
16.67	-100	-863	49	0.49	-912	10
41.67	-250	-776	121	0.48	-897	25
58.33	-350	-714	169	0.48	-883	39
83.33	-500	-616	243	0.49	-859	63
100	-600	-558	288	0.48	-846	76
125	-750	-449	362	0.48	-811	111
150	-900	-335	432	0.48	-767	155
166.67	-1000	-265	481	0.48	-746	176

TEMP = 45 C

C.D.	CURR	POT	IR	RESIST	IR-FREE	OVER
0	0	-920	0	0	-920	0
0.83	-5	-918	2	0.4	-920	0
1.67	-10	-915	4	0.4	-919	1
4.17	-25	-907	11	0.44	-918	2
8.33	-50	-896	21	0.42	-917	3
16.67	-100	-870	42	0.42	-912	8
41.67	-250	-796	106	0.42	-902	18
58.33	-350	-746	148	0.42	-894	26
83.33	-500	-669	211	0.42	-880	40
100	-600	-616	253	0.42	-869	51
125	-750	-527	317	0.42	-844	76
150	-900	-441	381	0.42	-822	98
166.67	-1000	-378	424	0.42	-802	118

TEMP = 55 C

C.D.	CURR	POT	IR	RESIST	IR-FREE	OVER
0	0	-917	0	0	-917	0
0.83	-5	-915	2	0.4	-917	0
1.67	-10	-912	4	0.4	-916	1
4.17	-25	-906	9	0.36	-915	2
8.33	-50	-896	18	0.36	-914	3
16.67	-100	-875	36	0.36	-911	6
41.67	-250	-813	91	0.36	-904	13
58.33	-350	-771	127	0.36	-898	19
83.33	-500	-706	181	0.36	-887	30
100	-600	-656	218	0.36	-874	43
125	-750	-592	271	0.36	-863	54
150	-900	-529	321	0.36	-850	67
166.67	-1000	-472	361	0.36	-833	84

TEMP = 65 C

C.D.	CURR	POT	IR	RESIST	IR-FREE	OVER
0	0	-911	0	0	-911	0
0.83	-5	-909	2	0.4	-911	0
1.67	-10	-907	3	0.3	-910	1
4.17	-25	-901	8	0.32	-909	2
8.33	-50	-892	16	0.32	-908	3
16.67	-100	-873	33	0.33	-906	5
41.67	-250	-819	82	0.33	-901	10
58.33	-350	-784	114	0.33	-898	13
83.33	-500	-729	161	0.32	-890	21
100	-600	-693	192	0.32	-885	26
125	-750	-630	245	0.33	-875	36
150	-900	-565	296	0.33	-861	50
166.67	-1000	-522	327	0.33	-849	62

TEMP = 75 C

C.D.	CURR	POT	IR	RESIST	IR-FREE	OVER
0	0	-906	0	0	-906	0
0.83	-5	-904	2	0.4	-906	0
1.67	-10	-903	3	0.3	-906	0
4.17	-25	-898	7	0.28	-905	1
8.33	-50	-889	15	0.3	-904	2
16.67	-100	-872	31	0.31	-903	3
41.67	-250	-823	76	0.3	-899	7
58.33	-350	-789	106	0.3	-895	11
83.33	-500	-734	155	0.31	-889	17
100	-600	-696	187	0.31	-883	23
125	-750	-645	229	0.31	-874	32
150	-900	-591	274	0.3	-865	41
166.67	-1000	-553	303	0.3	-856	50

APPENDIX-F

Computer program for for solving model equation developed in Chapter 7.

```
C
C       IN THE DATA FILE FEED FOLLOWING PARAMETERS IN THIS    ORDER:-
C            T = TEMPERATURE IN K
C       BARK  = EFFECTIVE CONDUCTIVITY
C       HK = HENERY'S CONSTANT
C       EXI    = EXCHANGE CURRENT DENSITY
C       ALPHA  = CHARGE TRANSFER COEFFICENT
C       DL     = DIFFUSIVITY IN PURE ELECTROLYTE
C       DLE    = DIFFUSIVITY IN POROUS GRAIN
C       DG     = DIFFUSIVITY IN MACROPORES
C       DEL    = THICKNESS OF THE FILM
C       R      = AVERAGE RADIAUS OF THE GRAIN
C       PPP    = A NON ZERO REAL NUMBER  FOR THE CONTINUATION        AND
ZERO FOR STOPPING
C       NNN    = # OF THE DATA SET (A NON ZERO INTEGER NUMBER FOR   THE
CONTINUATION AND ZERO FOR STOPPING)
              IMPLICIT REAL*8(A-H,O-Z)

              COMMON TA0,P0,AX,Y1,Y2,Y3,Y4,W1,W2,W3,W4,Z1,Z2,Z3,Z4,
     &        BARK,EPS,EXI,ALPHA,DL,DLE,DG,DEL,CS,HK,T,R,IET,NNN
              DIMENSION Y(12),DERY(12),AUX(8,12),A(4),B(4),C(4),PRMT(5)
              INTEGER IET
              EXTERNAL FCT,OUTP
              EPS=0.200
              P0=138.0
              CON0= P0*HK
7             READ(5,*) T,BARK,HK,EXI,ALPHA,DL,DLE,DG,DEL,R,PPP,MMM
       IF(PPP.EQ.0) GO TO 3000
              WRITE(7,222) MMM
              WRITE(8,999) T-273.15, R
              WRITE(7,333)
              WRITE(7,444)T,P0,HK,BARK,EPS,EXI,ALPHA,DL,DLE,DG,
     &       DEL,CON0
              WRITE(7,555)
              ETA0=0.000
              DETA0=0.00500
              DO 99 N=1,25
C
C
                        DAA= 0.0
                        DBB= 0.0
                              AA=-1.0
                              BB= 0.0
C
                   IET=0
```

```
10              AA=AA-DAA
                BB=BB-DBB
                IET=IET+1
                        PRMT(1)=0.000000001
                        PRMT(2)=0.032
                        PRMT(3)=0.008
                        PRMT(4)=0.000001
                        PRMT(5)=0.0
                        DERY(1)=0.083
                        DERY(2)=0.083
                        DERY(3)=0.083
                        DERY(4)=0.083
                        DERY(5)=0.083
                        DERY(6)=0.083
                        DERY(7)=0.083
                        DERY(8)=0.083
                        DERY(9)=0.083
                        DERY(10)=0.083
                        DERY(11)=0.085
                        DERY(12)=0.085
                        Y(1)=ETA0
                        Y(2)=AA
                        Y(3)=BB
                        Y(4)=0.0
C
                        Y(5)=0.0
                        Y(6)=1.0
                        Y(7)=0.0
                        Y(8)=0.0
                        Y(9) =0.0
                        Y(10)=0.0
                        Y(11)=1.0
                        Y(12)=0.0
                        NDIM=12
                CALL RKGS(PRMT,Y,DERY,NDIM,IHLF,FCT,OUTP,AUX)
                DY2= Y2-0.0
                DY3= Y3-P0
                DAA= (W3*DY2-W2*DY3)/(W3*Z2-W2*Z3)
                DBB= (Z3*DY2-Z2*DY3)/(Z3*W2-Z2*W3)
                SS=SQRT(DY2**2+DY3**2)
                IF(SS.GT.1.0E-3) GO TO 10
                NNN=IET
CC          USE  THESE STATEMENTS TO CHECK CRUDE RESULT
C
C               WRITE(7,*)'ITERATION #=',IET,NNN
```

```
C                   WRITE(7,*)AX,Y1,Y2,Y3,Y4,Z1,Z2,Z3,Z4,W1,W2,W3
     &              W4
99                  CONTINUE
              IF(PPP.GT.0) GO TO 7
C .
C             FORMAT  STATEMENTS
C ..........................................................
222           FORMAT('IN THE NAME OF ALLAH.....',///,'DATA SET #',I3, /)
333           FORMAT('MODEL PARAMETERS',/)
444           FORMAT(/,'T=',F8.2,/,'P0 =',F8.2,/,'HK=',E10.4,/,
     &        'BARK=',F8.4,/,'EPS=',F8.4,
     &        /, 'EXI=',E10.4,/,'ALPHA=',F5.2,/,'DL=',
     &        E10.4,/,'DLE=',E10.4,/,'DG=',E10.4,/,'DEL=',E10.4,
     &        /,'CON0=',E10.4//)
555           FORMAT('POLARIZATION DATA.....',//,
    &         ' ETA0   ',' CURRENT ',' PRESSURE')
999           FORMAT('TEMP =',F8.2,'   R=',E10.4)
C ..........................................................
3000  STOP
      END
CC=================================================================
=====
C                         PARAMETERS ARE PRMT(1),(2),(3),(4),(5)
C                         PRMT(1) IS THE LOWER LIMIT OF THE
C                         INDEPENDENT VARIABLE
C                         PRMT(2) IS THE UPPER LIMIT OF THE
C                         INDEPENDENT VARIABLE
C                         PRMT(3) IS THE INCREMENT IN THE
C                         INDEPENDENT VARIABLE
C                         PRMT(4) IS THE ERROR LIMIT
C                         PRMT(5) IF NOT EQUAL TO ZERO STOP
C                         Y(1),Y(2),..... ARE THE DEPENDENT VARIABLES
C                         GIVE THE INITIAL VALUE OF THEM
C
C                         DERY(1),DERY(2),.... ARE THE FUNCTIONS
C                         GIVEN AS WEIGHTED FUNCTIONS
C
C                         NDIM IS THE NO. OF EQUATIONS
C
C
C=========================================================C
C
C
              SUBROUTINE RKGS(PRMT,Y,DERY,NDIM,IHLF,FCT,OUTP,AUX)
               IMPLICIT REAL*8(A-H,O-Z)
```

```
      COMMON ETA0,P0,AX,Y1,Y2,Y3,Y4,W1,
     &      W2,W3,W4,Z1,Z2,Z3,Z4,
     &      BARK,EPS,EXI,ALPHA,DL,DLE,DG,DEL,CS,HK,T,R,IET,NNN
C
      DIMENSION Y(12),DERY(12),AUX(8,12),A(4),B(4),C(4),PRMT(5) 100
     CONTINUE
      DO 1 I=1,NDIM
1     AUX(8,I)=.06666667*DERY(I)
      X=PRMT(1)
      XEND=PRMT(2)
      H=PRMT(3)
      PRMT(5)=0.
      CALL FCT(NDIM,X,Y,DERY)
C     ERROR TEST
      IF (H*(XEND-X))38,37,2
C     PREPARATION FOR RUNGE-KUTTA METHOD
2     A(1)=.5
      A(2)=.2928932
      A(3)=1.707107
      A(4)=.1666667
      B(1)=2.
      B(2)=1.
      B(3)=1.
      B(4)=2.
      C(1)=.5
      C(2)=.2928932
      C(3)=1.707107
      C(4)=.5
C     PREPERATION OF FIRST RUNGE-KUTTA STEP
            DO 3 I=1,NDIM
            AUX(1,I)=Y(I)
            AUX(2,I)=DERY(I)
            AUX(3,I)=0.
3           AUX(6,I)=0.
            IREC=0
            H=H+H
            IHLF=-1
            ISTEP=0
            IEND=0
C.....
C           STATEMENTS FOR PRINTING POLARIZATION DATA
C.....
C           WRITE(7,*)'TEST',NNN
            IF (IET.EQ.NNN)WRITE(7,1111)Y(1)*1.0E03,
     &      -BARK*(1.0-EPS)*Y(2)*1.0E03,Y(3)
```

```
      IF (IET.EQ.NNN)WRITE(8,1111)Y(1)*1.0E03,
     &  -BARK*(1.0-EPS)*Y(2)*1.0E03,Y(3)
1111      FORMAT(F7.2,1X
     &           ,F7.2,3X,F7.2)
C.....
C         START OF A RUNGE-KUTTA STEP
4         IF((X+H-XEND)*H)7,6,5
5         H=XEND-X
6         IEND=1
C     RECORDING OF INITIAL VALUES OF THIS STEP
7         CALL OUTP(X,Y,DERY,IREC,NDIM,PRMT)
          IF(PRMT(5))40,8,40
8         ITEST=0
9         ISTEP=ISTEP+1
C
C
C     START OF INNERMOST RUNGE-KUTTA LOOP
          J=1
10        AJ=A(J)
          BJ=B(J)
          CJ=C(J)
          DO 11 I=1,NDIM
          R1=H*DERY(I)
          R2=AJ*(R1-BJ*AUX(6,I))
          Y(I)=Y(I)+R2
          R2=R2+R2+R2
11        IF(J-4)12,15,15
12        J=J+1 EL202160
          IF(J-3)13,14,13
13        X=X+.5*H
14        CALL FCT(NDIM,X,Y,DERY)
          G0 TO 10
C     END OF INNERMOST RUNGE-KUTTA LOOP
C     TEST OF ACCURACY
15        IF(ITEST)16,16,20
C     IN CASE ITEST=0 THERE IS NO POSSIBILITY FOR TESTING OF
C     ACCURACY
16        DO 17 I=1,NDIM
17        AUX(4,I)=Y(I)
          ITEST=1
          ISTEP=ISTEP+ISTEP-2
18        IHLF=IHLF+1
          X=X-H
          H=H*.5
          DO 19 I=1,NDIM
```

```
            Y(I)=AUX(1,I)
            DERY(I)=AUX(2,I)
19          AUX(6,I)=AUX(3,I)
            GO TO 9
C       IN CASE ITEST=1 TESTING OF ACCURACY IS POSSIBLE
20          IMOD=ISTEP/2
            IF(ISTEP-IMOD-IMOD)21,23,21
21          CALL FCT(NDIM,X,Y,DERY)
            DO 22 I=1,NDIM
            AUX(5,I)=Y(I)
22          AUX(7,I)=DERY(I)
            GO TO 9      EL202480
C       COMPUTATION OF TEST VALUE DELT
23          DELT=0
            DO 24 I=1,NDIM
24          DELT=DELT+AUX(8,I)*ABS(AUX(4,I)-Y(I))
            IF(DELT-PRMT(4))28,28,25
C       ERROR IS TOO GREAT
25          IF(IHLF-10)26,36,36
26          DO 27 I=1,NDIM
27          AUX(4,I)=AUX(5,I)
            ISTEP=ISTEP+ISTEP-4
            X=X-H
            IEND=0
            GO TO 18

C       RESULT VALUES ARE GOOD
28          CALL FCT(NDIM,X,Y,DERY)
            DO 29 I=1,NDIM
                        AUX(1,I)=Y(I)
                        AUX(2,I)=DERY(I)
                        AUX(3,I)=AUX(6,I)
                        Y(I)=AUX(5,I)
29          DERY(I)=AUX(7,I)
C*************************************************************
            CALL OUTP(X-H,Y,DERY,IHLF,NDIM,PRMT)
            IF(PRMT(5))40,30,40
30          DO 31 I=1,NDIM
                  Y(I)=AUX(1,I)
31          DERY(I)=AUX(2,I)
            IREC=IHLF
            IF(IEND)32,32,39
C       INCREMENT GETS DOUBLE
32          IHLF=IHLF-1
            ISTEP=ISTEP/2
```

```
            H=H+H
            IF(IHLF)4,33,33
33          IMOD=ISTEP/2
            IF(ISTEP-IMOD-IMOD)4,34,4
34           IF(DELT-.02*PRMT(4))35,35,4
35          IHLF=IHLF-1
            ISTEP=ISTEP/2
            H=H+H
            GO TO 4
C
C
C     RETURNS TO CALLING PROGRAM
36          IHLF=11
            CALL FCT(NDID,X,Y,DERY)
            GO TO 39
37          IHLF=12
            GO TO 39
38          IHLF=13
39          CALL OUTP(X,Y,DERY,IHLF,NDIM,PRMT)
C     ..........................................................................
C      IN ORDER TO PRINT FINAL VALUES OF X,ETA,CUR AND PR
C     REMOVE FROM THE FOLLOWING TWO STATEMENTS !!!!!!!!
C     ..........................................................................
C           IF (IET.EQ.4)WRITE(7,1112)X,Y(1)*1.0E03,
C     &     -BARK*(1.0-EPS)*Y(2)*1.0E03,Y(3)
1112        FORMAT('X=AL=',E10.4,1X,'ETAL=',F7.2,1X,
     &      'CURL=',F7.2,1X,'PR0=',F7.2)
40          RETURN
            END
C_____________________________________________________
            SUBROUTINE OUTP(X,Y,DERY,IHLF,NDIN,PRMT)
            IMPLICIT REAL*8(A-H,O-Z)
            COMMON ETA0,P0,AX,Y1,Y2,Y3,Y4,W1,W2,W3,W4,Z1,Z2,Z3,
     &      Z4, BARK,EPS,EXI,ALPHA,DL,DLE,DG,DEL,CS,HK,T,R,IET,NNN

C     REAL BARK,EPS
C     ----------------------------------------
C
            DIMENSION Y(12),DERY(12),PRMT(5)
            INTEGER IET
            HK=6.67E-10
C
            AX=X
            Y1=Y(1)
            Y2=Y(2)
```

```
            Y3=Y(3)
            Y4=Y(4)
            Z1=Y(5)
            Z2=Y(6)
            Z3=Y(7)
            Z4=Y(8)
            W1=Y(9)
            W2=Y(10)
            W3=Y(11)
            W4=Y(12)
C.....
C
C       USE THESE STATEMENTS TO PRINT P0(X),CS(X) ETC.
C
C.....
C            IF(IET.EQ.NNN)WRITE(7,111)X,Y(1)*1.0E03,
C     &      -BARK*(1.0-EPS)*Y(2)*1.0E03,Y(3)
C            IF(IET.EQ.NNN)WRITE(7,111)X,Y(1)*1.0E03
C                  IF(IET.EQ.NNN)WRITE(7,111)X,Y(3),CS/HK
111         FORMAT(E10.4,1X,F7.2,1X,F7.2,1X,F7.2)
C.....  .....
            RETURN
            END
C
C.....
            SUBROUTINE FCT(NDIM,X,Y,DERY)
            IMPLICIT REAL*8(A-H,O-Z)
            COMMON ETA0,P0,AX,Y1,Y2,Y3,Y4,W1,W2,W3,W4,Z1,Z2,Z3,
     &      Z4, BARK,EPS,EXI,ALPHA,DL,DLE,DG,DEL,CS,HK,T,R,IET,NNN

            DIMENSION DERY(12),Y(12)
C
            REAL TANH,SINH,EXP,SQRT,ABS
            INTRINSIC DTANH,DSINH,EXP,SQRT,ABS
C.....DEFINE PHYSICAL PARAMETERS
C
C
C
            EN=2.0
            AL = 0.320E-01
C           R=2.0E-03
            F=96484.56
            Z=1.0
            GASC=8.314
            SURF=5.40E+05
```

```
C
C.....CALCULATION
C
C      CALCULATIONS FOR ORIGINAL SET OF EQNS
C
               C0=HK*P0
               A1= EXI*SURF/(EN*F*DLE)
               A2=EXP(ALPHA*F*Z*Y(1)/(GASC*T) )
               A3=EXP(-(1-ALPHA)*F*Z*Y(1)/(GASC*T) )
               AW1=2.0*EN*F*DLE/(BARK*R)
               AW2=4*DLE*(1.0-EPS)/(AL*DG)
               P2=DEL*R*DLE/((DEL+R)*DL)
               RUT=SQRT(ABS(A1*A2/C0))
               SECOND=RUT/TANH(RUT*R) -1.0/R
               PR=P2*C0*SECOND*A3/A2
               CS= (HK*Y(3)+PR)/(1.0 +P2*SECOND)
               FIRST=CS-C0*A3/A2
               DERC= FIRST * SECOND
C              WRITE(7,*)EN,HK,AL,EPS,BARK,R,F,DLE,Z,GASC,T,EXI,
     &         ALPHA,SURF,DL,DG
C              WRITE(7,*)  C0,A1,A2,A3,AW1,AW2,RUT,B1,B2,CS,DERC
C
               DERY(1)=Y(2)
               DERY(2)=AW1*DERC
               DERY(3)=Y(4)
               DERY(4)=AW2*DERC
C
CCALCULATIONS FOR  SET OF EQNS OBTAINED BY DIFF. W.R.T. AA
C
               DA2A=ALPHA*Z*F*A2*Y(5)/(GASC*T)
               DA3A=-(1-ALPHA)*Z*F*A3*Y(5)/(GASC*T)
               DRUTA=0.5*DA2A*SQRT(ABS(A1/A2*C0))
               DSA=DRUTA*(-RUT*R/(DSINH(RUT*R))**2+ 1.0/DTANH(RUT*R))
               DPRA= P2*C0*(A2*(SECOND*DA3A + A3*DSA)-
     &         SECOND*A3*DA2A)/A2**2
               DCSA=((1.0 + P2*SECOND)*(HK*Y(7) +DPRA)-
     &         (HK*Y(3) +PR)*P2*DSA)/
     &         (1.0+P2*SECOND)**2
               DFA= DCSA - C0*(A2*DA3A-A3*DA2A)/A2**2
C
               DDERCA=FIRST*DSA + SECOND*DFA
               DERY(5)=Y(6)
               DERY(6)=AW1*DDERCA
               DERY(7)=Y(8)
               DERY(8)=AW2*DDERCA
```

```
C
C
C     CALCULATIONS FOR  SET OF EQNS OBTAINED BY DIFF. W.R.T. AA
C
C
            DA2B=ALPHA*Z*F*A2*Y(9)/(GASC*T)
            DA3B=-(1-ALPHA)*Z*F*A3*Y(9)/(GASC*T)
            DRUTB=0.5*DA2B*SQRT(ABS(A1/A2*C0))
            DSB=DRUTB*(-RUT*R/(DSINH(RUT*R))**2+ 1.0/DTANH(RUT*R))

            DPRB= P2*C0*(A2*(SECOND*DA3B + A3*DSB)-
     &      SECOND*A3*DA2B)/A2**2
            DCSB=((1.0 + P2*SECOND)*(HK*Y(11) +DPRB)-
     &      (HK*Y(3) +PR)*P2*DSB)/
     &      (1.0+P2*SECOND)**2
            DFB= DCSB - C0*(A2*DA3B-A3*DA2B)/A2**2
C
            DDERCB=FIRST*DSB + SECOND*DFB
            DERY(9)=Y(10)
            DERY(10)=AW1*DDERCB
            DERY(11)=Y(12)
            DERY(12)=AW2*DDERCB
            RETURN
            END
```

APPENDIX-G

A Sample Run of Electrode Preparation

Details of a sample electrode preparation are given this appendix. Following parameters are used for making this electrode.

PTFE Content : 8%
Cooling : ON
Clearance between the rolls : 400μm
Milling Time : 30 second

(i) Take 250 gm of Raney-Ni with water.

(ii) Wash the catalyst thoroughly with running distilled water.

(iii) Passivate the catalyst with oxygen using conventional method.

(iv) For making one electrode sample take 18.4 gm of dried and passivated catalyst and add 1.6 gm of PTFE powder. Mix these constituents thoroughly.

(v) Mill this mixture for 30 second while cooling ON.

(vi) Make a slurry using 500 ml distilled water, 2 ml Brij 96 (10% dilution) and 15 gm milled catalyst.

(vii) Filter the slurry on a filter paper applying 500 and 300 mbar in steps.

(viii) Roll the filter cake with paper after several hour of air drying.

(ix) Put a clean precut nickel mesh and roll again at 400 μm clearance.

(x) Boil the electrode in acetone for five minutes to remove the residual surfactant.

VITA

Personal:

Born on 20 August 1965 ... Excellent Health ... Indian ...Muslim ... Married (two year old daughter) ... Fluent in English.

Education :

Doctor of Philosophy in Chemical Engineering (1995)
King Fahd University of Petroleum and Minerals **(KFUPM)**,
Dhahran, Kingdom of Saudi Arabia.

Master of Technology Specialized in Petroleum and Coal (1990)
Indian Institute of Technology **(IIT)**,
Bombay, India.

Bachelor of Engineering (1987)
University of Roorkee **(UOR)**,
Roorkee, India.

Experience:

Lecturer in Chemical Engineering (April '91 to present)
Chemical Engineering Department,
King Fahd University of Petroleum and Minerals,
Dhahran, Kingdom of Saudi Arabia.

Project Engineer (March '90 to April '91)
Kinetics Technology International (KTI),
New Delhi, India.

Visiting Lecturer (March '89 to September '89)
K. G. Somaiya Institute of Technical Training and Research (SITTAR),
Bombay, India.

Production Trainee (August '87 to May '88)
PAMWI Specialty Tissues and Papers Limited (PAMWI),
Himachal Pradesh, India.

Publications :

1. M. C. Dwivedi and **Sleem-ur-Rahman**, ***"Asphalt Emulsions - A Review"***, 6th Symposium on Lubricants, Additives, Waxes and Petroleum Speciality Products, IIT: Bombay (1989).

2. M. A. Al-Saleh, S. Gultekin, **Sleem-ur-Rahman** and A. S. Al-Zakri, ***"Modified Flooded Spherical Agglomerate Model for Gas Diffusion Electrodes of Alkaline Fuel-Cells"***, Journal of Power Sources, Vol. *55*, No. 1, pp 43-49 (1995).

Address:

Rahman Manzil, Jhabrera-247665 (Haridwar) U.P., INDIA.